CATABOLITE CONTROL AND METABOLIC HOMEOSTASIS IN *RHIZOBIUM LEGUMINOSARUM*



Ann-Kathrin Maurer

Jesus College

University of Oxford

A thesis submitted for the degree of

Doctor of Philosophy

Trinity 2026

DECLARATION

I declare that all parts of this thesis are my own work and have not been submitted for any other qualifications, with the following exceptions in **Chapter 4**:

The construction of pOPS1850–54 and their conjugation into recipient rhizobial strains were performed by Dr Raphael Ledermann. Markerless deletions resulting in strains OPS3365 and OPS3367 were carried out in conjunction with Dr Raphael Ledermann. In addition, the conjugation resulting in strain OPS2516 was performed by Dr Raphael Ledermann.

The data from transcriptional *gusA*-reporter assays were generated during an internship undertaken at the Poole lab as part of my M.Sc. in Plant Sciences at Wageningen University & Research, the Netherlands, immediately prior to the start of my DPhil in the same research group. The work carried out during that time in the Poole lab was included in an internship report submitted in partial fulfilment of the requirements for the master's degree.

For the present thesis, these data have been re-analysed and are presented in newly generated figures and accompanying text, integrated with additional results obtained during the DPhil, to form a coherent and extended body of work. All other parts of this thesis represent original work conducted during the DPhil.

Ann-Kathrin Maurer

ABSTRACT

Biological nitrogen fixation by rhizobia in symbiosis with legume plants is a key resource for sustainable nitrogen inputs in agricultural systems, yet the regulatory mechanisms that coordinate bacterial metabolism during this interaction remain incompletely understood. In particular, detailed understanding of how rhizobia integrate environmental nutrient signals to control metabolic adaptation across their transition from free-living growth to the nitrogen-fixing bacteroid state is required to fully exploit this symbiosis.

In this thesis I investigate how metabolic and regulatory processes are coordinated in *Rhizobium leguminosarum*, with a focus on carbon utilisation, transport systems, and global regulatory mechanisms. Utilizing a combination of genetic, physiological, and transcriptomic approaches, three interconnected aspects of rhizobial regulation are explored.

First, carbon catabolite repression (CCR) was shown to be governed by intracellular C_4-dicarboxylate availability rather than dedicated sensing systems. Using luminescence-based reporters, I show that various alternative carbon transporters are repressed to prioritise C_4-dicarboxylates uptake, which is required to generate the CCR signal. Mechanistic analysis of the inositol pathway supports an inducer exclusion model, in which repression of this secondary carbon source is achieved through selective inhibition of substrate uptake.

Second, the native regulatory context of the dicarboxylate transport system (Dct) was found to be essential for coordinating growth on C_4-dicarboxylates with cellular physiology. Although not required for CCR signalling, disruption of the Dct regulatory context resulted in severe growth defects and impaired symbiotic nitrogen fixation, even when transport capacity was restored. These findings highlight the importance of regulatory integration, where the Dct system may function as an integrated transport–regulatory module that coordinates carbon uptake with broader metabolic networks, including those linking carbon and nitrogen metabolism.

Third, the integration of metabolic signals at the level of global regulation was investigated through the stringent response effector DksA. Functional characterisation of three DksA homologues revealed a clear division between canonical DksA, which is essential for transcriptional reprogramming and maintenance of metabolic homeostasis during symbiosis, and DksA-like proteins, which are oxygen-responsive but exhibit no major phenotypes under the conditions tested. Loss of DksA resulted in metabolic imbalance and a failure to fully establish the bacteroid state, with pronounced host-dependent effects.

Together, these findings support a hierarchical model of rhizobial regulation in which intracellular metabolites determine the metabolic state, transport systems coordinate substrate uptake, and global regulators integrate these signals to shape gene expression and symbiotic performance. This work provides new insights into the coordination of metabolism and regulation in rhizobia across their life cycle and outlines elementary principles governing symbiotic adaptation.

ACKNOWLEDGEMENTS

This thesis builds on the work and support of many others, and I am fortunate to have received such support over the past 3+ years.

First, I'd like to thank my primary supervisor, Phil Poole, whose unending excitement for science is truly inspiring. You worried about my project when I did not, and kept an eye on the bigger picture while I was deep in the details. You endured long discussions where I arrived with new data that often overturned previous hypotheses. You create a lab environment that supports and encourages us to become better microbiologists - fuelled by biscuits, film and book quotes, and stories from past and present. Likewise, I thank my second supervisor, Jani Bolla, for his support and for always being available to discuss ideas and answer questions.

I also thank the Clarendon Scholarship and Jesus College for their financial support, which allowed me to accept and undertake this PhD.

I am very grateful to have been part of the Poole lab. The people here, and their support and friendship, made this work possible.

Special thanks to the postdocs for generously sharing their knowledge. Alison, thank you for managing all of us and your input on expression datasets, ABC transporters, and navigating years of Poole lab publications. Carmen, thank you for your teaching, wisdom, and insights into the radiation lab and women in science. Isidro, thank you for shaping my approach to experimental design and teaching me how to ask the right questions. Tim and Andrzej, you were there at the very beginning, and among the first to move on to new endeavours; science is a transient place, and sometimes that makes me sad to see good people go. Hayley, thank you for answering my many questions over the years, and especially for your help in the final year. Bea, who taught me to always have controls and guided me through Golden Gate cloning and RNA-seq analysis, thank you. Albert, your unending enthusiasm for my projects and their associated hurdles kept me going and helped me see things from new perspectives. I am looking forward to keep working with you!

And lastly, to Raphael: thank you for everything you have taught me. I am happy and proud to carry forward your way of conducting science. Thank you for sharing a lab bench with me, and for putting up with my messiness, endless questions, and sometimes limited maths or chemistry skills. Thank you for reading various stages of my written work and for your rigorous feedback. I truly appreciate your eye for details, both in writing and in the lab, and your patience in answering my questions, no matter how many times I asked them or how basic they were. You shaped my experience more than either of us may realise. The Raphael way of doing things will stay with me, and I look forward to teach the next students all the things I could learn from you. Your leaving was an adjustment at first, yet it allowed me to grow into a more independent researcher.

Obviously, the biggest thanks to Helen and Lida, the lab fairies without whom none of our work would be possible, thank you for keeping the lab running so smoothly. I am also grateful to Rob, who always helped resolve the many requests I brought to his workshop or office.

To my fellow PhD students, past and present, thank you for the shared journey. We shared countless DPhil meetings, coffees and drinks, both in Oxford and during conferences, where colleagues became close friends. Thank you to Patrick, Clare, and Bergthor, who impressed me with their knowledge in my early days. Thank you to Jessie, Tom, and Olivia, who submitted just before me. All of you taught me different aspects of science, and I am very grateful for that. Particular thanks to Olivia, with whom I became especially close, for answering my never-ending questions and discussing PTS^{Ntr}, transport assays, rhizobial metabolism, and many other scientific and non-scientific topics. And all the Linacre lunches! A special thanks to Matt, who was there for most of this ride and as a fellow supervisee of Raphael; I am glad this PhD made us friends. I know that I can always bother you and have no hesitation in disrupting your work – just as you are always welcome to bother me. We helped each other, doing sanity math-checks, rolling on the floor to understand cloning techniques, and figuring out together what a post-Raphael PhD life looks like.

To Rachel, James, Hamish and Julian, I have no doubt that you will carry on the Poole lab legacy! Thank you also to the Master's students to contributing to the spirit. To Mairi, Evan, Henry, Laura, Jonathan, Tarka, Evelyn, and Ben, thank you for joining our lab, the

occasional drink, and the student meetings on Friday morning. Thanks to Lea for co-running experiments and, more than once, watering my plants.

I am immensely grateful to have learned from many of you, and in turn to have shared and passed on some of that knowledge, across old and new protocols, techniques, presentation feedback, and troubleshooting any of the above. Science is a collective effort, and you have all made it an exceptional group to be part of.

In a similar vein, I would also like to acknowledge Colm Reid. Although we have never met in person, I am still impressed by the scope and depth of your work on Dct, which I was able to build upon – quite literally, as your strains remain viable more than 30 years later.

To my friends outside of the lab, Nicole, Jisoo, and Casey, thank you for adopting me amongst the social scientists, and for sharing so many meals, formals, outings, and holidays with me. To Genia and Nick, thank you for the shared nights at High Table and other meals together.

To my family, to my mom, dad, Sarah and Sabrina: Danke für eure Unterstützung, auch wenn ihr nicht immer ganz verstanden habt, worum es ging oder wohin es als Nächstes ging. Auendorf bleibt meine Heimat und meine Herkunft eine wichtige Motivation für meine Arbeit. Likewise, I thank Johannes' family, for their warm welcome and continued interest in our endeavours over the years.

I also acknowledge one particular desk in the PH Freiburg library, Johannes' colleagues and the shared lunches, all of which sustained me while large parts of this thesis were written and completed.

Lastly, in acknowledging those who contributed to the successful completion of this thesis, there is one person who cannot go unmentioned. Johannes, thank you for all the support, guidance, and love that carried me through my time in Oxford. You always always listened, patiently endured biology refreshers in both theory and practice, and cooked dinner for me whenever I had yet another late evening in the lab. Oxford is where we began building our first home together. In the end, home is wherever you are, and I count myself incredibly lucky to have you by my side. You make me a better person, scientist, and partner every day.

TABLE OF CONTENTS

DECLARATION i
ABSTRACT ii
ACKNOWLEDGEMENTS iv
TABLE OF CONTENTS vii

1 GENERAL INTRODUCTION 1
1.1. The nitrogen crisis 2
1.2. Rhizobium-legume symbiosis 4
1.2.1. The rhizobial life cycle 5
1.3 Research contexts and aims 21
1.4 Thesis Outline 22
References 23

2 Carbon catabolite repression prioritizes C_4- dicarboxylates by selectively repressing transport of alternative carbon sources 33
Abstract 36
Introduction 37
Material and Methods 40
Results 49
Discussion 74
References 83
Supplementary Information 90

3 Misregulation of the Dct system uncouples C_4-dicarboxylate transport from physiological function 103
Abstract 105
Introduction 106
Material and Methods 111
Results 118
I: Spontaneous Dct regulatory mutants 118
II: Uncoupling *dctA* expression from DctBD through engineered constructs 126
Discussion 138
References 149
Supplementary Information 156

4 Functional diversification of canonical and oxygen-responsive DksA homologues in *Rhizobium leguminosarum* 169
Abstract 172
Introduction 173
Material and Methods 176
Results 186
Discussion 213
References 223
Supplementary Information 232

5 GENERAL DISCUSSION AND FUTURE PERSPECTIVES 254
References 263

1

GENERAL INTRODUCTION

GENERAL INTRODUCTION

1.1. The nitrogen crisis

Nitrogen is the most abundant element in the atmosphere and essential for life on Earth. It forms the backbone of nucleic acids like DNA and amino acid chains in proteins, and is therefore indispensable for all living systems. Despite its abundance, however, most nitrogen exists as molecular dinitrogen (N_2), a highly stable and largely inert gas composed of two nitrogen atoms joined by a strong triple bond. This chemical stability renders atmospheric nitrogen inaccessible to the majority of organisms, creating a fundamental paradox: nitrogen is ubiquitous, yet frequently the limiting nutrient for growth in both terrestrial and marine ecosystems.

The conversion of atmospheric nitrogen into biologically available forms is mediated by the global nitrogen cycle, a biogeochemical process carried out by interconnected microbial and abiotic processes that circulate nitrogen between atmospheric, terrestrial and aquatic environments. Central to this cycle is nitrogen fixation, in which N_2 is reduced to biologically available forms such as ammonia (NH_3), which is rapidly protonated to ammonium (NH_4^+) under physiological conditions. In natural ecosystems, this process is primarily carried out by specialized bacteria and archaea through biological nitrogen fixation (BNF), while abiotic processes such as lightning contribute comparatively small amounts of fixed nitrogen, predominantly in the form of nitrate (NO_3^-) (Fowler et al., 2013). Once fixed, nitrogen is subsequently incorporated into organic matter, transferred through food webs, and eventually returned to the environment through mineralisation, nitrification, and denitrification, thereby completing the cycle (Fowler et al., 2013).

In terrestrial ecosystems, and particularly in agricultural systems, nitrogen is often the primary limiting nutrient for plant growth (Lawlor et al., 2001; LeBauer & Treseder, 2008). To overcome this limitation and sustain high crop yields, modern agriculture relies heavily on the industrial production of reactive nitrogen via the Haber-Bosch process. Ever since its development in the 1910s, industrial nitrogen fixation has enabled the large-scale synthesis of ammonia from atmospheric nitrogen and hydrogen under high temperature and pressure conditions (Liu, 2013). Today, anthropogenic activities account for

approximately half of the global annual input of fixed nitrogen, estimated at around 210 Tg N per year (Fowler et al., 2013).

The widespread application of synthetic nitrogen fertilizers has been instrumental in supporting global food production and population growth, but dependence on this practice comes at significant environmental and economic costs (Tian et al., 2022). The Haber-Bosch process is highly energy-intensive and relies heavily on fossil fuels (Liu, 2013), contributing substantially to global greenhouse gas emissions. Moreover, excessive fertilizer application leads to nitrogen losses from agricultural systems, resulting in eutrophication of aquatic ecosystems, emissions of nitrous oxide (N_2O, a potent greenhouse gas), and broader soil and ecosystem degradation (FAO, 2025; Rockström et al., 2024). Together, these impacts highlight the unsustainability of current nitrogen management practices.

At the same time, continued population growth and increasing food demand place additional pressure on agricultural systems. Several of the United Nations Sustainable Development Goals (SDGs), including those addressing food security, climate action, and environmental sustainability, emphasize the urgent need to develop more sustainable approaches to nutrient management. Reducing reliance on synthetic nitrogen fertilizers while maintaining crop productivity therefore represents a major scientific and societal challenge (IPCC, 2023; Zhang et al., 2020).

In contrast to industrial nitrogen fixation, biological nitrogen fixation represents a more sustainable and energy-efficient alternative at the ecosystem level (Peoples et al., 1995). Consequently, considerable effort is being directed towards harnessing and improving BNF for agricultural applications. In particular, the symbiotic interaction between legume plants and nitrogen-fixing rhizobia bacteria provides a highly efficient mechanism for nitrogen input into agricultural systems, reducing the need for external fertilizer inputs. Understanding the biological principles that govern this symbiosis, including the metabolic and regulatory processes that underpin its efficiency, is therefore of central importance. This thesis aims to contribute to this understanding by investigating how *Rhizobium leguminosarum* coordinates metabolic and regulatory processes during free-living growth and symbiosis, with the long-term goal of informing strategies to enhance sustainable nitrogen fixation in agriculture.

1.2. Rhizobium-legume symbiosis

As primary producers, plants convert atmospheric CO_2 into organic compounds through photosynthesis. Yet, as sessile organisms, they rely on their surrounding environment for the acquisition of all other essential nutrients, including nitrogen, phosphorus, potassium, and sulfur, as well as various micronutrients and trace elements. To facilitate nutrient uptake under often limiting conditions, mutualistic interactions between plants and root-associated microorganisms have evolved. Among the most widespread of these is the symbiosis with arbuscular mycorrhizal (AM) fungi, which evolved more than 400 million years ago (Brundrett, 2002), and primarily enhances the uptake of phosphorus and other mineral nutrients, but may also improve the plant's access to nitrogen from organic and inorganic sources (Bennett & Groten, 2022).

In addition to these ancient associations, some land plants have evolved the ability to form symbiosis with nitrogen-fixing prokaryotes (Delaux et al., 2015; Griesmann et al., 2018). BNF is restricted to a subset of bacteria and archaea, collectively referred to as diazotrophs, which possess the nitrogenase enzyme required to reduce atmospheric nitrogen into bioavailable ammonia. While some diazotrophs exist as free-living organisms, others form intimate associations with plants, allowing for the direct transfer of fixed nitrogen to the host.

The most prominent of these associations is the rhizobium-legume symbiosis, in which nitrogen-fixing bacteria, collectively referred to as rhizobia (belonging to Alpha- and Betaproteabacteria; Masson-Boivin et al., 2009), form a highly specialized interaction with leguminous plants (Fabaceae, order Fabales). In this symbiosis, bacteria colonize plant roots and induce the formation of specialized root nodule organs, within which rhizobia differentiate into nitrogen-fixing bacteroids (Poole et al., 2018). These nodules provide a tightly regulated microenvironment that protects the oxygen-sensitive nitrogenase enzyme while supplying the bacteroids with carbon substrates derived from the host plant.

More generally, the ability to form so-called root nodule symbioses is largely confined to plant species within the monophyletic FaFaCuRo clade, comprising the Fabales, Fagales, Cucurbitales, and Rosales (Soltis et al., 1995). Within this clade, agriculturally

important nitrogen-fixing crops are predominantly found in the Fabales, including soybean (*Glycine max*), pea (*Pisum sativum*), common bean (*Phaseolus vulgaris*), cowpea (*Vigna unguiculata*), chickpea (*Cicer arietinum*), and peanut (*Arachis hypogaea*), as well as model legumes such as *Medicago* spp. and *Lotus japonicus*.

Although the capacity for nodulation is phylogenetically constrained, it is thought to have evolved independently at least ten times in land plants (Delaux et al., 2015) and has also been lost repeatedly during evolution, for instance at least eight independent times within the FaFaCuRo clade (Griesmann et al., 2018), highlighting both its adaptive value and its evolutionary plasticity.

Root nodule symbiosis shares components of its signalling machinery with the more ancient AM symbiosis (Radhakrishnan et al., 2020), suggesting that it evolved by recruiting pre-existing genetic pathways. Despite this shared foundation, the rhizobium–legume interaction has developed into a highly specialized system for nitrogen acquisition. While alternative nitrogen-fixing symbioses exist, such as those between actinorhizal plants and *Frankia* species (Gherbi et al., 2008), the rhizobium–legume symbiosis remains the most extensively characterized and is of particular relevance for agricultural systems.

1.2.1. The rhizobial life cycle

All root nodule symbioses ultimately result in the formation of specialized root nodule organs that host nitrogen-fixing microsymbionts called bacteroids. Although the specifics of these symbioses differ between strains and plants, the fundamental progression of symbiotic development is conserved. A variety of infection mechanisms and nodule morphologies have been described (Hadri et al., 1998; Sprent et al., 2017), and while rhizobia enter most often through root hairs, alternative routes such as crack entry in the root epidermis also exist (Chaintreuil et al., 2013).

The establishment of rhizobium–legume symbiosis is a multi-stage process involving tightly coordinated signalling and developmental changes in both partners (Oldroyd et al., 2011). During this transition, rhizobia differentiate from motile, free-living cells into a distinct physiological state optimized for nitrogen fixation.

This thesis focuses on the interaction between the α-proteobacterium species *Rhizobium leguminosarum* and its legume hosts, using this model to investigate how bacterial metabolic and regulatory processes are coordinated during free-living growth and symbiosis. In the following sections, the major stages of the rhizobial life cycle are outlined, with a focus on processes relevant to *R. leguminosarum* and to this work.

During the course of this PhD, the *R. leguminosarum* species complex underwent phylogenetic reclassification (Young et al., 2023), resulting, for instance, in the reassignment of strain 3841 to *Rhizobium johnstonii*. However, for consistency and clarity, the original nomenclature is retained throughout this thesis, and all strains are therefore referred to as *R. leguminosarum*.

Free-living rhizobia

Like other rhizobia, *R. leguminosarum* undergoes a complex life cycle that alternates between a free-living, soil-dwelling phase and a symbiotic, host-associated phase within root nodules (Figure 1.1). While the symbiotic phase has been extensively studied due to its importance for biological nitrogen fixation, the free-living stage represents a critical but comparatively less well understood phase in which rhizobia must persist, proliferate, and compete prior to host colonisation. This limited understanding may partly explain why rhizobial inoculants, commonly applied as biofertilizers, often fail to compete for nodule occupancy in the field, as selection has traditionally prioritised nitrogen fixation efficiency over traits required for persistence and competitiveness in complex soil environments (Checcucci et al., 2017; Mendoza-Suárez et al., 2021).

A key challenge in understanding this phase lies in the fact that most experimental work on rhizobia has been conducted under simplified laboratory conditions, typically using defined media and single strains. As a result, we lack a detailed spatial and temporal understanding of metabolic and genetic processes within rhizobia in natural environments, where they are exposed to fluctuating nutrient availability, spatial heterogeneity, and interactions with complex microbial communities. Recent advances, such as transposon insertion sequencing (INSeq), have begun to address this gap by

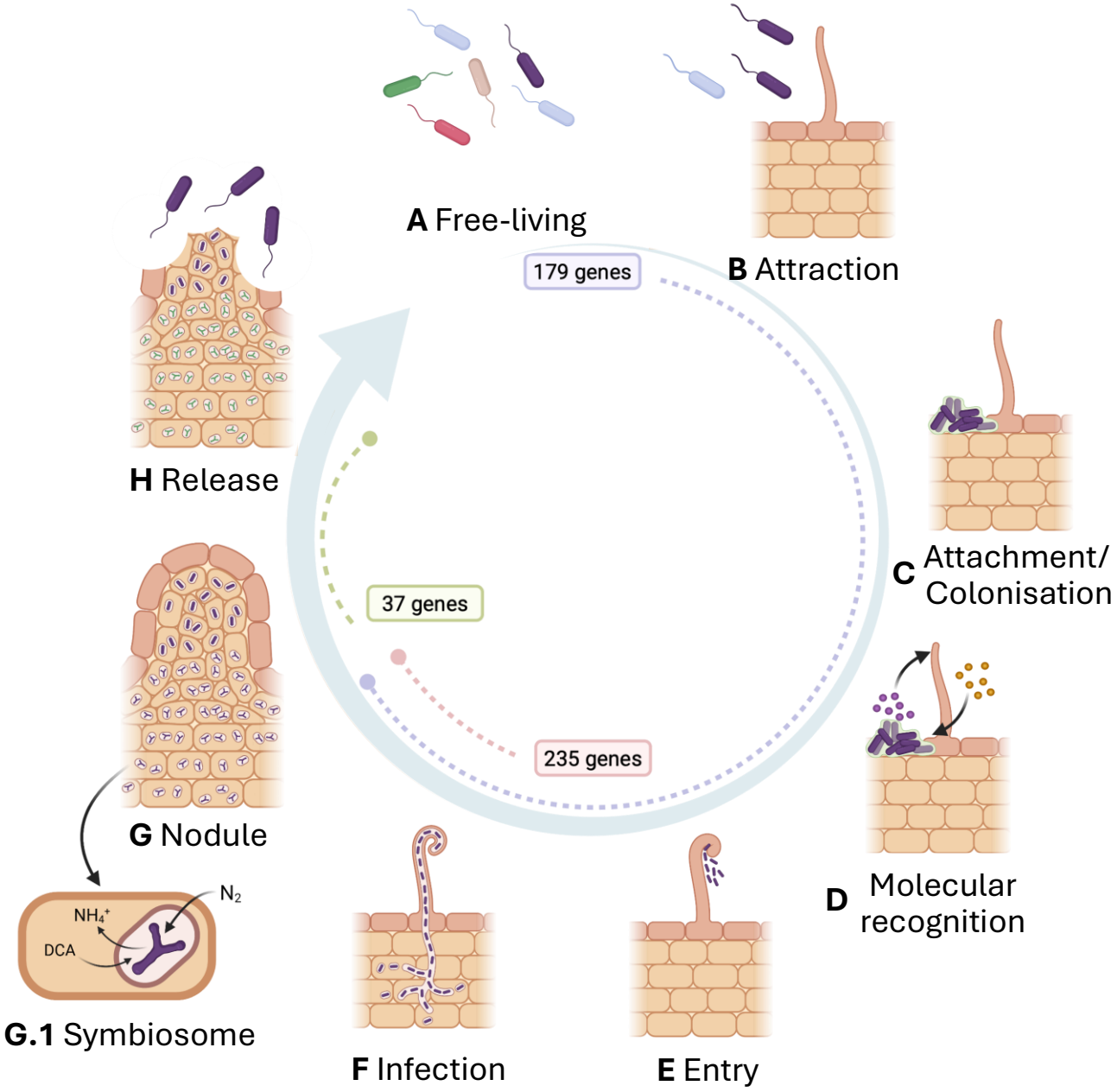


Figure 1.1 Rhizobial life cycle during symbiosis with legume plants. Rhizobia transition from free-living to a symbiotic state through a coordinated series of stages. **(A)** In the soil, rhizobia bacteria exist as free-living cells, competing against each other and other organisms for resources. **(B)** Upon sensing root-derived signals, rhizobia are attracted to the root surface and **(C)** attach and colonise the root surface, forming biofilms. **(D)** Symbiotic signalling, where legume roots exudate flavonoids and compatible rhizobial partners release Nod factors, leads to **(E)** root hair curling and bacterial entrapment. **(F)** Rhizobia then enter the root through infection threads, which guide them inward toward cortical cells. **(G)** Within the developing root nodule, bacteria are released into host cells and differentiate into nitrogen-fixing bacteroids (Y-shaped) **(G.1)** In this symbiotic state, rhizobia convert atmospheric nitrogen (N_2) into ammonia (NH_4^+), benefiting the plant host, in return for carbon, mainly C_4-dicarboxylates (DCA). **(H)** Eventually, when nodules senesce, bacteria are released back into the soil, returning to the free-living state and completing the cycle. Note, in terminally differentiated nodule symbioses, only nodule bacteria are released into the environment, whereas in non-terminally differentiated symbiosis, the bacteroids can revert to the free-living state. Numbers within the central circle indicate the number of genes required for specific stages of the symbiosis, as identified by genome-scale insertion sequencing (INSeq) in pea (Wheatley et al., 2020) and bean-nodulating rhizobia (Knights, Ledermann et al., in preparation). Figure modified from illustrations by Beatriz Jorrín and Hayley Knights, originally created with Biorender.com.

enabling genome-scale identification of genes required for growth under diverse conditions, including complex media, different carbon sources, and varying oxygen levels (Perry et al., 2016; Perry & Yost, 2014; Wheatley et al., 2017). Such studies provide insights into the genetic basis of rhizobial fitness across environmental contexts and can help link free-living and symbiotic lifestyles.

Like many natural environments, soil does not permit unconstrained microbial growth (Sterner & Elser, 2003). Instead, as oligotrophic organisms, free-living rhizobia are able to persist in highly heterogeneous and often nutrient-limited soil environments. Availability of key nutrients, including carbon and nitrogen sources, is often limiting and unevenly distributed (Pini et al., 2017), while abiotic factors such as soil pH (Angus et al., 2013; Frey & Blum, 1994) or nutrient availability (Elliott et al., 2009) further influence bacterial survival and competitiveness (Mendoza-Suárez et al., 2021). In addition, rhizobia themselves are members of complex soil communities and must compete with a diverse microbiota for access to these resources (Poole et al., 2018), making efficient nutrient acquisition and metabolic flexibility essential for persistence.

To cope with these challenges, rhizobia have evolved large genomes encoding a broad repertoire of metabolic functions and transport systems. In particular, they possess an unusually high number of ATP-binding cassette (ABC) transporters compared with many other bacteria, reflecting adaptation to the chemical complexity of soil and rhizosphere environments. For example, more than 200 ABC transporter genes have been identified in *Sinorhizobium meliloti*, 216 in *Mesorhizobium loti*, 269 in *R. leguminosarum*, and 240 in *Bradyrhizobium diazoefficiens*, compared with 67 in *Escherichia coli* and 124 in *Pseudomonas aeruginosa* (Mauchline et al., 2006). This diversity enables rhizobia to utilise a wide range of substrates and supports their ecological versatility (Prell & Poole, 2006).

Among available substrates, C_4-dicarboxylic acids such as succinate, malate and fumarate play a particularly prominent role in rhizobial metabolism. These compounds are preferentially utilised by free-living rhizobia over many alternative carbon sources (Iyer et al., 2016; Mandal & Chakrabartty, 1993), and later serve as the primary carbon and energy source during symbiotic nitrogen fixation (Mitsch et al., 2018; Ronson et al., 1981; see below). This preference reflects a hierarchical organisation of carbon

utilisation, typically mediated by carbon catabolite repression (CCR; cf. Chapter 2). The regulatory mechanisms underlying this carbon hierarchy in *R. leguminosarum* remain poorly resolved, yet understanding how rhizobia prioritise available substrates is particularly relevant to their adaptation to the chemically diverse rhizosphere and to the transition towards C_4-dicarboxylate-dependent metabolism in bacteroids (see below).

In parallel, free-living rhizobia must acquire and assimilate nitrogen from their environment, for instance through uptake of ammonium or organic nitrogen sources such as amino acids via dedicated transport systems (Hosie et al., 2002; Taté et al., 1998; Walshaw & Poole, 1996). These compounds are subsequently incorporated into central metabolism, primarily via the combined activities of glutamine synthetase and glutamate synthase (GS/GOGAT) (Mulley et al., 2011). As this pathway relies on key carbon intermediates from the TCA cycle, nitrogen assimilation is tightly coupled to central carbon metabolism, necessitating coordinated regulation of both nutrient inputs (Poole & Allaway, 2000; Prell & Poole, 2006).

Coordination between carbon and nitrogen metabolism, and integration of perturbations in these systems, is mediated by global regulatory networks, including the stringent response, involving the RelA and DksA proteins,and the PTS^{Ntr} system, comprising PtsP, NPr, PtsN, ManX (Calderón-Flores et al., 2005; Green et al., 2019; Prell et al., 2012; Sánchez-Cañizares et al., 2020; Tjahjono, 2025). These conserved systems enable rhizobia to sense and respond to fluctuations in nutrient availability, thereby adjusting metabolic activity to environmental conditions. While such regulatory mechanisms are broadly conserved across bacteria, their specific roles and regulatory wiring in rhizobia often deviate from those described in classical model organisms (Prell & Poole, 2006; Sánchez-Cañizares et al., 2020).

Host attraction and root colonisation

Rhizobia, like many soil microorganisms, are attracted to the rhizosphere (Figure 1.1B), the nutrient-rich zone surrounding plant roots, where root exudates provide a diverse array of substrates (Pini et al., 2017; Ramachandran et al., 2011). However, this environment is highly competitive, as microorganisms must compete for nutrients and niches. Plants strongly influence the rhizosphere microbiota (Tkacz et al., 2015; Turner et

al., 2013), and, as a consequence of plant selection, microbial diversity in the rhizosphere is generally lower than in bulk soil. Competitiveness in the rhizosphere is therefore a key determinant of symbiotic success and ultimately influences the likelihood of nodule formation (Mendoza-Suárez et al., 2021).

The large genomes and extensive pan-genomes of rhizobia provide the genetic basis for this adaptability. To exemplify, the nearly 8 Mb genome of the model strain *Rhizobium leguminosarum* bv. *viciae* 3841 (*Rlv*3841) comprises not only a chromosome but also six large plasmids. Notably, most genes required for nodulation (*nod*) and nitrogen fixation (*fix*) are located on plasmid pRL10, commonly referred to as the symbiotic plasmid. In addition, horizontal gene transfer facilitates rapid genetic exchange, including symbiotic loci, between strains. This process, potentially shaped by host plant environments (Ling et al., 2016), enables fast spread of advantageous traits through rhizobial populations (Kumar et al., 2015).

Successful colonisation of the rhizosphere and later rhizoplane therefore depends not only on metabolic versatility but also on the ability to sense and respond to plant-derived signals (Salas et al., 2017; Wheatley et al., 2020). Motility and chemotaxis enable rhizobia to move towards root exudates (Aroney et al., 2024), which contain sugars, organic acids, amino acids, and secondary metabolites such as flavonoids that act as chemoattractants (Geurts & Bisseling, 2002; Ramachandran et al., 2011).

Following attraction, rhizobia attach to the root surface (Figure 1.1C), a process mediated by a combination of surface structures and extracellular components. Production of extracellular polysaccharides (EPS), lipopolysaccharides (LPS), and other cell surface molecules facilitates adhesion to root hairs and contributes to the establishment of stable associations with the host (Knights et al., 2021).

In addition to above-mentioned INSeq experiments, the two most recent INSeq data sets focusing on symbiotic interactions enabled identification of genes required during rhizosphere growth, root colonisation, undifferentiated bacteria within the host, and (terminally) differentiated bacteroids in nodules of pea (Wheatley et al., 2020, Figure 1.1) and bean (Knights, Ledermann et al., in preparation). For instance, 390 genes are required for competitive nodulation of pea (Wheatley et al., 2020). Of these, 146 were classified

as rhizosphere-progressive, meaning they are required in the rhizosphere and at all subsequent stages. These genes are primarily involved in the biosynthesis of essential metabolites, including tryptophan, riboflavin, leucine, isoleucine, and cobalamin, as well as ABC transport, EPS and LPS production, and stress regulation. A further 33 root-progressive genes are required from root attachment onward and contribute to Nod factor synthesis, cell-surface and EPS formation, cytochrome biosynthesis and export. Finally, 211 genes were classified as nodule-general and are therefore required for infection as well as nodule development and function, with roles in Nod factor signalling, nitrogen fixation, respiration, cell-envelope remodelling, stress responses, metabolism, and transport. Together, these genome-scale studies demonstrate that successful symbiosis depends not only on canonical *nod*, *nif* and *fix* functions, but also on the coordinated regulation of nutrient acquisition, metabolism, transport and stress adaptation throughout the rhizobial life cycle. How all these metabolic functions are coordinated by transport and global regulatory networks, however, remains largely unexplored.

The rhizobium-legume symbiosis is highly specific and requires precise molecular recognition between host plant and bacterium. This specificity is primarily determined by signal exchange between both symbiotic partners (Figure 1.1D). Plant-derived flavonoids present in root exudates induce expression of nodulation (*nod*) genes in compatible rhizobia, leading to the synthesis of lipochitooligosaccharides (LCOs), also known as Nod factors. These molecules carry various chemical modifications, including acetylation, methylation, sulphation, and fucosylation (Long, 1996) and these Nod factor 'decorations' in turn determine host specificity. For example, differences in LCO composition contribute to host specificity, such that *Rhizobium leguminosarum* bv. *viciae* infects pea, whereas *R. leguminosarum* bv. *phaseoli* infects bean. Recognition of compatible Nod factors by the host plant triggers extensive reprogramming of root cells, including cortical cell division that leads to the formation of the nodule primordium. In parallel, Nod factors induce bending and curling of root hairs, forming the characteristic 'shepherd's crook' that may entrap rhizobia attached to curling root hairs and therefore promote the formation of microcolonies within so-called infection pockets (Poole et al., 2018, Figure 1.1E). As the microcolony is commonly derived from a single strain, this

process represents a critical bottleneck that determines which rhizobia successfully initiate infection (Gage, 2002). Importantly, competitiveness in the rhizosphere does not necessarily translate into successful nodulation. Rhizobial strains and mutants that efficiently colonise roots may nonetheless lack competitiveness during nodule formation (Fry et al., 2001; Ledermann et al., 2018), highlighting that both rely on distinct processes requiring different adaptations.

Infection and nodule development

In the majority of rhizobium–legume interactions, bacterial entry into the host occurs via infection threads (ITs, Figure 1.1F), plant-derived tubular structures that originate in curled root hairs and guide rhizobia through the root epidermis into underlying cortical tissues (Quilbé et al., 2022). Infection is initiated at the root hair tip, where localised degradation of the plant cell wall allows rhizobia to enter, followed by invagination of the plant membrane to form the growing IT. Within these structures, bacteria are thought to proliferate and are transported towards the developing nodule primordium, largely driven by cell division and possibly some motility (Brewin, 2004). Production of EPS and LPS plays important roles during this process, contributing to successful infection by mediating host recognition and suppressing plant immune responses (Ghosh & Maiti, 2016) .

The infection process is tightly controlled by the host plant, which directs the IT trajectory towards sites of cortical cell division (Batzenschlager et al., 2025; Gao et al., 2024). Upon reaching the nodule primordia (Figure 1.1G), bacteria are released into individual plant cells by endocytosis and become enclosed within a plant-derived membrane, forming the symbiosome. Within this compartment, rhizobial cells multiply until the plant cell is densely packed and bacteria differentiate into bacteroids, the specialised form capable of nitrogen fixation (Poole et al., 2018).

Although IT-mediated entry is the best-studied mechanism, alternative modes of infection have been described. These include crack entry, where rhizobia enter through natural openings in the root epidermis, and fixation threads, in which bacteria remain confined within plant-derived tubular structures rather than being released into symbiosomes (De Faria et al., 2022; Quilbé et al., 2022). The evolution of symbiosomes

has been proposed to enhance host control through tighter compartmentalization of rhizobial microsymbionts, promoting an intimate and therefore more stable symbiosis (De Faria et al., 2022).

The extent of bacteroid differentiation is strongly dependent on the host plant. In legumes belonging to the inverted repeat-lacking clade (IRLC), host-derived nodule-specific cysteine-rich (NCR) peptides induce extensive physiological changes in the bacterial partner. Up to several hundred (>650) different NCR peptides have been identified in individual legume species to date, of which only a small fraction has been functionally characterised (Downie & Kondorosi, 2021). These peptides trigger genome endoreduplication in their bacterial partner, resulting in polyploidy and cell enlargement. Consequently, bacteroids undergo terminal differentiation, as they cannot revert to a free-living state after endoreduplication has occurred (Mergaert et al., 2006; Van de Velde et al., 2010). Terminally differentiated bacteroids are typically elongated or irregular in shape, often forming Y-shaped cells (Figure 1.2), and symbiosomes within infected cells

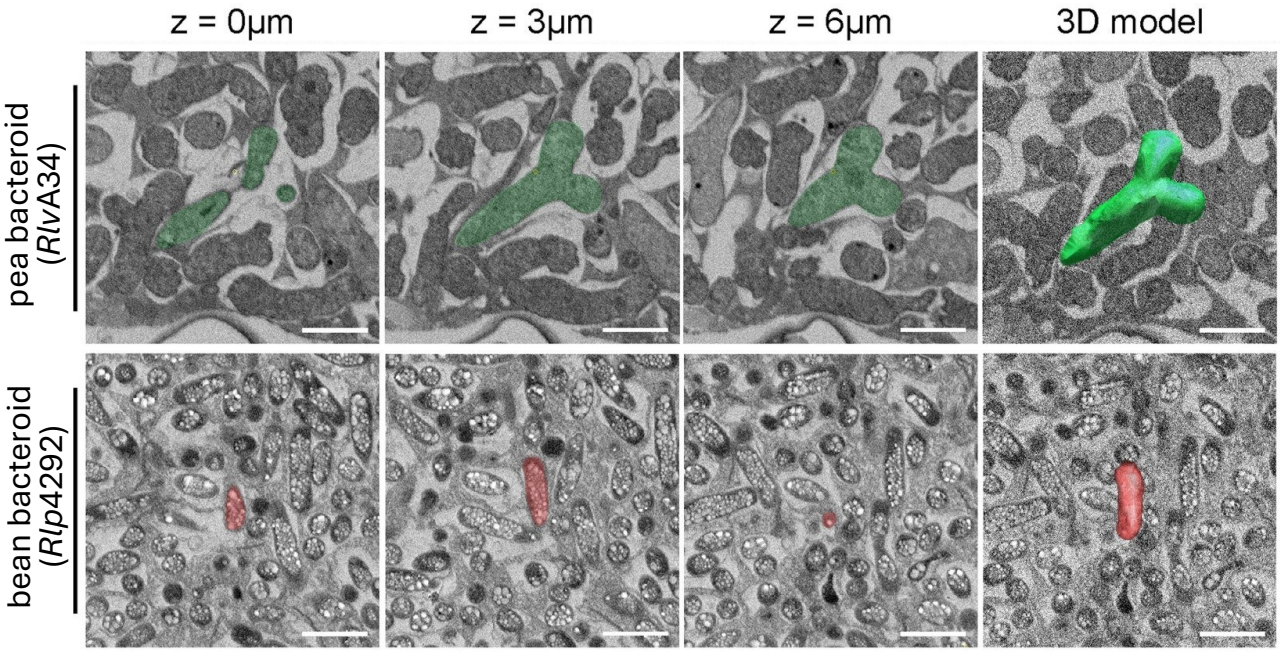


Figure 1.2 Differences between bean and pea bacteroids. Volume electron microscopy imaging of individual bacteroids show that bacteroids in pea (inoculated with *Rhizobium leguminosarum* bv. *viciae* A34 (*Rlv*A34), green) are swollen and Y-shaped, while bacteroids in bean (inoculated with *Rhizobium leguminosarum* bv. *phaseoli* (*Rlp*4292), red) are not. Serial Block Face-Scanning Electron Microscopy (SBF-SEM) imaging of representative bacteroids segmented across example Z slices and their subsequent 3D reconstruction. All scale bars = 2 *µ*m. Adapted from Sánchez-Cañizares et al. (2026).

generally contain a single bacteroid. By contrast, legumes that do not produce NCR peptides, such as common bean and soybean, host bacteroids that retain a morphology similar to free-living rhizobia (Figure 1.2), with multiple bacteroids housed within a single symbiosome (Maróti & Kondorosi, 2014; Poole et al., 2018). These cells retain the capacity to resume growth after release from the nodule.

Finally, legumes can be classified based on nodule morphology (Figure 1.3). Depending on the host plant, one of two nodule types is formed: determinate nodules lacking a persistent meristem, for example the spherical nodules formed by bean (cf. Figure 4.9), and indeterminate nodules, which maintain a persistent meristem and therefore exhibit indefinite growth, resulting in elongated, branched, or lobe-shaped nodules, such as those found on pea roots (cf. Figure 4.6) (Oldroyd et al., 2011; Poole et al., 2018; Udvardi & Poole, 2013). While NCR peptide production is associated with legumes of the IRLC, which form indeterminate nodules, indeterminate nodules are also found in legumes outside this clade that do not produce NCR peptides, indicating that nodule morphology and NCR peptide production are not strictly coupled.

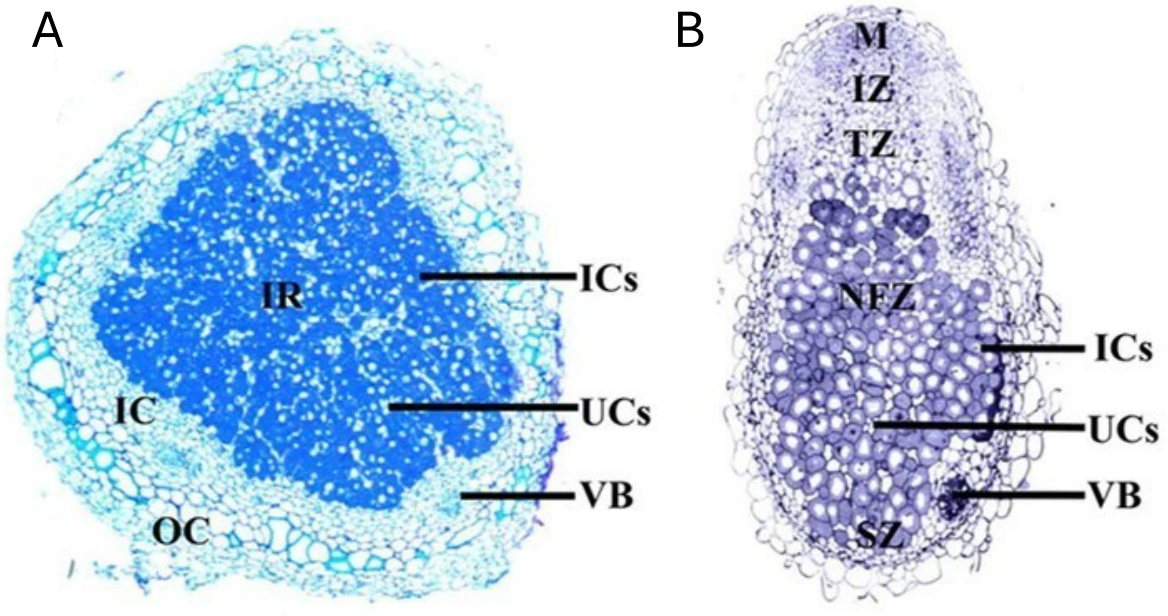


Figure 1.3 Cross sections of determinate and indeterminate root nodules. Longitudinal sections of a determinant soybean nodule **(A)** and an indeterminant *Medicago truncatula* nodule **(B)**. Determinate nodules consist of a central infected region (IR) containing infected cells (ICs; dark) interspersed with uninfected cells (UCs; light), surrounded by inner (IC) and outer cortex (OC) layers. Indeterminate nodules retain an active meristem and display distinct developmental zones, including the meristem (M), infection zone (IZ), transition zone (TZ), nitrogen fixation zone (NFZ), and senescence zone (SZ). Adapted from Brear et al. (2013).

Mature nodules and nitrogen fixation

Symbiosomes (Figure 1.1G.1) provide a controlled microenvironment in which differentiated bacteroids encounter optimal conditions to carry out their highly specialised physiological program dedicated to nitrogen fixation. In this form, bacterial metabolism is largely redirected towards the reduction of atmospheric nitrogen, with the nitrogenase enzyme converting N_2 into ammonia that is subsequently supplied to the host plant. In exchange, the plant provides bacteroids with carbon substrates and other nutrients, establishing a tightly coupled metabolic interaction (Udvardi & Poole, 2013). Common adaptations of bacteroid function have been summarised in a recent meta-analysis of transcriptomic and proteomic datasets (Ledermann et al., 2021), and the core principles relevant for this thesis are outlined below.

The iron-sulphur clusters of the nitrogenase enzyme are highly sensitive to oxygen (O_2), and nitrogenase is rapidly inactivated in its presence (Imlay, 2006). Paradoxically, nitrogen fixation requires high rates of respiration to meet the considerable energy demand of the enzyme. Hence, both partners of the symbiosis employ complementary strategies to resolve this 'oxygen paradox' and to ensure that levels of free oxygen within the symbiosome are kept in a nanomolar range (20-50 nM; King et al., 1988; Minchin, 1997).

On the one hand, the nodule cortex forms an oxygen diffusion barrier that limits oxygen entry into the nodule (Minchin, 1997). Nevertheless, to supply bacteroids with sufficient oxygen, legume plants produce leghaemoglobin, an iron-containing oxygen carrier protein that binds oxygen and facilitates its diffusion towards the bacteroids, thereby buffering free oxygen concentrations while ensuring sufficient oxygen transfer to the symbiosomes (Ledermann et al., 2021). The accumulation of leghaemoglobin also gives nodules their characteristic red colour.

On the other hand, rhizobia have evolved complex regulatory systems to sense surrounding oxygen levels and respond by coupling symbiotic gene expression to low oxygen conditions (Figure 1.4; reviewed in Rutten & Poole, 2019). In *R. leguminosarum*, the hFixL-FnrN cascade mediates adaptation to the microaerobic environment and, in response to lowering oxygen levels, activates transcription of downstream *fix* genes.

These include the high-affinity ccb_3-type oxidase (encoded by the *fixNOQP* operon, Figure 1.5), which enables respiration under microaerobic conditions (Preisig et al., 1996).

Lastly, the master regulator NifA, which controls a large regulon including the nitrogenase components *nifHDK,* is O_2-sensitive and coordinates gene expression required for the final differentiation into nitrogen fixing bacteroids (Dixon & Kahn, 2004).

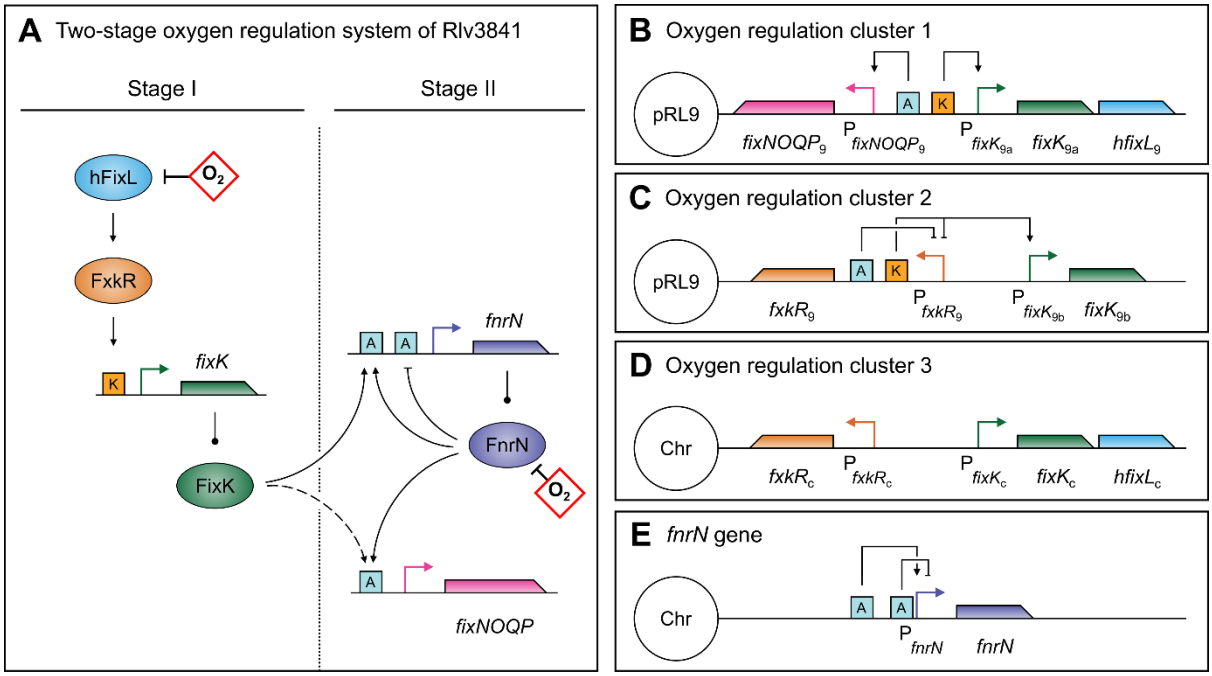


Figure 1.4 Oxygen regulatory network in *Rhizobium leguminosarum*. bv. *viciae* 3841 (*Rlv*3841). Proteins are shown as ellipses, genes as pointed rectangles and operator sites as square boxes. Oxygen is indicated in red diamonds. Promoter sites are shown as right-angled arrows. Lines ending in arrows, bars, or circles indicate activation, repression, and translation, respectively. **(A)** The oxygen regulation system constitutes of two stages. Stage I starts under microaerobic conditions, where hFixL activates FxkR, which binds to the K-box operator to induce expression of *fixK*. FixK binds to anaerobox operators upstream of *fnrN* and *fixNOQP* to induce expression. Stage II gets only activated at even lower oxygen levels. In this stage, FnrN binds anaeroboxes to induce *fixNOQP* expression and to auto-regulate itself positively and negatively. **(B-E)** *Rlv*3841 has multiple copies of several oxygen regulation genes, and many are arranged in clusters. They are situated either on megaplasmid pRL9 or on the chromosome. Figure from Rutten et al. (2021). For further details, see the original publication.

Only a limited subset of genes is specifically required for bacteroid function, comprising mostly *nod* and *fix* genes (Wheatley et al., 2020). This observation highlights that the majority of the rhizobial genome is required for transitions into and out of the bacteroid state, whereas bacteroid functionality itself is comparatively streamlined. Consistent

with this, global transcriptomic analyses show that most genes are downregulated in bacteroids (Ledermann et al., 2021), reflecting a reduction in physiological complexity and a shift towards a highly specialised metabolic programme dedicated to nitrogen fixation.

In contrast, a restricted set of genes directly supporting nitrogen fixation and energy metabolism is strongly upregulated. These include genes required for nitrogenase assembly (*nif* genes), electron transfer (*fix* genes), and transport systems for essential cofactors such as iron and molybdenum (Udvardi & Poole, 2013). In addition, increased expression of chaperones and enzymes involved in the detoxification of reactive oxygen species indicates that both the transition into and maintenance of the bacteroid state impose significant physiological stress on rhizobia (Ledermann et al., 2021).

Together, these patterns highlight the highly specialised nature of bacteroid metabolism. Accordingly, bacteroids have been described as 'ammonioplasts', emphasising their organelle-like behaviour. In this state, bacteroids become dependent on the host for carbon supply and are auxotrophic for several compounds, including amino acids and homocitrate (Figure 1.5).

This metabolic specialisation is centred on the supply of plant-derived C_4-dicarboxylates, which serve as the primary carbon and energy sources for bacteroids (Mitsch et al., 2018; Udvardi & Poole, 2013). Consistent with this, the bacteroid proteome is dominated by enzymes involved in C_4-dicarboxylate metabolism (Sánchez-Cañizares et al., 2026). The dependency on this carbon supply is further reflected in the essential role of the dicarboxylate transport system (Dct, Figure 1.5), which is required for effective nitrogen fixation but not for earlier stages of infection, as *dct* mutants can still form nodules but exhibit a Fix^- phenotype (Ronson et al., 1981). Together, these observations highlight the metabolic shift from the versatile substrate utilisation observed in free-living rhizobia to a highly specialised carbon metabolism within nodules.

Carbon metabolism in bacteroids is tightly constrained by oxygen availability and redox balance. Growth on C_4-dicarboxylates imposes high respiratory demand, while oxygen limitation restricts flux through the decarboxylating arm of the TCA cycle, thereby limiting assimilation of fixed nitrogen into amino acids (Schulte et al., 2021). Consequently,

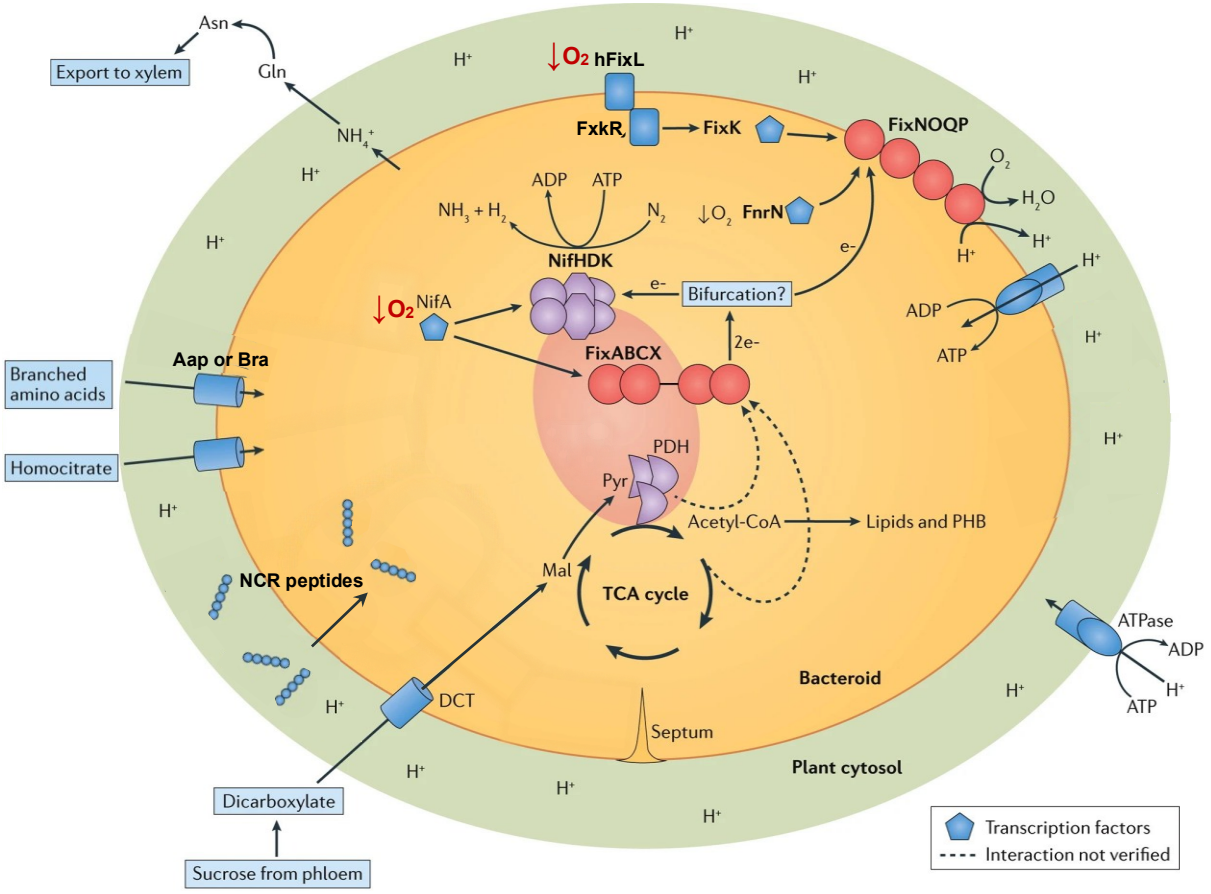


Figure 1.5 Nutrient exchange and regulation of bacteroid development. Schematic representation of central metabolic pathways, nutrient exchange, and oxygen-dependent regulatory networks in *Rhizobium leguminosarum* bacteroids. Oxygen (O_2) is the key signal controlling bacteroid development through two major regulatory circuits. The first involves the hFixL-FxkR cascade, which activates the transcriptional regulators FixK and FnrN, leading to expression of the high-affinity terminal oxidase FixNOQP (cbb_3-type oxidase). The second involves the nitrogen fixation regulator NifA, which induces expression of *nifHDK* (encoding the nitrogenase complex) and autoinduces the *fixABCX-nifA* operon. The FixABCX complex functions as an electron-bifurcating system, likely transferring electrons to ferredoxin or to flavodoxin, thereby supporting nitrogenase acitivity. Electron supply may additionally be linked to central carbon metabolism via pyruvate dehydrogenase (PDH), the tricarboxylic acid (TCA) cycle, and associated redox carriers. Under low O_2 conditions, flux through the TCA cycle is restricted, resulting in diversion of acetyl-CoA towards lipid and polyhydroxybutyrate (PHB) synthesis. Bacteroid differentiation is further influenced by nodule cysteine-rich (NCR) peptides. The plant host supplies bacteroids with C4-dicarboxylates as the primary carbon source, as well as additional metabolites such as amino acids and homocitrate, while bacteroids export fixed nitrogen to the plant. Aap, amino acid permease; Bra, branched amino acid permease; DCT, dicarboxylate transporter; Mal, malate; Pyr, pyruvate. Modified from Poole et al. (2018).

bacteroids secrete ammonium to the host rather than incorporating it into glutamate, reinforcing their dependence on the plant and rendering them symbiotic auxotrophs for compounds such as branched-chain amino acids (Lodwig et al., 2003; Prell et al., 2009).

Differences in bacteroid differentiation between host plants further influence metabolic efficiency. Terminally differentiated bacteroids, such as in pea, exhibit increased packing density, higher relative abundance of nitrogenase, and enhanced C_4-dicarboxylate metabolism compared to bacteroids in hosts such as bean. As a result, pea bacteroids achieve higher nitrogen fixation efficiency per unit bacteroid protein and per unit nodule mass (Sánchez-Cañizares et al., 2026).

Pea bacteroids and those from the IRLC are further characterised by their nongrowing state. Genes associated with cell division, translation (ribosomal proteins), motility, and cell envelope biogenesis (outer membrane proteins, peptidoglycan, and exopolysaccharide synthesis) are generally downregulated, resembling aspects of free-living growth arrest (Ledermann et al., 2021). However, in contrast to free-living bacteria in stationary phase, bacteroids are not nutrient-limited but remain highly metabolically active to sustain nitrogen fixation. The mechanisms underlying this uncoupling of metabolic activity and cell division remain poorly understood.

Nodule senescence

Following the nitrogen-fixing phase, nodules eventually undergo senescence, a plant-controlled process driven by developmental cues and influenced by environmental conditions and symbiotic performance (Kazmierczak et al., 2020). It is often triggered when nitrogen fixation becomes inefficient or when external nitrogen sources are available, leading to reduced carbon allocation to nodules and the activation of degradation pathways, ultimately resulting in the release or breakdown of bacterial cells (Figure 1.1H).

The fate of rhizobia during this process depends largely on the type of bacteroid differentiation imposed by the host. In legumes that enforce terminal differentiation through NCR peptides, only undifferentiated bacteria, such as those residing in ITs or early infection zones, are capable of surviving and re-entering the soil environment. In contrast, in legumes that do not induce terminal differentiation, bacteroids retain the

capacity to dedifferentiate and may be released, thereby re-entering soil populations and contributing to subsequent infection cycles.

The molecular basis of bacteroid regrowth and dedifferentiation remains comparatively underexplored. A recent genome-scale study on bean bacteroids has begun to identify genes required for regrowth from nodules (Knights, Ledermann et al., in preparation). Their findings indicate that dedifferentiation is a phased and tightly regulated process in which symbiotic identity is rapidly lost and genes associated with free-living growth are sequentially reactivated. These include stress response pathways, core metabolic processes, and motility, all of which are downregulated in bacteroids but are essential for re-establishing a free-living lifestyle.

The regulation of metal homeostasis appears to be particularly critical during this transition. For example, iron export systems are required for successful regrowth (Knights, Ledermann et al., in preparation), likely reflecting the need to detoxify excess intracellular iron accumulated during symbiosis in the leghaemoglobin-rich nodule environment.

1.3 Research contexts and aims

The rhizobium-legume symbiosis represents a highly specialised metabolic interaction that requires tight coordination between bacterial and plant processes to sustain efficient nitrogen fixation. As outlined above, this coordination depends on the integration of carbon and nitrogen metabolism, adaptation to fluctuating environmental conditions, and precise regulatory control across distinct life stages. While many aspects of symbiotic development and bacteroid physiology have been well characterised, the regulatory mechanisms linking nutrient availability to metabolic adaptation in *R. leguminosarum* remain incompletely resolved.

In particular, it is unclear how rhizobia prioritise carbon sources in complex environments, how uptake and metabolism of key substrates such as C_4-dicarboxylates are coordinated with broader physiological processes, and how global regulatory systems contribute to adaptation during both free-living growth and symbiosis.

In this thesis therefore my aim was to investigate the integration of metabolic and regulatory networks in *R. leguminosarum*, with a particular focus on carbon utilisation, transport systems, and global regulation. Specifically, this work (i) examines the basis of carbon source hierarchy and carbon catabolite repression, (ii) characterises the role of the dicarboxylate transport system in coordinating transport and physiology, and (iii) explores the contribution of global regulators, mainly DksA, to bacterial adaptation during symbiosis. Together, these studies contribute to a more comprehensive understanding of how rhizobia coordinate metabolism and regulation across their life cycle, and how these processes influence symbiotic performance.

1.4 Thesis Outline

This thesis is structured around three central research chapters (Chapters 2-4), each presented in manuscript format. Although each results chapter is designed to be read independently, including its own introduction, method, and discussion sections, they are conceptually linked. In particular, Chapters 2 and 3 originate from a shared line of investigation and therefore include cross-references where appropriate.

Chapter 2 investigates the basis of carbon source hierarchy in *Rhizobium leguminosarum*, focussing on the mechanisms underlying carbon catabolite repression and the preferential utilisation of C_4-dicarboxylates.

Chapter 3 further explores this theme by examining the role of the dicarboxylate transport system in coordinating substrate uptake with broader physiological responses.

Chapter 4 expands the scope to global regulatory processes, investigating the role of the three DksA homologues in mediating bacterial adaptation during free-living growth and symbiosis.

The result chapters are framed by a general introduction (Chapter 1) and a general discussion and outlook (Chapter 5).

Chapter 1 provides the broader biological context, outlining the motivation for this work and introducing key aspects of the rhizobial life cycle relevant to the studies presented.

Chapter 5 concludes the thesis by synthesising the main findings, discussing their implications, and outlining directions for future research.

Figures and tables are labelled according to their respective chapter numbers to integrate the individual chapters into a coherent body of work.

References

Angus, A. A., Lee, A., Lum, M. R., Shehayeb, M., Hessabi, R., Fujishige, N. A., Yerrapragada, S., Kano, S., Song, N., Yang, P., Estrada De Los Santos, P., De Faria, S. M., Dakora, F. D., Weinstock, G., & Hirsch, A. M. (2013). Nodulation and effective nitrogen fixation of Macroptilium atropurpureum (siratro) by Burkholderia tuberum, a nodulating and plant growth promoting beta-proteobacterium, are influenced by environmental factors. *Plant and Soil*, *369*(1–2), 543–562. https://doi.org/10.1007/s11104-013-1590-7

Aroney, S. T. N., Pini, F., Kessler, C., Poole, P. S., & Sánchez-Cañizares, C. (2024). The motility and chemosensory systems of Rhizobium leguminosarum , their role in symbiosis, and link to PTS^{NTR} regulation. *Environmental Microbiology*, *26*(2), e16570. https://doi.org/10.1111/1462-2920.16570

Batzenschlager, M., Lace, B., Zhang, N., Su, C., Boiger, A., Egli, S., Krohn, P., Salfeld, J., Ditengou, F. A., Laux, T., & Ott, T. (2025). Competence for transcellular infection in the root cortex involves a post-replicative, cell-cycle exit decision in Medicago truncatula. *eLife*, *12*, RP88588. https://doi.org/10.7554/eLife.88588.3

Bennett, A. E., & Groten, K. (2022). The costs and benefits of plant–arbuscular mycorrhizal fungal interactions. *Annual Review of Plant Biology*, *73*(1), 649–672. https://doi.org/10.1146/annurev-arplant-102820-124504

Brear, E. M., Day, D. A., & Smith, P. M. C. (2013). Iron: An essential micronutrient for the legume-rhizobium symbiosis. *Frontiers in Plant Science*, *4*. https://doi.org/10.3389/fpls.2013.00359

Brewin, N. J. (2004). Plant cell wall remodelling in the rhizobium–legume symbiosis. *Critical Reviews in Plant Sciences*, *23*(4), 293–316. https://doi.org/10.1080/07352680490480734

Brundrett, M. C. (2002). Coevolution of roots and mycorrhizas of land plants. *New Phytologist*, *154*(2), 275–304. https://doi.org/10.1046/j.1469-8137.2002.00397.x

Calderón-Flores, A., Du Pont, G., Huerta-Saquero, A., Merchant-Larios, H., Servín-González, L., & Durán, S. (2005). The stringent response is required for amino acid and nitrate utilization, nod factor regulation, nodulation, and nitrogen fixation in Rhizobium etli. *Journal of Bacteriology*, *187*(15), 5075–5083. https://doi.org/10.1128/JB.187.15.5075-5083.2005

Chaintreuil, C., Arrighi, J., Giraud, E., Miché, L., Moulin, L., Dreyfus, B., Munive-Hernández, J., Villegas-Hernandez, M. D. C., & Béna, G. (2013). Evolution of symbiosis in the legume genus Aeschynomene. *New Phytologist*, *200*(4), 1247–1259. https://doi.org/10.1111/nph.12424

Checcucci, A., DiCenzo, G. C., Bazzicalupo, M., & Mengoni, A. (2017). Trade, diplomacy, and warfare: The quest for elite rhizobia inoculant strains. *Frontiers in Microbiology*, *8*, 2207. https://doi.org/10.3389/fmicb.2017.02207

De Faria, S. M., Ringelberg, J. J., Gross, E., Koenen, E. J. M., Cardoso, D., Ametsitsi, G. K. D., Akomatey, J., Maluk, M., Tak, N., Gehlot, H. S., Wright, K. M., Teaumroong, N., Songwattana, P., De Lima, H. C., Prin, Y., Zartman, C. E., Sprent, J. I., Ardley, J., Hughes, C. E., & James, E. K. (2022). The innovation of the symbiosome has enhanced the evolutionary stability of nitrogen fixation in legumes. *New Phytologist*, *235*(6), 2365–2377. https://doi.org/10.1111/nph.18321

Delaux, P.-M., Radhakrishnan, G., & Oldroyd, G. (2015). Tracing the evolutionary path to nitrogen-fixing crops. *Current Opinion in Plant Biology*, *26*, 95–99. https://doi.org/10.1016/j.pbi.2015.06.003

Dixon, R., & Kahn, D. (2004). Genetic regulation of biological nitrogen fixation. *Nature Reviews Microbiology*, *2*(8), 621–631. https://doi.org/10.1038/nrmicro954

Downie, J. A., & Kondorosi, E. (2021). Why should nodule cysteine-rich (NCR) peptides be absent from nodules of some groups of legumes but essential for symbiotic N-fixation in others? *Frontiers in Agronomy*, *3*, 654576. https://doi.org/10.3389/fagro.2021.654576

Elliott, G. N., Chou, J., Chen, W., Bloemberg, G. V., Bontemps, C., Martínez-Romero, E., Velázquez, E., Young, J. P. W., Sprent, J. I., & James, E. K. (2009). Burkholderia spp. are the most competitive symbionts of Mimosa, particularly under N-limited conditions. *Environmental Microbiology*, *11*(4), 762–778. https://doi.org/10.1111/j.1462-2920.2008.01799.x

FAO. (2025). *Sustainable nitrogen management in agrifood systems*. Rome. https://doi.org/10.4060/cd3388en

Fowler, D., Coyle, M., Skiba, U., Sutton, M. A., Cape, J. N., Reis, S., Sheppard, L. J., Jenkins, A., Grizzetti, B., Galloway, J. N., Vitousek, P., Leach, A., Bouwman, A. F., Butterbach-Bahl, K., Dentener, F., Stevenson, D., Amann, M., & Voss, M. (2013). The global nitrogen cycle in the twenty-first century. *Philosophical Transactions of the Royal Society B: Biological Sciences*, *368*(1621), 20130164. https://doi.org/10.1098/rstb.2013.0164

Frey, S. D., & Blum, L. K. (1994). Effect of pH on competition for nodule occupancy by type I and type II strains of Rhizobium leguminosarum bv. phaseoli. *Plant and Soil*, *163*(2), 157–164. https://doi.org/10.1007/BF00007964

Fry, J., Wood, M., & Poole, P. S. (2001). Investigation of *myo*-inositol catabolism in Rhizobium leguminosarum bv. viciae and its effect on nodulation competitiveness. *Molecular Plant-Microbe Interactions*, *14*(8), 1016–1025. https://doi.org/10.1094/MPMI.2001.14.8.1016

Gage, D. J. (2002). Analysis of infection thread development using Gfp- and DsRed-expressing Sinorhizobium meliloti. *Journal of Bacteriology*, *184*(24), 7042–7046. https://doi.org/10.1128/JB.184.24.7042-7046.2002

Gao, J.-P., Liang, W., Liu, C.-W., Xie, F., & Murray, J. D. (2024). Unraveling the rhizobial infection thread. *Journal of Experimental Botany*, *75*(8), 2235–2245. https://doi.org/10.1093/jxb/erae017

Geurts, R., & Bisseling, T. (2002). *Rhizobium* Nod Factor Perception and Signalling. *The Plant Cell*, *14*(suppl 1), S239–S249. https://doi.org/10.1105/tpc.002451

Gherbi, H., Markmann, K., Svistoonoff, S., Estevan, J., Autran, D., Giczey, G., Auguy, F., Péret, B., Laplaze, L., Franche, C., Parniske, M., & Bogusz, D. (2008). SymRK defines a common genetic basis for plant root endosymbioses with arbuscular mycorrhiza fungi, rhizobia, and *Frankia* bacteria. *Proceedings of the National Academy of Sciences*, *105*(12), 4928–4932. https://doi.org/10.1073/pnas.0710618105

Ghosh, P. K., & Maiti, T. K. (2016). Structure of extracellular polysaccharides (EPS) produced by rhizobia and their functions in legume–bacteria symbiosis: — A Review. *Achievements in the Life Sciences*, *10*(2), 136–143. https://doi.org/10.1016/j.als.2016.11.003

Green, R. T., East, A. K., Karunakaran, R., Downie, J. A., & Poole, P. S. (2019). Transcriptomic analysis of Rhizobium leguminosarum bacteroids in determinate and indeterminate nodules. *Microbial Genomics*, *5*(2). https://doi.org/10.1099/mgen.0.000254

Griesmann, M., Chang, Y., Liu, X., Song, Y., Haberer, G., Crook, M. B., Billault-Penneteau, B., Lauressergues, D., Keller, J., Imanishi, L., Roswanjaya, Y. P., Kohlen, W., Pujic, P., Battenberg, K., Alloisio, N., Liang, Y., Hilhorst, H., Salgado, M. G., Hocher, V., … Cheng, S. (2018). Phylogenomics reveals multiple losses of nitrogen-fixing root nodule symbiosis. *Science*, *361*(6398), eaat1743. https://doi.org/10.1126/science.aat1743

Hadri, A.-E., Spaink, H. P., Bisseling, T., & Brewin, N. J. (1998). Diversity of root nodulation and rhizobial infection processes. In H. P. Spaink, A. Kondorosi, & P. J. J. Hooykaas (Eds), *The Rhizobiaceae* (pp. 347–360). Springer Netherlands. https://doi.org/10.1007/978-94-011-5060-6_18

Hosie, A. H. F., Allaway, D., Galloway, C. S., Dunsby, H. A., & Poole, P. S. (2002). Rhizobium leguminosarum has a second general amino acid permease with unusually broad substrate specificity and high similarity to branched-chain amino acid transporters (Bra/LIV) of the ABC family. *Journal of Bacteriology*, *184*(15), 4071–4080. https://doi.org/10.1128/JB.184.15.4071-4080.2002

Imlay, J. A. (2006). Iron-sulphur clusters and the problem with oxygen. *Molecular Microbiology*, *59*(4), 1073–1082. https://doi.org/10.1111/j.1365-2958.2006.05028.x

Intergovernmental Panel on Climate Change (IPCC). (2023). *Climate Change 2022 – Impacts, Adaptation and Vulnerability: Working Group II Contribution to the Sixth Assessment Report of the Intergovernmental Panel on Climate Change*. Cambridge University Press. https://doi.org/10.1017/9781009325844

Iyer, B., Rajput, M. S., Jog, R., Joshi, E., Bharwad, K., & Rajkumar, S. (2016). Organic acid mediated repression of sugar utilization in rhizobia. *Microbiological Research*, *192*, 211–220. https://doi.org/10.1016/j.micres.2016.07.006

Kazmierczak, T., Yang, L., Boncompagni, E., Meilhoc, E., Frugier, F., Frendo, P., Bruand, C., Gruber, V., & Brouquisse, R. (2020). Chapter Seven—Legume nodule senescence: A coordinated death mechanism between bacteria and plant cells. In P. Frendo, F. Frugier, & C. Masson-Boivin (Eds), *Regulation of Nitrogen-Fixing Symbioses in Legumes* (Vol. 94, pp. 181–212). Academic Press. https://doi.org/https://doi.org/10.1016/bs.abr.2019.09.013

King, B. J., Hunt, S., Weagle, G. E., Walsh, K. B., Pottier, R. H., Canvin, D. T., & Layzell, D. B. (1988). Regulation of O_2 concentration in soybean nodules observed by *in situ* spectroscopic measurement of leghemoglobin oxygenation. *Plant Physiology*, *87*(2), 296–299. https://doi.org/10.1104/pp.87.2.296

Knights, H. E., Jorrin, B., Haskett, T. L., & Poole, P. S. (2021). Deciphering bacterial mechanisms of root colonization. *Environmental Microbiology Reports*, *13*(4), 428–444. https://doi.org/10.1111/1758-2229.12934

Knights, H. E., Ledermann, R., Jorrin, B., Abreu, I., Campbell, M. J., Cocker, C. R., Dolliver, J., East, A. K., Hague, K., Maurer, A.-K., Palomero-Gómez, M., Prescott, H., Terpolilli, J., Tjahjono, O., Tronca, M. N., Underwood, T. J., & Poole, P. S. (in preparation). *Mechanisms behind nodule infection and bacteroid dedifferentiation in Rhizobium leguminosarum* [Unpublished manuscript].

Kumar, N., Lad, G., Giuntini, E., Kaye, M. E., Udomwong, P., Shamsani, N. J., Young, J. P. W., & Bailly, X. (2015). Bacterial genospecies that are not ecologically coherent: Population genomics of Rhizobium leguminosarum. *Open Biology*, *5*(1), 140133. https://doi.org/10.1098/rsob.140133

Lawlor, D. W., Lemaire, G., & Gastal, F. (2001). Nitrogen, plant growth and crop yield. In P. J. Lea & J.-F. Morot-Gaudry (Eds), *Plant Nitrogen* (pp. 343–367). Springer Berlin Heidelberg. https://doi.org/10.1007/978-3-662-04064-5_13

LeBauer, D. S., & Treseder, K. K. (2008). Nitrogen limitation of net primary productivity in terrestrial ecosystems is globally distributed. *Ecology*, *89*(2), 371–379. https://doi.org/10.1890/06-2057.1

Ledermann, R., Bartsch, I., Müller, B., Wülser, J., & Fischer, H.-M. (2018). A functional general stress response of Bradyrhizobium diazoefficiens is required for early stages of host plant infection. *Molecular Plant-Microbe Interactions*, *31*(5), 537–547. https://doi.org/10.1094/MPMI-11-17-0284-R

Ledermann, R., Schulte, C. C. M., & Poole, P. S. (2021). How rhizobia adapt to the nodule environment. *Journal of Bacteriology*, *203*(12). https://doi.org/10.1128/JB.00539-20

Ling, J., Wang, H., Wu, P., Li, T., Tang, Y., Naseer, N., Zheng, H., Masson-Boivin, C., Zhong, Z., & Zhu, J. (2016). Plant nodulation inducers enhance horizontal gene transfer of Azorhizobium caulinodans symbiosis island. *Proceedings of the National Academy of Sciences*, *113*(48), 13875–13880. https://doi.org/10.1073/pnas.1615121113

Liu, H. (2013). *Ammonia synthesis catalysts: Innovation and practice*. World Scientific.

Lodwig, E. M., Hosie, A. H. F., Bourdès, A., Findlay, K., Allaway, D., Karunakaran, R., Downie, J. A., & Poole, P. S. (2003). Amino-acid cycling drives nitrogen fixation in the legume–Rhizobium symbiosis. *Nature*, *422*(6933), 722–726. https://doi.org/10.1038/nature01527

Long, S. R. (1996). Rhizobium symbiosis: Nod factors in perspective. *The Plant Cell*, *8*(10), 1885–1898. https://doi.org/10.1105/tpc.8.10.1885

Mandal, N. C., & Chakrabartty, P. K. (1993). Succinate-mediated catabolite repression of enzymes of glucose metabolism in root-nodule bacteria. *Current Microbiology*, *26*(5), 247–251. https://doi.org/10.1007/BF01575912

Maróti, G., & Kondorosi, Ã. (2014). Nitrogen-fixing rhizobium-legume symbiosis: Are polyploidy and host peptide-governed symbiont differentiation general principles of endosymbiosis? *Frontiers in Microbiology*, *5*. https://doi.org/10.3389/fmicb.2014.00326

Masson-Boivin, C., Giraud, E., Perret, X., & Batut, J. (2009). Establishing nitrogen-fixing symbiosis with legumes: How many rhizobium recipes? *Trends in Microbiology*, *17*(10), 458–466. https://doi.org/10.1016/j.tim.2009.07.004

Mauchline, T. H., Fowler, J. E., East, A. K., Sartor, A. L., Zaheer, R., Hosie, A. H. F., Poole, P. S., & Finan, T. M. (2006). Mapping the Sinorhizobium meliloti 1021 solute-binding protein-dependent transportome. *Proceedings of the National Academy of Sciences*, *103*(47), 17933–17938. https://doi.org/10.1073/pnas.0606673103

Mendoza-Suárez, M., Andersen, S. U., Poole, P. S., & Sánchez-Cañizares, C. (2021). Competition, nodule occupancy, and persistence of inoculant strains: Key factors in the rhizobium-legume symbioses. *Frontiers in Plant Science*, *12*, 690567. https://doi.org/10.3389/fpls.2021.690567

Mergaert, P., Uchiumi, T., Alunni, B., Evanno, G., Cheron, A., Catrice, O., Mausset, A.-E., Barloy-Hubler, F., Galibert, F., Kondorosi, A., & Kondorosi, E. (2006). Eukaryotic control on bacterial cell cycle and differentiation in the Rhizobium –legume symbiosis. *Proceedings of the National Academy of Sciences*, *103*(13), 5230–5235. https://doi.org/10.1073/pnas.0600912103

Minchin, F. R. (1997). Regulation of oxygen diffusion in legume nodules. *Soil Biology and Biochemistry*, *29*(5–6), 881–888. https://doi.org/10.1016/S0038-0717(96)00204-0

Mitsch, M. J., diCenzo, G. C., Cowie, A., & Finan, T. M. (2018). Succinate transport is not essential for symbiotic nitrogen fixation by Sinorhizobium meliloti or Rhizobium leguminosarum. *Applied and Environmental Microbiology*, *84*(1), e01561-17. https://doi.org/10.1128/AEM.01561-17

Mulley, G., White, J. P., Karunakaran, R., Prell, J., Bourdes, A., Bunnewell, S., Hill, L., & Poole, P. S. (2011). Mutation of GOGAT prevents pea bacteroid formation and N2 fixation by globally downregulating transport of organic nitrogen sources. *Molecular Microbiology*, *80*(1), 149–167. https://doi.org/10.1111/j.1365-2958.2011.07565.x

Oldroyd, G. E. D., Murray, J. D., Poole, P. S., & Downie, J. A. (2011). The rules of engagement in the legume-rhizobial symbiosis. *Annual Review of Genetics*, *45*(1), 119–144. https://doi.org/10.1146/annurev-genet-110410-132549

Peoples, M. B., Herridge, D. F., & Ladha, J. K. (1995). Biological nitrogen fixation: An efficient source of nitrogen for sustainable agricultural production? *Plant and Soil*, *174*(1–2), 3–28. https://doi.org/10.1007/BF00032239

Perry, B. J., Akter, M. S., & Yost, C. K. (2016). The use of transposon insertion sequencing to interrogate the core functional genome of the legume symbiont Rhizobium leguminosarum. *Frontiers in Microbiology*, *7*. https://doi.org/10.3389/fmicb.2016.01873

Perry, B. J., & Yost, C. K. (2014). Construction of a mariner-based transposon vector for use in insertion sequence mutagenesis in selected members of the Rhizobiaceae. *BMC Microbiology*, *14*(1), 298. https://doi.org/10.1186/s12866-014-0298-z

Pini, F., East, A. K., Appia-Ayme, C., Tomek, J., Karunakaran, R., Mendoza-Suárez, M., Edwards, A., Terpolilli, J. J., Roworth, J., Downie, J. A., & Poole, P. S. (2017). Bacterial biosensors for in vivo spatiotemporal mapping of root secretion. *Plant Physiology*, *174*(3), 1289–1306. https://doi.org/10.1104/pp.16.01302

Poole, P., & Allaway, D. (2000). Carbon and nitrogen metabolism in Rhizobium. In *Advances in Microbial Physiology* (Vol. 43, pp. 117–163). Elsevier. https://doi.org/10.1016/S0065-2911(00)43004-3

Poole, P., Ramachandran, V., & Terpolilli, J. (2018). Rhizobia: From saprophytes to endosymbionts. *Nature Reviews Microbiology*, *16*(5), 291–303. https://doi.org/10.1038/nrmicro.2017.171

Preisig, O., Zufferey, R., Thöny-Meyer, L., Appleby, C. A., & Hennecke, H. (1996). A high-affinity cbb3-type cytochrome oxidase terminates the symbiosis-specific respiratory chain of Bradyrhizobium japonicum. *Journal of Bacteriology*, *178*(6), 1532–1538. https://doi.org/10.1128/jb.178.6.1532-1538.1996

Prell, J., Mulley, G., Haufe, F., White, J. P., Williams, A., Karunakaran, R., Downie, J. A., & Poole, P. S. (2012). The PTS^{Ntr} system globally regulates ATP-dependent transporters in Rhizobium leguminosarum: Global regulation by PTS in R. leguminosarum. *Molecular Microbiology*, *84*(1), 117–129. https://doi.org/10.1111/j.1365-2958.2012.08014.x

Prell, J., & Poole, P. (2006). Metabolic changes of rhizobia in legume nodules. *Trends in Microbiology*, *14*(4), 161–168. https://doi.org/10.1016/j.tim.2006.02.005

Prell, J., White, J. P., Bourdes, A., Bunnewell, S., Bongaerts, R. J., & Poole, P. S. (2009). Legumes regulate Rhizobium bacteroid development and persistence by the supply of branched-chain amino acids. *Proceedings of the National Academy of Sciences*, *106*(30), 12477–12482. https://doi.org/10.1073/pnas.0903653106

Quilbé, J., Montiel, J., Arrighi, J.-F., & Stougaard, J. (2022). Molecular mechanisms of intercellular rhizobial infection: Novel findings of an ancient process. *Frontiers in Plant Science*, *13*, 922982. https://doi.org/10.3389/fpls.2022.922982

Radhakrishnan, G. V., Keller, J., Rich, M. K., Vernié, T., Mbadinga Mbadinga, D. L., Vigneron, N., Cottret, L., Clemente, H. S., Libourel, C., Cheema, J., Linde, A.-M., Eklund, D. M., Cheng, S., Wong, G. K. S., Lagercrantz, U., Li, F.-W., Oldroyd, G. E. D., & Delaux, P.-M. (2020). An ancestral signalling pathway is conserved in intracellular symbioses-forming plant lineages. *Nature Plants*, *6*(3), 280–289. https://doi.org/10.1038/s41477-020-0613-7

Ramachandran, V. K., East, A. K., Karunakaran, R., Downie, J. A., & Poole, P. S. (2011). Adaptation of Rhizobium leguminosarum to pea, alfalfa and sugar beet rhizospheres investigated by comparative transcriptomics. *Genome Biology*, *12*(10), R106. https://doi.org/10.1186/gb-2011-12-10-r106

Rockström, J., Donges, J. F., Fetzer, I., Martin, M. A., Wang-Erlandsson, L., & Richardson, K. (2024). Planetary boundaries guide humanity's future on Earth. *Nature Reviews Earth & Environment*, *5*(11), 773–788. https://doi.org/10.1038/s43017-024-00597-z

Ronson, C. W., Lyttleton, P., & Robertson, J. G. (1981). C_4-dicarboxylate transport mutants of Rhizobium trifolii form ineffective nodules on Trifolium repens. *Proceedings of the*

National Academy of Sciences, *78*(7), 4284–4288. https://doi.org/10.1073/pnas.78.7.4284

Rutten, P. J., & Poole, P. S. (2019). Oxygen regulatory mechanisms of nitrogen fixation in rhizobia. In *Advances in Microbial Physiology* (Vol. 75, pp. 325–389). Elsevier. https://doi.org/10.1016/bs.ampbs.2019.08.001

Rutten, P. J., Steel, H., Hood, G. A., Ramachandran, V. K., McMurtry, L., Geddes, B., Papachristodoulou, A., & Poole, P. S. (2021). Multiple sensors provide spatiotemporal oxygen regulation of gene expression in a rhizobium-legume symbiosis. *PLOS Genetics*, *17*(2), e1009099. https://doi.org/10.1371/journal.pgen.1009099

Salas, M. E., Lozano, M. J., López, J. L., Draghi, W. O., Serrania, J., Torres Tejerizo, G. A., Albicoro, F. J., Nilsson, J. F., Pistorio, M., Del Papa, M. F., Parisi, G., Becker, A., & Lagares, A. (2017). Specificity traits consistent with legume-rhizobia coevolution displayed by Ensifer meliloti rhizosphere colonization. *Environmental Microbiology*, *19*(9), 3423–3438. https://doi.org/10.1111/1462-2920.13820

Sánchez-Cañizares, C., Ledermann, R., McKenna, J., Underwood, T. J., Mendoza-Suárez, M., Green, R., Ramakrishnan, K., East, A. K., Webb, I., Kirchhelle, C., Jorrín, B., Saalbach, G., James, E. K., Moreira-Leite, F., Terpolilli, J., & Poole, P. S. (2026). Developmental fates and N2-fixing efficiency of terminally-differentiated versus undifferentiated bacteroids from legume nodules. *Plant Physiology*, *200*(3), kiaf613. https://doi.org/10.1093/plphys/kiaf613

Sánchez-Cañizares, C., Prell, J., Pini, F., Rutten, P., Kraxner, K., Wynands, B., Karunakaran, R., & Poole, P. S. (2020). Global control of bacterial nitrogen and carbon metabolism by a PTS^{Ntr} -regulated switch. *Proceedings of the National Academy of Sciences*, *117*(19), 10234–10245. https://doi.org/10.1073/pnas.1917471117

Schulte, C. C. M., Borah, K., Wheatley, R. M., Terpolilli, J. J., Saalbach, G., Crang, N., De Groot, D. H., Ratcliffe, R. G., Kruger, N. J., Papachristodoulou, A., & Poole, P. S. (2021). Metabolic control of nitrogen fixation in rhizobium-legume symbioses. *Science Advances*, *7*(31), eabh2433. https://doi.org/10.1126/sciadv.abh2433

Soltis, D. E., Soltis, P. S., Morgan, D. R., Swensen, S. M., Mullin, B. C., Dowd, J. M., & Martin, P. G. (1995). Chloroplast gene sequence data suggest a single origin of the predisposition for symbiotic nitrogen fixation in angiosperms. *Proceedings of the National Academy of Sciences*, *92*(7), 2647–2651. https://doi.org/10.1073/pnas.92.7.2647

Sprent, J. I., Ardley, J., & James, E. K. (2017). Biogeography of nodulated legumes and their nitrogen-fixing symbionts. *New Phytologist*, *215*(1), 40–56. https://doi.org/10.1111/nph.14474

Sterner, R. W., & Elser, J. J. (2003). *Ecological Stoichiometry: The Biology of Elements from Molecules to the Biosphere*. Princeton University Press. https://doi.org/10.1515/9781400885695

Taté, R., Riccio, A., Merrick, M., & Patriarca, E. J. (1998). The Rhizobium etli amtB gene coding for an NH_4^+ transporter is down-regulated early during bacteroid differentiation. *Molecular Plant-Microbe Interactions*, *11*(3), 188–198. https://doi.org/10.1094/MPMI.1998.11.3.188

Tian, H., Bian, Z., Shi, H., Qin, X., Pan, N., Lu, C., Pan, S., Tubiello, F. N., Chang, J., Conchedda, G., Liu, J., Mueller, N., Nishina, K., Xu, R., Yang, J., You, L., & Zhang, B. (2022). History of anthropogenic nitrogen inputs (HaNi) to the terrestrial biosphere: A 5 arcmin resolution annual dataset from 1860 to 2019. *Earth System Science Data*, *14*(10), 4551–4568. https://doi.org/10.5194/essd-14-4551-2022

Tjahjono, O. (2025). *Regulation of global metabolism by PTS-NTR in Rhizobium leguminosarum*. PhD thesis, University of Oxford.

Tkacz, A., Cheema, J., Chandra, G., Grant, A., & Poole, P. S. (2015). Stability and succession of the rhizosphere microbiota depends upon plant type and soil composition. *The ISME Journal*, *9*(11), 2349–2359. https://doi.org/10.1038/ismej.2015.41

Turner, T. R., Ramakrishnan, K., Walshaw, J., Heavens, D., Alston, M., Swarbreck, D., Osbourn, A., Grant, A., & Poole, P. S. (2013). Comparative metatranscriptomics reveals kingdom level changes in the rhizosphere microbiome of plants. *The ISME Journal*, *7*(12), 2248–2258. https://doi.org/10.1038/ismej.2013.119

Udvardi, M., & Poole, P. S. (2013). Transport and metabolism in legume-rhizobia symbioses. *Annual Review of Plant Biology*, *64*(1), 781–805. https://doi.org/10.1146/annurev-arplant-050312-120235

Van De Velde, W., Zehirov, G., Szatmari, A., Debreczeny, M., Ishihara, H., Kevei, Z., Farkas, A., Mikulass, K., Nagy, A., Tiricz, H., Satiat-Jeunemaître, B., Alunni, B., Bourge, M., Kucho, K., Abe, M., Kereszt, A., Maroti, G., Uchiumi, T., Kondorosi, E., & Mergaert, P. (2010). Plant peptides govern terminal differentiation of bacteria in symbiosis. *Science*, *327*(5969), 1122–1126. https://doi.org/10.1126/science.1184057

Walshaw, D. L., & Poole, P. S. (1996). The general L-amino acid permease of Rhizobium leguminosarum is an ABC uptake system that also influences efflux of solutes. *Molecular Microbiology*, *21*(6), 1239–1252. https://doi.org/10.1046/j.1365-2958.1996.00078.x

Wheatley, R. M., Ford, B. L., Li, L., Aroney, S. T. N., Knights, H. E., Ledermann, R., East, A. K., Ramachandran, V. K., & Poole, P. S. (2020). Lifestyle adaptations of Rhizobium from

rhizosphere to symbiosis. *Proceedings of the National Academy of Sciences*, *117*(38), 23823–23834. https://doi.org/10.1073/pnas.2009094117

Wheatley, R. M., Ramachandran, V. K., Geddes, B. A., Perry, B. J., Yost, C. K., & Poole, P. S. (2017). Role of O_2 in the growth of Rhizobium leguminosarum bv. viciae 3841 on glucose and succinate. *Journal of Bacteriology*, *199*(1). https://doi.org/10.1128/JB.00572-16

Young, J. P. W., Jorrin, B., Moeskjær, S., & James, E. K. (2023). Rhizobium brockwellii sp. nov., Rhizobium johnstonii sp. nov. And Rhizobium beringeri sp. nov., three genospecies within the Rhizobium leguminosarum species complex. *International Journal of Systematic and Evolutionary Microbiology*, *73*(7). https://doi.org/10.1099/ijsem.0.005979

Zhang, X., Davidson, E. A., Zou, T., Lassaletta, L., Quan, Z., Li, T., & Zhang, W. (2020). Quantifying nutrient budgets for sustainable nutrient management. *Global Biogeochemical Cycles*, *34*(3), e2018GB006060. https://doi.org/https://doi.org/10.1029/2018GB006060

2

Carbon catabolite repression prioritizes C_4 - dicarboxylates by selectively repressing transport of alternative carbon sources

Chapter 2

This thesis chapter is presented in the form of a completed manuscript intended for publication. Minor formatting modifications, along with additional background information, have been included to ensure that it conforms to the format of a thesis.

Carbon catabolite repression prioritizes C_4-dicarboxylates by selectively repressing transport of alternative carbon sources

Ann-Kathrin Maurer[1], Raphael Ledermann[1], Philip Poole[1]

[1] Department of Biology, University of Oxford, Oxford, UK

Abstract

Rhizobium leguminosarum, a symbiotic nitrogen-fixing bacterium, prioritizes succinate and related C_4-dicarboxylates by exerting carbon catabolite repression (CCR) upon multiple ABC transporter operons encoding uptake systems for less preferred carbon sources, including glucose, fructose, xylose, sucrose, mannitol, erythritol, and inositol. However, the mechanisms underlying CCR in rhizobia remain poorly resolved. In a luminescence-based genetic screen designed to identify strains impaired in their succinate-mediated CCR, we predominantly isolated mutants impaired in the Dct system, the dedicated C_4-dicarboxylate transport system, indicating that C_4-dicarboxylate uptake is required to generate the CCR signal. To separate Dct-specific signalling from transport, we replaced the native C_4-dicarboxylate permease with a distantly related malate transporter, which restored repression, supporting a model in which intracellular C_4-dicarboxylate availability, rather than Dct-specific sensing, triggers CCR. Focusing on the inositol system as a mechanistic example, we show that repression primarily targets the transport operon *intABC*, whose expression is governed by the transcriptional repressor IolR and additional post-transcriptional regulation. This is consistent with inducer-exclusion, whereby blocked uptake prevents inducer accumulation and sustains regulon-wide repression. Together, these findings establish that intracellular C_4-dicarboxylate availability underlies rhizobial CCR, which is executed primarily through selective repression of competing uptake systems.

KEYWORDS Carbon catabolite repression, C_4-dicarboxylates, inducer exclusion, ABC transporters, rhizobia, inositol.

Introduction

Rhizobium leguminosarum, a soil-dwelling α-proteobacteria belonging to the rhizobia, establishes nitrogen-fixing symbiosis with legumes and represents a cornerstone of agro-environmental sustainability. This family of bacteria transitions between heterogenous bulk soil and the plant root environment, where they encounter significant shifts in nutrient availability and must compete with other microorganisms for root colonization (Wheatley et al., 2020). The rhizosphere, enriched by plant root exudates, is a nutrient-rich yet selective environment. To thrive in this chemically complex environment (Bertin et al., 2003; Pini et al., 2017), rhizobia encode an extensive repertoire of transport systems, including approximately 170 ATP-binding cassette (ABC) transporters, compared to 47 in *Escherichia coli* (Mauchline et al., 2006). This diversity is thought to have evolved in response to the nutritional complexity, enabling rhizobia to access a broader spectrum of nutrients found in the soil and rhizosphere (Prell & Poole, 2006).

Among available substrates, C_4-dicarboxylic acids play a prominent role in both free-living and symbiotic states. C_4-dicarboxylates such as succinate, malate, and fumarate are the primary, if not sole, carbon sources that fuel nitrogen fixation in bacteroids (Arwas et al., 1985; Finan et al., 1983; Glenn & Brewin, 1981; Mitsch et al., 2018; Ronson et al., 1981) and are preferentially utilized by free-living rhizobia over many sugars and alternative substrates (Mandal & Chakrabartty, 1993). This preference manifests as hierarchical carbon utilization, typically governed by carbon catabolite repression (CCR). CCR enables rhizobia to selectively assimilate C_4-dicarboxylates from complex substrate mixtures by downregulating cellular processes linked to utilization of secondary carbon sources. Consistent with this hierarchy, Bringhurst & Gage (2002) showed that in *Sinorhizobium meliloti*, intracellular accumulation of secondary carbon sources, lactose and raffinose, is prevented in the presence of succinate in a process referred to as inducer exclusion. Similarly, in *R. leguminosarum*, catabolism of the secondary carbon source *myo*-inositol is strongly reduced in the presence of C_4-dicarboxylates (Poole et al., 1994). Although well documented in various *Rhizobium* sp., the according molecular basis by which C_4-dicarboxylates enforce repression of alternative carbon sources in rhizobia is poorly understood.

The classical example of CCR is the preferential use of glucose over lactose in *E. coli*, first described by Monod (1942) as diauxic growth and later formalized under the broader concept of 'catabolite repression' (Magasanik, 1961). Although CCR is often portrayed as a canonical regulatory module, its mechanistic basis is highly diverse and often lineage-specific. Presently, two major types of CCR mechanisms have been described: (i) preference for glucose by Enterobacteriaceae (e.g. *E. coli*) and Bacillota (e.g. *Bacillus subtilis*), mediated through the phosphorylation state of phosphotransferase system (PTS) components; and (ii) preferential utilization of organic acids in pseudomonads, mediated primarily through the posttranscriptional regulators Hfq and Crc (all reviewed in Sonnleitner (2025)).

The mechanism of CCR in *E. coli* and *B. subtilis* are among the best studied. Although they differ notably in regulatory architecture, both systems rely on the phosphorylation state of key PTS proteins to reflect the physiological state of the cell, and pathways for less preferred carbon sources are generally transcriptionally activated only after depletion of glucose (Deutscher, 2008; Görke & Stülke, 2008; Nair & Sarma, 2021).

In contrast, for several other bacterial species, including *Rhizobium* (Ucker & Signer, 1978), *Pseudomonas aeruginosa* (Sonnleitner et al., 2018), *Streptomyces* (Świątek et al., 2012), *Streptococcus* (Van Den Bogaard et al., 2000), and *Bifidobacterium* (Parche et al., 2006), glucose serves only as a secondary carbon source, and instead other substrates are preferentially assimilated. To highlight the inverted hierarchy, this is occasionally referred to as 'reverse CCR'.

This type of CCR is mainly described for *Pseudomonas*, where regulation occurs through post-transcriptional repression of target genes via the RNA chaperone Hfq and its corepressor Crc (catabolite repression control protein). Upon depletion of preferred substrates such as succinate, repression is relieved by the regulatory RNA CrcZ which sequesters Hfq (Bharwad & Rajkumar, 2019; Sonnleitner et al., 2018).

Together, these examples illustrate that CCR is not mechanistically uniform across bacteria. Numerous taxa lack the hallmark regulators identified in enteric models, and even when homologous components exist, regulatory wiring and physiological roles can differ substantially. In rhizobia, for instance, homologues of the PTS system and the RNA

chaperone Hfq have been implicated in carbon regulation (García-Tomsig et al., 2022; Pinedo et al., 2008; Sánchez-Cañizares et al., 2020), yet their reported roles do not conform to the established CCR models outlined above. Additional regulatory elements have been proposed; for example, Garcia et al. (2010) described a two-component regulatory system encoded by *sma0113-sma0114* that partially relieves succinate-mediated repression in *S. meliloti*. However, no clear homologues of this system are present in *R. leguminosarum*, suggesting that CCR mechanisms may differ even among closely related rhizobia.

Thus, despite the ecological importance of C_4-dicarboxylates in rhizobia, we still lack a detailed understanding of how they induce repression of other carbon sources (Iyer et al., 2016). Although individual components have been linked to carbon regulation, no central CCR regulator has been definitively identified in rhizobia. Here, we investigate how carbon hierarchy is established and at which regulatory level repression occurs in *R. leguminosarum*. We first demonstrate that C_4-dicarboxylates are the preferred carbon source in the model strain *Rhizobium leguminosarum* biovar *viciae* 3841 (*Rlv*3841) and quantify repression of alternative substrates using luminescent reporters and visualize diauxic growth. We then employ a genetic approach to identify components required for CCR and, using repression of the inositol pathway as an example, apply targeted regulatory mapping to localize the level at which repression is implemented. Together, this framework defines how C_4-dicarboxylates impose carbon hierarchy in a symbiosis-relevant bacterium adapted to fluctuating nutrient environments.

Material and Methods

Bacterial strains and growth conditions

E. coli strains were grown at 37°C in liquid or solid Luria-Bertani (LB) medium (Sambrook et al., 1989) and *R. leguminosarum* strains were grown at 28°C in either tryptone yeast (TY) complex medium (Beringer, 1974) or universal minimal salts (UMS) minimal medium (Pini et al., 2017). If not stated otherwise, UMS was supplemented with 10 mM NH_4Cl as nitrogen source and 20 mM succinate as carbon source. Antibiotics were added when necessary, at the following final concentrations (μg mL^{-1}): ampicillin (100), gentamicin (10 for *E. coli*; 20 for *R. leguminosarum*), kanamycin (20; for *E. coli*) or neomycin (40; for *R. leguminosarum*), streptomycin (500), spectinomycin (100), and tetracycline (10 for *E. coli*; 1 in liquid and 5 in solid media for *R. leguminosarum*). The bacterial strains and plasmids used in this study are listed in Table 2.1 and Table 2.2.

Table 2.1 Strains used in this study.

Strains	Relevant phenotype and genotype	Reference or Source
Escherichia coli		
DH5α	*supE44 ΔlacU169* (ϕ80 *lacZ*ΔM15) *hsdR17 recA1 gyrA96 thi-1 relA2*	Hanahan, 1983
ST18	Sm^r Sp^r *pro thi hsdR* chromosome::RP4-2 Tc::Mu-Kan::Tn7/ λ*pir* Δ*hemA*	Thoma & Schobert, 2009
Rhizobium leguminosarum		
3841	Sm^r derivative of *R. leguminosarum* bv. *viciae* strain 300; in this study referred to as wild-type (WT)	Johnston & Beringer, 1975; Glenn et al., 1980
LMB590	Sm^r Tc^r 3841 × pLMB684 [xylose biosensor]	Pini et al., 2017
LMB592	Sm^r Tc^r 3841 × pLMB686 [*myo*-inositol biosensor]	Pini et al., 2017
LMB593	Sm^r Tc^r 3841 × pLMB687 [sucrose biosensor]	Pini et al., 2017
LMB614	Sm^r Tc^r 3841 × pLMB714 [C_4-dicarboxylate biosensor]	Pini et al., 2017
LMB617	Sm^r Tc^r 3841 × pLMB705 [mannitol biosensor]	Pini et al., 2017
LMB619	Sm^r Tc^r 3841 × pLMB717 [erythritol biosensor]	Pini et al., 2017
LMB622	Sm^r Tc^r 3841 × pLMB725 [glucose biosensor]	A. K. East, unpublished
LMB667	Sm^r Tc^r 3841 × pLMB757 [fructose biosensor]	Pini et al., 2017
OPS3566	Sm^r Tc^r Nm^r *dctA*::Himar1 × pLMB686	this work
OPS3567	Sm^r Tc^r Nm^r *dctA*::Himar1 × pLMB686	this work
OPS3568	Sm^r Tc^r Nm^r *dctA*::Himar1 × pLMB686	this work

OPS3569	Sm^r Tc^r Nm^r *dctB*::Himar1 × pLMB686	this work
OPS3570	Sm^r Tc^r Nm^r *dctB*::Himar1 × pLMB686	this work
OPS3571	Sm^r Tc^r Nm^r *dctB*::Himar1 × pLMB686	this work
OPS3572	Sm^r Tc^r Nm^r *dctB*::Himar1 × pLMB686	this work
OPS3573	Sm^r Tc^r Nm^r *dctB*::Himar1 × pLMB686	this work
OPS3574	Sm^r Tc^r Nm^r *dctB*::Himar1 × pLMB686	this work
OPS3575	Sm^r Tc^r Nm^r *dctD*::Himar1 × pLMB686	this work
OPS3576	Sm^r Tc^r Nm^r *dctD*::Himar1 × pLMB686	this work
OPS3577	Sm^r Tc^r Nm^r *rpoN*::Himar1 × pLMB686	this work
OPS3578	Sm^r Tc^r Nm^r *iolR*::Himar1 × pLMB686	this work
OPS3601	Sm^r Sp^r Tc^r RU727 × pLMB686	this work
OPS3602	Sm^r Sp^r Tc^r *dctB*::Ω × pLMB686	this work
OPS3603	Sm^r Sp^r Tc^r Δ*dctD*::Ω × pLMB686	this work
OPS3604	Sm^r Sp^r Tc^r Δ*dctABD*::Ω × pLMB686	this work
OPS3605	Sm^r Sp^r Tc^r Δ*dctBD*::Ω × pLMB686	this work
OPS4112	Sm^r Nm^r *iolR*::Himar1	this work
OPS4172	Sm^r Gm^r 3841 Tn*7*::P_{23106}–*gusA*	this work
OPS4173	Sm^r Gm^r 3841 Tn*7*::P_{intA}–5'UTR–*intA*(SP)*–*gusA*	this work
OPS4174	Sm^r Gm^r 3841 Tn*7*::P_{intA} (until TSS)–*gusA*	this work
OPS4175	Sm^r Gm^r 3841 Tn*7*::P_{23106}–*gusA*	this work
OPS4176	Sm^r Gm^r 3841 Tn*7*::P_{iolC}–5'UTR–*gusA*	this work
OPS4177	Sm^r Nm^r Gm^r *iolR*::Himar1 Tn*7*::P_{23106}–*gusA*	this work
OPS4178	Sm^r Nm^r Gm^r *iolR*::Himar1 Tn*7*::P_{intA}–5'UTR–*intA*(SP)*–*gusA*	this work
OPS4179	Sm^r Nm^r Gm^r *iolR*::Himar1 Tn*7*::P_{intA} (until TSS)–*gusA*	this work
OPS4180	Sm^r Nm^r Gm^r *iolR*::Himar1 Tn*7*::P_{23106}–*gusA*	this work
OPS4181	Sm^r Nm^r Gm^r *iolR*::Himar1 Tn*7*::P_{iolC}–5'UTR–*gusA*	this work
OPS4223	Sm^r Gm^r 3841 Tn*7*::P_{intA}–5'UTR–*intA*(SP):*phoA*	this work
OPS4224	Sm^r Gm^r 3841 Tn*7*::J_{23106}–5'UTR–*intA*(SP):*phoA*	this work
OPS4225	Sm^r Nm^r Gm^r *iolR*::Himar1 Tn*7*::P_{intA}–5'UTR–*intA*(SP):*phoA*	this work
OPS4226	Sm^r Nm^r Gm^r *iolR*::Himar1 Tn*7*::J_{23106}–5'UTR–*intA*(SP):*phoA*	this work
OPS4234	Sm^r Sp^r Gm^r Tc^r Δ*dctABD*::Ω × pTH600, pLMB686	this work
OPS4235	Sm^r Sp^r Gm^r Tc^r Δ*dctABD*::Ω × pTH648, pLMB686	this work
OPS4236	Sm^r Sp^r Gm^r Tc^r *dctA*::Ω × pTH600, pLMB686	this work
OPS4237	Sm^r Sp^r Gm^r Tc^r *dctA*::Ω × pTH648, pLMB686	this work
RU711	Sm^r Sp^r Δ*dctD*::Ω	Reid et al., 1996

RU714	Sm^r Sp^r Δ*dctABD*::Ω	Reid et al., 1996
RU727	Sm^r Sp^r *dctA*::Ω	Reid et al., 1996
RU730	Sm^r Sp^r *dctB*::Ω	Reid et al., 1996
RU865	Sm^r Sp^r Δ*dctBD*::Ω	Reid et al., 1996

Gm: gentamicin; Nm: neomycin; Tc: tetracycline; Sm: streptomycin; Sp: spectinomycin; ^{r}: resistance; *intA*(SP): *intA* signal peptide (first 26 codons); * contains extra stop codon

Table 2.2 Plasmids used in this study.

Plasmid	Relevant phenotype and genotype / Description	Reference or Source
pJET1.2/blunt	commercial cloning vector for PCR products	Thermo Fisher
pLMB686	Tc^r (pIJ11268) P_{intA}-*luxCDABE* (*myo*-inositol biosensor)	Pini et al. (2017)
pOPS1850	Ap^r Gm^r (pUC18T-mini-Tn*7*T-Gm) promoterless *gusA* in mTn*7* delivery plasmid for promoter fusions	this work
pOPS2353	Ap^r Gm^r (pOPS1850) P_{J23106}–*gusA* (constitutive *gusA* control)	this work
pOPS2354	Ap^r Gm^r (pOPS1850) P_{intA}–5'UTR–*intA*(SP)*–*gusA*	this work
pOPS2355	Ap^r Gm^r (pOPS1850) P_{intA} (until TSS)–*gusA*	this work
pOPS2356	Ap^r Gm^r (pOPS1850) P_{J23106} – 5'UTR–*intA*(SP)*–*gusA*	this work
pOPS2357	Ap^r Gm^r (pOPS1850) P_{iolC}–5'UTR–*gusA*	this work
pOPS2358	Ap^r Gm^r (pUC18T-mini-Tn*7*T-Gm) P_{intA}–5'UTR–*intA*(SP):*phoA*	this work
pOPS2359	Ap^r Gm^r (pUC18T-mini-Tn*7*T-Gm) J_{23106}–5'UTR–*intA*(SP):*phoA*	this work
pRK2013	Km^r self-transmissible helper plasmid	Ditta et al., (1980)
pTH600	Gm^r (pBBR1mcs-5) P_{dme}-*maeP*	Mitsch et al. (2018)
pTH648	Gm^r (pBBR1mcs-5) P_{dctA}-*maeP*	Mitsch et al. (2018)
pTNS3	Ap^r *oriT oriV* (R6K) *tnsABCD* Tn*7* helper plasmid	Choi et al. (2008)
pUC18T-mini-Tn*7*T-Gm	Ap^r Gm^r *oriT oriV* (ColE1) Tn*7* delivery vector	Choi et al. (2005)

Ap: Ampicillin; Gm: gentamicin; Km: kanamycin; Tc: tetracycline; ^{r}: resistance

intA(SP): *intA* signal peptide (first 26 codons); * contains extra stop codo**n**

Strain construction

All ligations were transformed into chemically competent *E. coli* DH5α or ST18. Plasmids were mobilized into recipient *R. leguminosarum* strains by bi-, tri-, or tetraparental mating using the helper plasmid pRK2013 and the Tn*7* transposase-encoding plasmid pTNS3 when necessary. Transconjugants were restreaked twice on TY with respective antibiotics. For chromosomal Tn*7* integration, transposition events were selected on TY

supplemented with appropriate antibiotics and final strains were verified by PCR using primer pairs oxp2307/oxp3060 and oxp2308/oxp3061 amplifying across the left and right Tn*7* integration sites. All primers are listed in Table S2.1.

Transductions were carried out with the bacteriophage RL38 as previously described (Buchanan-Wollaston, 1979).

Carbon source biosensors

We employed a collection of previously validated strains expressing *lux*-based biosensors (Pini et al., 2017) that are responsive to distinct carbon sources, i.e. erythritol (LMB619), fructose (LMB667), glucose (LMB622), *myo*-inositol (LMB592), mannitol (LMB617), sucrose (LMB593), and xylose (LMB590). To visualize repression of their respective uptake systems in presence of dicarboxylates, the biosensor strains were grown on TY slopes for three days, washed three times in 10 mM $MgCl_2$, and inoculated at OD_{595}=0.01 into 10 mL of liquid UMS or spotted in 15 µL dots onto UMS agar containing 10 mM of its respective inducing substrate with and without 20 mM succinate. Liquid cultures were grown at 28°C overnight and luminescence and absorbance determined in a plate reader (FLUOstar Omega, BMG Labtech) when cultures had reached OD_{595} ~0.5. Agar plates were incubated at 28°C and imaged after three, four, and five days. Luminescence (in counts per second (cps)) was measured using a CCD camera in the NightOWL imaging system (Berthold Technologies). CCD images of light output were exposed for 20 s and photographed under 'low gain' settings. Images were analysed with the imaging software IndiGO (Berthold Technologies), in which settings and background correction were adjusted to each biosensor's intensity and per image.

For strains impaired in their ability to grow on one or more of the tested carbon sources, (i.e. *dct* mutants), plate reader assays were methodologically adapted. Rhizobial strains were grown in TY liquid to exponential phase, washed three times in 10mM $MgCl_2$, and inoculated into 5 mL UMS containing the required carbon sources to an OD_{595} ~ 0.5. Luminescence and OD_{595} were measured using a plate reader after approximately 1.5 h incubation at 28°C.

Diauxic growth curves

A single colony of LMB592 was streaked onto UMS agar slopes and incubated for three days. Cultures were washed twice and inoculated into UMS containing different carbon source combinations to an OD_{595} of 0.05. 400 µl aliquots were incubated in a 24-well plate in a FLUOstar Omega plate reader (BMG Labtech) plate reader at 28°C and 500 rpm, with absorbance and luminescence measured every 30 min. OD_{595} and luminescence values were blank-corrected and averaged across four replicates.

Transport assays

Rhizobia cultures were grown in UMS with 10 mM NH_4Cl and respective carbon sources overnight, washed twice in UMS minus carbon and nitrogen sources, and cells adjusted to OD_{595} of 1 and starved for 2 hours. Each uptake assay contained either 0.125 µCi (4.625 kBq) [1,2-^{3}H(N)]-*myo*-inositol, [^{14}C(U)]-glucose, or [2,3-^{14}C]-succinic acid (ARC Inc.), with a total solute concentration of 25 µM, following previously described protocols (Poole et al., 1985). Five samples of 100 µL were taken at intervals of 1 min, millipore filtered and counted via a scintillation counter (Hidex 300 SL) to calculate rate of transport in one biological sample.

Screening for carbon catabolite repression-defective mutants

Mutants which show a defective CCR phenotype were isolated from a *Rlv*3841 random-barcode transposon-site (RB-TnSeq) library (Knights et al., 2024). The inositol luminescent biosensor plasmid (pLMB686) was introduced into the RB-TnSeq library by biparental conjugation, with increased volumes to accommodate the whole library. Serial dilutions of the conjugants were plated onto solid UMS plates containing selective antibiotics,10 mM *myo*-inositol, and 20 mM succinate. NightOWL images were taken after plates were incubated until colonies were large but still well separated (typically 4-5 days). In total, approximately 15,000 colonies were screened for increased luminescence.

Colonies depicting increased luminescence were purified and phenotyped by comparing their luminescence to the WT strain (LMB592) on UMS plates with 10 mM *myo*-inositol or 10 mM *myo*-inositol plus 20 mM succinate; as well as for growth on 20 mM succinate as

the sole carbon source. Only candidates showing consistent increased luminescence were selected for further characterisation. Transposon-insertion sites were identified by a combination of transductional analysis, arbitrary-primed PCR, and Sanger sequencing of gel-purified PCR products.

RNA work and (q)RT-PCR

*Rlv*3841 cultures were grown in UMS supplemented with 10 mM ammonia and the indicated carbon sources in three biological replicates. At harvest, an equal volume of RNAlater™ was added to each culture, followed by incubation for 5 min at room temperature before cells were collected by centrifugation at 4°C. Cells were lysed using a FastPrep-24 5G instrument (MP Biomedicals) and total RNA was extracted from the lysate using the Qiagen RNeasy Plus Mini Kit according to the manufacturer's instructions. Residual genomic DNA (gDNA) was depleted by treatment with Invitrogen's TURBO™ DNase. RNA quantity and purity were assessed using a Qbit 2.0 fluorometer and NanoDrop One spectrophotometer.

For cDNA synthesis, 500 ng of purified RNA was reverse-transcribed using the Invitrogen SuperScript™ IV Reverse Transcriptase kit, following the manufacturer's recommendations. Quantitative PCR (qPCR) reactions were performed in a total volume of 10 µL, containing 5 µL PowerUp™ SYBR™ Green Master Mix, 300 nM of each primer, and 5 ng of cDNA template. Reactions were run in 384-well plates on a QuantStudio™ 5 Real-Time PCR System (Thermo Fisher Scientific) in technical triplicates.

Primer pairs used for RT-qPCR are listed in Table S2.1. Primer amplification efficiency and specificity were validated by generating a standard curve (Figure S2.4) and by testing against gDNA. Relative expression levels were calculated using the Pfaffl method, normalising against the housekeeping gene *rpoD*, previously validated as a stable reference (Tjahjono, 2025). Values are shown relative to WT grown on *myo*-inositol and were $\log_2$ transformed for visualization and statistical analysis.

cDNA was used for PCR analysis of the *intABC* transcriptional organisation using primer pairs listed in Table S2.1. For mapping of transcription start sites of *intABC* by 5' RACE, the 5'/3' RACE kit, 2nd generation (Roche Diagnostics AG) was used following manufacturer's

recommendations, with additionally required primers listed in Table S2.1. Reaction products were cloned into pJET1.2/blunt if required and sent for sequencing.

Transcriptional and translational fusions

For transcriptional *gusA* fusions, the promoter region and 5' untranslated region (5'UTR) of *iolC*, *intA*, as well as truncation variations containing either the *intA* promoter or the 5'UTR were amplified using primers listed in the Table S2.1. All fragments were ligated into *Pst*I-*Spe*I digested pOPS1850, a promoterless *gusA* in a mTn*7* delivery plasmid, using HiFi assembly (NEB). The resulting plasmids pOPS2354-57 are listed in Table 2.2. Fragments containing the *intA* 5'UTR were expressed under the control of the constitutive promoter J23106 (https://parts.igem.org/Promoters/Catalog/Anderson), which was included in the forward HiFi-primers oxp7296 and oxp7534 as a spacer. The *intA* signal peptide was predicted using TOPCONS (Tsirigos et al., 2015) and an extra stop codon (UGA) was integrated into the design of oxp7297 to prevent *intA* translation. Plasmid pOPS2353 (P_{23106}–*gusA*) served as a constitutive control and was created by ligating a *Spe*I-*Pst*I digested pOPS1850 with oxp7293 in an HiFi reaction adapted for ligating backbones with single stranded DNA oligos (NEB).

To create congruent *phoA* translational fusions to the existing *gusA* reporter plasmids, truncations of the *intA* promoter region and 5'UTR until the *intA* signal peptide (primers see Table S2.1) were fused to the *E. coli* K12 *phoA* chain lacking its own signal peptide (amplified with oxp7301-7332) and HiFi assembled into the *Kpn*I-*Hind*III digested pUC18T-mini-Tn7T-Gm backbone, resulting in plasmids pOPS2358 and pOPS2359.

All reporter plasmids were Tn*7*-integrated into rhizobial strains via tetraparental conjugations. The resulting strains were grown in UMS liquid cultures with required carbon sources and cells harvested by centrifugation when they had reached exponential phase.

For quantifying β-glucuronidase activity, the protocol described in Ledermann (2017) was followed. In short, 85 µL of cells (washed twice with 0.9% NaCl, concentrated to OD_{595} < 5.0) were added to 915 µL of β-glucuronidase assay buffer (50 mM $NaPO_4$ pH 7.0, 10 mM β-mercaptoethanol, 2 mM EDTA, 0.1% sarkosyl, 0.1% Triton X-100) and permeabilised by addition of 30 µL of chloroform and thorough vortexing. The enzyme

reaction was started by adding 200 µL of PNPG solution (p-nitrophenyl-β-glucuronide, 13.5 mM in water) and placed at 37°C. The reaction was stopped by adding 500 µL of 2 M Na_2CO_3 when visible yellow colouration of the reaction mixture was observed compared to the control (85 µL of NaCl instead of cells in the reaction mixture).

For quantifying alkaline phosphatase activity, the same protocol was used, with the following adaptations: 100 µL of cells (washed twice with 0.1 M Tris-HCl pH 8.0, concentrated to $OD_{595} < 5.0$) were added to 700 µL 0.1 M Tris-HCl (pH 8.0) and permeabilised by adding 20 µL of chloroform and 10 µL SDS (10%) and thorough vortexing. Tubes were incubated at 30°C for 5 min before adding 100 µL of pNPP (p-nitrophenyl phosphate, 4 mg mL^{-1} in 0.1 M Tris-HCl, pH 8.0) to start the enzyme reaction. The reaction was stopped with 100 µL of 1 M K_2HPO_4.

Reaction mixtures were cleared by centrifugation and absorbance of supernatants was measured at 405 nm for β-glucuronidase assays and at 420 nm for alkaline phosphatase assays. Reporter activities were calculated analogously to those of β-galactosidase (Miller, 1972), expressed in adapted Miller units (MU):

$$adapted\ MU = \frac{OD_X \times 1000}{V \times OD_{600} \times t}$$

where OD_X denotes OD_{405} for β-glucuronidase and OD_{420} for alkaline phosphatase, V denotes volume of cell sample in mL, and t denotes the time difference between start and stop point in decimal minutes.

One biological replicate was defined as an independent culture, and each replicate was assayed in technical duplicates. β-glucuronidase activity is shown as relative activity to a constitutive control (J_{23106}-*gusA*, pOPS2353).

Statistical analysis and visualization

All statistical analyses were performed using GraphPad Prism v10.6.1. Differences between groups were assessed using Student's *t*-tests or analysis of variance (ANOVA). When multiple comparisons were conducted, appropriate post hoc tests with correction for multiple testing were applied. In cases where assumptions of equal variance were not

met, Welch's alternative of tests or mixed effect models were applied. Data were visualized using GraphPad Prism and Inkscape v1.4.3.

Results

C_4-dicarboxylates impose hierarchical carbon utilization in *R. leguminosarum*

To visualise C_4-dicarboxylate-mediated catabolite repression (CCR), we utilized a set of previously characterised *lux*-based biosensors responsive to distinct carbon sources (Pini et al., 2017). Each biosensor reports transcriptional activity from the promoter of a solute-specific ABC transporter in response to its corresponding inducer and is sensitive to its inducer in or below the millimolar range.

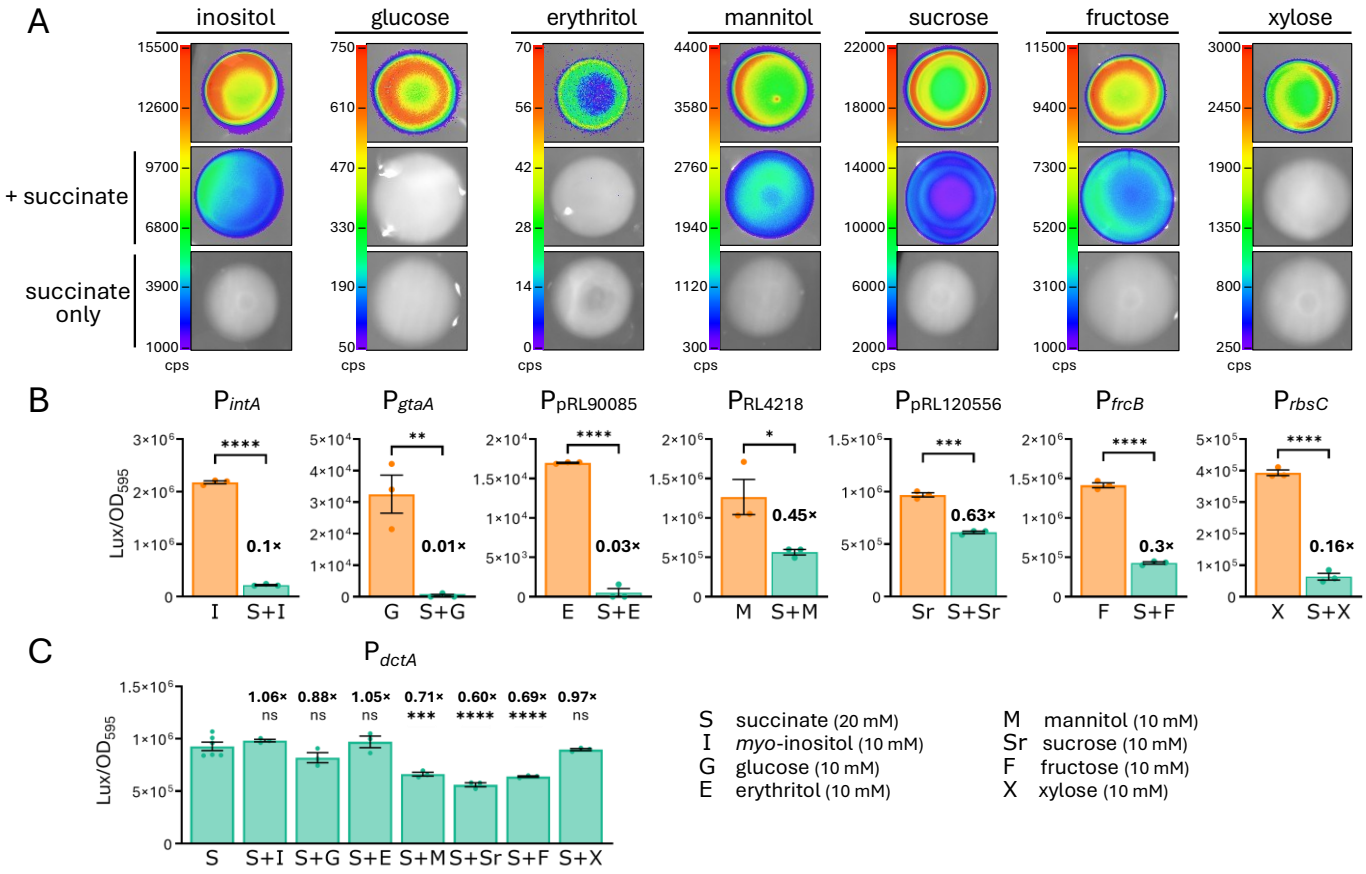


Figure 2.1 Presence of succinate represses expression of alternate carbon uptake systems.
(A) Representative NightOWL luminescence images of *lux*-reporter strains spotted onto solid UMS containing 10 mM inducer (top row), 10 mM inducer plus 20 mM succinate (middle row), or 20 mM of succinate (bottom row). Images were taken five days after incubation with colour scaling adjusted individually for each biosensor to account for differences in absolute luminescence. cps: counts per second. **(B, C)** Quantification of luminescence from liquid cultures during mid-exponential growth (OD_{595}~0.5), normalised to OD_{595} and measured using a plate reader).Bars show mean ± SEM from three independent cultures grown in either 10 mM inducer (orange) or 10 mM inducer + 20 mM succinate (green). Numbers above bars indicate fold change relative to the leftmost bar in each plot (inducing condition for each respective *lux*-reporter strain). Statistical significance was assessed using Student's *t*-test (B) or one-way ANOVA with Dunnet's multiple comparisons test (C). Asterisks indicate significance levels: **** $p < 0.0001$, *** $p < 0.001$, ** $p < 0.01$, * $p < 0.05$, ns not significant.

When plated on UMS agar containing the respective inducing substrate as the sole carbon source, all biosensor strains displayed strong luminescence signals (Figure 2.1A). In contrast, the addition of succinate resulted in a pronounced repression of luminescence for all biosensors. In some cases, i.e. glucose, erythritol, and xylose, presence of succinate reduced luminescence intensities to levels undistinguishable from the background (succinate only). No luminescence was detected on plates containing succinate as the sole carbon source, confirming that succinate does not induce any of the biosensors.

These qualitative observations were quantitatively confirmed in liquid cultures using plate reader measurements (Figure 2.1B). All measurements were taken during mid-exponential growth (OD_{595} ~0.5), ensuring sufficient growth on the respective carbon sources prior to measurement. For all biosensors, luminescence values normalised to optical density were significantly reduced in cultures supplemented with succinate in addition to the inducer, demonstrating consistent CCR across a range of alternative carbon sources.

Overall signal strength and repression magnitude from inducing to repressing conditions varied between biosensors (Figure 2.1A,B), consistent with differences in promoter activity and inducer specificity (Pini et al., 2017). The inositol reporter exhibited the highest luminescence output (~2,000,000 relative light units (RLU)), and one of the largest fold changes between inducing and repressing conditions, together with glucose and erythritol. Based on overall signal intensity and dynamic range, biosensors were ranked for CCR visualisation as follows: inositol > xylose > sucrose ≈ mannitol > fructose > erythritol. Although the erythritol biosensor displayed clear repression (Figure 2.1), its low absolute signal limited sensitivity.

Consequently, the inositol biosensor was selected for subsequent CCR analyses due to its high luminescence output and clear and reproducible contrast between conditions. (Figure 2.1A,B).

Repression of alternative carbon source uptake was independent of the specific C_4-dicarboxylate present, as the inositol reporter is equally repressed in the presence of succinate, malate or fumarate (Figure 2.2), equalling approximately 10-30% of its level in cells grown on *myo*-inositol as the sole carbon source.

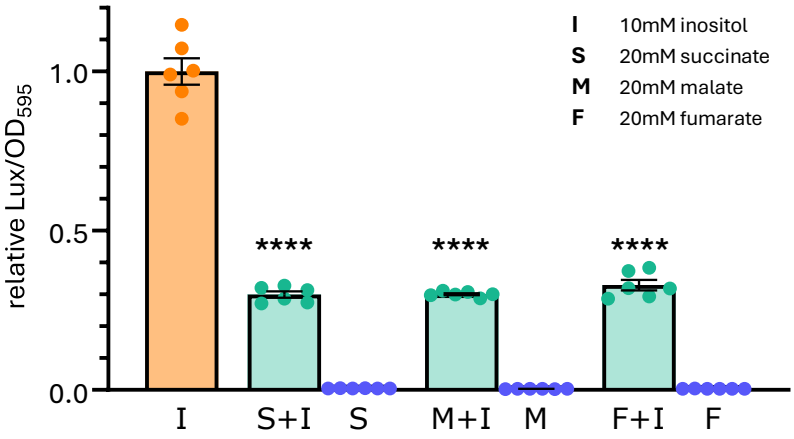


Figure 2.2 C_4-dicarboxylate–mediated carbon catabolite repression of *myo*-inositol–dependent luminescence. Luminescence normalised to optical density (Lux/OD_{595}) from an inositol biosensor strain (LMB592) was quantified from liquid cultures grown to mid-exponential phase (OD_{595} ~0.5) in UMS containing *myo*-inositol alone (I), *myo*-inositol plus a C_4-dicarboxylate (S+I, M+I, F+I), or a C_4-dicarboxylate alone (S, M, F). Bars represent mean ± SEM (n = 6), with values expressed relative to the *myo*-inositol-only condition. Statistical analysis was performed using Welch's ANOVA followed by a Dunnett-type multiple comparisons test comparing CCR-inducing conditions to the *myo*-inositol control; asterisks indicate significant differences **** $p < 0.0001$.

In contrast, expression of *dctA*, the gene encoding the C_4-dicarboxylate permease, was not reduced by the presence of alternative carbon sources (Figure 2.1.C). This observation is consistent with transport assays where transport rates of C_4-dicarboxylates were unchanged under these conditions (Figure 2.4.C). Together, the data supports a hierarchical carbon utilisation strategy in *R. leguminosarum*, in which uptake of preferred C_4-dicarboxylates occurs independently of the availability of and without the competition from alternative carbon sources.

Hierarchical carbon utilization manifests as diauxic growth

Further support for a hierarchical carbon utilisation strategy mediated by CCR was provided by the observation that *Rlv*3841 exhibits classical diauxic growth. When grown on mixed carbon sources, *Rlv*3841 displayed two distinct exponential growth phases, indicative of preferential utilisation of C_4-dicarboxylates over *myo*-inositol (Figure 2.3). To visualize this, growth of strain LMB592 (WT carrying the inositol biosensor) was examined under different carbon source combinations. Although the mean generation time (MGT) in 10 mM *myo*-inositol (4.43 ± 0.05h; mean ± SEM) as the single carbon source was comparable to that observed in 20 mM succinate (4.16 ± 0.09 h; mean ± SEM), growth on *myo*-inositol was preceded by a lag phase approximately twice as long as that of succinate-grown cultures when strains were precultured on TY (Figure S2.1).

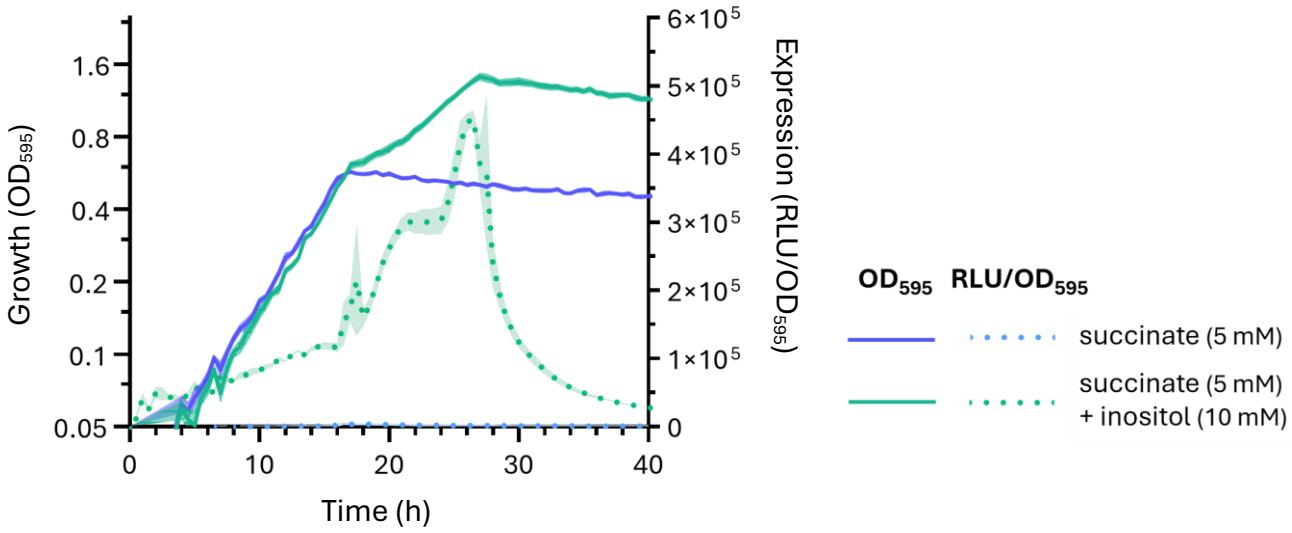


Figure 2.3 Diauxic growth of *R. leguminosarum* LMB592 (WT carrying the inositol biosensor plasmid) when grown on succinate and *myo*-inositol. Blank-corrected average OD_{595} (solid lines) and RLU (relative luminescence units) normalised to optical density (dotted lines) (four replicates; SEM shown as bands) in 5 mM succinate (blue), or 5 mM succinate plus 10 mM *myo*-inositol (green) as carbon sources. Optical density and luminescence were measured every 30 min.

To enforce diauxic growth, succinate concentrations were reduced to ensure depletion of the preferred carbon source before cultures reached stationary phase. When succinate concentrations were lowered from the standard 20 mM to 5 mM in media supplemented with 10 mM *myo*-inositol, growth consistently resolved into two distinct exponential phases (Figure 2.3). Cultures containing 5 mM succinate as the sole carbon

source ceased growing after approximately 16 h, consistent with exhaustion of the available succinate. When the medium additionally contained 10 mM *myo*-inositol, succinate exhaustion resulted in only a transient slowing of growth, after which bacterial cultures resumed exponential growth, typical for diauxie.

As expected, the deflection in the growth curve coincided with a change in luminescence from the inositol biosensor, increasing from $\leq 1 \times 10^5$ RLU/OD_{595} during the first exponential growth phase to approximately 3×10^5 RLU/OD_{595} during the second exponential growth phase (Figure 2.3). Notably, a pronounced spike in luminescence was observed around the time of the presumed metabolic shift. While this could reflect a genuine biological signal, it is more likely that the spike results from the transient accumulation of Lux proteins per cell during the growth pause following succinate exhaustion, as a similar increase was also observed upon entry into stationary phase.

Asymmetric inducer exclusion favours C_4-dicarboxylate uptake over alternative carbon sources

CCR strongly affected carbon transport in *Rlv*3841 in a substrate-dependent manner (Figure 2.4). *Myo*-inositol transport was markedly repressed by the presence of succinate, decreasing from 4.80±0.57 to 1.06±0.17 (mean ± SEM) nmol min^{-1} mg $protein^{-1}$, corresponding to an approximately 4.5-fold reduction (~22% of the transport rate of cells grown only on *myo*-inositol). With succinate present in the growth medium, *myo*-inositol transport was no longer significantly different from background uptake observed in cells grown on succinate alone (Figure 2.4A).

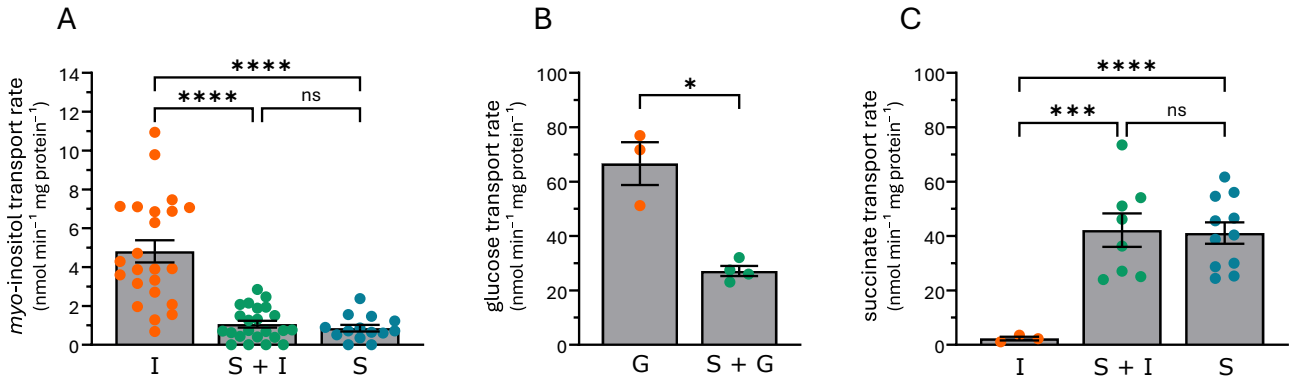


Figure 2.4 Carbon catabolite repression differentially regulates *myo*-inositol, glucose, and succinate transport. Transport rates of *myo*-inositol (A), glucose (B), and succinate (C) were measured in WT cells grown on the indicated carbon sources: *myo*-inositol (I, 10 mM), glucose (G, 10 mM), succinate (S, 20 mM), or combinations thereof. Bars indicate mean ± SEM with individual biological replicates shown. Data stem from multiple independent experiments. Statistical analyses were performed using Welch's ANOVA with Dunnett-type post hoc tests or Welch's t-tests, as appropriate. Statistical significance is indicated as follows: ns, not significant; $p < 0.05$ (*); $p < 0.001$ (***); $p < 0.0001$ (****).

It is worth noting that the low inositol transport rates observed with -[1,2-^{3}H(N)]-*myo*-inositol are likely attributable to isotope-related limitations rather than inherently weak uptake. Supporting this interpretation, Fry et al. (2001) observed substantially higher uptake rates in *Rlv*3841 WT (47.0 ± 1.7 (mean ± SD) nmol min^{-1} mg $protein^{-1}$) using ^{14}C-labelled *myo*-inositol, indicating that ^{3}H-labelling likely underestimates true transport capacity. Poole et al. (1994) similarly reported low transport rates with tritiated inositol and proposed that these may result from loss of the label to volatile components or steric hindrance associated with tritium substitution.

Glucose transport was likewise subject to repression in the presence of a C_4-dicarboxylate, although to a lesser extent (Figure 2.4B). Cells grown on succinate plus glucose exhibited a significant reduction in glucose uptake equalling approximately 40% of the level measured in glucose-grown cells.

In contrast, succinate transport was not repressed by the presence of *myo*-inositol (Figure 2.4C). Succinate uptake rates were comparable in cells grown in succinate or succinate plus *myo*-inositol, and both were significantly higher than background uptake in *myo*-inositol-grown cells (uninduced state).

Together, these results demonstrate that CCR in *R. leguminosarum* selectively downregulates alternative carbon source uptake, with strong repression of *myo*-inositol transport, effectively abolishing measurable uptake, and moderate repression of glucose transport. Importantly, CCR preserves the carbon hierarchy through directional regulation, leaving succinate transport rates unaffected by other carbon sources.

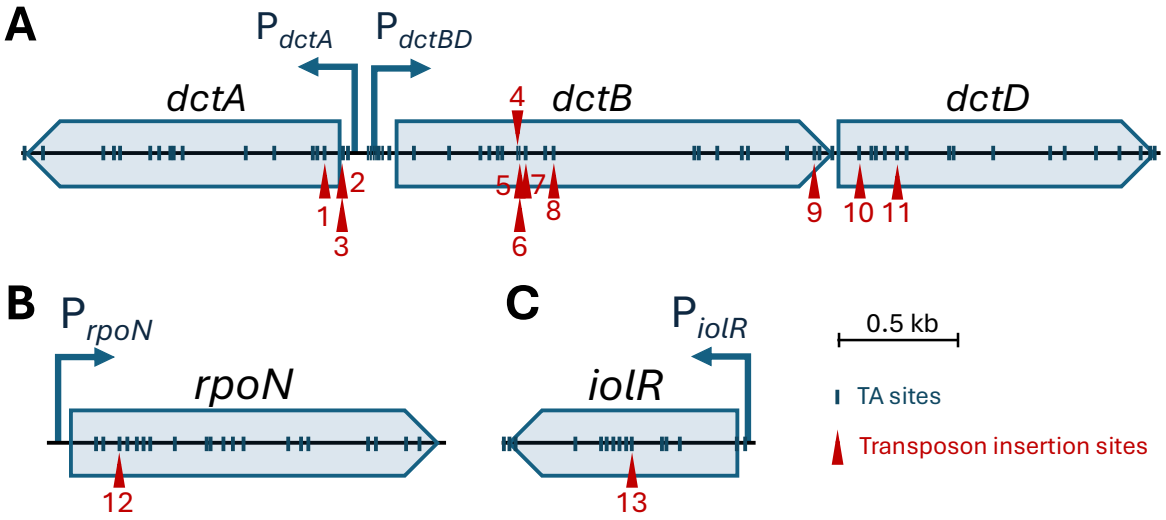
A genetic screen identifies the dicarboxylate transport (Dct) system as essential for CCR

To identify genetic components required for CCR, an RB-TnSeq library carrying the inositol reporter plasmid (pLMB686) was screened for mutants defective in succinate-mediated repression. As established above, in WT *R. leguminosarum*, luminescence of the reporter is reduced to ~30% of its maximum level in the presence of a C_4-dicarboxylate (Figure 2.2). The original RB-TnSeq library comprised 341,471 transposon insertions, covering 82% of potential *mariner* transposon insertion sites (TA dinucleotides) and 90% of protein-coding genes (Knights et al., 2024).

Approximately 15,000 colonies were screened on UMS containing *myo*-inositol and succinate. The majority of colonies exhibited low luminescence, consistent with effective succinate-mediated repression of P_{intA}-*lux*. However, 13 mutants reproducibly displayed elevated luminescence under these conditions, indicating a transposon-insertion in a genomic location important for establishing CCR.

Mapping of transposon insertion sites and transductions revealed that 11 of the 13 mutants carried insertions within the dicarboxylate transport system (Dct) cluster (Figure 2.5). These included six independent insertions in the open reading frame of *dctB* (OPS3569-74), two in *dctD* (OPS3575, OPS3576) and one within the coding region of *dctA* (OPS3566). In addition, two mutants (OPS3567, OPS3568) contained transposon insertions upstream of *dctA*, located 12 nucleotides before the start codon, likely disrupting normal expression from the *dctA* promoter and potentially affecting expression of *dctBD*. The pairs OPS3570/OPS3571 and OPS3567/OPS3568 appear to be sibling isolates originating from the same transposon insertion event.

In addition to *dct* mutants, two CCR-defective strains were identified with insertions in *rpoN* (OPS3577), the gene encoding the alternative sigma factor σ^{54} which is required for *dctA* expression (Dombrecht et al., 2002; Ronson et al., 1987, Figure 3.1), and in *iolR* (OPS3578), which encodes the transcriptional repressor of various genes involved in *myo*-inositol metabolism (Figure 2.8). In the *iolR* mutant, disruption of the negative regulator resulted in constitutive expression of the biosensor, even in absence of its inducer inositol.



D

	Candidate	Orientation of inserted transposon	Insertion site **gene** (TA site location)
1	**OPS3566**	reverse	***dctA*** (3 599 257bp)
2	**OPS3567**	reverse	upstream of ***dctA*** (3 599 335bp)
3	**OPS3568**	reverse	upstream of ***dctA*** (3 599 335bp)
4	**OPS3569**	reverse	***dctB*** (3 600 080bp)
5	**OPS3570**	forward	***dctB*** (3 600 078bp)
6	**OPS3571**	forward	***dctB*** (3 600 078bp)
7	**OPS3572**	forward	***dctB*** (3 600 107bp)
8	**OPS3573**	reverse	***dctB*** (3 600 226bp)
9	**OPS3574**	reverse	***dctB*** (3 601 333bp)
10	**OPS3575**	forward	***dctD*** (3 601 519bp)
11	**OPS3576**	reverse	***dctD*** (3 601 686bp) – no TA site
12	**OPS3577**	reverse	***rpoN*** (459 000bp)
13	**OPS3578**	reverse	***iolR*** (1 563 864bp)

Figure 2.5 Transposon insertion sites of the 13 CCR-defective mutants. Genomic regions of *dct* cluster **(A),** *rpoN* **(B)** and *iolR* **(C)**, with all TA sites representing potential *mariner* transposon insertion sites (blue bars) and TA insertions sites of mutants (red triangles; numbers correspond to strains listed in **(D)**) marked. Genes are shown as pentagon arrows and transcription start sites as right-angled arrows.

Intracellular C_4-dicarboxylate accumulation, rather than Dct signalling, mediates repression

C_4-dicarboxylate uptake in *R. leguminosarum* is mediated by the dicarboxylate transport system (Dct). The Dct consists of the transporter permease DctA and the two-component sensor-regulator DctB/DctD, which sense extracellular C_4-dicarboxylates and induce *dctA* expression (c.f. Chapter 3). To confirm that components of the Dct system contribute to CCR, we employed a systematic genetic approach in which individual elements of the Dct system were disrupted and the effects on CCR were assessed. Following from this, the inositol biosensor plasmid (pLMB686) was conjugated into already existing *dct* mutants, generating strains OPS3601-05. Subsequent testing validated the finding that *dct* mutants show increased P_{intA} expression under conditions where WT *Rlv*3841 elicits strong CCR (Figure 2.6A and Figure S2.7).

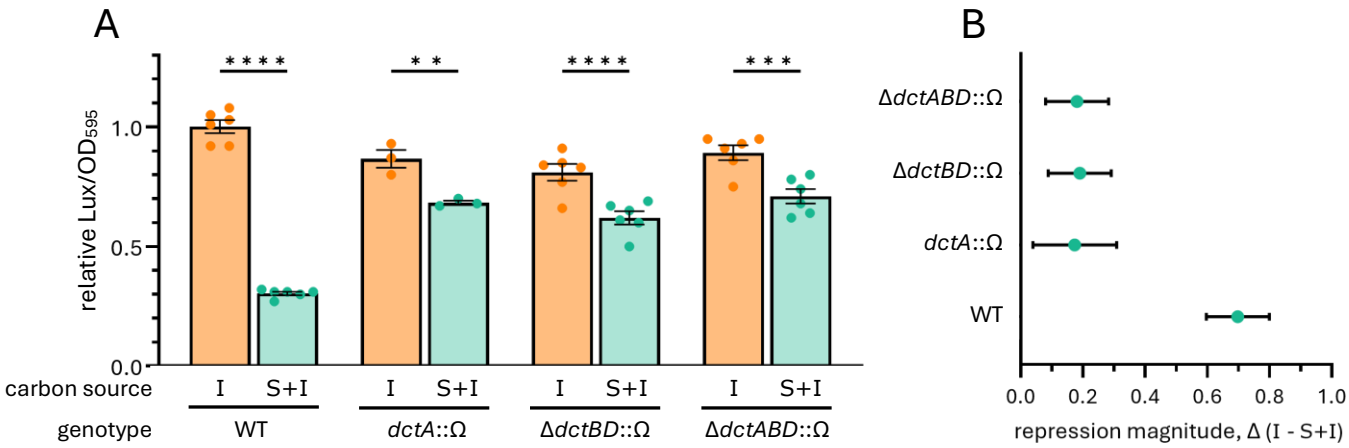


Figure 2.6 Mutants in *dct* genes no longer show full CCR. (A) Luminescence of a *myo*-inositol biosensor in WT *Rlv*3841 and *dct* mutant strains, normalised to optical density (Lux/OD_{595}) and expressed relative to WT grown in *myo*-inositol. Luminescence was quantified from liquid cultures grown in TY and inoculated into UMS containing either 10 mM *myo*-inositol (I, orange), or 20 mM succinate plus 10 mM *myo*-inositol (S+I, green) at OD_{595} ~ 0.5. Bars represent mean ± SEM (n ≥ 3). Statistical significance reflects Sidak-corrected comparisons between growth conditions within each genotype following a two-way mixed-effects model, where **** $p < 0.0001$, *** $p < 0.001$, ** $p < 0.01$. **(B)** Model-estimated repression magnitudes shown as difference between *myo*-inositol alone and succinate plus *myo*-inositol conditions (Δ = I − S+I). Points represent estimated (LS) mean differences derived from the mixed-effects model, and horizontal bars indicate Sidak-adjusted 95% confidence intervals.

While succinate still significantly reduced biosensor activity in all strains, a significant genotype × carbon source interaction ($F(3,24) = 67.46$, $p < 0.0001$) indicates that CCR is substantially weaker in *dct* mutants compared to WT. Succinate strongly repressed biosensor activity in WT ($\Delta = 0.7$, $p < 0.0001$), whereas repression in *dct* mutants was significantly weaker ($\Delta \approx 0.17–0.19$) (Figure 2.6B). Reduced repression observed in luminescence is consistent with unaltered transcript levels of inositol-related genes in the Δ*dctA* and Δ*dctABD* backgrounds (Figure S2.5).

As DctB and DctD are the regulating circuit controlling *dctA* expression, all loss-of-function mutants – whether generated by targeted gene disruption or spontaneous transposon insertion – display the same functional phenotype: Disruption of any of the three *dct* genes results either in the absence of *dctA* expression or yields a nonfunctional DctA transporter. Consequently, these mutants do not allow discrimination between transport-dependent and signalling-dependent effects. (Attempts to resolve this by engineering the native Dct system are discussed in more detail in Chapter 3).

To determine whether the Dct system is intrinsically required for CCR signalling – or whether intracellular C_4-dicarboxylate accumulation alone is sufficient – we functionally uncoupled C_4-dicarboxylate transport from Dct-dependent sensing. This was achieved by replacing the DctA C_4-dicarboxylate transporter with the distantly related, malate-specific transporter MaeP.

The *maeP* gene from *Streptococcus gallolyticus* encodes a membrane symporter with functional analogy to DctA, yet it is specific for malate transport and is unable to recognize succinate or fumarate as substrates (Kawai et al., 1997; Mitsch et al., 2018). DctA and MaeP share low sequence similarity (16.5%) and their AlphaFold-predicted structures exhibit limited structural overlap (TM-align score = 0.35 (Zhang & Skolnick, 2005)), making functional complementation beyond malate transport unlikely. Moreover, MaeP is not expected to be subject to DctBD-dependent regulation when introduced into *R. leguminosarum*.

Medium-copy-number plasmids expressing *maeP* under control of either the constitutive *S. meliloti dme* promoter (P_{dme}-*maeP*) or the *S. meliloti dctA* promoter (P_{dctA}-*maeP*) were conjugated together with the inositol biosensor into *dct* mutants to generate strains

OPS4234-4237. Three of the four strains regained the ability to grow on L-malate as the sole carbon source, with the exception of OPS4235 (Δ*dctABD* strain carrying P_{dctA}-*maeP*), indicating that the *S. meliloti dctA* promoter is subject to DctBD-dependent activation in *R. leguminosarum*.

As expected, none of the strains grew on succinate as the sole carbon source, confirming that MaeP does not transport succinate. Consequently, no CCR was observed when these strains were grown on succinate and *myo*-inositol (Figure S2.8), consistent with the phenotype of the corresponding parental *dct* mutants (Figure 2.6A).

In contrast, when grown on malate and *myo*-inositol, all strains expressing functional MaeP displayed restored CCR comparable to wild type levels in both Δ*dctA* and Δ*dctABD* backgrounds (Figure 2.7). Notably, this occurred despite malate transport rates in the mutants are only a fraction of those in the WT (Mitsch et al., 2018). Only the Δ*dctABD* strain carrying the inactive P_{dctA}-MaeP construct failed to restore proper repression, consistent with the absence of malate uptake.

Together, these results demonstrate that malate uptake alone is sufficient to restore CCR in *dct* mutants, indicating that the Dct signalling system is not intrinsically required for repression, as long as C_4-dicarboxylate uptake is enabled.

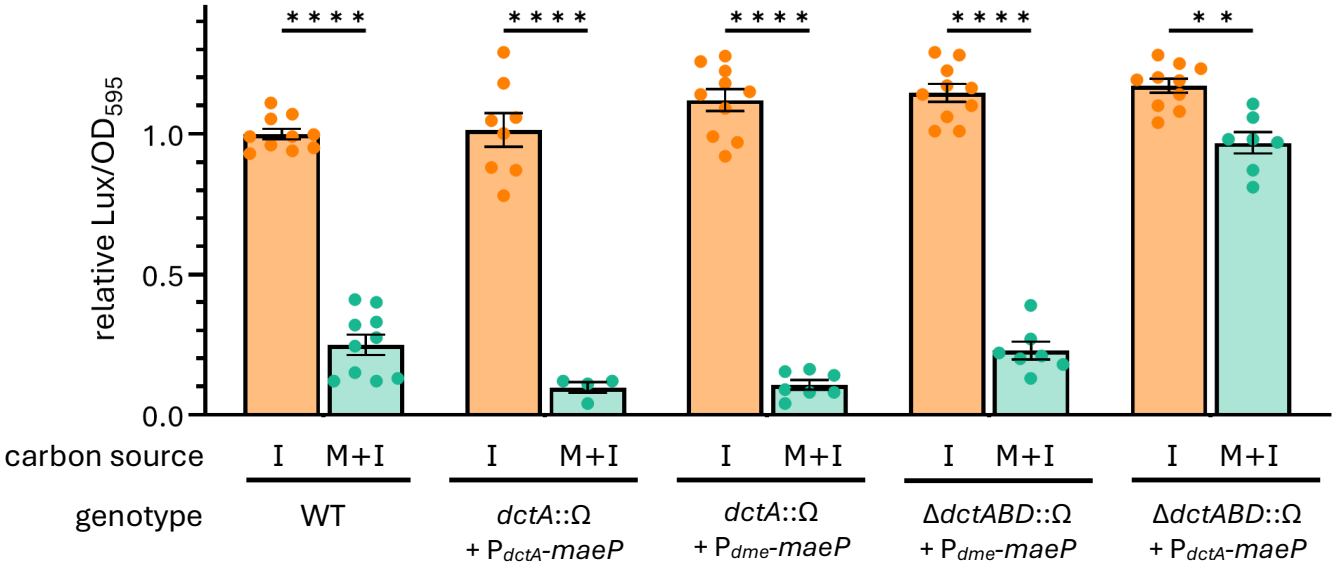


Figure 2.7 Complementation with a distantly-related malate transporter restores CCR in Dct mutants. Luminescence of a inositol biosensor in WT *Rlv*3841 and *dct* mutants complemented with the malate-specific transporter *maeP* from *Streptococcus gallolyticus* driven by either the native *dctA* promoter (P_{dctA}) or the *dme* promoter (P_{dme}). Cultures were grown in UMS containing 10 mM *myo*-inositol (I, orange) or 20 mM malate plus 10 mM *myo*-inositol (M+I, green) to mid-exponential phase (OD_{595} ~0.5) and luminescence was normalized to optical density (Lux/OD_{595}) and expressed relative to WT grown in *myo*-inositol. Bars represent mean ± SEM (n ≥ 4), with data stemming from three independent experiments. Statistical significance reflects Sidak-corrected comparisons between growth conditions within each genotype following a mixed-effects model, where **** $p < 0.0001$, ** $p < 0.01$.

The inositol utilization pathway as a model system to localize CCR

Results from the mutant screen and subsequent experiments demonstrate that C_4-dicarboxylate entry is required to trigger repression of alternative carbon sources such as *myo*-inositol. However, the mechanism by which this repression is mediated remains unclear. To address this question, we used the inositol pathway as an example system and first defined its transcriptional organization and regulatory architecture as a foundation for the subsequent experiments.

Inositol transport, catabolism, and their regulation form a conserved functional module across diverse α-proteobacteria (Boutte et al., 2008; Figure 2.8A). In *Rlv*3841, inositol uptake depends on a CUT2-family ATP-binding cassette (ABC) transporter encoded by the *intABC* operon (RL4655-RL4653; Figure 2.8B). As is typical for ABC transporters, *intA* encodes the periplasmic solute-binding protein (SBP), which is responsible for substrate recognition and delivery to the transporter complex. An IntC dimer is predicted to form the transmembrane domains (TMD) coupled to an an ATPase dimer of IntB in the cytoplasm that powers transport via ATP hydrolysis (Schneider, 2001). Homologous transporter operons in other α-proteobacteria are often referred to as *ibpA–iatAP*.

Transcriptomic data show that *intABC* is strongly induced during growth on *myo*-inositol (Karunakaran et al., 2009). PCR analysis of cDNA confirmed that the three genes are co-transcribed as an operon (Figure S2.2) with expression driven from a primary promoter upstream of *intA*. Mapping of the transcription start site (TSS) by 5'RACE located the +1 site 78 bp upstream of the *intA* start codon (Figure S2.2A), establishing the promoter region used for subsequent reporter analyses. Additional regulatory features likely modulate transcript levels, including a predicted stem-loop structure in the 69 bp *intA–intB* intergenic region which may function as a transcriptional attenuator, and two secondary 5'RACE bands suggest additional internal transcription start sites upstream of *intB* and *intC* (Figure S2.2A). It is unclear whether those additional TSS are genuine and to what extent they contribute to transcriptional output and it is possible that they are degradation/processing products of the longer transcript.

Following uptake, *myo*-inositol is degraded by enzymes encoded by the conserved catabolic gene cluster comprising *idhA*, *iolCDEB*, and *iolA*, yielding, aside from NADH

and NADPH, dihydroxyacetone phosphate (DHAP), and acetyl-coenzyme A (Herrou & Crosson, 2013; Karunakaran et al., 2009), which can subsequently enter central carbon metabolism via the Embden-Meyerhof-Parnas pathway and the TCA cycle, respectively (Figure 2.8D).

All inositol-related genes in *Rlv*3841, including *intABC* and the catabolic genes, are negatively regulated by the transcriptional repressor IolR, which blocks transcription by binding to conserved operator motifs in their promoter regions (Figure 2.8A,C). MEME analysis suggests that all promoters of inositol-related genes in *Rlv*3841 contain variations of the putative IolR-binding motif GGAA-N_6-TTCC (Figure S2.3).

IolR also autoregulates its own expression via an IolR-binding motif overlapping the predicted TSS of *iolR* (Figure 2.8A; Figure S2.3). Negative autoregulation is typical for transcriptional repressors and reduces response time while stabilizing steady-state repressor levels (Alon, 2007). This supports robust induction in the presence of inositol and rapid re-repression of the *int* and *iol* genes once inositol is depleted.

Importantly, pathway induction is not triggered by *myo*-inositol itself but by a downstream catabolic intermediate (Fry et al., 2001), most likely DKHP (2-deoxy-5-keto-D-gluconic acid 6-phosphate), the product of the IolC-catalysed reaction. DKHP has been shown to be the inducer in *S. meliloti* (Kohler et al., 2011) and *B. subtilis* (Yoshida et al., 2008) and is thought to interact with the phosphosugar-binding domain (SIS) of IolR, thereby releasing the repressor from its target operators. As the different inositol isomers (*myo-, scyllo-*, and D-*chiro*-inositol) commonly co-occur in soil (Turner et al., 2002) and can all be metabolized by rhizobia (Kohler et al., 2010), a shared catabolic intermediate provides a unified induction signal for pathway activation.

With this regulatory framework defined, we next thought to pinpoint the level at which CCR intervenes into the inositol utilization pathway.

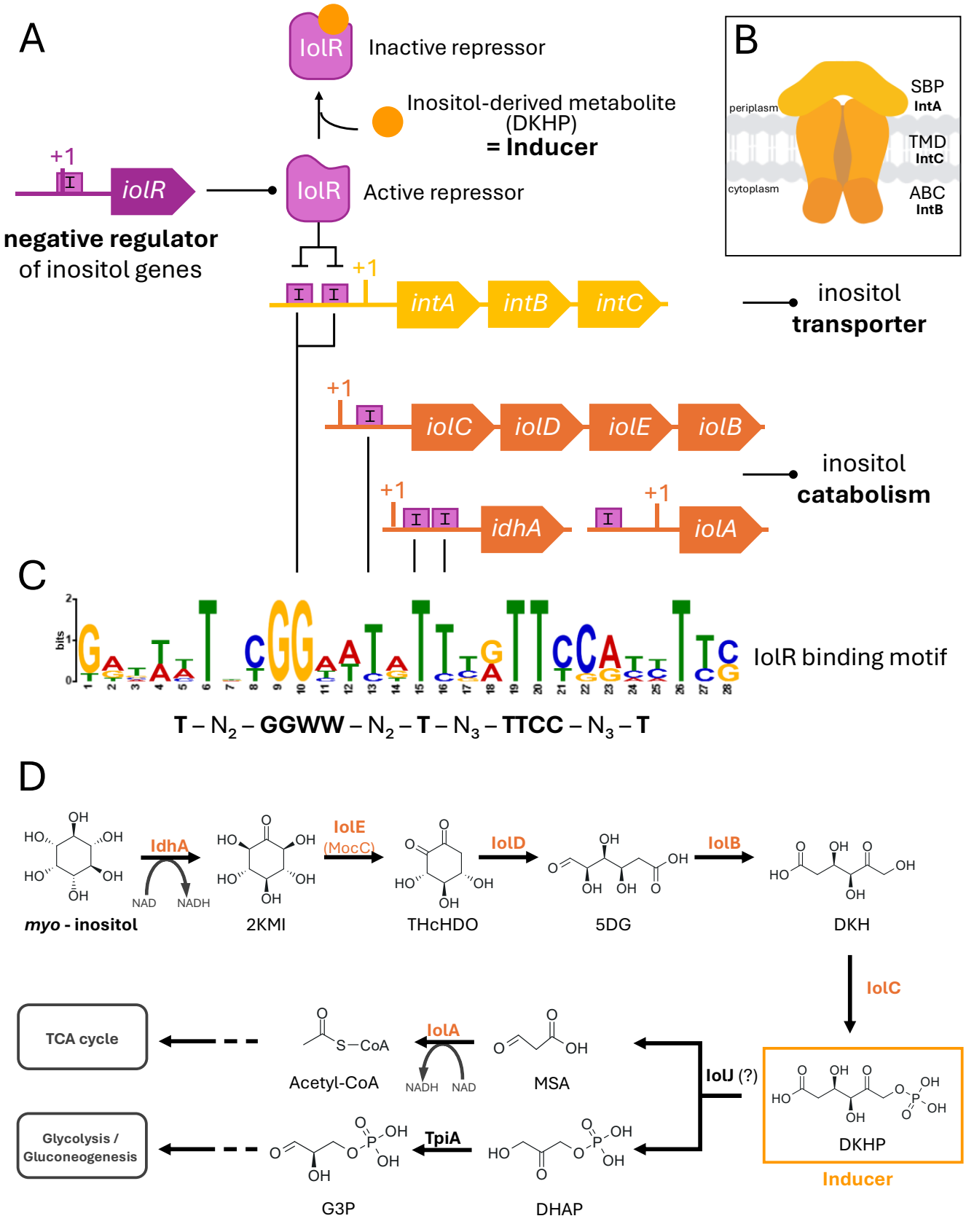

A
IolR
Inactive repressor
Inositol-derived metabolite
(DKHP)
= Inducer
+1
I
iolR
IolR
Active repressor
negative regulator
of inositol genes
+1
I I
intA
intB
intC
B
periplasm
SBP
IntA
TMD
IntC
cytoplasm
ABC
IntB
inositol
transporter
+1
I
iolC
iolD
iolE
iolB
inositol
catabolism
+1
I I
idhA
+1
I
iolA
C
bits
IolR binding motif
T – N2 – GGWW – N2 – T – N3 – TTCC – N3 – T
D
IdhA
NAD
NADH
IolE
(MocC)
IolD
IolB
myo - inositol
2KMI
THcHDO
5DG
DKH
IolC
TCA cycle
IolA
Acetyl-CoA
NADH
NAD
MSA
IolJ (?)
DKHP
Inducer
Glycolysis /
Gluconeogenesis
TpiA
G3P
DHAP

Figure 2.8 Inositol metabolism and respective genetic loci in *Rhizobium leguminosarum*. (A) Genes are shown as arrows, proteins as indented squares, and transcription start sites (+1) as ticks. Line endings indicate interaction (arrow), inhibition (blunt end) and translation (filled circle). The *intABC* operon (yellow) encodes an ABC transporter for inositol uptake, while inositol catabolic genes (orange) are distributed across the genome, with *iolCDEB* forming the main catabolic operon. Expression of all inositol-associated genes is negatively regulated by IolR (purple), which binds conserved operator motifs (purple squares) in promoter regions and inhibits transcription in the absence of an inducer. Following uptake and initial metabolism of inositol, an inositol-derived metabolite (yellow circle) acts as the inducer by binding to and thus releasing IolR from its operator sites, thereby enabling transcriptional upregulation. **(B)** Inositol ABC transporter in inner membrane, consisting of the solute-binding protein (SBP) IntA, the transmembrane channel (TMD) formed by an IntC dimer and two IntB ATP-hydrolysing proteins (ABC). **(C)** MEME output for the identification of a conserved partially palindromic motif (MEME E-value $3.2\times e^{-4}$), which loosely fits the IolR binding motif GGAA-N_6-TTCC described by Boutte et al. (2008). For more details see Figure S2.3. **(D)** Biochemical pathway of *myo*-inositol catabolism in *R. leguminosarum*. All genes for this catabolic pathway are present in *Rlv*3841, except the *iolJ* gene. 2KMI, 2-Keto-*myo*-inositol; THcHDO, 3D-(3,4/5) trihydroxycyclohexane-1,2-dione; 5DG, 5-deoxy glucuronic acid; DKH, 2-deoxy-5-keto-D-gluconic acid; DKHP, 2-Deoxy-5-keto-D-gluconic acid 6-phosphate; DHAP, Dihydroxyacetone phosphate; MSA, Malonic semialdehyde; acetyl-CoA, acetyl coenzyme A; G3P, glyceraldehyde-3-phosphate. Pathway based on KEGG-pathway rle00562.

Transcription of *intABC*, but not *iolC* or *iolR*, involves regulation beyond IolR

To determine where CCR interferes with the inositol utilisation pathway, we examined the regulation of the inositol-specific ABC transporter (IntABC) at the transcriptional level and compared it to the regulation of other genes induced by inositol and required for its utilisation. As CCR mechanisms identified in related bacteria act at multiple regulatory levels, ranging from transcriptional to post-transcriptional control (see Introduction), we therefore applied complementary approaches to examine regulatory control of the inositol utilisation pathway. To account for internal regulation by the inositol-specific regulator IolR, both WT and *iolR*-mutant strains were included in the following analyses. The *iolR* mutant (OPS4112) was constructed by transducing the mariner transposon from OPS3578 into a clean WT background.

To assess whether CCR modulates inositol gene expression in response to the presence of preferred carbon sources, we first examined how addition of succinate alters transcript levels of transport, metabolic, and regulatory genes. To this end, we quantified expression of the *intABC* transport operon, the inositol catabolic gene *iolC*, and the transcriptional regulator *iolR* by RT-qPCR in cells grown on *myo*-inositol, succinate, or a combination of both (Figure 2.9). To ensure that *iolR* transcript measurement reflected transcriptional output from its promoter, qPCR primers were designed to amplify the 5' region upstream of the transposon insertion.

In WT cells, *intA*, the first gene of the *intABC* transport operon, was strongly induced during growth on inositol and was significantly reduced upon addition of succinate (Figure 2.9A). Two-way ANOVA revealed a significant genotype × carbon source interaction ($F(2,11) = 176.8$, $p < 0.0001$). Resulting simple-effects analysis confirmed significant repression of *intA* in WT, whereas in the *iolR* mutant this repression was distinctly attenuated but remained significant, indicating partial dependence on IolR. The downstream genes *intB* and *intC* exhibited the same qualitative expression pattern as *intA* in both genotypes (Figure 2.9B and C), consistent with operon-wide regulation. These findings are consistent with inositol transport assays performed on the *iolR* mutant (Figure 2.10). Although transport rates were only modestly higher than in the WT, *myo*-inositol transport was no longer repressed in the presence of succinate. Moreover, in succinate-grown cultures, the *iolR* mutant maintained measurable *myo*-inositol uptake,

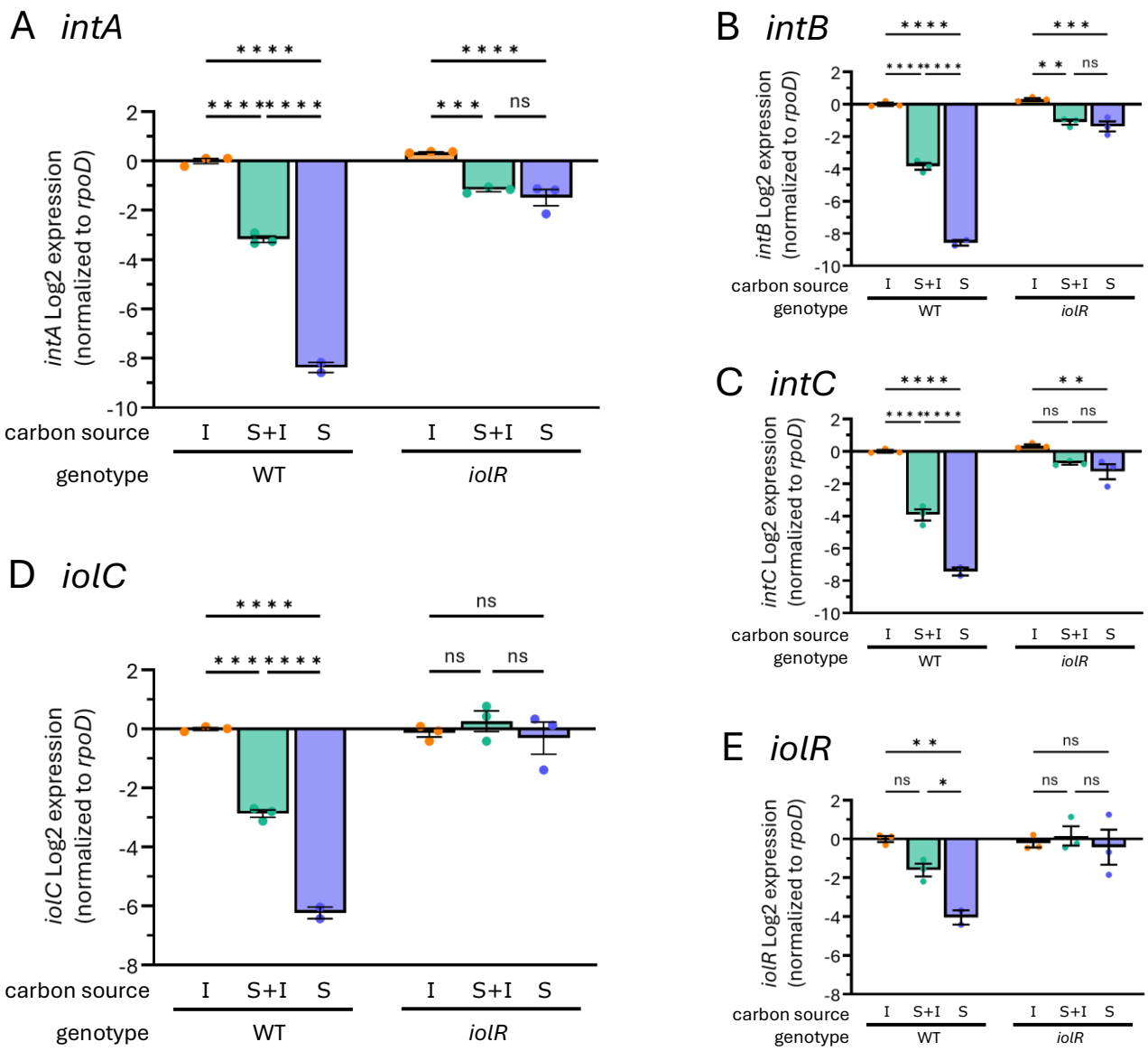


Figure 2.9 Succinate-mediated CCR selectively represses the inositol transport operon (*intABC*) and is partially dependent on IolR. qPCR analysis of genes encoding the inositol ABC transporter (*intA* **(A)**, *intB* **(B)**, *intC* **(C)**), the first inositol catabolism gene *iolC* **(D)** and the transcriptional regulator *iolR* **(E)** in WT and *iolR*, grown on *myo*-inositol (I, orange), succinate plus *myo*-inositol (S+I; green), or succinate (S, blue). Bars represent mean ± SEM of $\log_2$-transformed Pfaffl relative expression (n=3), normalized to *rpoD* and expressed relative to WT grown on *myo*-inositol Data were analysed by two-way ANOVA (genotype x carbon source), followed by Sidak-adjusted planned pairwise comparisons. Adjusted *p*-values are shown above comparisons with ns, not significant, **** $p < 0.0001$, *** $p < 0.001$, ** $p < 0.01$, * $p < 0.05$.

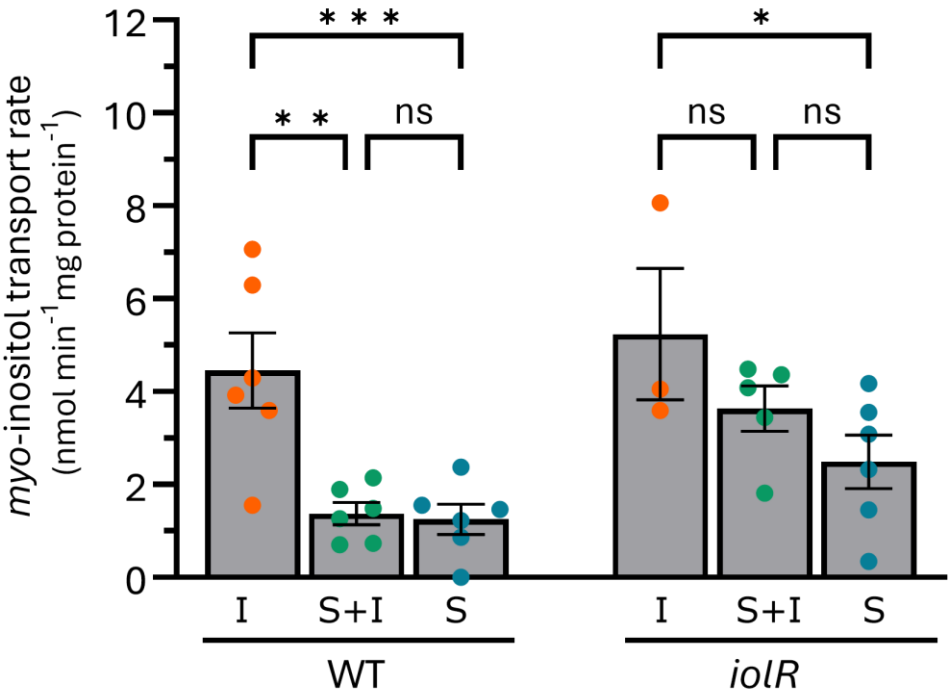


Figure 2.10 *iolR* mutant shows constitutive inositol transport and partial relief of CCR. Transport rates of tritiated *myo*-inositol measured in WT or *iolR* mutant cells grown on *myo*-inositol (I, orange), succinate and *myo*-inositol (S+I, green), or succinate (S, blue). Bars indicate mean ± SEM with individual biological replicates shown. The data is derived from two independent experiments. Statistical analyses were performed using a mixed effects model with Sidak-type post hoc tests. Statistical significance is indicated as follows: ns, not significant; $p < 0.05$ (*); $p < 0.01$ (**); $p < 0.001$ (***).

consistent with partial derepression of *intABC* expression in the absence of IolR. This observation is also consistent with our mutant screen, in which the *iolR* mutant was identified based on increased expression of the P_{intA}-*lux* bioreporter.

In contrast, expression of *iolC*, encoding the first enzyme of the inositol catabolism operon (*iolCDEB*), only showed succinate-dependent repression in the WT but not in the *iolR* strain (Figure 2.9D). Similarly, *iolR* transcript levels were significantly affected by carbon source only in the WT (Figure 2.9E), suggesting regulation of *iolC* and *iolR* is fully dependent on IolR and not on the presence of intracellular C_4-dicarboxylates.

In line with earlier findings, unaltered transcript levels of inositol-related genes were observed in the Δ*dctA* and Δ*dctABD* background (Figure S2.5).

Together, these data indicate that transcription of inositol-related genes is significantly downregulated in the presence of C_4-dicarboxylates and that IolR mediates a substantial

but not exclusive component of this regulatory response, specifically at the transporter operon. While CCR of the regulatory and catabolic genes appears to be mediated solely through IolR, repression of at the *intABC* operon also contains an IolR-independent component.

CCR at the *intA* promoter requires IolR

As established earlier, the *intABC* genes are transcribed as an operon under the control of one primary promoter, hereafter referred to as the *intA* promoter (P_{intA}). To pinpoint where CCR acts within this region, we constructed a series of transcriptional and translational fusions spanning the intergenic region between RL4656 and *intA*, which contains the P_{intA} and 5' untranslated region (5'UTR) (Figure 2.11A). These fusions enabled systematic dissection of cis-regulatory elements contributing to CCR.

Transcriptional fusions were generated by placing the designated *intA* promoter and/or 5'UTR fragments upstream of *gusA* (Figure 2.11), and the resulting transcriptional output was used to assess whether the fragment contributed to CCR. Fragments extending upstream of the TSS also included predicted IolR binding motifs. All constructs were tested in both WT and *iolR* backgrounds to distinguish IolR-mediated regulation from additional, theoretically IolR-independent, effects.

As expected, transcriptional fusions containing the full *intA* promoter region exhibited strong succinate-dependent repression in the WT strain (Figure 2.11B and Figure S2.6). In contrast to P_{iolC}, where succinate repression was completely abolished in the absence of IolR, repression of P_{intA} was partially retained in the *iolR* mutant (Figure 2.11B and Figure S2.6). These results are consistent with earlier findings (Figure 2.9) and indicate that, although IolR is a major mediator of CCR, additional regulatory mechanisms operate specifically at the *intA* locus but not at *iolC*.

To further localize CCR-relevant sequences upstream of the TSS, a truncated P_{intA} construct lacking the 5'UTR was analysed (Figure 2.11C). This construct remained responsive to succinate-dependent repression in the WT background but completely lost repression when tested in cells lacking IolR, demonstrating that CCR at the *intA* promoter level strictly requires IolR. Overall reporter activity was reduced compared to the full P_{intA}-5'UTR fusion (Figure 2.11B vs. C), suggesting a positive contribution of downstream

sequences to expression. This effect may, at least in part, reflect improved promoter – transcription start-site spacing. Consistent with this, a promoter fragment that extended 20 bp downstream of the TSS already modestly increased reporter activity (data not shown), although it did not restore CCR in the absence of IolR. Alternatively, the higher activity observed in the full construct may result from the presence of two ribosome binding sites, compared to only one in the truncated variant.

To evaluate whether the 5'UTR contributes directly to CCR, potentially through an additional regulator acting within this region, a fusion containing only the 5'UTR was examined (Figure 2.11D). This construct did not show succinate-dependent repression in either WT or an *iolR* mutant background, indicating that the 5'UTR alone is insufficient to mediate CCR. The low reporter activity further suggests that the native P_{intA} promoter is substantially stronger than the synthetic promoter (P_{J23106}) used in this construct.

Finally, additional truncations of the upstream region (−90 bp and −40 bp relative to the TSS) were generated to further delimit CCR-relevant sequences. The −90 bp fragment retains both predicted IolR binding sites, while the −40 bp fragment contains no complete binding motif. Although both fragments should theoretically contain all regulatory elements of a canonical σ^{70} promoter, neither construct showed detectable GusA activity under any tested condition and were therefore excluded from further analysis. These results indicate that these truncated fragments lack a functional promoter, suggesting that the P_{intA} architecture may deviate from the canonical σ^{70} model and/or requires activating elements located further upstream (see discussion).

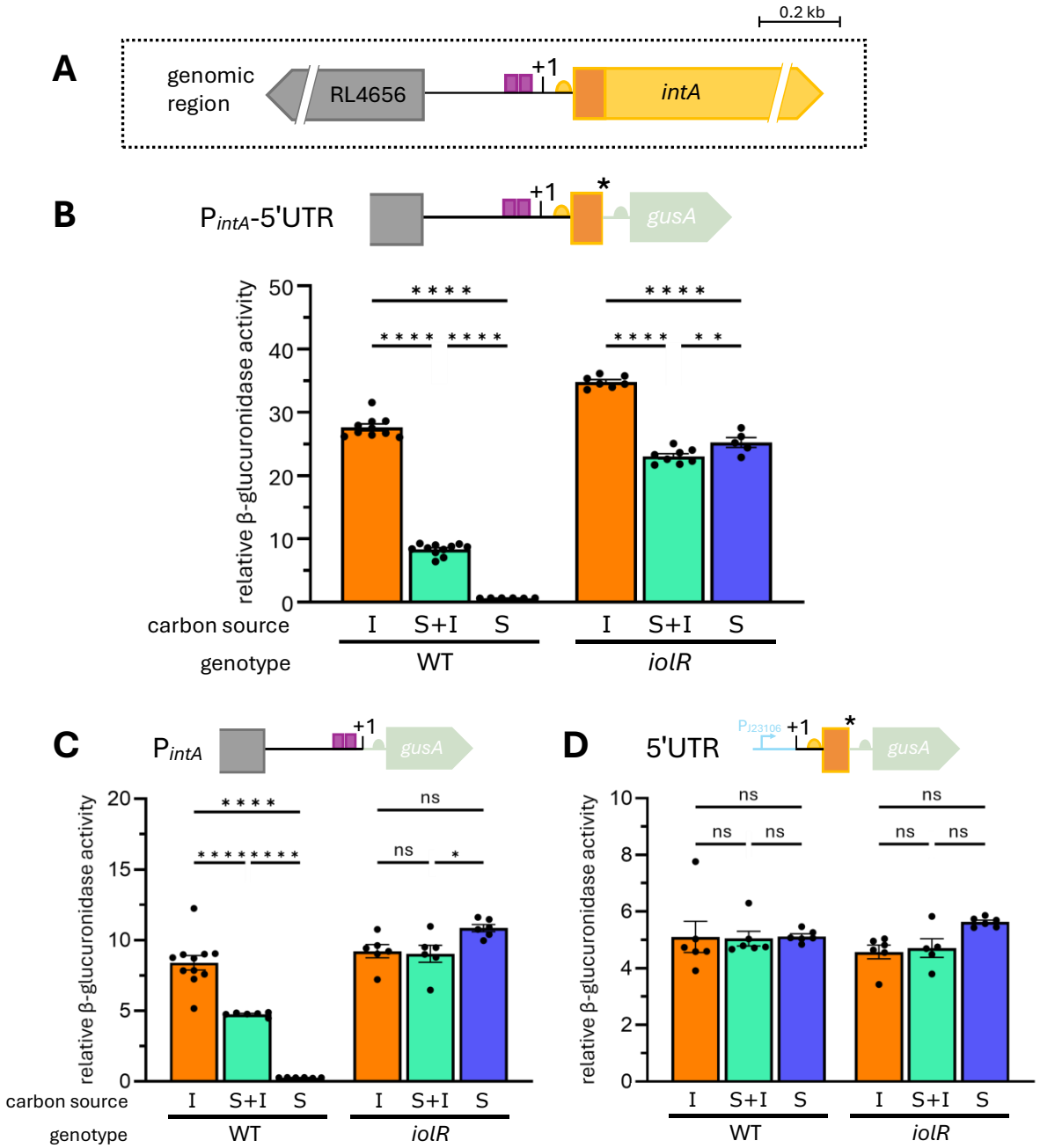


Figure 2.11 Mapping of carbon catabolite repression at *intA* identifies promoter-proximal sequence required for IolR-dependent regulation. (A) The genome region of *intA* is shown at the top, including the upstream gene (grey) and the *intA* coding sequence (yellow). The ribosome binding site is indicated as a half-circle, and the predicted N-terminal signal peptide (SP) is indicated in orange. Purple boxes denote predicted IolR binding motifs, and the experimentally confirmed transcription start site (TSS, +1) is indicated. Schematic representation of *intA* promoter fragments used in transcriptional *gusA* fusions are shown above each data panel. Transcriptional *gusA* fusions include fragments of the *intA* promoter (P_{intA}, extending to the TSS) and/or the 5' untranslated region (5'UTR, extending to the SP). Asterisks indicate constructs in which an additional stop codon was introduced to prevent translation of *intA*. Expression of the 5'UTR fragment was driven by the constitutive promoter J_{23106}. Relative β-glucuronidase activity of the full P_{intA}- 5'UTR **(B)**, only the P_{intA} **(C)**, or only the 5'UTR **(D)** driving *gusA* expression, measured in the WT and *iolR* strain grown on 10 mM *myo*-inositol (I, orange), 20 mM succinate plus 10 mM *myo*-inositol (S+I, green), or 20 mM succinate (S, blue) as the carbon source. Bars represent mean ± SEM (n ≥ 5), with values expressed relative to the adapted Miller units measured for a constitutive control (J23106-*gusA*). Statistical significance reflects Tukey-corrected comparisons between growth conditions within each genotype following a two-way mixed-effects model; ns, not significant, **** $p < 0.0001$, ** $p < 0.01$, * $p < 0.05$.

CCR at *intA* includes an IolR-independent post-transcriptional component

Because IolR is subject to autoregulation, we hypothesized that regulatory effects acting downstream of transcription could propagate upstream through feedback loops, thereby affecting apparent transcriptional outputs. To assess whether regulation of *intABC* extends beyond IolR-mediated control at P_{intA}, complementary translational fusions to alkaline phosphatase (*phoA*) were analysed (Figure 2.12).

The full P_{intA}-5'UTR-*phoA* fusion exhibited strong succinate-dependent repression in the WT strain and partial relief in the *iolR* background (Figure 2.12B), mirroring the behaviour of the corresponding transcriptional *gusA* reporter (Figure 2.11B). Notably, succinate-mediated reduction of expression in the *iolR* mutant was significantly reduced, reaching ~46% of the level observed in inositol-only conditions.

In addition, a *phoA* fusion containing only the 5'UTR, driven by a constitutive promoter, showed a modest yet significant reduction in activity under repressing conditions in both the WT and, importantly, also in the *iolR* mutant background (Figure 2.12C). Although this effect was small relative to promoter-mediated regulation, it cannot be readily explained by promoter activity alone and occurs again independently of IolR.

Together, these results demonstrate that *intABC* expression is subject to an additional layer of post-transcriptional regulation. Importantly, this regulation operates independently of, and in addition to, IolR-mediated transcriptional control.

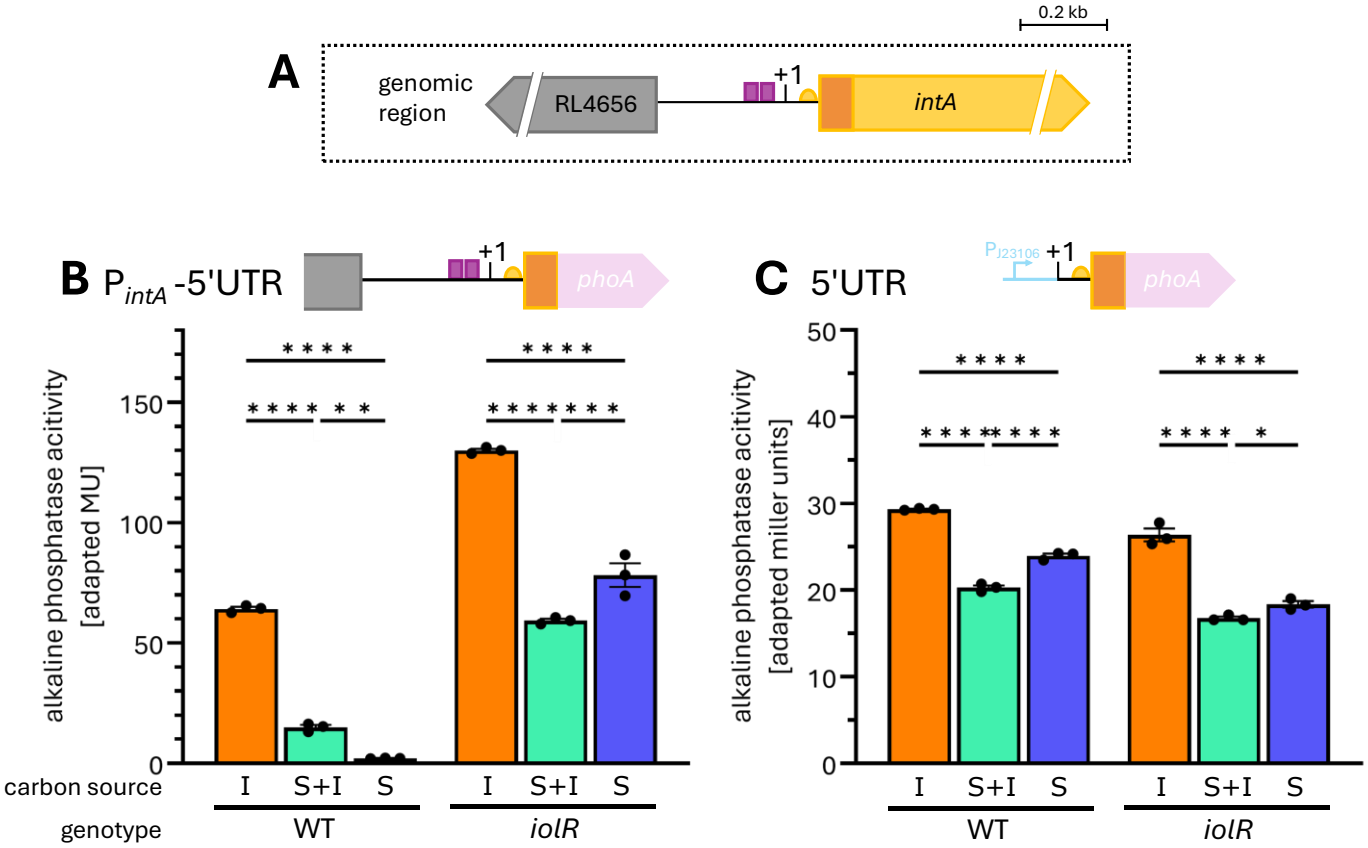


Figure 2.12 PhoA translational reporter analysis of succinate-mediated CCR at the *intA* locus. **(A)** Schematic representation of *intA* promoter fragments used in translational *phoA* fusions. The genomic context of *intA* is shown at the top, including the upstream gene (grey) and the *intA* coding sequence (yellow). The ribosome binding site is indicated as a half-circle, and the predicted N-terminal signal peptide (SP) is indicated in orange. Purple boxes denote predicted IolR binding motifs, and the experimentally confirmed transcription start site (TSS, +1) is indicated. Schematic representation of fragments used in translational *phoA* fusions are shown above each data panel. Translational *phoA* fusions include the full *intA* promoter (P_{intA}, extending to the TSS) and/or the 5' untranslated region (5'UTR, extending to the SP). Expression of 5'UTR fragments was driven by the constitutive promoter J_{23106}. Alkaline phosphatase activity of the full P_{intA}- 5'UTR fusion **(B)**, or only the 5'UTR **(C)** fused to *phoA*, measured in the WT and *iolR* strain grown on 10 mM *myo*-inositol (I, orange), 20 mM succinate plus 10 mM *myo*-inositol (S+I, green), or 20 mM succinate (S, blue) as the carbon source. Bars represent mean ± SEM (n = 3), and statistical significance reflects Tukey-corrected comparisons between growth conditions within each genotype following a two-way ANOVA; ns, not significant, **** $p < 0.0001$, ** $p < 0.01$, * $p < 0.05$.

Discussion

CCR selectively targets transport to establish carbon hierarchy

CCR enables bacteria to prioritize favourable substrates when multiple carbon sources are available. In *R. leguminosarum*, C_4-dicarboxylates such as malate, succinate and fumarate constitute the preferred carbon source in free-living bacteria and the primary carbon supply during symbiosis. Here, we show that C_4-dicarboxylates strongly repress uptake systems of alternative carbon sources, establishing a clear hierarchy in carbon utilization.

Using luminescent biosensors, diauxic growth curves, and transport assays, we show that C_4-dicarboxylates represses ABC transport systems for a wide array of substrates, including monosaccharides (glucose, fructose, xylose), disaccharides (sucrose), and polyols (mannitol, erythritol, inositol) (Figure 2.1). The extent of repression varies between transport systems, ranging from ~40% reduction to near-complete repression at the transcriptional level, with corresponding decreases in transport rates of ~60% to levels indistinguishable from background (Figure 2.4). This variability likely reflects differences in regulatory architecture or substrate specificity. For example, three glucose ABC transporters (*gtaABC* (RL3624-26), *gtbABCD* (RL1824-27), *gtcABCD* (RL4249-52)) have been identified (Karunakaran et al., 2009), with tentative evidence that one is the primary glucose transporter, whereas the others may function as constitutive or secondary systems (Karunakaran, unpublished). Likewise, many ABC transporters display broad substrate specificity; for instance, they can be induced by multiple substrates (Pini et al., 2017), and redundancy between transport systems enables parallel uptake of the same substrate(s) (Jensen et al., 2002), albeit with differing affinities. Such transporters may be less stringently repressed, as their inhibition would restrict multiple substrates.

In contrast, the inositol pathway is tightly regulated by the transcriptional repressor IolR and is therefore strongly repressed in the absence of its substrate but induced in its presence. Inositol uptake is mediated via the ABC transporter encoded by *intABC*. All three genes are markedly upregulated in microarrays of inositol-grown cultures relative to glucose-grown cultures, with expression of *intA* and *intC* increasing 71- and 33-fold,

respectively, and *intB* increasing ~ two-fold (Karunakaran et al., 2009), consistent with RT-qPCR data from this work. This sharply defined regulatory switch makes the inositol pathway a particularly suitable system for mechanistic dissection of CCR.

CCR requires C_4-dicarboxylate uptake

Our genetic screen highlights the central role of C_4-dicarboxylate uptake in CCR. The predominant recovery of insertions in the *dct* locus (*dctA*, *dctB*, *dctD*) and *rpoN* indicates that C_4-dicarboxylate transport is required to generate the CCR signal. However, as DctB, DctD and RpoN are required for *dctA* expression, disruption of any of these genes ultimately reduces DctA-mediated uptake, resulting in a shared transport-deficient phenotype.

Therefore, a key question arising from our screen was whether CCR depends on Dct-mediated signalling/transport or on intracellular C_4-dicarboxylate accumulation itself. To distinguish these possibilities, we replaced the native DctA transporter with the heterologous malate transporter MaeP, restoring malate uptake in *dct* mutants independently of DctBD regulation. Importantly, CCR was reinstated in these strains (Figure 2.7) despite malate transport rates being substantially lower than in the WT (Mitsch et al., 2018) and despite the absence of DctBD-mediated sensing. Thus, intracellular C_4-dicarboxylates are sufficient to trigger repression, arguing against a direct involvement of the Dct system beyond enabling substrate uptake and pointing instead to a signal downstream of transport.

The molecular nature of this signal remains unresolved. Because all three C_4-dicarboxylate feed directly into the TCA cycle, plausible mechanisms include sensing of metabolic flux, redox balance (e.g. NADH/NAD^+ ratios), energy state, or accumulation of downstream metabolites. Alternatively, intracellular C_4-dicarboxylate levels could be sensed by a yet-unidentified CCR-mediating factor, or the relevant signal may arise from broader metabolic reprogramming during C_4-dicarboxylate catabolism. Metabolic model predictions suggest that C_4-dicarboxylates catabolism may yield a more favourable NADH/NAD^+ ratio than sugars, which may be particularly relevant under the microaerobic conditions within nodules and has been proposed as one explanation for why bacteroids are fuelled by C_4-dicarboxylates (Schulte et al., 2021). Distinct metabolic states

associated with C_4-dicarboxylate versus sugar catabolism may therefore provide intrinsic cues that redirect carbon utilization.

The conducted transposon screen identified all known or expected targets and regulators of both C_4-dicarboxylate and inositol uptake. Although only a subset of the original library was screened, the recovery of independent insertions in the same genes suggests substantial coverage. On average, the approximately 15,000 colonies screened correspond to more than two mutants per protein-coding gene; however, as mutant representation following conjugation was not quantified, individual gene coverage cannot be assumed. The absence of additional candidates suggests either that CCR in *R. leguminosarum* does not rely on a dedicated global regulator analogous to CRP-cAMP in *E. coli*, or that such a regulator is essential or at least its mutants unrecoverable under the screening conditions used. Because selection required good growth and sufficient ATP to sustain luminescence output, mutations that severely impair central metabolism or energy homeostasis were likely counter-selected. Similar biases have been noted in other CCR screens, where transport-related mutations dominate recovery (Bringhurst & Gage, 2002). Consequently, while our data clearly demonstrate the requirement for C_4-dicarboxylate transport, additional regulatory layers cannot be excluded.

In *S. meliloti*, the phosphotransferase system (PTS) protein Hpr and its kinase/phosphatase HprK have been implicated in succinate-mediated catabolite repression (Pinedo et al., 2008; Pinedo & Gage, 2009), with HPrK regulating CCR via phosphorylation of HPr at a conserved serine residue. Because PTS mutations often severely impair growth (Pinedo & Gage, 2009; Sánchez-Cañizares et al., 2020), such mutants would likely fail to compete in our screen. Indeed, when we tested an Δ*hprK* mutant of *Rlv*3841 (Figure S2.9), we observed a modest enhancement of CCR, although less pronounced than reported for *S. meliloti*. This suggests PTS-related components may contribute to CCR in rhizobia, although their precise mechanism of action remains to be established.

Post-transcriptional regulation may represent another layer contributing to carbon hierarchy. Such mechanisms would not necessarily be detected in a screen based on transcriptional repression of a promoter fusion. In *R. leguminosarum*, the RNA chaperone Hfq regulates numerous ABC transporters (Mulley et al., 2011), and recent work in

S. meliloti shows that two sRNAs AbcR1/AbcR2, in conjunction with Hfq, downregulate multiple transporters and metabolic genes. Although *intABC* was not among those targets and we observed no loss of repression in a *AbcR1/AbcR2* double mutant (Figure S2.10), these findings highlight the capacity of sRNA to modulate transporter expression. Given the expanding repertoire of sRNAs and our tentative evidence for post-transcriptional modulation of *intABC*, additional sRNA involvement remains a plausible possibility.

Notably, disruption of *iolR* yielded constitutive activation of the inositol transporter, indicating that hierarchical control cannot be maintained in this background even in the presence of succinate. This is consistent with a model in which CCR reinforces IolR-mediated repression to prevent inducer accumulation. Similarly, a genetic screen in *S. meliloti* demonstrated that removal of a negative repressor controlling a transporter can overwhelm the inducer exclusion mechanisms, permitting uptake of an otherwise repressed carbon source (Bringhurst & Gage, 2002).

CCR acts primarily at promoter level via IolR

Our combined qPCR, enzymatic assays, and reporter analyses demonstrate that succinate-mediated repression of the inositol transporter operon (*intABC*) operates through a two-layer regulatory mechanism, comprising IolR-dependent transcriptional control as the primary determinant and an additional IolR-independent post-transcriptional modulation.

Although succinate repression is largely sustained by IolR, a residual repression persists in a *iolR* mutant background specifically at the transporter level (Figure 2.9A-C, Figure 2.11B), indicating that additional regulatory contributions act at *intABC*. This contrasts with *iolC* and *iolR*, which appear to be regulated exclusively via IolR, highlighting a locus-specific regulatory architecture at *intABC*.

Promoter mapping supports a predominantly IolR-dependent transcriptional mechanism. Across *intA* promoter and 5'UTR fragments, we were unable to identify any cis-acting element capable of mediating CCR independently of IolR. All constructs lost full succinate-dependent repression in an *iolR* background, demonstrating that IolR is the dominant mediator at the transcriptional levels under our assay conditions. Together with

the qPCR data, these findings localize the primary CCR response to the promoter–TSS junction and establish transcriptional repression as the major regulatory layer. While downstream sequences contribute to overall expression output, their ability to mediate CCR remains IolR-dependent.

In contrast, translational fusion analyses reveal a second layer of regulation acting downstream of transcription initiation. All translational fusions exhibited significant and reproducible repression even in the absence of IolR, indicating that this effect cannot be attributed to promoter activity and is therefore independent of transcriptional initiation control. Although smaller in magnitude than the transcriptional effect, this observation supports the presence of post-transcriptional modulation, potentially mediated through mRNA structure, stability, or translational efficiency.

Posttranscriptional regulation has been described in *S. meliloti*, where post-transcriptional silencing via sRNAs was shown to fine-tune transcriptional output. (García-Tomsig et al., 2022). While the two sRNAs identified in that study, *AbcR1* and *AbcR2*, do not appear to regulate the *intABC* operon in our system (Figure S2.10), the large number of uncharacterized sRNAs suggests that additional regulatory factors may remain to be identified.

Our findings are consistent with previous work demonstrating conservation of IolR regulation across α-proteobacteria. In *Rlv*3841, the IolR regulon includes *intABC*, *iolCDEB* and *iolR* itself, and the IolR-binding motif identified here (Figure 2.8 and Figure S2.3) closely matches the palindromic consensus defined by Boutte et al. (2008). In *Caulobacter crescentus,* disruption of this motif abolishes basal repression and increases promoter activity, paralleling our observation that reporter constructs lacking the motif lose IolR-mediated repression (Figure 2.11D).

Comparative data from *S. meliloti* support divergence in regulatory architecture within the inositol system. Kohler et al. (2011) reported that none of the catabolic genes of the inositol pathway were subject to CCR, besides *iolA*, the enzyme catalysing the last step. Notably, no IolR-binding motif was identified in the *iolA* promoter in *S. meliloti*, whereas our MEME analysis predicts a putative motif in the *iolA* promoter of *Rlv*3841, suggesting species-specific differences in regulatory wiring.

Two truncated promoter constructs failed to produce GusA activity above background, raising the possibility that the experimentally mapped TSS does not fully capture the functional promoter architecture. Promoter prediction using BPROM (Solovyev & Salamov, 2011) predicts a σ^{70}-dependent -10/-35 motif further upstream, consistent with an alternative TSS mapped in an *Rlv*3841 TSS library (V. K. Ramachandran, unpublished). If validated, this arrangement would position the IolR operator overlapping or slightly downstream of the core promoter elements, rather than upstream, allowing IolR to function as a transcriptional roadblock analogous to LacI repression of the *lac* operon in *E. coli*.

Together, our results support a model in which CCR at the *intABC* locus is primarily executed through IolR-dependent repression at the promoter, while an additional, IolR-independent post-transcriptional mechanism fine-tunes expression. This layered regulatory architecture distinguishes *intABC* from other members of the IolR regulon and highlights the integration of transcriptional and post-transcriptional control in carbon source-dependent gene regulation.

Inducer exclusion sustains IolR-mediated repression

Our data support an inducer exclusion-like mechanism in *R. leguminosarum* in which CCR primarily represses transport of alternative carbon sources. For the inositol pathway, CCR selectively targets *intABC*, whereas repression of downstream catabolic genes is solely dependent on IolR (Figure 2.13). This selective targeting identifies transport as the principal control node in hierarchical carbon utilization.

When inositol is available, low basal expression of catabolic enzymes (Kohler et al., 2011) likely permits minimal production of the IolR-antagonizing effector. Initial inducer accumulation rapidly alleviates IolR-mediated repression, activating both transporter and catabolic genes and establishing a positive feedback loop in which increased transport reinforces induction.

In contrast, in the presence of C_4-dicarboxylates, CCR prevents this loop from initiating. By reducing expression of *intABC*, CCR blocks inositol uptake and thereby prevents inducer accumulation. Without inducer, IolR repression is maintained and the entire inositol regulon remains inactive. Thus, CCR effectively excludes inositol uptake at the

earliest possible step. Selective repression of transport therefore provides an efficient mechanism to enforce hierarchy, as even modest reductions in uptake are sufficient to prevent formation of the induction cascade. Transport measurements support this model: in the presence of succinate, little to no inositol is transported across the cell membrane (Figure 2.4A).

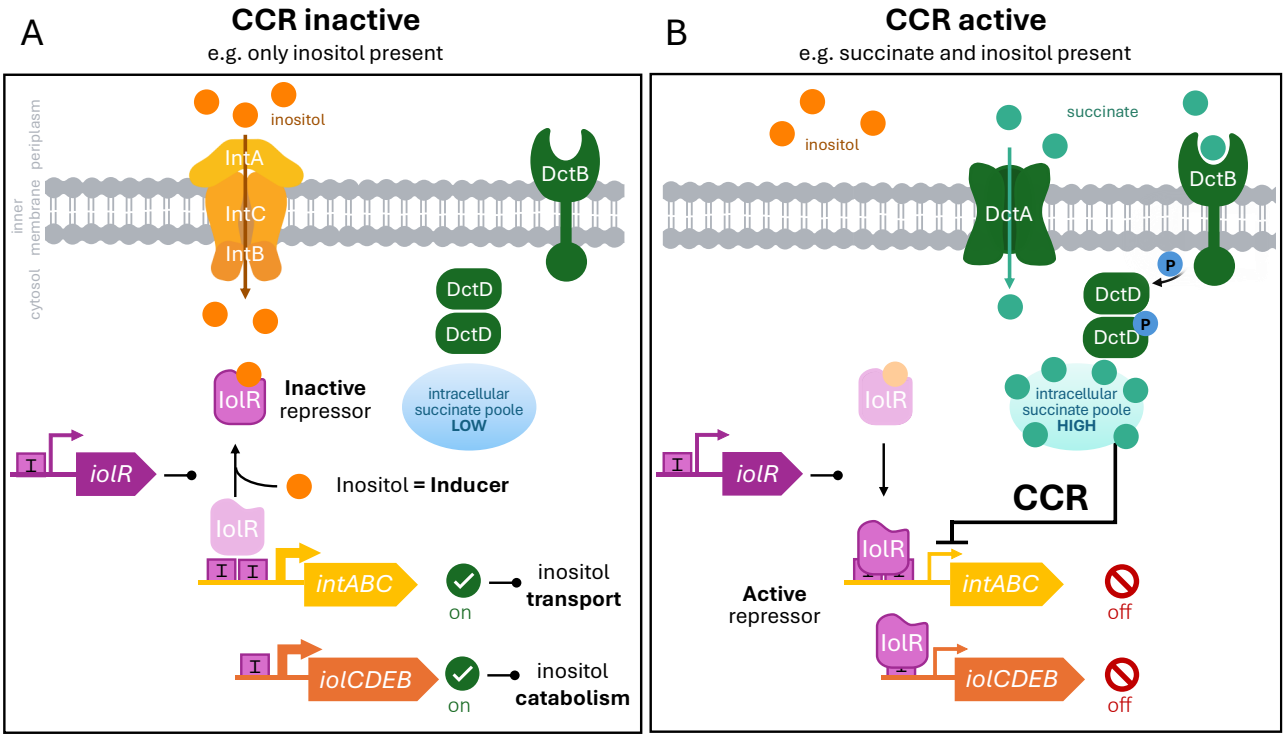


Figure 2.13 Proposed model for carbon catabolite repression (CCR) via inducer exclusion in *Rhizobium leguminosarum*. Genes are depicted as arrows, promoters as right-angled arrows, conserved IolR operator motifs as purple squares, and proteins as organic shapes. **(A)** In the absence of CCR, inositol (orange circles) is transported via the IntABC transporter, leading to relief of IolR-mediated repression of inositol-related genes. This enables expression of the inositol transporter (*intABC*) and catabolic genes (e.g. *iolCDEB*), allowing more inositol uptake and metabolism. **(B)** In the presence of preferred C_4-dicarboxylates such as succinate (green circles), the DctB-DctD two-component sensor-regulator activates transcription of *dctA*, enabling C_4-dicarboxylate uptake and consequently raising intercellular C_4-dicarboxylate levels. CCR represses *intABC* expression, preventing inositol import and thereby maintaining IolR-mediated repression of all inositol-related genes.

Ecological and symbiotic implications of hierarchical carbon utilization

The biological significance of CCR in rhizobia is not immediately apparent. Unlike classical CCR systems, preferential utilization of C_4-dicarboxylates does not translate into faster growth in *R. leguminosarum*. The MGT of *Rlv*3841 on glucose as the sole

carbon source (3.42±0.11 h, mean ± SEM; Sánchez-Cañizares et al., 2020) is shorter than on succinate (4.16±0.09 h) or *myo*-inositol (4.43±0.05 h; Figure S2.1). Thus, prioritization cannot be explained by growth-rate maximization alone. Instead, C_4-dicarboxylate preference may reflect adaptation to the rhizosphere and symbiotic nodule environment. This aligns with metabolic modelling by McGill et al. (2021), who predicted that C_4-dicarboxylate-mediated CCR in *P. aeruginosa* does not maximize growth rate but rather follows a multidimensional strategy that minimizes overall resource investment. Similarly, CCR in rhizobia may optimize metabolic efficiency rather than growth speed per se.

Diauxic growth enforces strict sequential carbon utilization: Only after depletion of the preferred C_4-dicarboxylate is repression of the inositol pathway relieved, allowing the bacteria to switch to the next available substrate. This hierarchy ensures preferential consumption of even small amounts of C_4-dicarboxylates and may be more efficient than co-utilization by minimizing unnecessary expression of secondary transport and catabolic systems and avoiding metabolic interference between competing pathways. In fluctuating soil environments and early infection stages, where carbon availability is heterogeneous, this strategy likely optimizes resource allocation and improves competitive fitness. For example, inositol is a prominent component of plant root exudate (Pini et al., 2017) and its catabolism contributes to competitive root colonization and nodule formation in peas (Fry et al., 2001; Knights, 2021; Kohler et al., 2010). However, this pathway is not upregulated in bacteroids, indicating that inositol utilization is mainly relevant in the rhizosphere or early infection (Karunakaran et al., 2009). In our hands, a *iolR* mutant did not display significant differences in nodule number or nitrogen fixation on pea (Figure S2.11), although it apparently regrows significantly less well from nodule extracts than WT (Ford, 2021). More generally, inappropriate upregulation of metabolic pathways at inappropriate times can hinder the bacteria's ability to transition into the nodule environment (Pardo Díaz, 2022). Together, these observations suggest that tight regulation of carbon uptake is critical during niche transitions, and hierarchical carbon control likely optimizes metabolic allocation across the rhizobial life cycle.

Conclusion

Here we show that C_4-dicarboxylates impose a broad hierarchy in *R. leguminosarum* by repressing multiple alternative ABC transport operons. By replacing DctA with MaeP to uncouple Dct signalling from uptake, we demonstrate that intracellular C_4-dicarboxylate availability is sufficient to trigger repression, arguing against a direct signalling role for the Dct system beyond transport. Using the inositol pathway as a mechanistically tractable model, we localize CCR to transporter control at *intABC* and show that repression is reinforced through an inducer exclusion–like mechanism that sustains IolR-mediated regulation of the inositol regulon.

Together, our data support a model in which CCR prioritizes preferred substrates by targeting uptake pathways, with pathway-specific repressors translating transport control into coordinated regulon-level shutdown. This framework provides a basis for future work aimed at identifying the downstream intracellular signal that links C_4-dicarboxylate uptake to global transporter repression.

References

Arwas, R., McKay, I. A., Rowney, F. R. P., Dilworth, M. J., & Glenn, A. R. (1985). Properties of organic acid utilization mutants of rhizobium leguminosarum strain 300. *Microbiology*, *131*(8), 2059–2066. https://doi.org/10.1099/00221287-131-8-2059

Beringer, J. E. (1974). R Factor transfer in Rhizobium leguminosarum. *Microbiology*, *84*(1), 188–198. https://doi.org/10.1099/00221287-84-1-188

Bertin, C., Yang, X., & Weston, L. A. (2003). The role of root exudates and allelochemicals in the rhizosphere. *Plant and Soil*, *256*(1), 67–83. https://doi.org/10.1023/A:1026290508166

Bharwad, K., & Rajkumar, S. (2019). Rewiring the functional complexity between Crc, Hfq and sRNAs to regulate carbon catabolite repression in Pseudomonas. *World Journal of Microbiology and Biotechnology*, *35*(9), 140. https://doi.org/10.1007/s11274-019-2717-7

Boutte, C. C., Srinivasan, B. S., Flannick, J. A., Novak, A. F., Martens, A. T., Batzoglou, S., Viollier, P. H., & Crosson, S. (2008). Genetic and computational identification of a conserved bacterial metabolic module. *PLoS Genetics*, *4*(12), e1000310. https://doi.org/10.1371/journal.pgen.1000310

Bringhurst, R. M., & Gage, D. J. (2002). Control of inducer accumulation plays a key role in succinate-mediated catabolite repression in Sinorhizobium meliloti. *Journal of Bacteriology*, *184*(19), 5385–5392. https://doi.org/10.1128/JB.184.19.5385-5392.2002

Buchanan-Wollaston, V. (1979). Generalized transduction in Rhizobium leguminosarum. *Journal of General Microbiology*, *112*(1), 135–142. https://doi.org/10.1099/00221287-112-1-135

Choi, K.-H., Gaynor, J. B., White, K. G., Lopez, C., Bosio, C. M., Karkhoff-Schweizer, R. R., & Schweizer, H. P. (2005). A Tn7-based broad-range bacterial cloning and expression system. *Nature Methods*, *2*(6), 443–448. https://doi.org/10.1038/nmeth765

Choi, K.-H., Mima, T., Casart, Y., Rholl, D., Kumar, A., Beacham, I. R., & Schweizer, H. P. (2008). Genetic tools for select-agent-compliant manipulation of Burkholderia pseudomallei. *Applied and Environmental Microbiology*, *74*(4), 1064–1075. https://doi.org/10.1128/AEM.02430-07

Deutscher, J. (2008). The mechanisms of carbon catabolite repression in bacteria. *Current Opinion in Microbiology*, *11*(2), 87–93. https://doi.org/10.1016/j.mib.2008.02.007

Ditta, G., Stanfield, S., Corbin, D., & Helinski, D. R. (1980). Broad host range DNA cloning system for gram-negative bacteria: Construction of a gene bank of Rhizobium meliloti. *Proceedings of the National Academy of Sciences*, *77*(12), 7347–7351. https://doi.org/10.1073/pnas.77.12.7347

Dombrecht, B., Marchal, K., Vanderleyden, J., & Michiels, J. (2002). Prediction and overview of the RpoN-regulon in closely related species of the rhizobiales. *Genome Biology*, *3*(12), research0076.1. https://doi.org/10.1186/gb-2002-3-12-research0076

Finan, T. M., Wood, J. M., & Jordan, D. C. (1983). Symbiotic properties of C_4-dicarboxylic acid transport mutants of Rhizobium leguminosarum. *Journal of Bacteriology*, *154*(3), 1403–1413. https://doi.org/10.1128/jb.154.3.1403-1413.1983

Ford, B. L. (2021). *Investigating the basis of competitive nodulation and bacteroid development in Rhizobium leguminosarum*. PhD thesis, University of Oxford.

Fry, J., Wood, M., & Poole, P. S. (2001). Investigation of myo-inositol catabolism in Rhizobium leguminosarum bv. viciae and its effect on nodulation competitiveness. *Molecular Plant-Microbe Interactions*, *14*(8), 1016–1025. https://doi.org/10.1094/MPMI.2001.14.8.1016

Garcia, P. P., Bringhurst, R. M., Arango Pinedo, C., & Gage, D. J. (2010). Characterization of a two-component regulatory system that regulates succinate-mediated catabolite repression in Sinorhizobium meliloti. *Journal of Bacteriology*, *192*(21), 5725–5735. https://doi.org/10.1128/JB.00629-10

García-Tomsig, N. I., Robledo, M., diCenzo, G. C., Mengoni, A., Millán, V., Peregrina, A., Uceta, A., & Jiménez-Zurdo, J. I. (2022). Pervasive RNA regulation of metabolism enhances the root colonization ability of nitrogen-fixing symbiotic α-rhizobia. *mBio*, *13*(1), e03576-21. https://doi.org/10.1128/mbio.03576-21

Glenn, A. R., & Brewin, N. J. (1981). Succinate-resistant mutants of Rhizobium leguminosarum. *Microbiology*, *126*(1), 237–241. https://doi.org/10.1099/00221287-126-1-237

Glenn, A. R., Poole, P. S., & Hudman, J. F. (1980). Succinate uptake by free-living and bacteroid forms of Rhizobium leguminosarum. *Microbiology*, *119*(1), 267–271. https://doi.org/10.1099/00221287-119-1-267

Görke, B., & Stülke, J. (2008). Carbon catabolite repression in bacteria: Many ways to make the most out of nutrients. *Nature Reviews Microbiology*, *6*(8), 613–624. https://doi.org/10.1038/nrmicro1932

Hanahan, D. (1983). Studies on transformation of Escherichia coli with plasmids. *Journal of Molecular Biology*, *166*(4), 557–580. https://doi.org/10.1016/S0022-2836(83)80284-8

Herrou, J., & Crosson, S. (2013). Myo-inositol and D-ribose ligand discrimination in an ABC periplasmic binding protein. *Journal of Bacteriology*, *195*(10), 2379–2388. https://doi.org/10.1128/JB.00116-13

Iyer, B., Rajput, M. S., Jog, R., Joshi, E., Bharwad, K., & Rajkumar, S. (2016). Organic acid mediated repression of sugar utilization in rhizobia. *Microbiological Research*, *192*, 211–220. https://doi.org/10.1016/j.micres.2016.07.006

Jensen, J. B., Peters, N. K., & Bhuvaneswari, T. V. (2002). Redundancy in periplasmic binding protein-dependent transport systems for trehalose, sucrose, and maltose in Sinorhizobium meliloti. *Journal of Bacteriology*, *184*(11), 2978–2986. https://doi.org/10.1128/JB.184.11.2978-2986.2002

Johnston, A. W. B., & Beringer, J. E. (1975). Identification of the rhizobium strains in pea root nodules using genetic markers. *Journal of General Microbiology*, *87*(2), 343–350. https://doi.org/10.1099/00221287-87-2-343

Karunakaran, R., Ramachandran, V. K., Seaman, J. C., East, A. K., Mouhsine, B., Mauchline, T. H., Prell, J., Skeffington, A., & Poole, P. S. (2009). Transcriptomic analysis of Rhizobium leguminosarum biovar viciae in symbiosis with host plants Pisum sativum and Vicia cracca. *Journal of Bacteriology*, *191*(12), 4002–4014. https://doi.org/10.1128/JB.00165-09

Kawai, S., Suzuki, H., Yamamoto, K., & Kumagai, H. (1997). Characterization of the L-malate permease gene (maeP) of Streptococcus bovis ATCC 15352. *Journal of Bacteriology*, *179*(12), 4056–4060. https://doi.org/10.1128/jb.179.12.4056-4060.1997

Knights, H. E. (2021). *Genome-wide identification of colonisation determinants in Rhizobium leguminosarum using BarSeq*. PhD thesis, University of Oxford.

Knights, H. E., Ramachandran, V. K., Jorrin, B., Ledermann, R., Parsons, J. D., Aroney, S. T. N., & Poole, P. S. (2024). Rhizobium determinants of rhizosphere persistence and root colonization. *The ISME Journal*, *18*(1), wrae072. https://doi.org/10.1093/ismejo/wrae072

Kohler, P. R. A., Choong, E.-L., & Rossbach, S. (2011). The RpiR-like repressor IolR regulates inositol catabolism in Sinorhizobium meliloti. *Journal of Bacteriology*, *193*(19), 5155–5163. https://doi.org/10.1128/JB.05371-11

Kohler, P. R. A., Zheng, J. Y., Schoffers, E., & Rossbach, S. (2010). Inositol catabolism, a key pathway in Sinorhizobium meliloti for competitive host nodulation. *Applied and Environmental Microbiology*, *76*(24), 7972–7980. https://doi.org/10.1128/AEM.01972-10

Ledermann, R. (2017). *Role of general stress response in trehalose biosynthesis for functional rhizobia-legume symbiosis*. PhD thesis, ETH Zurich https://doi.org/10.3929/ETHZ-B-000202317

Magasanik, B. (1961). Catabolite Repression. *Cold Spring Harbor Symposia on Quantitative Biology*, *26*(0), 249–256. https://doi.org/10.1101/SQB.1961.026.01.031

Mandal, N. C., & Chakrabartty, P. K. (1993). Succinate-mediated catabolite repression of enzymes of glucose metabolism in root-nodule bacteria. *Current Microbiology*, *26*(5), 247–251. https://doi.org/10.1007/BF01575912

Mauchline, T. H., Fowler, J. E., East, A. K., Sartor, A. L., Zaheer, R., Hosie, A. H. F., Poole, P. S., & Finan, T. M. (2006). Mapping the Sinorhizobium meliloti 1021 solute-binding protein-

dependent transportome. *Proceedings of the National Academy of Sciences*, *103*(47), 17933–17938. https://doi.org/10.1073/pnas.0606673103

McGill, S. L., Yung, Y., Hunt, K. A., Henson, M. A., Hanley, L., & Carlson, R. P. (2021). Pseudomonas aeruginosa reverse diauxie is a multidimensional, optimized, resource utilization strategy. *Scientific Reports*, *11*(1), 1457. https://doi.org/10.1038/s41598-020-80522-8

Miller, J. H. (1972). *Experiments in Molecular Genetics*. Cold Spring Harbor Laboratory Press.

Mitsch, M. J., diCenzo, G. C., Cowie, A., & Finan, T. M. (2018). Succinate transport is not essential for symbiotic nitrogen fixation by Sinorhizobium meliloti or Rhizobium leguminosarum. *Applied and Environmental Microbiology*, *84*(1), e01561-17. https://doi.org/10.1128/AEM.01561-17

Monod, J. (1942). Recherches Sur La Croissance. In *Des Cultures Bactériennes* (2nd edn). Hermann.

Mulley, G., White, J. P., Karunakaran, R., Prell, J., Bourdes, A., Bunnewell, S., Hill, L., & Poole, P. S. (2011). Mutation of GOGAT prevents pea bacteroid formation and N2 fixation by globally downregulating transport of organic nitrogen sources. *Molecular Microbiology*, *80*(1), 149–167. https://doi.org/10.1111/j.1365-2958.2011.07565.x

Nair, A., & Sarma, S. J. (2021). The impact of carbon and nitrogen catabolite repression in microorganisms. *Microbiological Research*, *251*, 126831. https://doi.org/10.1016/j.micres.2021.126831

Parche, S., Beleut, M., Rezzonico, E., Jacobs, D., Arigoni, F., Titgemeyer, F., & Jankovic, I. (2006). Lactose-over-glucose preference in Bifidobacterium longum NCC2705: glcP, encoding a glucose transporter, is subject to lactose repression. *Journal of Bacteriology*, *188*(4), 1260–1265. https://doi.org/10.1128/JB.188.4.1260-1265.2006

Pardo Díaz, J. (2022). *Construction of gene coexpression networks and transcriptomic analysis for Rhizobium leguminosarum*. PhD thesis, University of Oxford.

Pinedo, C. A., Bringhurst, R. M., & Gage, D. J. (2008). Sinorhizobium meliloti mutants lacking phosphotransferase system enzyme HPr or EIIA are altered in diverse processes, including carbon metabolism, cobalt requirements, and succinoglycan production. *Journal of Bacteriology*, *190*(8), 2947–2956. https://doi.org/10.1128/JB.01917-07

Pinedo, C. A., & Gage, D. J. (2009). HPrK regulates succinate-mediated catabolite repression in the gram-negative symbiont Sinorhizobium meliloti. *Journal of Bacteriology*, *191*(1), 298–309. https://doi.org/10.1128/JB.01115-08

Pini, F., East, A. K., Appia-Ayme, C., Tomek, J., Karunakaran, R., Mendoza-Suárez, M., Edwards, A., Terpolilli, J. J., Roworth, J., Downie, J. A., & Poole, P. S. (2017). Bacterial

biosensors for in vivo spatiotemporal mapping of root secretion. *Plant Physiology*, *174*(3), 1289–1306. https://doi.org/10.1104/pp.16.01302

Poole, P. S., Blyth, A., Reid, C. J., & Walters, K. (1994). Myo-inositol catabolism and catabolite regulation in Rhizobium leguminosarum bv. viciae. *Microbiology*, *140*(10), 2787–2795. https://doi.org/10.1099/00221287-140-10-2787

Poole, P. S., Franklin, M., Glenn, A. R., & Dilworth, M. J. (1985). The transport of L-glutamate by Rhizobium leguminosarum involves a common amino acid carrier. *Microbiology*, *131*(6), 1441–1448. https://doi.org/10.1099/00221287-131-6-1441

Prell, J., & Poole, P. (2006). Metabolic changes of rhizobia in legume nodules. *Trends in Microbiology*, *14*(4), 161–168. https://doi.org/10.1016/j.tim.2006.02.005

Reid, C. J., Walshaw, D. L., & Poole, P. S. (1996). Aspartate transport by the Dct system in Rhizobium leguminosarum negatively affects nitrogen-regulated operons. *Microbiology*, *142*(9), 2603–2612. https://doi.org/10.1099/00221287-142-9-2603

Ronson, C. W., Lyttleton, P., & Robertson, J. G. (1981). C_4-dicarboxylate transport mutants of Rhizobium trifolii form ineffective nodules on Trifolium repens. *Proceedings of the National Academy of Sciences*, *78*(7), 4284–4288. https://doi.org/10.1073/pnas.78.7.4284

Ronson, C. W., Nixon, B. T., Albright, L. M., & Ausubel, F. M. (1987). Rhizobium meliloti ntrA (rpoN) gene is required for diverse metabolic functions. *Journal of Bacteriology*, *169*(6), 2424–2431. https://doi.org/10.1128/jb.169.6.2424-2431.1987

Sambrook, J., Fritsch, E. F., Maniatis, T., Russell, D. W., & Green, M. R. (1989). *Molecular cloning: A laboratory manual*. Cold Spring Harbor Laboratory Press.

Sánchez-Cañizares, C., Prell, J., Pini, F., Rutten, P., Kraxner, K., Wynands, B., Karunakaran, R., & Poole, P. S. (2020). Global control of bacterial nitrogen and carbon metabolism by a PTS^{Ntr} -regulated switch. *Proceedings of the National Academy of Sciences*, *117*(19), 10234–10245. https://doi.org/10.1073/pnas.1917471117

Schneider, E. (2001). ABC transporters catalyzing carbohydrate uptake. *Research in Microbiology*, *152*(3–4), 303–310. https://doi.org/10.1016/S0923-2508(01)01201-3

Schulte, C. C. M., Borah, K., Wheatley, R. M., Terpolilli, J. J., Saalbach, G., Crang, N., De Groot, D. H., Ratcliffe, R. G., Kruger, N. J., Papachristodoulou, A., & Poole, P. S. (2021). Metabolic control of nitrogen fixation in rhizobium-legume symbioses. *Science Advances*, *7*(31), eabh2433. https://doi.org/10.1126/sciadv.abh2433

Solovyev, V., & Salamov. (2011). Automatic annotation of microbial genomes and metagenomic sequences. In *Metagenomics and its Applications in Agriculture, Biomedicine and Environmental Studies* (pp. 61–78). Nova Science Publishers.

Sonnleitner, E. (2025). A comparative analysis: Molecular mechanisms of carbon catabolite repression in bacteria. *Annual Review of Microbiology*, *79*(1), 241–262. https://doi.org/10.1146/annurev-micro-050624-031622

Sonnleitner, E., Wulf, A., Campagne, S., Pei, X.-Y., Wolfinger, M. T., Forlani, G., Prindl, K., Abdou, L., Resch, A., Allain, F. H.-T., Luisi, B. F., Urlaub, H., & Bläsi, U. (2018). Interplay between the catabolite repression control protein Crc, Hfq and RNA in Hfq-dependent translational regulation in Pseudomonas aeruginosa. *Nucleic Acids Research*, *46*(3), 1470–1485. https://doi.org/10.1093/nar/gkx1245

Świątek, M. A., Urem, M., Tenconi, E., Rigali, S., & Van Wezel, G. P. (2012). Engineering of N-acetylglucosamine metabolism for improved antibiotic production in Streptomyces coelicolor A3(2) and an unsuspected role of NagA in glucosamine metabolism. *Bioengineered*, *3*(5), 280–285. https://doi.org/10.4161/bioe.21371

Thoma, S., & Schobert, M. (2009). An improved Escherichia coli donor strain for diparental mating. *FEMS Microbiology Letters*, *294*(2), 127–132. https://doi.org/10.1111/j.1574-6968.2009.01556.x

Tjahjono, O. (2025). *Regulation of global metabolism by PTS-NTR in Rhizobium leguminosarum*. PhD thesis, University of Oxford.

Tsirigos, K. D., Peters, C., Shu, N., Käll, L., & Elofsson, A. (2015). The TOPCONS web server for consensus prediction of membrane protein topology and signal peptides. *Nucleic Acids Research*, *43*(W1), W401–W407. https://doi.org/10.1093/nar/gkv485

Turner, B. L., Papházy, M. J., Haygarth, P. M., & Mckelvie, I. D. (2002). Inositol phosphates in the environment. *Philosophical Transactions of the Royal Society of London. Series B: Biological Sciences*, *357*(1420), 449–469. https://doi.org/10.1098/rstb.2001.0837

Ucker, D. S., & Signer, E. R. (1978). Catabolite-repression-like phenomenon in Rhizobium meliloti. *Journal of Bacteriology*, *136*(3), 1197–1200. https://doi.org/10.1128/jb.136.3.1197-1200.1978

Van Den Bogaard, P. T. C., Kleerebezem, M., Kuipers, O. P., & De Vos, W. M. (2000). Control of lactose transport, β-galactosidase activity, and glycolysis by CcpA in Streptococcus thermophilus: Evidence for carbon catabolite repression by a Non-phosphoenolpyruvate-dependent phosphotransferase system sugar. *Journal of Bacteriology*, *182*(21), 5982–5989. https://doi.org/10.1128/JB.182.21.5982-5989.2000

Wheatley, R. M., Ford, B. L., Li, L., Aroney, S. T. N., Knights, H. E., Ledermann, R., East, A. K., Ramachandran, V. K., & Poole, P. S. (2020). Lifestyle adaptations of Rhizobium from rhizosphere to symbiosis. *Proceedings of the National Academy of Sciences*, *117*(38), 23823–23834. https://doi.org/10.1073/pnas.2009094117

Yoshida, K., Yamaguchi, M., Morinaga, T., Kinehara, M., Ikeuchi, M., Ashida, H., & Fujita, Y. (2008). Myo-inositol catabolism in Bacillus subtilis. *Journal of Biological Chemistry*, *283*(16), 10415–10424. https://doi.org/10.1074/jbc.M708043200

Zhang, Y., & Skolnick, J. (2005). TM-align: A protein structure alignment algorithm based on the TM-score. *Nucleic Acids Research*, *33*(7), 2302–2309. https://doi.org/10.1093/nar/gki524

Supplementary Information

Table S2.1 Primers used in this work.

Primer	Sequence 5' → 3'	Description
oxp2327	GATGATCTTCTCGCTGCCGA	primer pair amplifying the *glmS*-RL2383 intergenic region
oxp2328	GCTCTGGCCAATGAGGTTCT	
oxp3060	CACAGCATAACTGGACTGATTTC	primers binding on end of Tn*7* transposable element
oxp3061	ATTAGCTTACGACGCTACACCC	
oxp0270	CATTCCGCTGGTTTACGT	primer pair amplifying *intA* internal fragment
oxp6815	CGAATTCAATGCCGCTGGAG	
oxp0271	CGTCAAGGACTTCGTCAC	primer pair amplifying across *intA*-*intB* intergenic region
oxp6816	CCGGCGAGGATCTTCATCAA	
oxp2506	CCGCATGACCGAGGAATTG	primer pair amplifying *intB* internal fragment
oxp1742	CGTTCTTGAAGACGCCGTT	
oxp6817	CGAAGCAACGCAGATCAAGG	primer pair amplifying across *intB*-*intC* intergenic region
oxp1741	GTCAGACGCTGCGAATTC	
oxp2504	GATCGTCGTTGGTCTGCTG	primer pair amplifying *intC* internal fragment
oxp6818	TAGACCTTGACGAGATGCGC	
oxp5439	ATTCCTGCTCGTTGGAAGCA	SP1-SP3 used in 5'RACE of *intA*
oxp5440	GACGTAAACCAGCGGAATGC	
oxp5441	GAAACGTCGTTCTGTGCGTC	
oxp5437	TCACGCCGTGATCGATGAAA	SP1-SP3 used in 5'RACE of *intB*
oxp5438	ATCCCATTCTCGAGTGCGTC	
oxp6816	CCGGCGAGGATCTTCATCAA	
oxp6992	GATCAGCAGACCAACGACGA	SP1-SP3 used in 5'RACE of *intC*
oxp6993	CGGTGATGATGACCTGCGTA	
oxp1741	GTCAGACGCTGCGAATTC	
oxp6980	GATGAAGTCGATCGGCAATCTG	RT-qPCR primers for *rpoD*
oxp6981	GCTTCGACCATTTCCTTCTTGG	
oxp7001	GATCTCGACGTCACGGTGTT	RT-qPCR primers for *intA*
oxp7002	GTGACGAGCTGGAAGGGAAT	
oxp7003	CGCACTCGAGAATGGGATTG	RT-qPCR primers for *intB*
oxp7004	CGCCGTGATCGATGAAACC	
oxp7009	AGCATGGGTGTCGGATATGA	RT-qPCR primers for *intC*
oxp7010	GTCATGACGCCGAGGATGAT	
oxp7274	ATGGGCTGCATCGTCTATGA	RT-qPCR primers for *iolC*
oxp7275	AGGAAGCCGGACATGAAGG	
oxp7276	TTTTCCGACCTGCAGAGCAT	RT-qPCR primers for *iolR*
oxp7277	AAGCCGGAGAGCAGATTGG	

oxp7293	GCTAATTCGATCATGCATGAG CTCA**TTTACGGCTAGCTCAGT CCTAGGTATAGTGCTAGC**TGC AGGAATTCCTCGAGATAGACTG	Single stranded DNA oligo containing J23106 (bold) used in HiFi assembly of pOPS2353
oxp7294	TTCGATCATGCATGAGCTCAAG GCGAGCAGTCACCAATATAGC	Forward amplification primer for P_{intA} amplification for HiFi assembly of pOSP2354, pOPS2355, pOPS2358
oxp7295	TATCTCGAGGAATTCCTGCATTC CCCGCGCCACCTCTC	Reverse amplification primer for P_{intA} amplification for HiFi assembly of pOPS2355
oxp7296	TTCGATCATGCATGAGCTCA**TTTACG GCTAGCTCAGTCCTAGGTATAGTGC TAGC**TTGCGGCTTCAGAGCAAATG	Forward amplification primer binding to 5'UTR of *intA,* for HiFi assembly of pOPS2356 and pOPS2359; contains J23106 as spacer(bold)
oxp7297	TATCTCGAGGAATTCCTGCATCAG ACGCCGACAGTTTCCGC	Reverse amplification primer for *intA*(SP)* amplification for HiFi assembly of pOSP2354, and pOPS2356; * denotes extra stop codon (UGA)
oxp7299	TATCTCGAGGAATTCCTGCACTG TGAACCCGGATTCGATTG	Reverse amplification primer for P_{iolC} amplification for HiFi assembly of pOSP2357
oxp7300	ACAGGCATTTCTGGTGTCCGGAC GCCGACAGTTTCCGC	Reverse amplification primer for *intA*(SP):*phoA* fusion for HiFi assembly of pOPS2358 and pOPS2359
oxp7301	CGGACACCAGAAATGCCTGTTC	Forward amplification primer for *E. coli* K12 *phoA* chain for HiFi assembly of pOPS2358 and pOPS2359
oxp7303	TTCGATCATGCATGAGCTCACAG GAGCTTGCCGACCGC	Forward amplification primer for P_{iolC} amplification for HiFi assembly of pOSP2357
oxp7332	CTTCTCGAGGAATTCCTGCATTATT TCAGCCCCAGAGC	Reverse amplification primer for *E. coli* K12 *phoA* chain for HiFi assembly of pOPS2358 and pOPS2359

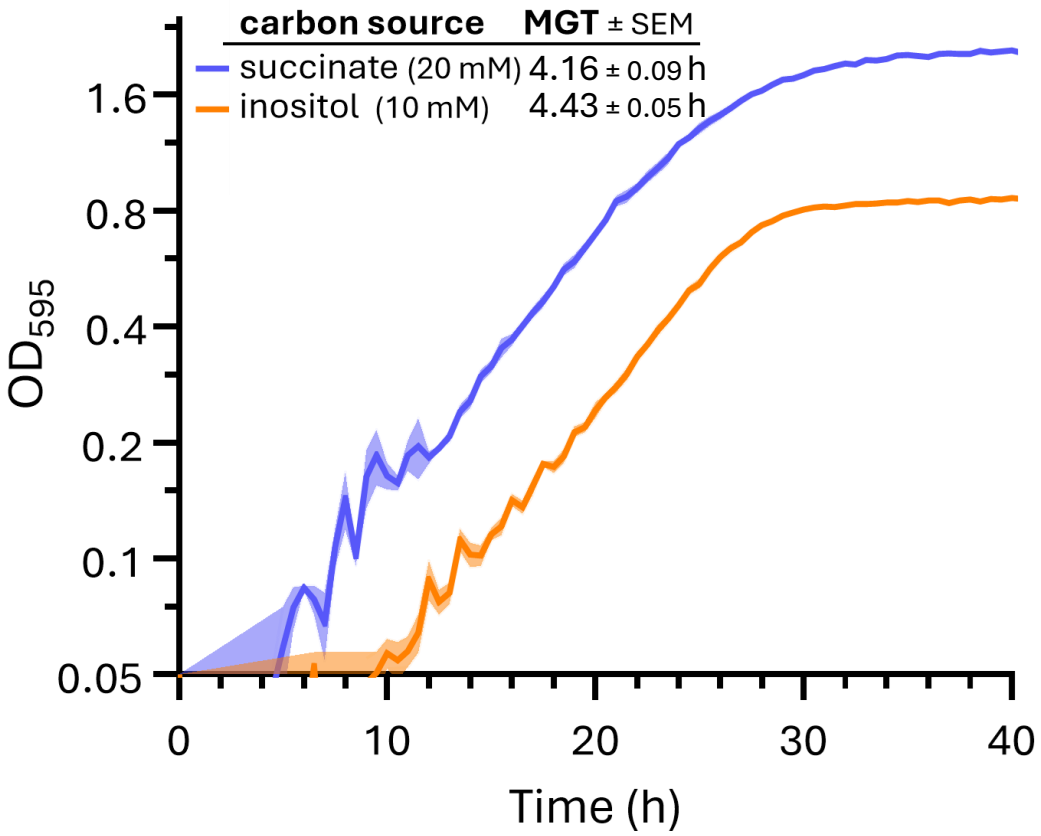


Figure S2.1 Growth curves of *R. leguminosarum* on single carbon sources. Blank-corrected average OD_{595} (four replicates; SEM shown as bands) in UMS with 20 mM succinate (blue), or 10 mM *myo*-inositol (orange) as the carbon source. Optical density was measured every 30 min and mean generation time (MGT ± SEM) was calculated from the exponential growth phase of each replicate.

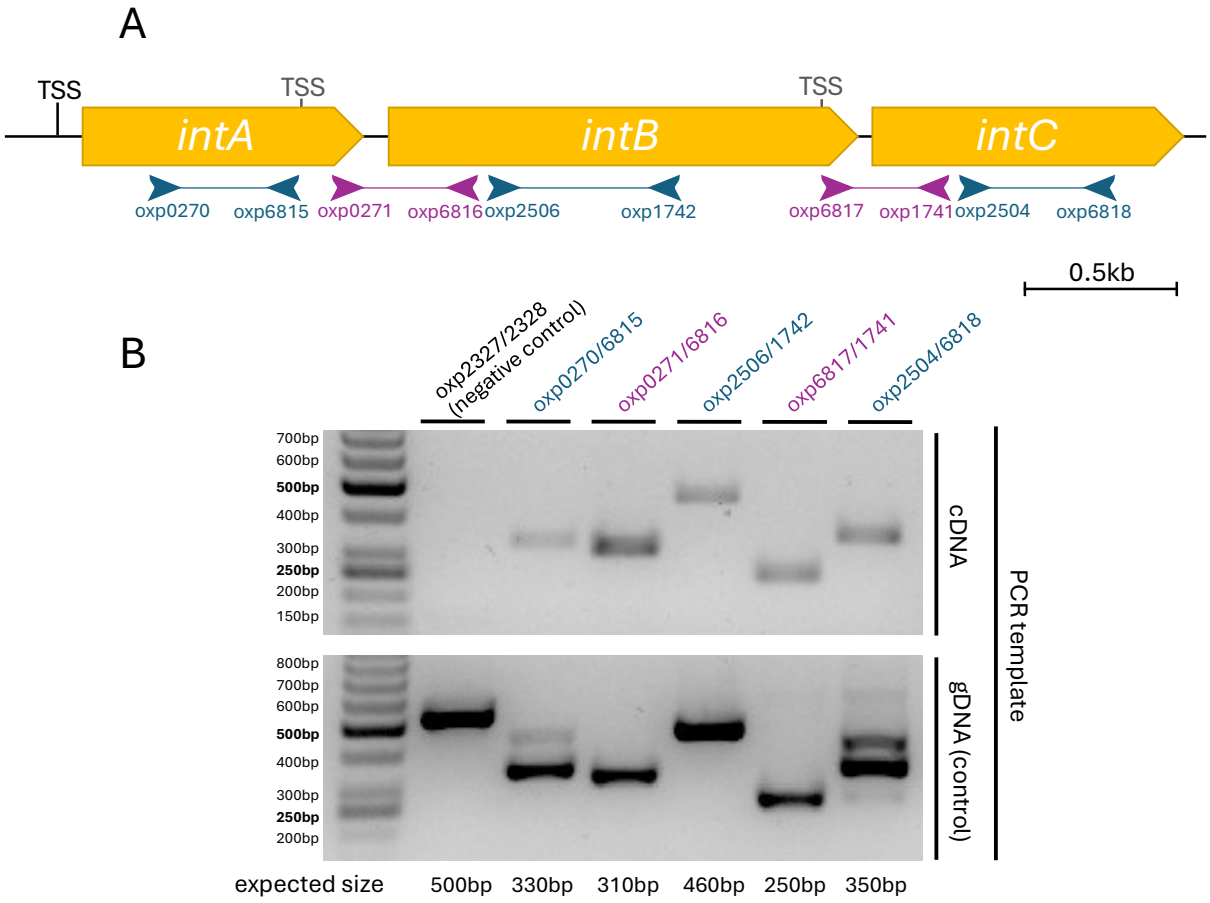


Figure S2.2 Transcriptional organisation and regulation of the *R. leguminosarum intABC* operon. (A) Genomic organisation of the *intABC* locus, with coding sequences shown as yellow arrows and transcription start sites (TSS) identified by 5'-RACE indicated as vertical lines (primary TSS in black, additional putative TSS in grey). Primer binding sites used for RT-PCR are indicated below the genes, with blue primers amplifying internal gene fragments and purple primers spanning intergenic regions. Primers used for 5'-RACE are listed in Table S2.1. **(B)** RT-PCR results demonstrating co-transcription of *intA*, *intB*, and *intC*. Total RNA was extracted from WT cells grown on UMS with 10 mM *myo*-inositol and reverse-transcribed using random hexamer primers. PCR amplification was performed using the primer pairs shown in (A). Amplification of intergenic (purple) regions support transcription as an operon. Control reactions include the amplification of the *glmS*-RL2383 intergenic region (oxp2327/2328) and testing all primers on genomic DNA (gDNA). Expected amplicon sizes are indicated below each lane.

A

Gene	Strand[1]	Start[2]		End[2]	*P*-value	Upstream motif
RL0776 (*iolA*)	+	208	-	181	$2.37\times e^{-9}$	GGGTTTGCGGCTCATCGGTTTGACCTCC
RL1495 (*iolC*)	-	105	-	78	$5.38\times e^{-12}$	GTCAATTCGGAATGTTTATTCCATTTTG
RL1496 (*iolR*)	+	40	-	13	$1.20\times e^{-12}$	GATAATATGGAATATTTGTTTCATCTCG
RL4655 (*intA*)	-	165	-	138	$6.49\times e^{-12}$	TGTTCTGCGGAATATTCATTCCATTTTC
	+	137	-	110	$5.13\times e^{-13}$	GATTTTACGGTTTGTTTGTTCCGTTTTG
RL3622 (*idhA*)	-	69	-	42	$3.92\times e^{-11}$	GAATTTCTGGAATTTTCATTCCACCTTC
	+	41	-	14	$8.10\times e^{-12}$	GATAATTCGGTTTATTTGTTCCGAATTC

[1] The motif was found on the same strand (+) or on the reverse complement strand (-) in relation to the coding sequence of the corresponding gene. [2] Start and end mark the position of the motif in base-pairs in relation to the start-codon of the coding sequence of the corresponding gene.

B

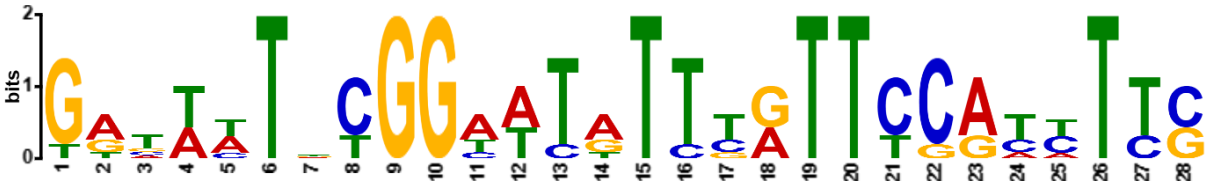


Figure S2.3 Identification of the conserved IolR-binding motif in the promoters of known inositol-regulated genes. (A) The upstream regions of genes and operons that are known to be required for *myo*-inositol transport and catabolism were searched for common sequence motifs using MEME (Bailey et al., 2015), as previously done by Boutte et al., (2008). **(B)** This search identified a conserved partially palindromic motif (MEME *E*-value $3.2\times e^{-4}$), which is shown as a weblogo cartoon (Crooks et al., 2004), where the relative nucleotide frequency at each of the 28 positions of the motif is depicted in proportion to the height of the letter.

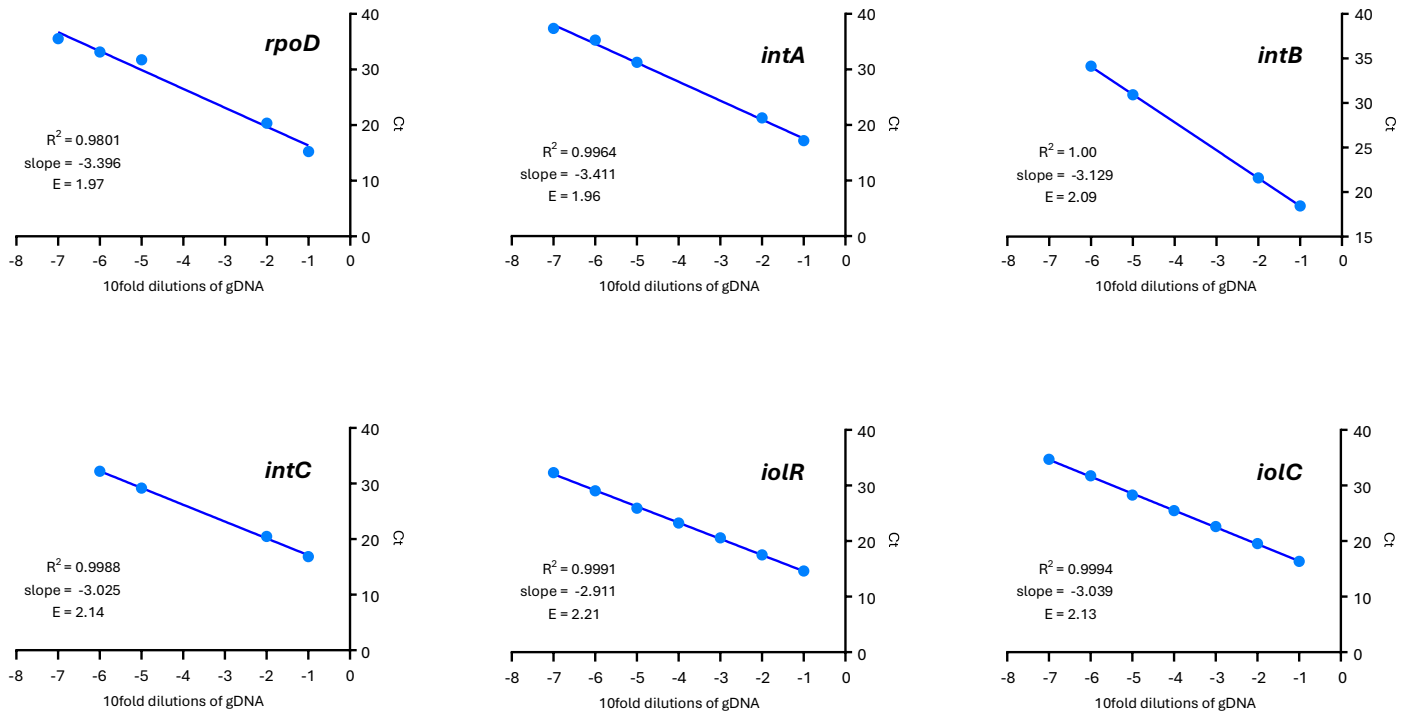


Figure S2.4 Standard curves used to calculate amplification efficiencies for RT-qPCR primers.

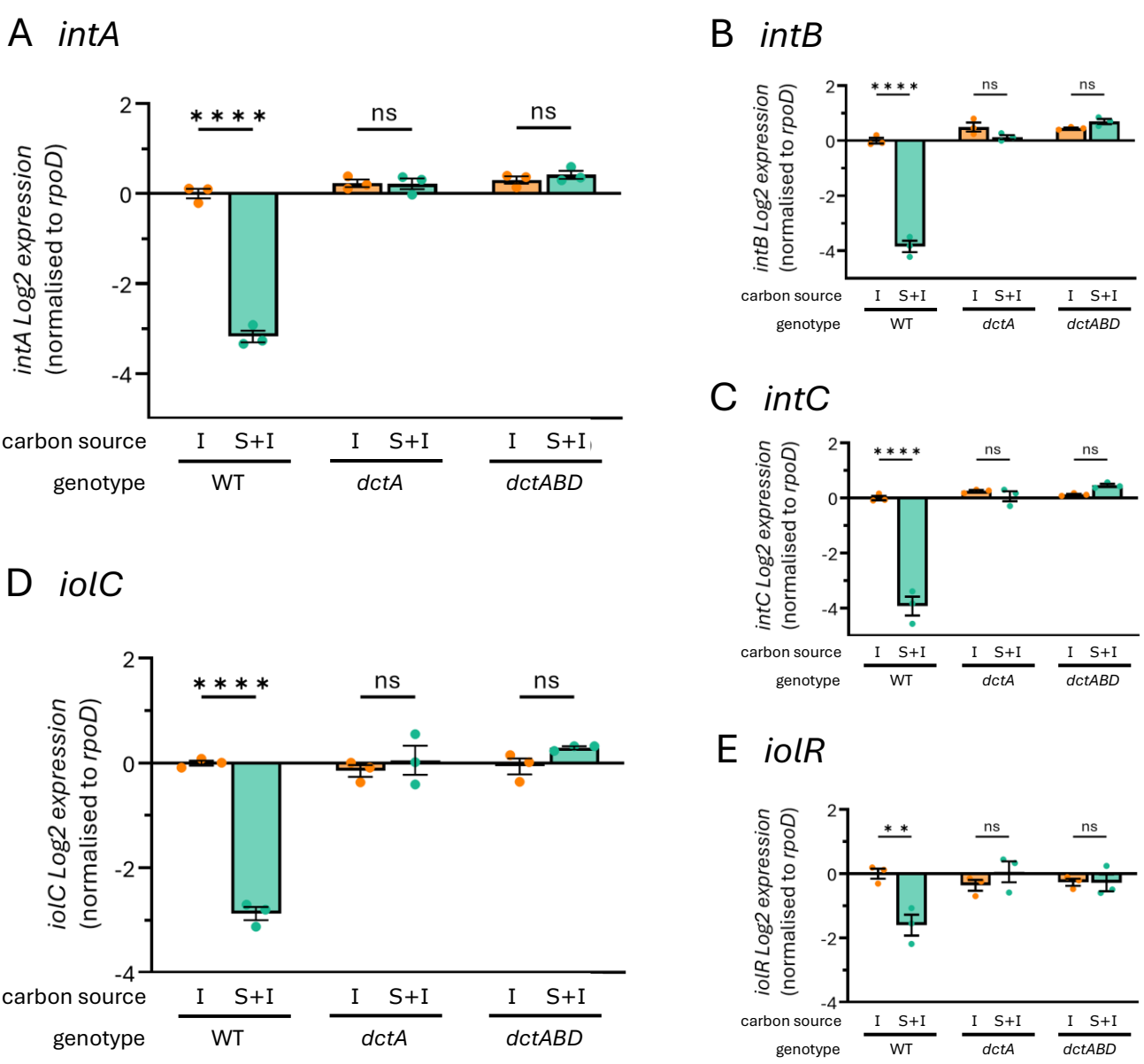


Figure S2.5 *Dct* mutants do not display succinate-mediated CCR of inositol utilisation genes. qPCR analysis of genes encoding the inositol ABC transporter (*intA* **(A)**, *intB* **(B)**, *intC* **(C)**), the first inositol catabolism gene *iolC* **(D)** and the transcriptional regulator *iolR* **(E)** in WT, *dctA*, and *dctABD*, grown on *myo*-inositol (I, orange), succinate plus *myo*-inositol (S+I; green), or succinate (S, blue). Bars represent means ± SEM of $\log_2$-transformed Pfaffl relative expression (n=3), normalized to *rpoD* and expressed relative to WT grown on *myo*-inositol. WT data are the same as shown in Figure 2.9. Data were analysed by two-way ANOVA (genotype x carbon source), followed by Sidak-adjusted planned pairwise comparisons. Adjusted *p*-values are shown above comparisons with ns, not significant, **** $p < 0.0001$, ** $p < 0.01$.

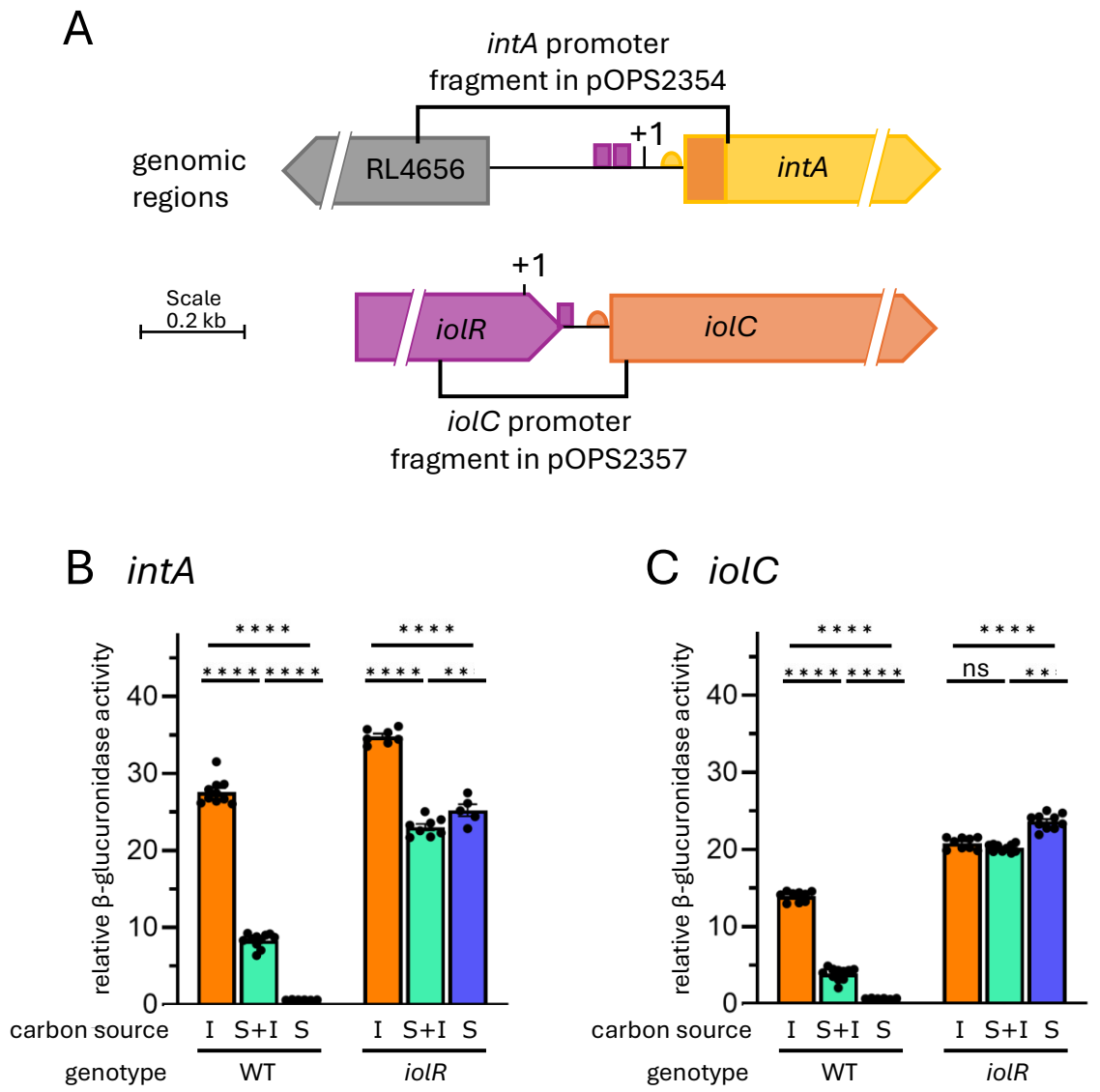


Figure S2.6 Partial and complete IolR-dependence distinguish succinate-mediated CCR of *intA* and *iolC*. (A) Schematic representation of the genomic context and promoter fragments of *intA* (top) and *iolC* (bottom) used for transcriptional *gusA* fusions. Genes are shown as arrows, ribosome binding sites are indicated as half-circles, and the predicted N-terminal signal peptide of IntA is indicated in orange. Purple boxes denote predicted IolR binding motifs, and experimentally confirmed or predicted transcription start sites (TSS, +1) are indicated. Relative β-glucuronidase activity of the P_{intA}–*gusA* fusion **(B)** or P_{iolC}–*gusA* fusion **(C)** measured in WT and *iolR* strains grown on 10 mM *myo*-inositol (I, orange), 20 mM succinate plus 10 mM *myo*-inositol (S+I, green), or 20 mM succinate (S, blue). In WT cells, succinate strongly represses both promoters, consistent with carbon catabolite repression (CCR). In the *iolR* background, repression of P_{iolC} is fully abolished, whereas repression of P_{intA} is only partially relieved. Bars represent mean ± SEM ($n \geq 5$), with values expressed relative to a constitutive control (J_{23106}-*gusA*). Statistical significance reflects Sidak-corrected comparisons between growth conditions within each genotype following a two-way mixed-effects model; ns, not significant, **** $p < 0.0001$, ** $p < 0.01$. Data for the P_{intA}–*gusA* fusion are identical to those presented in Figure 2.11B and are replotted here for direct comparison with the P_{iolC}–*gusA* fusion.

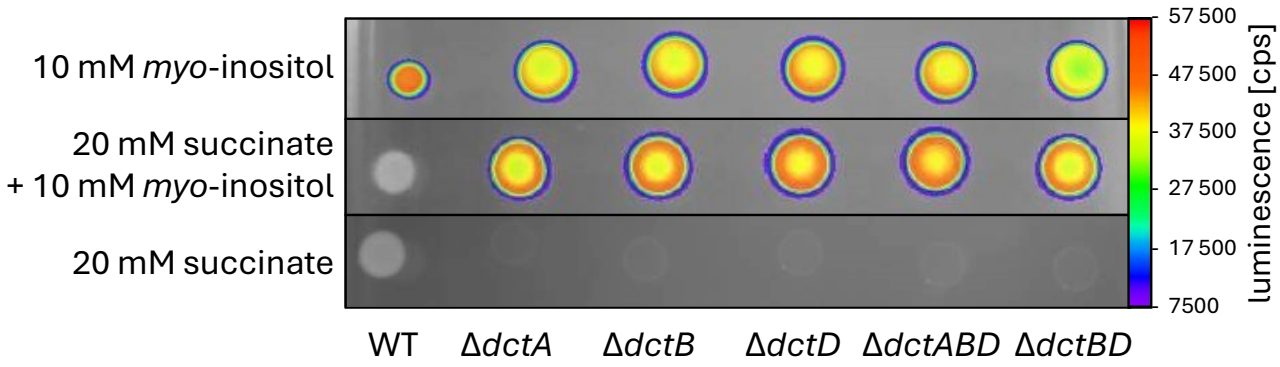


Figure S2.7 Luminescence of *myo*-inositol biosensor in WT Rlv3841 and *dct* mutants (OPS3601-05). Under CCR conditions (succinate and *myo*-inositol), the WT strain exhibits strongly repressed P_{intA} – *lux* expression (below the detection level) while *dct* mutants exhibit levels comparable to when plated on *myo*-inositol alone. On succinate no luminescence is observed and all *dct* mutants show only residual growth. Strains were spotted onto UMS plates containing the mentioned carbon sources and imaged in the NightOWL.

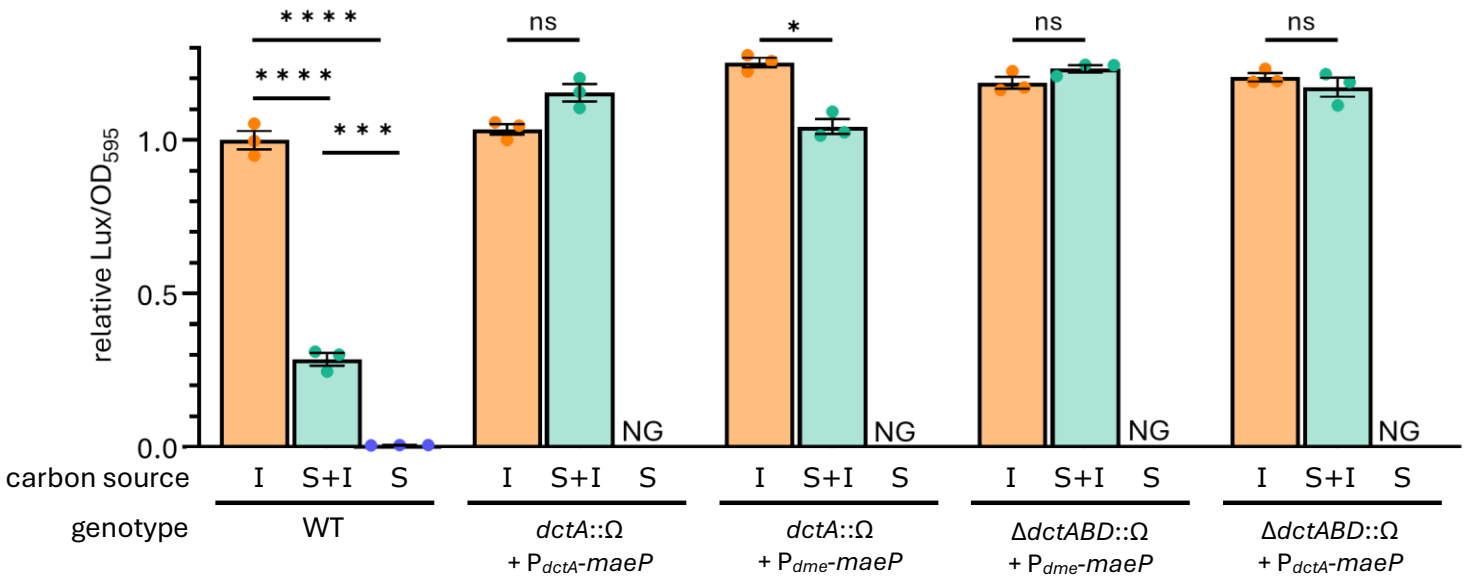


Figure S2.8 Complementation with malate-specific transporter does not restore CCR on succinate. Luminescence of a *myo*-inositol biosensor in WT *Rlv*3841 and *dct* mutants complemented with the malate-specific MaeP transporter from *Streptococcus gallolyticus* driven by two promoters, normalised to optical density (Lux/OD_{595}) and expressed relative to WT grown in *myo*-inositol. Luminescence was quantified from liquid cultures grown in UMS containing 10 mM *myo*-inositol (I, orange), 20 mM succinate plus 10 mM *myo*-inositol (S+I, green), or 20 mM succinate (S, blue). Bars represent mean ± SEM (n =3). NG = no growth observed in this condition. Statistical significance reflects Tukey-corrected comparisons between growth conditions within the WT following a One-way ANOVA and Sidak-corrected comparisons between growth conditions within each genotype following a mixed-effects model for all others, where **** $p < 0.0001$, *** $p < 0.001$, * $p < 0.05$, ns not significant.

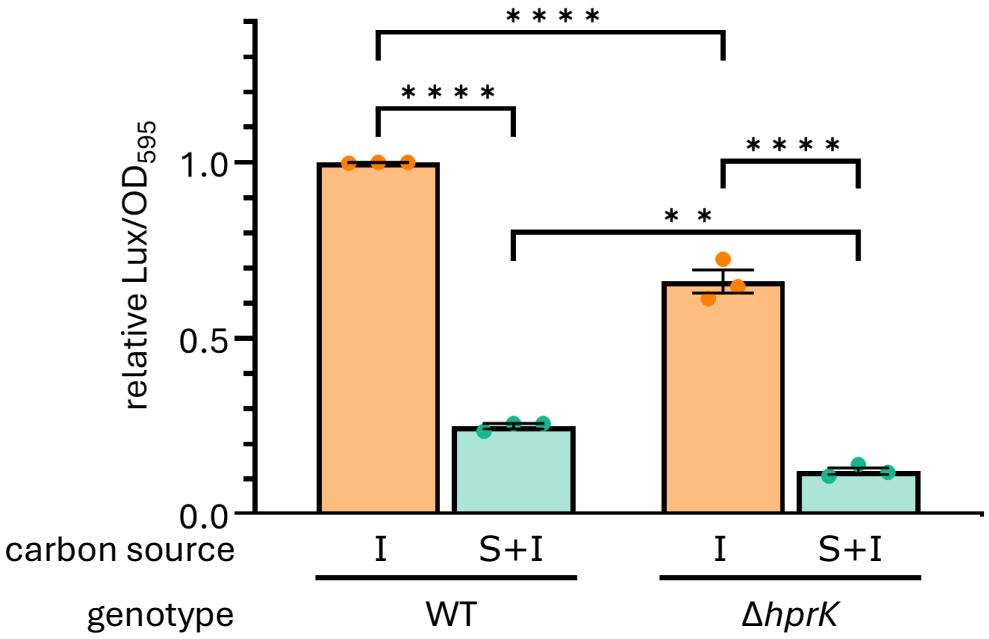


Figure S2.9 Δ*hprK* mutants shows enhanced CCR. Luminescence normalised to optical density (Lux/OD_{595}) from a *myo*-inositol biosensor strain was quantified from liquid cultures grown in UMS containing 10 mM *myo*-inositol (I, orange), or 20 mM succinate plus 10 mM *myo*-inositol (S+I, green). Bars represent mean ± SEM (n = 3), with values expressed relative to WT grown in *myo*-inositol. Statistical significances reflect Sidak-corrected planned comparisons following a two-way ANOVA, with **** $p < 0.0001$, ** $p < 0.01$.

Additional context:

According to Pinedo et al. (2008), the PTS protein Hpr plays a role in succinate-mediated catabolite repression in *S. meliloti*, and, later, they confirmed this was due to phosphorylation of Hpr by HprK (Pinedo and Gage 2009). We tested a *hprK* mutant (OPS3656 = AA081 (*Rlv*3841 *hprK*::ΩSpec; Sánchez-Cañizares et al., 2020) × pLMB686) and found that, indeed, it shows significantly strengthened or enhanced CCR compared to the WT strain (Fig. S6). In the presence of succinate, it repressed the *myo*-inositol biosensor more severely than the WT and even in the absence of a C_4-dicarboxylate there is less luminescence from the *myo*-inositol bioreporter. This support Pinedo et al.'s (2009) idea that a Δ*hprK* mutant is "stuck" in its repressive state; which is in agreement with the severely reduced growth rate of this mutant observed on various carbon sources (Sánchez-Cañizares et al., 2020).

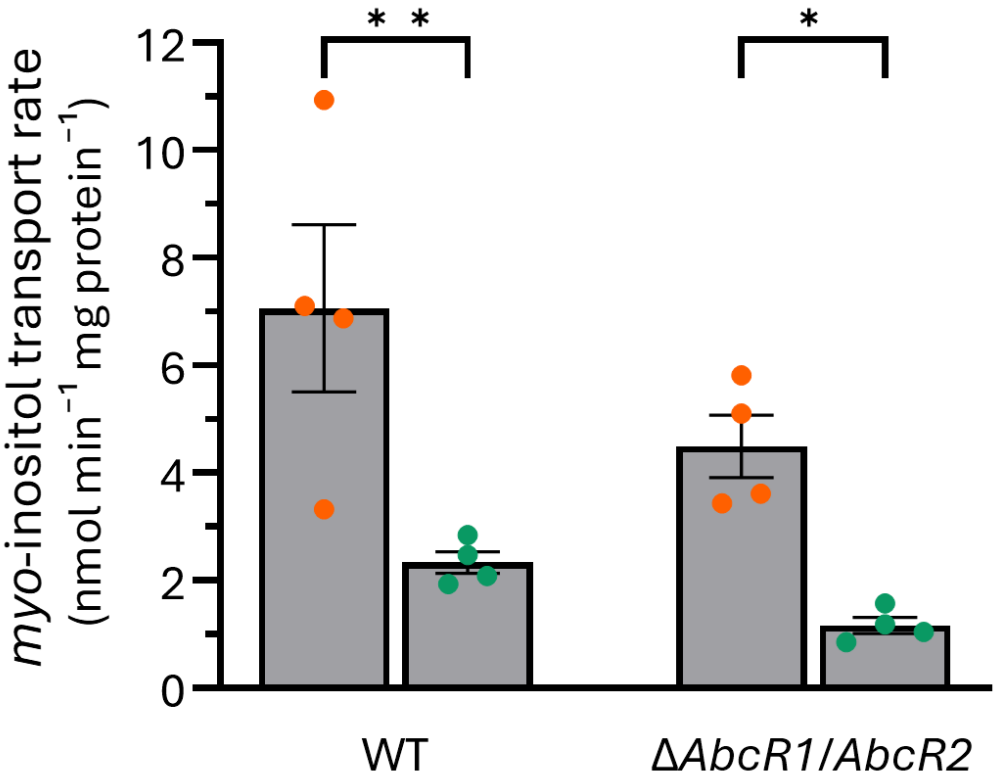


Figure S2.10 Δ*AbcR1/AbcR2* double mutant still shows succinate-dependent CCR. Transport rates of tritiated *myo*-inositol measured in WT or a mutant where the two sRNAs *AbcR1/AbcR2* were deleted (OPS3804, made by Olivia Tjahjono, unpublished). Cells were grown on *myo*-inositol (I, orange) or succinate and *myo*-inositol (S+I, green) before transport rates were measured. Bars indicate mean ± SEM with individual biological replicates shown. Statistical analyses were performed using a mixed effects model with Sidak-type post hoc tests. Statistical significance is indicated as follows: $p < 0.05$ (*); $p < 0.01$ (**).

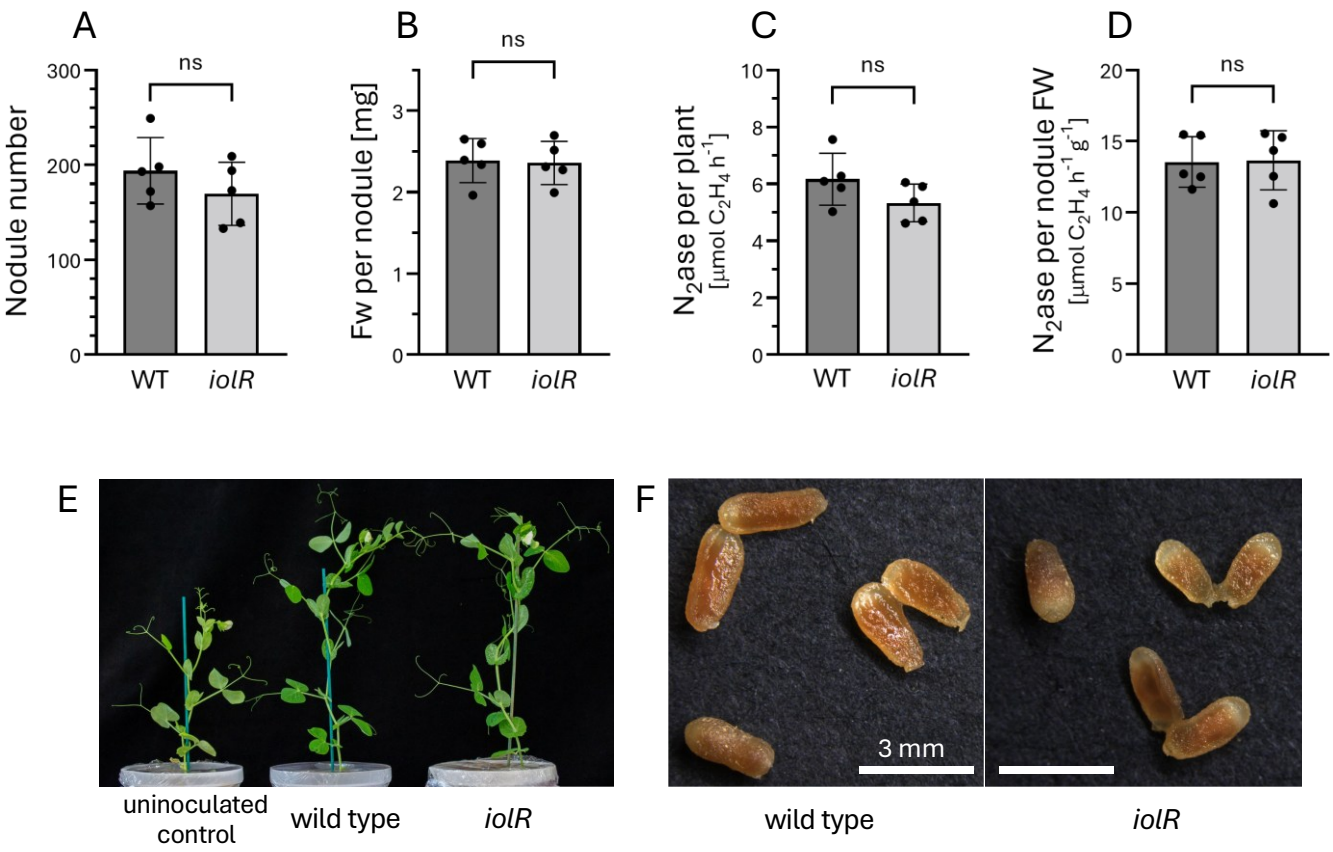


Figure S2.11 A *iolR* mutant is not affected in its symbiosis with pea plants. *Pisum sativum* cv. Avola seedlings were inoculated with wild-type or *iolR R. leguminosarum*. Plants were assayed for nodule number **(A)**, fresh weight (FW) per nodule **(B)**, nitrogenase activity per plant **(C)**, and nitrogenase activity per nodule fresh weight **(D)**. Exemplary plants **(E)** and nodules cross sections **(F)** inoculated with WT or *iolR* mutants. Each strain was tested on n = 5 plants. Statistical significance was determined with two-tailed unpaired *t*-tests, with ns = not significant.

Supplementary Methods – Assessing the iolR mutant on pea plants

Pea plant set-up, inoculation, and symbiotic performance assessment were done as described in Chapter 4. Plants were harvested after 25 dpi.

3

Misregulation of the Dct system uncouples C_4-dicarboxylate transport from physiological function

Chapter 3

This chapter is presented in the form of a manuscript to maintain structural consistency across the thesis. The work described here originated as part of the carbon catabolite repression study (Chapter 2) but has since developed into a distinct line of investigation.

This chapter is not intended for publication in its current form as additional work would be required to fully resolve the underlying mechanisms. Instead, it is presented here to reflect the chronological development of the study and to contextualize these findings within the broader scope of the thesis

To facilitate integration with preceding results, minor adaptations to the conventional manuscript structure have been made to facilitate cross-referencing between Chapters 2 and 3.

Misregulation of the Dct system uncouples C_4-dicarboxylate transport from physiological function

Abstract

C_4-dicarboxylates, primarily succinate and malate, are central to rhizobial metabolism during both free-living and symbiotic stages, and their uptake is mediated by the DctA permease under the control of the DctBD two-component regulatory system. Despite extensive characterisation of this system, it remains unclear whether broader cellular responses to C_4-dicarboxylates depend primarily on transport activity, DctBD signalling, or their coordinated interaction. In this study, two complementary approaches were employed to uncouple DctA-mediated transport from DctBD-dependent regulation in order to disentangle their individual contributions in *Rhizobium leguminosarum*. Complementing findings from Chapter 2, we show that misregulation within the dicarboxylate transport system – through spontaneous mutations or engineered constructs – consistently results in growth defects and impaired symbiotic nitrogen fixation. Remarkably, these phenotypes occur despite restoration of C_4-dicarboxylate transport, indicating that transport capacity alone does not determine physiological outcome. Instead, alternative explanations, including interference with nitrogen signalling pathways are explored. Together, these findings demonstrate that proper physiological function depends on the integration of DctA-mediated transport with the DctBD regulatory system and its coordination with broader metabolic networks, particularly those linking carbon and nitrogen metabolism. This highlights the Dct system as an integrated transport–regulatory module rather than a simple uptake pathway.

KEYWORDS *Rhizobium leguminosarum*, C_4-dicarboxylate transport, Dct system, carbon–nitrogen coordination; metabolic regulation

Introduction

Biological nitrogen fixation by rhizobia in symbiosis with legume plants represents a central process in global nitrogen cycling. Within root nodules, differentiated bacteroids reduce atmospheric nitrogen to ammonia, which is supplied to the host plant in exchange for carbon sources and other nutrients derived from photosynthesis (Poole & Allaway, 2000; Udvardi & Poole, 2013). Carbon supply is, in fact, a major limiting factor for nitrogen fixation (Hardy, 1977). Nitrogen fixation is a highly energetic process, where the nitrogenase enzyme requires a minimum of 16 ATP to reduce one molecule of N_2 (Hoffman et al., 2014), making it one of the most energetically expensive biological reactions known. Accordingly, the plant must sustain a continuous and substantial flux of carbon towards the bacteroids. The photosynthate sucrose is produced by the plant and transported from the shoot to the nodules, where it is converted to C_4-dicarboxylates such as malate, succinate, and fumarate, which are then supplied to the bacteroids as their primary energy source for nitrogen fixation (Day & Copeland, 1991; Vance et al., 1998). Despite the central importance of this metabolic exchange, the regulatory basis for the preferential utilisation of C_4-dicarboxylates over other available carbon sources remains incompletely understood (see Chapter 2 for detailed discussion).

As C_4-dicarboxylates are the primary carbon source for bacteroids, their uptake is essential for effective symbiosis across a variety of rhizobial species, and disruption of this process results in a Fix^- phenotype (Arwas et al., 1985; Finan et al., 1983; Glenn & Brewin, 1981; Ronson et al., 1981). In contrast, mutations in genes encoding transport and metabolism of other sugars do not affect symbiosis, indicating that they are not important or of lesser importance for a functional symbiosis (Wheatley et al., 2020). Consistent with this, nodules infected by rhizobial mutants impaired in C_4-dicarboxylate uptake accumulate excessive starch and show signs of early senescence, indicating an inability to utilise plant-derived carbon (Mitsch et al., 2018; Ronson et al., 1981; Yurgel & Kahn, 2005).

Although the capacity to transport C_4-dicarboxylates is broadly conserved among bacteria, its physiological relevance differs markedly between species. In *Escherichia coli*, for example, C_4-dicarboxylates are readily utilised through dedicated aerobic and

anaerobic transport systems, although they are typically secondary to preferred substrates such as glucose (Davies et al., 1999; Six et al., 1994). By contrast, rhizobia depend predominantly on C_4-dicarboxylates during symbiosis and assimilate them preferentially also during free-living growth, underscoring the central role of their uptake system in these organisms.

In rhizobia, uptake of C_4-dicarboxylates is mediated by the dicarboxylate transport system (Dct) (Figure 3.1; reviewed in Yurgel & Kahn, 2004), which is highly conserved across most members of the Rhizobiaceae family and consists of three genes : *dctB* and *dctD,* which encode a two-component regulatory system that responds to the presence of C_4-dicarboxylates and induces expression of *dctA*, which encodes the transport protein itself. Importantly, this means that C_4-dicarboxylate sensing and transport are mediated by distinct components, DctBD and DctA, respectively.

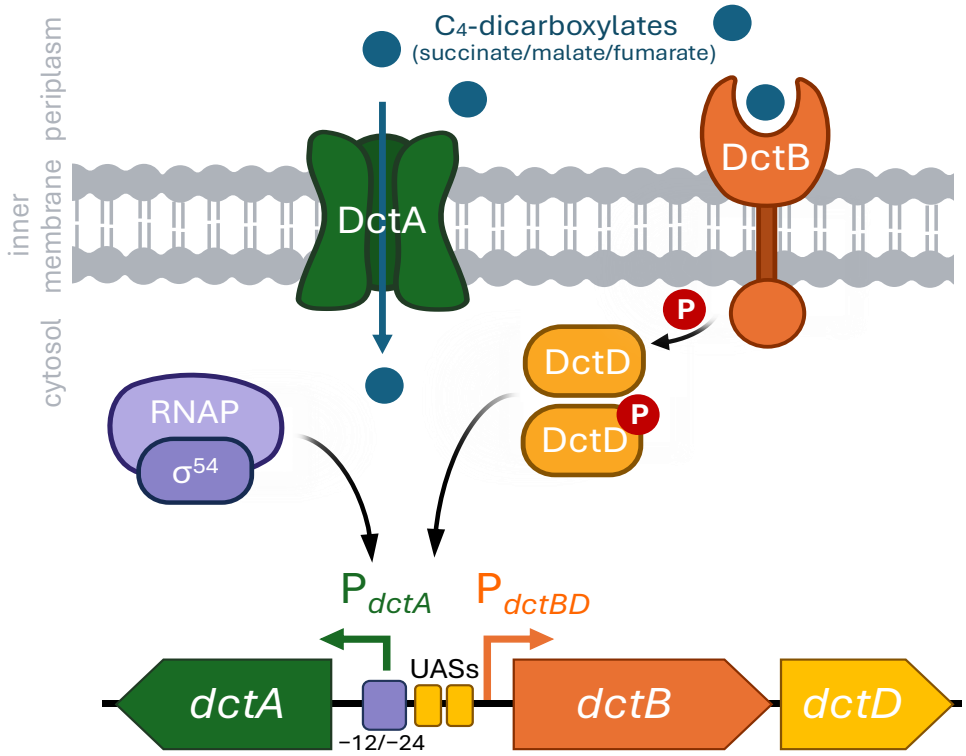


Figure 3.1 The dicarboxylate transport system (Dct) in *Rhizobium leguminosarum*. The Dct system comprises three proteins: DctA, the membrane-bound C_4-dicarboxylate transporter; DctB, the membrane-associated sensor histidine kinase; and DctD, the cytoplasmic response regulator. The *dctB* and *dctD* genes are co-transcribed from a constitutive promoter (P_{dctBD}), whereas *dctA* only gets expressed after the DctB-DctD cascade is activated through the presence of C_4-dicarboxylates or other feasible substrates in the periplasm. DctB senses C_4-dicarboxylates and consequently phosphorylates DctD. Phosphorylated DctD binds as a dimer to tandem upstream activation sequences (UASs) in the *dctA* promoter region, activating transcription by the σ^{54}-dependent RNA polymerase (RNAP, σ^{54} encoded by *rpoN*). Genes are depicted as pentagon arrows, proteins as organic shapes, arrows indicate transport, phosphorylation, or regulatory interactions.

All three genes are contained within the same genetic locus, but *dctA* is transcribed divergently from *dctB and dctD* (Figure 3.1). In *R. leguminosarum*, a shared promoter drives expression of *dctBD* (Reid & Poole, 1998), whereas in *S. meliloti*, *dctD* may be transcribed from an independent promoter (Jording et al., 1993; Watson, 1990).

Most members of the Rhizobiaceae encode only this single Dct system, with a few reported exceptions that harbour additional homologues of one or more *dct* genes (Batista et al., 2001; Burriolo, 2024; Van Slooten et al., 1992); however, their functional relevance remains poorly characterised.

Expression of *dctB* and *dctD* occurs at low constitutive levels (Reid & Poole, 1998; Ronson et al., 1987), and the resulting proteins form a two-component sensor-regulator signalling cascade that initiates expression of *dctA* upon sensing of C_4-dicarboxylates in the periplasm. DctB, a sensor histidine kinase located in the inner membrane (Figure 3.1), possesses two major domains: an N-terminal periplasmic sensing domain that binds C_4-dicarboxylates and similar substrates in a ligand-binding pocket, triggering a conformational change (Nan et al., 2010), and a cytoplasmic kinase domain that autophosphorylates in response. The phosphoryl group is subsequently transferred to a conserved aspartate residue in DctD, the associated response regulator (Giblin et al., 1995). Phosphorylated DctD acts as a transcriptional activator, binding as a dimer to two upstream activation sequences (UASs) in the *dctA* promoter (Ledebur et al., 1990; Ledebur & Nixon, 1992), thereby facilitating open complex formation by the σ^{54}-RNA polymerase holoenzyme and activating *dctA* expression (Wang et al., 1997).

This regulatory architecture resembles other two-component systems, such as the NtrB/NtrC nitrogen regulatory system (Nixon et al., 1986). In particular, DctD shares functional domains with the transcriptional activators NtrC and NifA, both of which require the alternative sigma factor RpoN (σ^{54}) for transcriptional activation as well (Dombrecht et al., 2002; Kustu et al., 1989). Given this similarity, it has been proposed that the Dct system may interact with the regulation of other sensing operons, including potential crosstalk with *nif* and *nod* genes (Birkenhead et al., 1990; Mavridou et al., 1995; Ronson et al., 1987; Watson, 1990). It has been postulated that DctA and DctB interact within the cytoplasmic membrane, potentially preventing inappropriate activation of

DctB in the absence of substrate and refining its sensing specificity (Reid & Poole, 1998). However, this hypothesis remains experimentally unverified.

Taken together, this regulatory framework ensures DctA transporter expression is tightly coupled to the DctB-DctD cascade and therefore C_4-dicarboxylate availability. Conversely, the Dct system can also be induced by, and transport, a range of other substrates, often structurally similar to C_4-dicarboxylates (Yurgel et al., 2000). For example, aspartate strongly induces the Dct system despite being transported with low affinity, and is therefore readily outcompeted in the presence of preferred substrates such as succinate (Reid et al., 1996; Watson et al., 1993). Beyond substrate-dependent regulation, *dctA* expression may also be induced by other environmental factors, including osmotic stress and nitrogen limitation (Reid & Poole, 1998).In addition, integration host factor (IHF) facilitates *dctA* transcription by bending the promoter DNA, thereby promoting interactions required for optimal DctD-mediated transcriptional activation (Sojda et al., 1999).

Collectively, the tight coupling of *dctA* expression to DctBD-dependent sensing, together with various (postulated) layers of additional regulatory inputs, make it difficult to disentangle the respective contributions of substrate sensing, transport, and regulation to downstream phenotypes.

The forward genetic screen described in Chapter 2 predominantly recovered mutants impaired in C_4-dicarboxylate sensing or transport (Figures 2.5), prompting closer investigation of the Dct system itself. Interpretation of *dct* mutants, however, is inherently complicated by the regulatory architecture of the locus. Due to the regulatory coupling of *dctA* expression to DctBD-mediated signalling, all loss-of-function mutations in any component of the Dct system – whether through targeted gene disruption or through spontaneous transposon insertion – ultimately produce the same functional outcome: loss of DctA activity, either through lack of *dctA* expression or transcription of a nonfunctional DctA protein. Consequently, such mutants do not permit discrimination of defects in C_4-dicarboxylate sensing from defects in transport, limiting mechanistic analysis of the individual contributions of Dct proteins to downstream phenotypes, including carbon catabolite repression (CCR) and symbiotic nitrogen fixation.

In Chapter 2, we concluded that C_4-dicarboxylate-mediated CCR depends on a metabolite-derived signal rather than on a direct signalling role of the Dct system itself, as demonstrated by the restoration of CCR when the native Dct system was replaced by a heterologous malate-specific transporter. In this chapter, we sought to test this conclusion directly within the native Dct framework by uncoupling DctA-mediated transport from DctBD-dependent regulation, using two complementary approaches based on both existing mutants and engineered constructs.

Material and Methods

Bacterial strains and growth conditions

The bacterial strains and plasmids used in this study are listed in Table 3.1.

Table 3.1 Strains and plasmids used in this study.

Strain or plasmid	Relevant phenotype and genotype	Reference or Source
Escherichia coli		
DH5α	*supE44 ΔlacU169* (ϕ80 *lacZ*ΔM15) *hsdR17 recA1 gyrA96 thi-1 relA2*	Hanahan, 1983
EC100D™ *pir+*	Sm^r F$^-$ *mcrA* Δ(*mrr-hsdRMS-mcrBC*) ϕ80dlacZΔM15 ΔlacX74 *recA1 endA1 araD139* Δ(*ara, leu*)7697 *galU galK* λ$^-$ *rpsL nupG* pir+(DHFR)	Lucigen
ST18	Sm^r Sp^r *pro thi hsdR* chromosome::RP4-2 Tc::Mu-Kan::Tn7/ λ*pir* Δ*hemA*	Thoma & Schobert, 2009
Rhizobium leguminosarum		
3841	Sm^r derivative of *R. leguminosarum* bv. *viciae* strain 300; in this study referred to as wild type (WT)	Johnston & Beringer, 1975; Glenn et al., 1980
LMB592	Sm^r Tet^r 3841 ×pLMB686	Pini et al., 2017
OPS3732	Sm^r Nm^r Tet^r RU150 ×pLMB686	this work
OPS3941	Sm^r Sp^r Nm^r Δ*dctABD*::Ω Tn*7*::J23104-R28-*dctA*-DT16	this work
OPS3942	Sm^r Sp^r Nm^r Δ*dctABD*::Ω Tn*7*::J23106-R1-*dctA*-DT16	this work
OPS3943	Sm^r Sp^r Nm^r Δ*dctABD*::Ω Tn*7*::J23106-R28-*dctA*-DT16	this work
OPS3944	Sm^r Sp^r Nm^r Δ*dctABD*::Ω Tn*7*::P_{rpoD}-R28-*dctA*-DT16	this work
OPS3948	Sm^r Sp^r Nm^r *dctA*::Ω Tn*7*::J23104-R28-*dctA*-DT16	this work
OPS3949	Sm^r Sp^r Nm^r *dctA*::Ω Tn*7*::J23106-R1-*dctA*-DT16	this work
OPS3950	Sm^r Sp^r Nm^r *dctA*::Ω Tn*7*::J23106-R28-*dctA*-DT16	this work
OPS3951	Sm^r Sp^r Nm^r *dctA*::Ω Tn*7*::P_{rpoD}-R28-*dctA*-DT16	this work
OPS3956	Sm^r Sp^r Nm^r Tet^r OPS3941 ×pLMB686	this work
OPS3957	Sm^r Sp^r Nm^r Tet^r OPS3943 ×pLMB686	this work
OPS3958	Sm^r Sp^r Nm^r Tet^r OPS3944 ×pLMB686	this work
OPS3962	Sm^r Sp^r Nm^r Tet^r OPS3948 ×pLMB686	this work
OPS3963	Sm^r Sp^r Nm^r Tet^r OPS3950 ×pLMB686	this work
OPS4116	Sm^r Sp^r *dctA*::Ω Tn*7*:: P_{native}-*dctA*	this work
OPS4119	Sm^r Sp^r Δ*dctABD*::Ω Tn*7*:: P_{native}-*dctA*	this work
OPS4241	Sm^r Sp^r Nm^r Tet^r OPS3942 ×pLMB686	this work
OPS4242	Sm^r Nm^r Tet^r RU152-22 ×pLMB686	this work
OPS4297	Sm^r Sp^r Nm^r Tet^r OPS3949 ×pLMB686	this work

OPS4298	Sm^r Sp^r Nm^r Tet^r OPS3951 ×pLMB686	this work
OPS4307	Sm^r Sp^r Tc^r *dctA*::Ω Tn*7*:: P_{native}-*dctA* ×pLMB686	this work
RU150	Sm^r Nm^r *dctA-dctB* IR::Tn*5*	Reid & Poole, 1998
RU152-22	RU150 suppressor; full genotype see Figure 3.4	Reid & Poole, 1998
RU714	Sm^r Sp^r Δ*dctABD*::Ω	Reid et al., 1996
RU727	Sm^r Sp^r *dctA*::Ω	Reid et al., 1996
Plasmids		
pLMB686	Tc^r (pIJ11268) P_{intA}-*luxCDABE* (inositol biosensor)	Pini et al., 2017
pOGG073	Sp^r pL0V-P destination vector	B.Geddes, unpublished
pOGG120	Sp^r pL0M-P J23104	Geddes et al., 2019b
pOGG121	Sp^r pL0M-P J23106	K. Grant, unpublished
pOGG144	Sp^r pL0M-U R1	K. Grant, unpublished
pOGG157	Sp^r pL0M-T DT16	Geddes et al., 2019a
pOGG272	Sp^r pL0M-U R28	T. Haskett, unpublished
pOGG446	Sp^r pL0M-P P_{rpoD}	this work
pOGG447	Spr pL0V-SC *dctA*	this work
pOPS2196	Ap^r Km^r (pTn*7*-SCOUT12) J23104-R28-*dctA*-DT16	this work
pOPS2197	Ap^r Km^r (pTn*7*-SCOUT12) J23106-R1-*dctA*-DT16	this work
pOPS2198	Ap^r Km^r (pTn*7*-SCOUT12) J23106-R28-*dctA*-DT16	this work
pOPS2199	Ap^r Km^r (pTn*7*-SCOUT12) P_{rpoD}-R1-*dctA*-DT16	this work
pOPS2200	Ap^r Km^r (pTn*7*-SCOUT12) P_{rpoD}-R28-*dctA*-DT16	this work
pOPS2284	Ap^r Gm^r (pUC18T-mini-Tn*7*T-Gm) P_{native}-*dctA*	this work
pRK2013	Km^r self-transmissible helper plasmid	Ditta et al., 1980
pTn*7*-SCOUT12	Ap^r Km^r pL1V-Lv1-pUC18R6K-miniTn*7*T-Km	Jorrin et al., 2024
pTNS3	Ap^r *oriT oriV* (R6K) *tnsABCD* Tn*7* helper plasmid	Choi et al., 2008
pUC18T-mini-Tn*7*T-Gm	Ap^r Gm^r *oriT oriV* (ColE1) Tn*7* delivery vector	Choi et al., 2005

Ap, ampicillin; Gm, gentamicin; Km, kanamycin; Nm, neomycin; Sm, streptomycin; Sp, spectinomycin; r, resistance; IR, intergenic region

E. coli strains were grown in Luria-Bertani (LB) medium (Sambrook et al., 1989) at 37°C and *R. leguminosarum* strains were grown in either tryptone yeast (TY) rich medium (Beringer, 1974) or universal minimal salts (UMS) minimal medium (Pini et al., 2017) at 28°C. If not stated otherwise, UMS was supplemented with 10 mM NH_4Cl as the nitrogen source and 20 mM succinate as the carbon source. Antibiotics were added when necessary, at the following concentrations (μg mL^{-1}): ampicillin (100), gentamicin (10 for *E. coli*; 20 for *R. leguminosarum*), kanamycin (20; for *E. coli*), neomycin (40;

R. leguminosarum), streptomycin (500), spectinomycin (100), and tetracycline (10 for *E. coli*; 1 in liquid and 5 in solid media for *R. leguminosarum*).

Genotyping RU150 and whole-genome sequencing of RU152-22

The Tn*5* transposon insertion in RU150 was originally mapped by a combination of Southern blotting, transductional analysis, complementation, and cloning of the Tn*5* insertion site (cf. Reid, 1995). This mapping was subsequently refined by PCR amplification of the *dctA-dctB* intergenic region from RU150 gDNA; combining the genome specific primers oxp6485 and oxp6486 with a Tn*5* specific primer (all listed in Table S3.1). Resulting amplicons were gel-purified and sent for Sanger sequencing.

Repeated attempts to genotype RU152-22 using similar PCR-based approaches were unsuccessful, as amplification of the expected flanking region (IS50R), presumed to be adjacent to *dctB*, could not be achieved. Instead, RU150 was sent for hybrid whole genome sequencing, combining Oxford Nanopore Technology long reads (50×) with 2× 250 bp Illumina short reads (30×), carried out by MicrobesNG (Birmingham, UK). The genotype was resolved by mapping the resulting reads to *in silico* versions of *Rlv*3841 WT, RU150 and the suspected RU152-22 genotype.

Golden Gate Cloning

To generate an array of plasmids with varying *dctA* expression independent of DctB-DctD signalling, transcriptional units were assembled by Golden Gate cloning (Geddes et al., 2019a). Each level 1 construct consisted of a P-module (promoter), U-module (ribosome binding site (RBS)), SC-module (open reading frame (ORF)), and T-module (terminator), assembled into the backbone pTn7-SCOUT12, which later allows integration of the units into the chromosome of rhizobial strains via Tn*7*.

To obtain a range of expression strengths, one of three constitutive promoters, P_{rpoD} (weak, pOGG446), J23106 (intermediate, pOGG121), J23104 (strong, pOGG120) was combined with one of two synthetic ribosome-binding sites, R28 (weak, pOGG272) or R1 (strong, pOGG144), and placed upstream of the *Rlv*3841 *dctA* ORF (pOGG447), followed by the terminator DT16 (pOGG157) (Figure 3.2). J23106 and J23104, from the Anderson promoter collection (https://parts.igem.org/Promoters/Catalog/Anderson) display

approximately 4.5-fold and 160-fold higher activity than the native *rpoD* promoter in *Rlv*3841, respectively (H. Knights, Poole Lab, unpublished). Differences in U-module strength further modulated expression levels, with R28 and R1 representing weak and strong RBSs, and R1 conferring approximately 180-fold higher expression than R28 (T. Haskett, Poole Lab, unpublished).

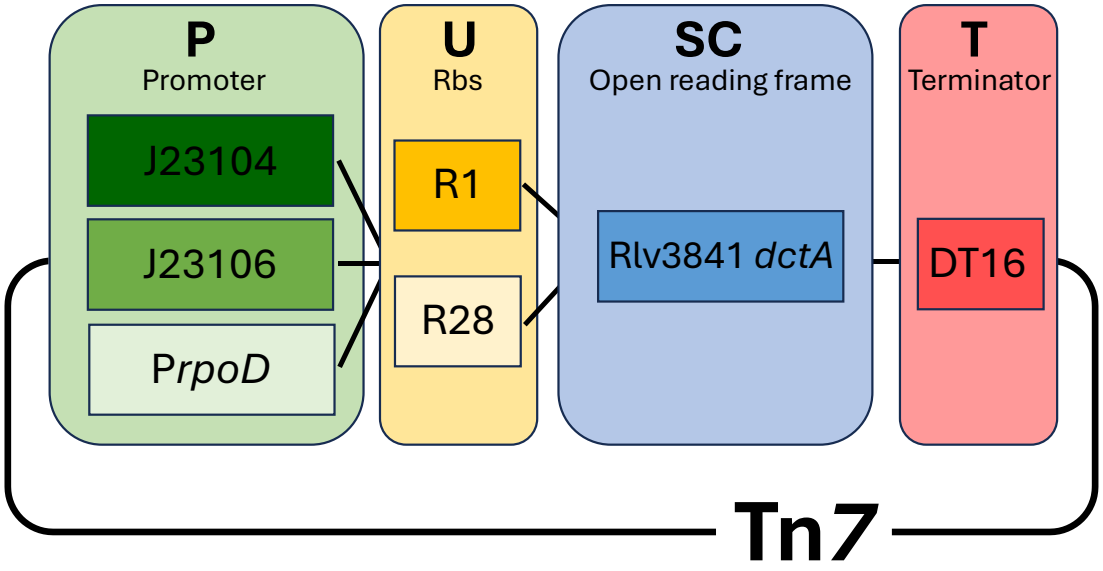


Figure 3.2 Modular structure of the constitutive *dctA* expression constructs, assembled via Golden Gate cloning. For details see main text.

Golden Gate assemblies were performed in 15 µL reactions containing 1.5 µL T4 DNA ligase buffer, 1.5 µL BSA (2 mg mL^{-1}), 1 µL *Bsa*I, 2,000,000 units T4 DNA ligase (Thermo Fisher Scientific), and 40 fmol DNA of each Golden Gate part. Reactions were placed in a thermocycler with 25 cycles of 3 min at 37°C and 4 min at 16°C, followed by incubation at 50°C for 5 min and heat inactivation at 80°C for 5 min.

Missing level 0 Golden Gate modules were constructed as follows. For the P-module carrying P_{rpoD}, the corresponding promoter sequence was amplified using primers oxp2898 and oxp6509 and assembled into pOGG073 (Lv0-P-empty) via a *Bpi*I Golden Gate reaction, generating pOGG446 (pL0M-P P_{rpoD}). Because the *dctA* coding sequence contains two internal *Bpi*I sites, standard MoClo assembly was not possible. Instead, the *Rlv*3841 *dctA* ORF was amplified from gDNA using oxp6558/oxp6559 and ligated into *Eco*RV-digested pJET1.2 using the blunt-end protocol of the CloneJET PCR Cloning Kit (Thermo Fisher Scientific), yielding pOGG447 (pL0M-SC *dctA*).

The resulting plasmids were transformed into *E. coli* EC100D *pir*+ and mobilized into RU727 and RU714 by tetra-parental mating, using the helper plasmid pRK2013 and the Tn*7* transposase-encoding plasmid pTNS3. Transposition events were selected on TY supplemented with neomycin, and final strains were verified by PCR using primer pairs oxp2327/oxp3060 amplifying the left Tn*7* end and oxp2328/oxp3061 amplifying the right end of the Tn*7* integration.

Native *dctA* complementation plasmid

For native *dctA* complementation, a fragment encompassing the native promoter, *dctA* coding sequence, and native terminator was amplified using primers oxp6975-76 and cloned into *Bam*HI – *Hin*dIII digested pUC18T-mini-Tn7T-Gm using HiFi assembly (NEB). The resulting plasmid, pOPS2284, was transformed into *E. coli* DH5α, mobilized into rhizobial strains, and successful chromosomal integration was verified via PCR as described above.

RNA extraction and real-time qPCR analysis

*Rlv*3841 cultures were grown in UMS supplemented with 10 mM ammonia or 10 mM glutamine as the nitrogen source and 20 mM succinate as the carbon source in three independent biological replicates. RNA was extracted and RT-qPCR performed following the same protocols as described in Chapter 2.

Primer pairs used for RT-qPCR are listed in Table S3.1. Primer amplification efficiency was assessed by generating a standard curve (Figure S3.1) and primer specificity was confirmed by amplification of gDNA. Relative gene expression was determined using the Pfaffl method, normalised to the housekeeping gene *rpoD*, which has been previously validated as a stable reference (Tjahjono, 2025). Expression values are reported relative to WT and were $\log_2$ transformed prior to visualization and statistical analysis.

Transport assays

Transport assays were conducted as described in Chapter 2.

Growth assessment on drop plates

10 µL of cell suspensions of *Rlv*3841 WT and mutant strains were spotted in serial tenfold dilutions starting from OD_{595} = 0.1 onto UMS plates supplemented with different carbon and nitrogen source combinations. Growth was visually assessed after three to five days of incubation.

Assessment of carbon catabolite repression using an inositol *lux* biosensor

The inositol biosensor plasmid pLMB686 (Pini et al., 2017) was used to visualize repression of alternative carbon uptake pathways in the presence of C_4-dicarboxylates, as validated in Chapter 2.

To assess repression of the inositol uptake system, pLMB686 was conjugated into strains of interest. Strains were grown on TY slopes for three days, washed three times in 10 mM $MgCl_2$, and inoculated into 10 mL of liquid UMS at an initial OD_{595} of 0.01. Media was supplemented with either 10 mM *myo*-inositol (positive control, unrepressed state), 20 mM C_4-dicarboxylate (succinate or malate) and 10 mM *myo*-inositol (CCR condition), or 20 mM succinate or 20 mM malate alone (negative controls). Cultures were incubated at 28°C overnight and luminescence and absorbance determined in a plate reader (FLUOstar Omega, BMG Labtech) when cultures had reached OD_{595} ~0.5.

As several *dct* mutant strains exhibited impaired growth on one or more of the tested carbon and nitrogen source combinations, the assay conditions were modified accordingly. Rhizobial strains were grown in TY liquid to exponential phase, washed three times in 10mM $MgCl_2$, and inoculated into 5 mL UMS containing the required carbon and nitrogen sources to an OD_{595} ~ 0.5. Following incubation at 28°C for ~1.5 hours, luminescence and OD_{595} were measured using a plate reader.

Plant growth and ARA

Pea plants were prepared, inoculated and grown as described in Chapter 4. Plants were harvested after 25 dpi and nitrogenase activity assessed via acetylene reduction following the protocol stated in Chapter 4.

Statistical analysis and visualization

Data were analysed and visualized using GraphPad Prism v10.6.1. Differences between groups were assessed with analysis of variance (ANOVA). When multiple comparisons were conducted, appropriate post hoc tests with correction for multiple testing were applied. In cases where assumptions of equal variance were not met, mixed effect models were applied.

Results

In the following, results of two complementary approaches aiming to uncouple C_4-dicarboxylate transport (via DctA) from C_4-dicarboxylate sensing (via DctB-DctD) are presented.

I: Spontaneous Dct regulatory mutants

Strains RU150 and its suppressor RU152-22 were originally isolated and described by Reid (1995). Here, their genotypes were verified and, in the case of RU152-22, revised, and their phenotypic characterisation was extended to include analysis of CCR and symbiotic function, providing a basis for reinterpretation of earlier findings.

RU150 uncouples dctA *expression from native DctBD regulation*

The strain RU150 was originally isolated in a random Tn*5* mutagenesis screen for mutants defective in C_4-dicarboxylate utilisation (Reid & Poole, 1998). It carries a Tn*5* insertion in the *dctA*–*dctB* intergenic region (*dctA*-*dctB* IR::Tn*5*), located 19 bp upstream of the *dctA* start codon (Figure S3.2) as confirmed by sequencing and consistent with earlier mapping.

This insertion disrupts the native promoter architecture controlling *dctA*. Instead of being inducible, *dctA* is expressed constitutively at a low level — approximately twofold higher than WT under non-inducing conditions, but ~1/8 of the fully induced level (Reid, 1995). Importantly, *dctA* expression is uncoupled from DctBD regulation, in which P_{dctA} is normally activated via σ^{54}-dependent RNA polymerase and DctD binding to UAS (Figure 3.1). Instead, *dctA* expression in RU150 is most likely driven by a weak outward-reading promoter within the Tn*5* element.

By contrast, expression of *dctB* and *dctD* is only modestly affected. Reid (1995) measured an approximately twofold increase in *dctB* and a slight increase in *dctD* compared to WT levels with various reporter probes, while our qPCR analysis revealed slightly decreased expression levels compared to the WT (Figure S3.3). Importantly, the DctBD signalling system remains functionally intact. It retains its ability to respond to C_4-dicarboxylates and promotes transcription from the native P_{dctA} in a substrate-dependent manner. Thus,

RU150 represents a system in which *dctA* expression is uncoupled from an otherwise functional DctBD regulatory circuit.

RU150 shows impaired growth on succinate/ammonia despite constitutive succinate transport

Consistent with constitutive *dctA* expression, RU150 transports succinate also under non-inducing conditions (e.g. glucose/ammonia) and succinate transport rates of RU150 are comparable to those of induced WT cells (Figure S3.4).

Despite this, RU150 displays a pleiotropic growth defect. Most notably, it grows very poorly on succinate as the carbon source in conjunction with ammonia as the nitrogen source (generation time ~30 h), while growth on other carbon sources, such as glucose, is unaffected. Growth on succinate is rescued when combined with various amino acids, including aspartate, glutamate, glutamine, asparagine, serine, alanine, proline or histidine (Reid, 1995). This is particularly interesting as, as noted above, succinate transport rates are not impaired compared to WT. Instead, Reid (1995) concluded that RU150 has a specific impairment in ammonia assimilation or nitrogen metabolism when succinate is provided as the carbon source, rather than a general defect in carbon or nitrogen metabolism.

Regardless of this phenotype, nitrogen regulation via the NTR system remains intact. P_{glnII} expression and aspartate uptake respond normally to nitrogen excess (Reid, 1995). Solely, when grown on glucose/aspartate, aspartate uptake via the AAP was elevated compared to repressed WT state under this growth condition.

RU150 is defective in carbon catabolite repression

Since succinate transport contributes to repression of alternative carbon utilisation pathways (cf. Chapter 2), RU150 was next assessed for its ability to mediate CCR using the inositol transcriptional reporter. As RU150 ability to grow on succinate in conjunction with ammonia is impaired, cells were grown in rich medium and inoculated into test conditions at higher cell density, as described previously for strains with growth defects (Chapter 2).

In the *Rlv*3841 WT, the presence of succinate strongly repressed reporter output when cells were grown on succinate and *myo*-inositol. In contrast, this repression was abolished in RU150: reporter expression remained high in succinate plus *myo*-inositol, resembling the signal strength observed in cells grown on *myo*-inositol alone (Figure 3.3).

These data show that RU150 is defective in succinate-mediated CCR despite retaining succinate transport.

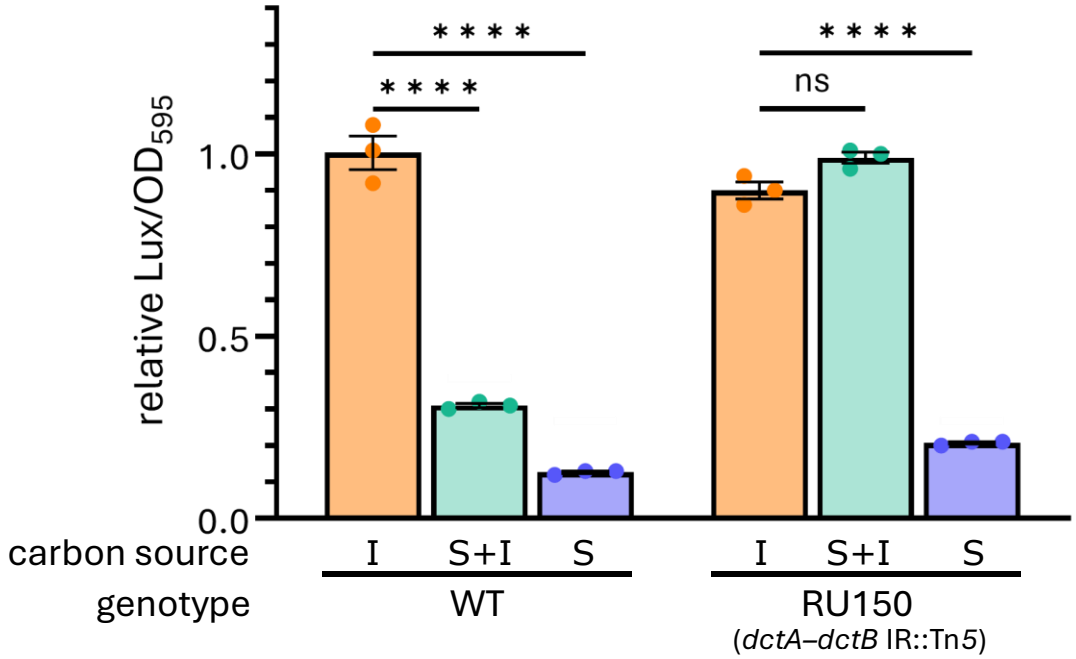


Figure 3.3 RU150 is defective in succinate-mediated carbon catabolite repression (CCR). Luminescence of a *myo*-inositol biosensor in WT *Rlv*3841 and RU150, normalised to optical density (Lux/OD_{595}) and expressed relative to WT grown in *myo*-inositol. RU150 carries a Tn*5* insertion in the *dctA-dctB* intergenic region (IR), resulting in low level constitutive *dctA* expression independent of DctBD signalling. Luminescence was quantified from liquid cultures grown in TY and inoculated into UMS containing either 10 mM *myo*-inositol (I, orange), 20 mM succinate plus 10 mM *myo*-inositol (S+I, green), or 20 mM succinate (S, blue) at OD_{595} ~ 0.5. Bars represent mean ± SEM (n = 3). Statistical significance was determined by two-way ANOVA with Sidak-corrected comparisons to the inositol condition within each genotype (**** $p < 0.0001$; ns, not significant).

A suppressor of RU150 carries a major rearrangement of the dct *locus*

The unusual growth phenotype of RU150, foremost its inability to grow on ammonia in combination with C_4-dicarboxylates, prompted Reid (1995) to isolate second-site suppressor mutants capable of growth on succinate/ammonia. RU150 was plated on succinate/ammonia without kanamycin, and colonies displaying WT-like growth were screened for retention of kanamycin resistance to ensure the original Tn*5* insertion was maintained. Transductional analysis identified several suppressor mutants, of which three carried second-site mutations closely linked to the *dct* region.

Two strains, RU152-1 and RU152-14, were previously shown to contain additional copies of *dctA*, supported by increased *dctA* transcript levels, Southern blot analysis, and (partial) mapping via inverse PCR (Reid & Poole, 1998). It was proposed that these duplications restore growth on succinate/ammonia by rebalancing the ratio of DctA to DctBD.

The third suppressor, RU152-22, was of particular interest, as earlier work suggested that it carried a deletion affecting *dctB,* distinct from site-directed deletion of *dctB*, *dctD*, or *dctBD* in the RU150 background (Reid, 1995; Reid & Poole, 1998). Because the original isolate was no longer available, the strain used in this study was reconstructed by curing the reporter plasmid from archived derivatives, thereby reconstituting the original mutant genotypes.

Previous restriction mapping of RU152-22 DNA had indicated an approximately 0.5 kb deletion on the *dctB* side of the Tn*5* insertion (Reid & Poole, 1998). This deletion was proposed to remove approximately 200 bp of the intergenic region, including the *dctB* promoter, and ~300 bp from the 5' end of *dctB*. However, this deletion could not be confirmed by PCR, as multiple primer combinations failed to amplify across the regions flanking the suspected deletion site. We therefore proceeded with whole-genome sequencing using a hybrid approach combining long and short reads, as short-read sequencing alone had previously failed to resolve this region due repetitive sequences within the Tn*5* element.

Hybrid assembly revealed that RU152-22 carries a more complex rearrangement than previously thought (Figure 3.4). Consistent with earlier inference, the intergenic region

downstream of the Tn*5* insertion, including a substantial portion of the *dctB* coding sequence, is deleted. Yet, this deletion is considerably larger than originally proposed, leaving only 272 bp of *dctB* remaining.

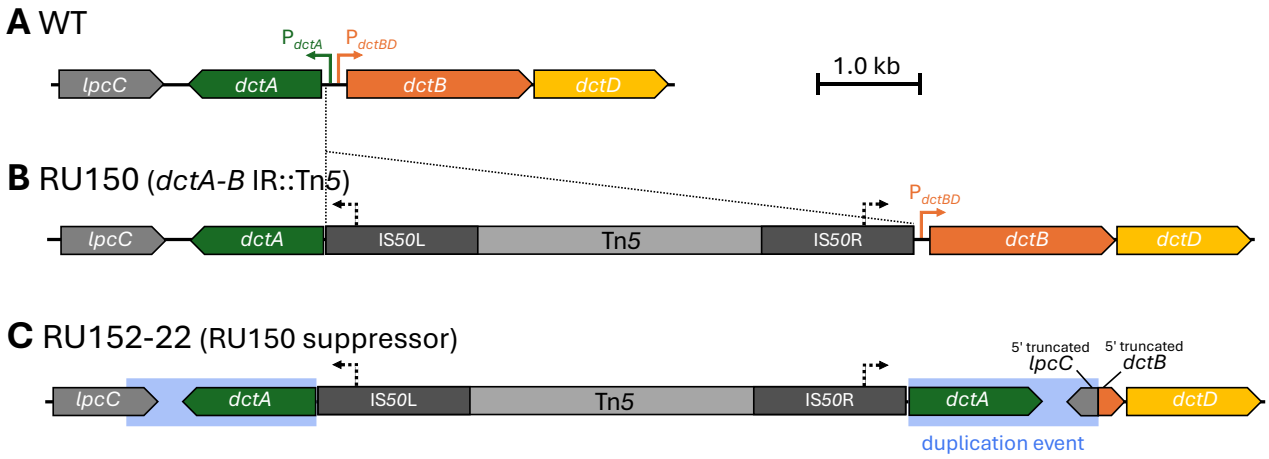


Figure 3.4 Genomic organization of the *dct* region in strain RU150 and its suppressor mutant RU152-22. (A) *Dct* locus in *Rhizobium leguminosarum* bv. *viciae* 3841 WT. **(B)** Genotype of RU150, in which a Tn*5* transposon is inserted in the *dctA–dctB* intergenic region, disrupting the native *dctA* promoter (see Figure S3.2 for details). **(C)** Genotype of the suppressor mutant RU152-22, in which the intergenic region and the 5' end of *dctB* are deleted and replaced by a duplicated 1.9 kb fragment (highlighted in blue) containing the full *dctA* and 3' end of *lpcC*. Genes are depicted as arrows indicating transcriptional orientation and promoters are shown as right-angled arrows. Putative outward-reading promoters within the Tn*5* transposon are shown as dotted right-angled arrows.

More importantly, the analysis uncovered an additional rearrangement event. The entire *dctA* coding sequence is duplicated and inserted on the opposite side of the Tn*5* element, at the original location of dct*B*. Thus, rather than a simple deletion, RU152-22 harbours a complex rearrangement comprising an extensive *dctB* truncation together with duplication and relocation of *dctA*.

The duplication also includes a segment of the upstream *lppC* gene; however, this duplicated fragment is unlikely to constitute a functional transcriptional unit.

Restoration of dctA *expression in RU152-22 reinstates growth and CCR*

The functional consequence of this rearrangement was assessed by comparing expression and phenotype across RU150 and RU152-22. Compared to RU150, RU152-22 is restored for growth on succinate/ammonia and also in the CCR phenotype. Utilising

the inositol biosensor, presence of succinate again repressed reporter expression in RU152-22 (Figure 3.5), indicating recovery of succinate-mediated CCR.

qPCR analysis further showed that *dctA* transcript levels were restored in RU152-22 (Figure S3.5). In RU150, *dctA* expression was reduced to approximately 18% of WT levels, whereas in RU152-22 transcript levels returned to induced WT levels. These data indicate that that duplication of *dctA* is sufficient to restore *dctA* expression in the absence of a functional DctBD regulatory system.

Although RU152-22 was initially considered a model to dissect the respective contributions of DctA and DctB to growth on succinate/ammonia and CCR, our findings instead necessitate a reinterpretation of this strain. RU152-22 represents, in line with RU152-1 and RU152-14, another example in which both growth and CCR are restored through increased *dctA* expression, thereby compensating for the low expression levels observed in RU150. Together, these results support the conclusion that reduced *dctA* expression in RU150 underlies both phenotypes.

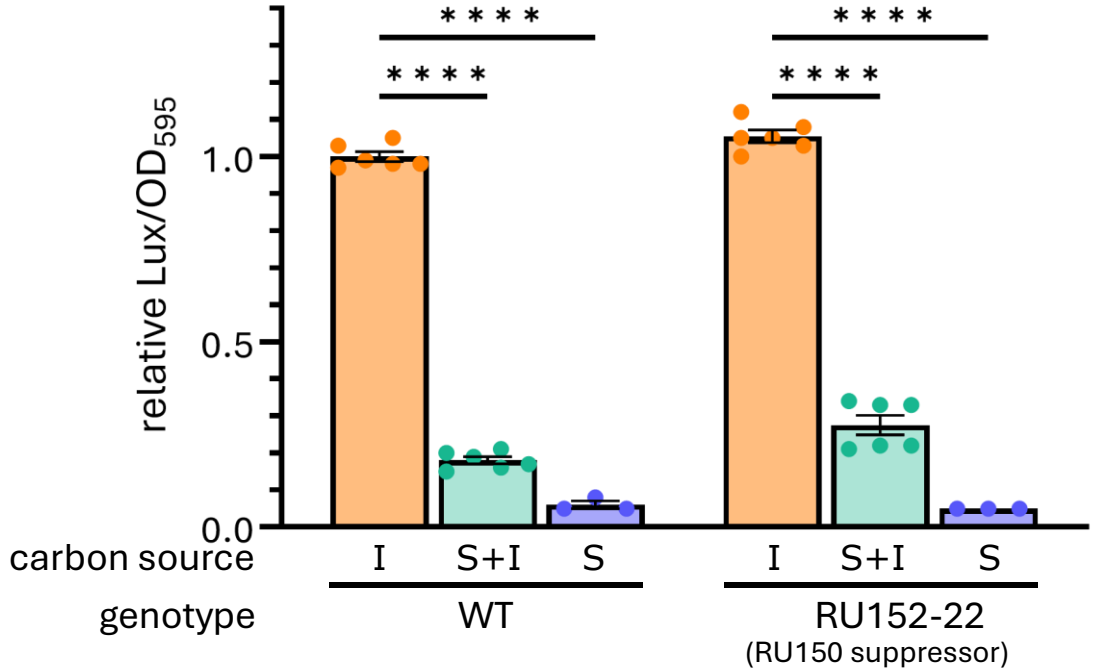


Figure 3.5 Succinate-mediated carbon catabolite repression (CCR) is restored in a RU150 suppressor mutant RU152-22. Luminescence of a *myo*-inositol biosensor in WT *Rlv*3841 and RU152-22, a spontaneous suppressor of RU150 (for detailed genotype see Figure 4.4), normalised to optical density (Lux/OD_{595}) and expressed relative to WT grown on myo-inositol. Luminescence was quantified from liquid cultures grown in TY and inoculated into UMS containing either 10 mM *myo*-inositol (I, orange), 20 mM succinate plus 10 mM *myo*-inositol (S+I, green), or 20 mM succinate (S, blue) at OD_{595} ≈ 0.5. Bars represent mean ± SEM (n ≥ 3) from two independent experiments. Statistical significance was determined by two-way ANOVA with Sidak-corrected comparisons to the inositol condition within each genotype (**** $p < 0.0001$).

Misregulation of the Dct system in RU150 compromises symbiotic nitrogen fixation

During symbiosis, bacteroids are primarily fuelled by C_4-dicarboxyaltes to support energy-demanding nitrogen fixation. Accordingly, mutants lacking a functional Dct systems are typically unable to fix nitrogen. To assess the consequences of *dct* misregulation on symbiotic performance, pea plants were inoculated with WT, RU150 or RU152-22 and analysed for various symbiotic parameters (Figure 3.6).

All strains formed similar numbers of nodules (Figure 3.6A). However, nodules induced by RU150 were significantly smaller (Figure 3.6B) and appeared white rather than pink (Figure 3.6F), consistent with a Fix^- phenotype. Nitrogenase activity of RU150 was severely impaired and nearly abolished, although low residual fixation was still detectable (Figure 3.6C,D). Correspondingly, plants inoculated with RU150 were visibly smaller and exhibited chlorotic leaves, resembling uninoculated control (Figure 3.6E). In contrast, RU152-22 restored symbiotic performance to WT levels across all properties measured.

These data show that disruption of the normal relationship between *dctA* expression and DctBD signalling has major consequences not only for laboratory growth phenotypes but also for symbiotic function in planta.

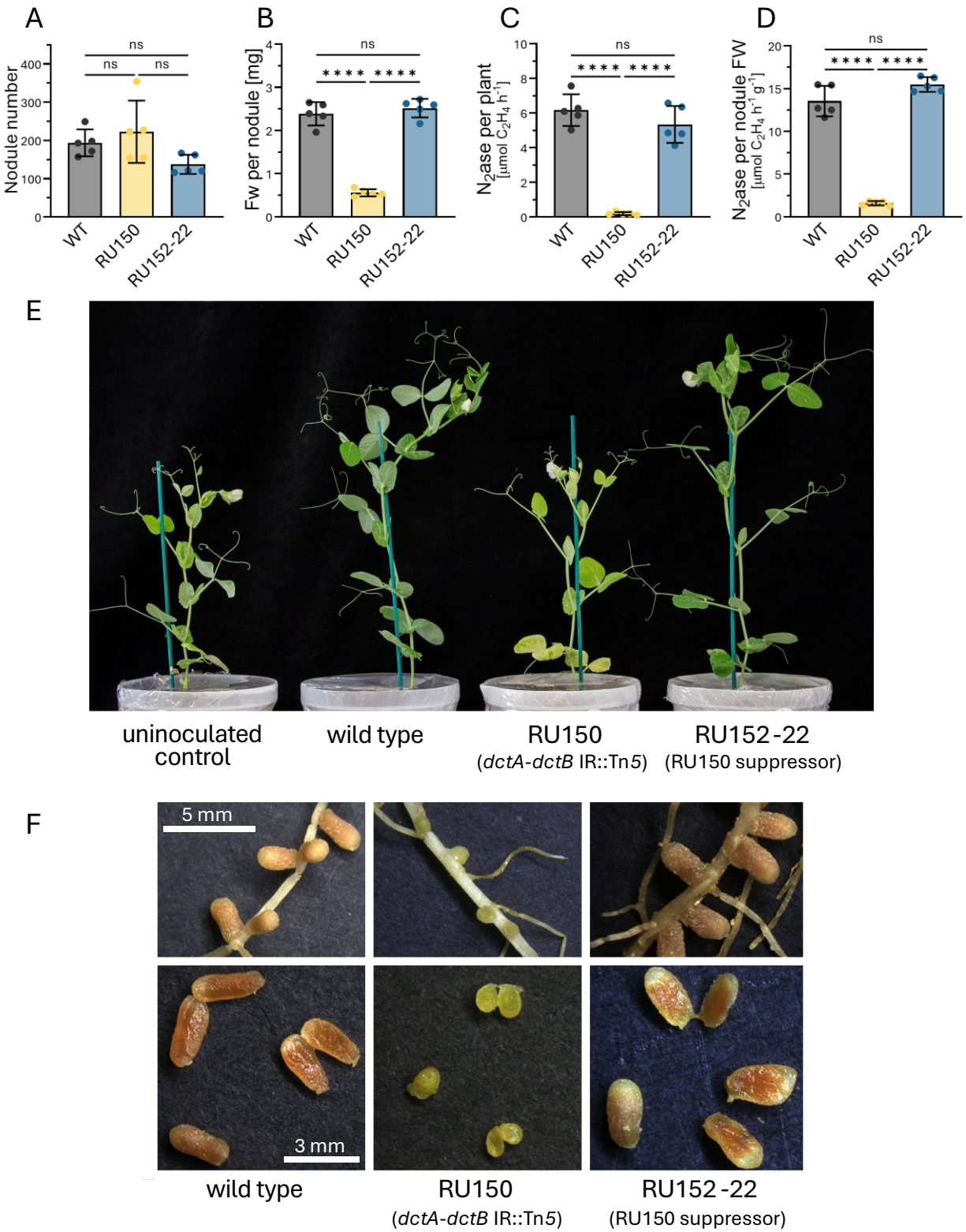


Figure 3.6 Impaired *dct* regulation in RU150 severely compromises nitrogen fixation; this defect is rescued in the suppressor strain RU152-22. *Pisum sativum* cv. Avola seedlings were inoculated with *Rlv*3841 wild-type (WT), RU150, or RU152-22 and grown for 24 dpi. RU150 carries a Tn*5* insertion in the *dctA-dctB* intergenic region (IR), resulting in low level constitutive *dctA* expression independent of DctBD signalling. RU152-22 is a spontaneous suppressor of RU150 (see Figure 4.4 for detailed genotype). Plants were assayed for nodule number **(A)**, fresh weight (FW) per nodule **(B)**, nitrogenase activity per plant **(C)**, and nitrogenase activity per nodule FW **(D)**. Representative plants **(E)** as well as nodules and nodule cross sections **(F)** are shown for the indicated strains. Scale bars in (F) apply per row. Each strain was tested on n = 5 plants, with bars showing mean ± SD. Statistical analysis was performed using one-way ANOVA followed by Tukey's multiple comparisons tests. Asterisks indicate significant differences with (**** $p < 0.0001$); ns, not significant.

II: Uncoupling *dctA* expression from DctBD through engineered constructs

As outlined above, mutations in *dctA*, *dctB* or *dctD* all disrupt the normal Dct circuit, therefore conventional *dct* mutants cannot easily separate defects in transport from defects in signalling. In addition, analysis of RU150 suggested that *dctA* expression level is a key determinant of downstream phenotypes.

To address this directly, we sought to uncouple *dctA* expression from the DctB-DctD sensing-cascade by placing *dctA* under the control of a set of constitutive promoters.

Previous attempts to express *dctA* from non-native promoters have highlighted the challenges of this approach: Reid (1995) overexpressed *dctA* using plasmids carrying constitutive promoters of varying strength, all predicted to be stronger than the native P_{dctA} under inducing conditions. Resulting strains failed to fully complement growth on C_4-dicarboxylates and frequently exhibited high rates of reversion or mutation. This instability was attributed to toxic overaccumulation of C_4-dicarboxylates resulting from unregulated *dctA* overexpression, leading to impaired growth and strong selection for mutations that reduce or eliminate *dctA* expression.

Aiming to circumvent these complications, we designed a tuneable expression system that avoids strong overexpression while enabling graded *dctA* expression independently of DctBD. This strategy combined (i) weak to intermediate-strength constitutive promoters, (ii) two ribosome-binding site (RBS) variants to further modulate expression levels, and (iii) single-copy chromosomal integration via the Tn*7* system to minimise copy-number effects.

Six expression plasmids spanning a range of predicted *dctA* expression levels were designed (Figure 3.2). However, not all promoter-RBS combinations were successfully obtained. One construct (J23104-R1-*dctA*-DT16) yielded no transformants following heat shock into competent *E. coli* cells, despite repeated attempts. A second construct acquired an insertion originating from an *E. coli* transposon within the promoter, suggesting strong selective pressure against the intact construct in the cloning host. Notably, both constructs combined a strong promoter with the strong R1 RBS. These observations indicate that high constitutive expression of *dctA* is poorly tolerated in *E. coli*.

Of the six intended constructs, five expression plasmids (pOPS2196-pOPS2200) were successfully generated and subsequently conjugated into RU727 (*dctA*) and RU714 (*dctABD*). Conjugation efficiencies varied between constructs, and pOPS2199, which contains the strong RBS R1, consistently failed to transfer into *R. leguminosarum* despite multiple attempts. This further supports the conclusion that strong constitutive *dctA* expression is detrimental in both *E. coli* and *R. leguminosarum* and is consistent with earlier reports and reinforce the notion that *dctA* expression must be tightly balanced to avoid toxicity. Strains resulting from successfully integrated plasmids are listed in Table 3.1.

Functional validation of the dctA *complementation system*

All successfully generated complementation strains were first assessed for their (ability to complement) growth on succinate as the sole carbon source with ammonia as the nitrogen source (Figure 3.7). As controls, all strains grew normally on rich medium (TY; not shown) and on glucose/ammonia (Figure 3.7), indicating that the introduced constructs did not cause general growth defects.

In contrast, the different *dctA* complementation constructs exhibited clear differing abilities to grow on succinate/ammonia (Figure 3.7). While the WT grew robustly on succinate/ammonia, the *dctA* and *dctABD* mutants failed to grow, as expected. Among the complementation strains, the majority of constructs did not restore growth on succinate/ammonia. Only a single construct, in which *dctA* expression is driven by the J23104-R28 promoter–RBS combination, supported growth comparable to the WT in both the *dctA* and *dctABD* deletion backgrounds.

These results indicate that most engineered expression constructs, despite being designed to drive constitutive *dctA* expression, are insufficient to restore growth on succinate. This limited and non-uniform complementation prompted further investigation into *dctA* expression levels across constructs to determine whether differences in transcript abundance could explain the observed phenotypic variation.

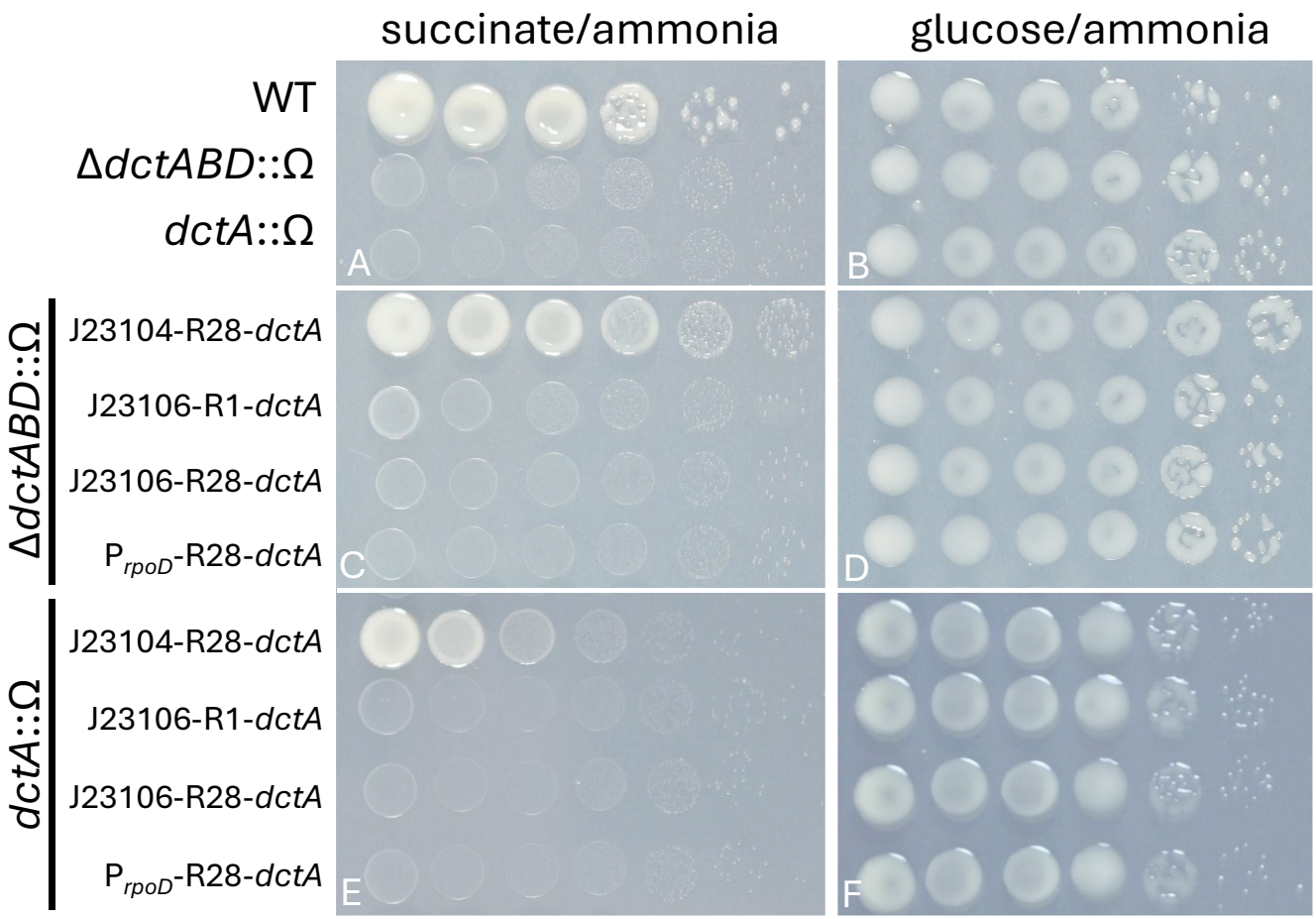


Figure 3.7 Only one constitutive *dctA* complementation enables growth on succinate/ammonia. 10 µL of serial tenfold dilutions (starting from OD595 = 0.1) of *R. leguminosarum* bv. *viciae* 3841 wild type (WT), Δ*dctABD*::Ω [RU714], *dctA*::Ω [RU727], and constitutive *dctA* complementation strains [OPS3941-44, OPS3948-51] were spotted onto UMS minimal medium supplemented with 10 mM ammonia as the nitrogen source and either 20 mM succinate **(A,C,E)** or 10 mM glucose **(B,D,F)** as the carbon source.

Constitutive constructs generate a gradient of dctA *expression levels*

To validate the expression strength of the *dctA* complementation constructs and to determine whether growth differences reflected differences in transcript abundance, *dctA* transcript levels were quantified by qPCR (Figure 3.8). Because not all complementation strains were able to grow on succinate with ammonia as the sole nitrogen source, expression was assessed primarily in succinate/glutamine. For the subset of strains capable of growth on succinate/ammonia, *dctA* expression was measured under both conditions. In these strains, *dctA* transcript levels were approximately twofold higher in succinate/ammonia compared to succinate/glutamine; however, the relative differences between constructs were preserved across conditions. Based on this consistency, succinate/glutamine can be used as a proxy to assess strain-specific *dctA* expression.

Across all constructs, *dctA* transcript levels were never lower than those observed from the induced native promoter and, in most cases, rather elevated relative to the WT, indicating that even the weakest constitutive promoters drive expression above physiological levels (Figure 3.8). This may be contributing to the growth defects observed in some strains.

Within each genetic background, the constructs produced a graded range of *dctA* expression levels; however, the overall differences between constructs were modest and, unexpectedly, did not follow the expected hierarchy based on individual promoter and RBS strength. This indicates that promoter and RBS strengths are not simply additive or multiplicative in this context.

In addition, *dctA* expression levels differed between genetic backgrounds. For identical constructs, transcript abundance was consistently higher in the Δ*dctABD* background compared to the *dctA* strain. This suggests that the presence of the DctB/D regulatory system may influence *dctA* expression independently of promoter control. In the *dctABD* background, all constructs exhibited expression levels significantly higher than WT, spanning a good dynamic range. In contrast, in the *dctA* deletion background, expression of most constructs was not significantly different from WT, and only one construct (J23106-R28) reached *dctA* expression levels significantly above WT. Thus, identical

promoter–RBS combinations produce different absolute expression levels depending on whether the DctB/D regulatory system is present.

Taken together, these results demonstrate that the engineered constructs generate a range of *dctA* expression levels, but that expression output is shaped by both combination of regulatory components and strain background. Importantly, all constructs exceed native expression levels, and the strongest constructs drive disproportionately high expression, which may contribute to the growth defects and instability observed for certain strains.

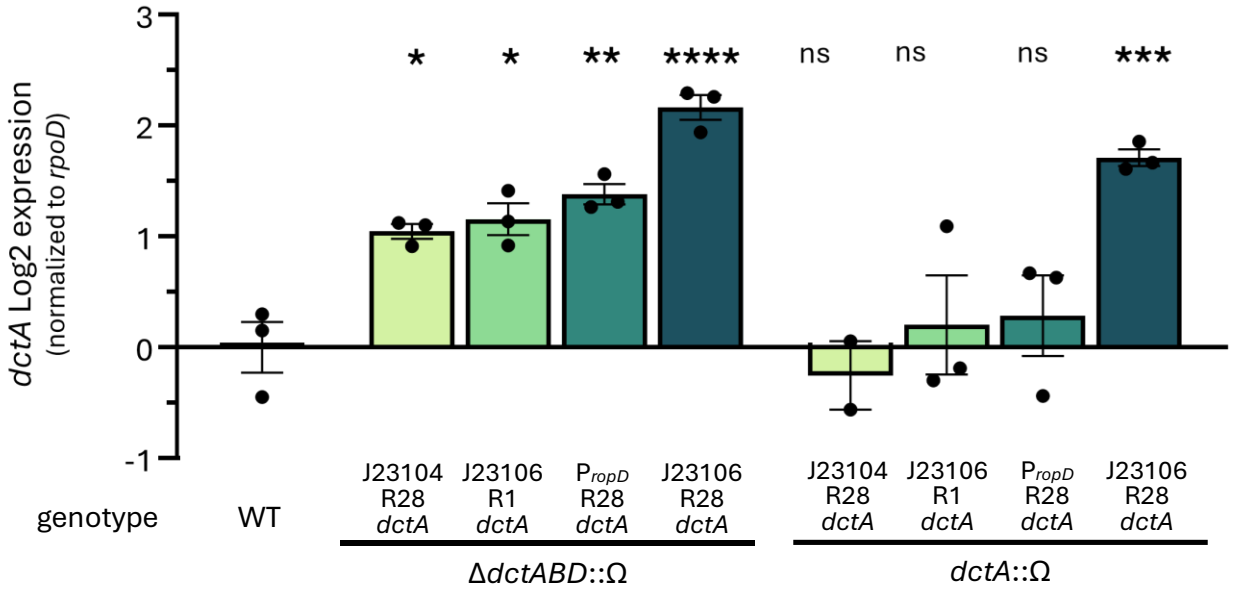


Figure 3.8 Varying *dctA* expression strength in constitutive *dctA* complementation strains. *dctA* expression levels were quantified by qPCR in WT *Rlv*3841 and *dct* mutant strains complemented with constructs driving constitutive *dctA* expression of increasing strength. Constructs consist of combinations of constitutive promoters (J23104, J23106, P_{rpoD}) and ribosome binding sites (R1, R28), integrated into the chromosome of either a Δ*dctABD*::Ω or *dctA*::Ω background (see main text for details). Cells were grown in UMS supplemented with 20 mM succinate and 10 mM glutamine. Expression levels are shown as $\log_2$-transformed relative expression (Pfaffl method), normalised to *rpoD* and expressed relative to WT. Bars represent mean ± SEM (n = 3). Asterisks indicate expression levels significantly different from WT *dctA* expression, as determined by one-way ANOVA with Dunnett's correction compared to WT (ns, not significant, **** $p < 0.0001$, *** $p < 0.001$, ** $p < 0.01$, * $p < 0.05$).

Growth issues in dctA *complementation strains are possibly related to ammonia utilisation*

Given that *dctA* expression was detectable and robust across all complementation constructs, the absence of growth on succinate/ammonia cannot be readily explained by lack of or insufficient *dctA* transcription. In particular, in the *dctA* background, the Golden Gate complementation should, in principle, restore a near wild type configuration with all Dct components present. These observations motivated us to test whether the observed growth defects are specific to the combination of succinate and ammonia, similar to growth issues reported in strain RU150.

To address this, all constructs were assessed for growth on succinate in combination with alternative nitrogen sources. Aspartate, glutamate, glutamine, and ornithine were selected as they represent amino acids with distinct uptake routes and metabolic entry points. Aspartate is structurally and metabolically closely related to C_4-dicarboxylates; it can induce the native Dct system and is also transported, albeit with low affinity, by DctA (Watson et al., 1993). In contrast, glutamate and glutamine are solely transported by the amino acid specific transporters Aap and Bra and function as key indicators of cellular nitrogen status, with glutamine representing nitrogen-rich and glutamate corresponding to relatively nitrogen-limited conditions (Tjahjono, 2025). Ornithine was included as it apparently cannot support growth as the sole carbon and nitrogen source (Hosie et al., 2002).

As noted above, all strains were capable of growth on succinate/glutamine. In addition, growth of all complementation strains was observed on succinate supplemented with aspartate, glutamate, or ornithine (Figure S3.6). However, even the parental *dctA* and *dctABD* mutants grew under these conditions, indicating that all these amino acids serve, at least in part, also as carbon sources. Consequently, observed growth cannot be attributed solely to succinate utilisation, limiting their usefulness for assessing functional complementation of C_4-dicarboxylate transport.

Closer inspection of growth on succinate/ammonia revealed that the phenotype of the complementation strains is not a strict absence of growth. Rather, most strains display very slow or delayed growth. Upon prolonged incubation, most complementation strains

exhibited residual growth exceeding that of the parental mutants, suggesting at least a degree of functional restoration. Consistent with this, even the construct that effectively complements growth (J23104-R28-*dctA*) exhibits a markedly prolonged lag phase when transferred from rich medium (TY) to succinate/ammonia minimal medium, before eventually entering exponential growth comparable to WT (Figure S3.7).

Together, these results that most complementation strains remain impaired under succinate/ammonia conditions, and it is difficult to examine this observed growth impairment by utilising alternative nitrogen sources. Rather than complete absence of growth, many strains exhibited delayed or reduced growth, indicating a defect in adaptation to these conditions. Notably, the phenotype of the complementation strains resembled that observed for the Tn*5* mutant RU150.

Constitutive dctA *expression restores succinate transport but not CCR*

The key question was whether recovery of DctA-mediated uptake would also restore downstream regulatory responsnes. Since J23104-R28-*dctA* was the only construct that restored growth on succinate/ammonia, this construct was analysed further for succinate transport (Figure 3.9).

In both *dctA* and *dctABD* backgrounds, the parental mutants exhibited neglectable succinate transport rates, confirming that disruption of the Dct abolishes C_4-dicarboxylate uptake. In contrast, introduction of *dctA* under control of the J23104-R28 promoter-RBS combination restored succinate transport to levels comparable to, or exceeding, those observed in the WT in both genetic backgrounds. Thus, these results confirm that constitutive *dctA* transcription effectively restored functional C_4-dicarboxyalte transport, even in the absence of the native DctBD regulatory system.

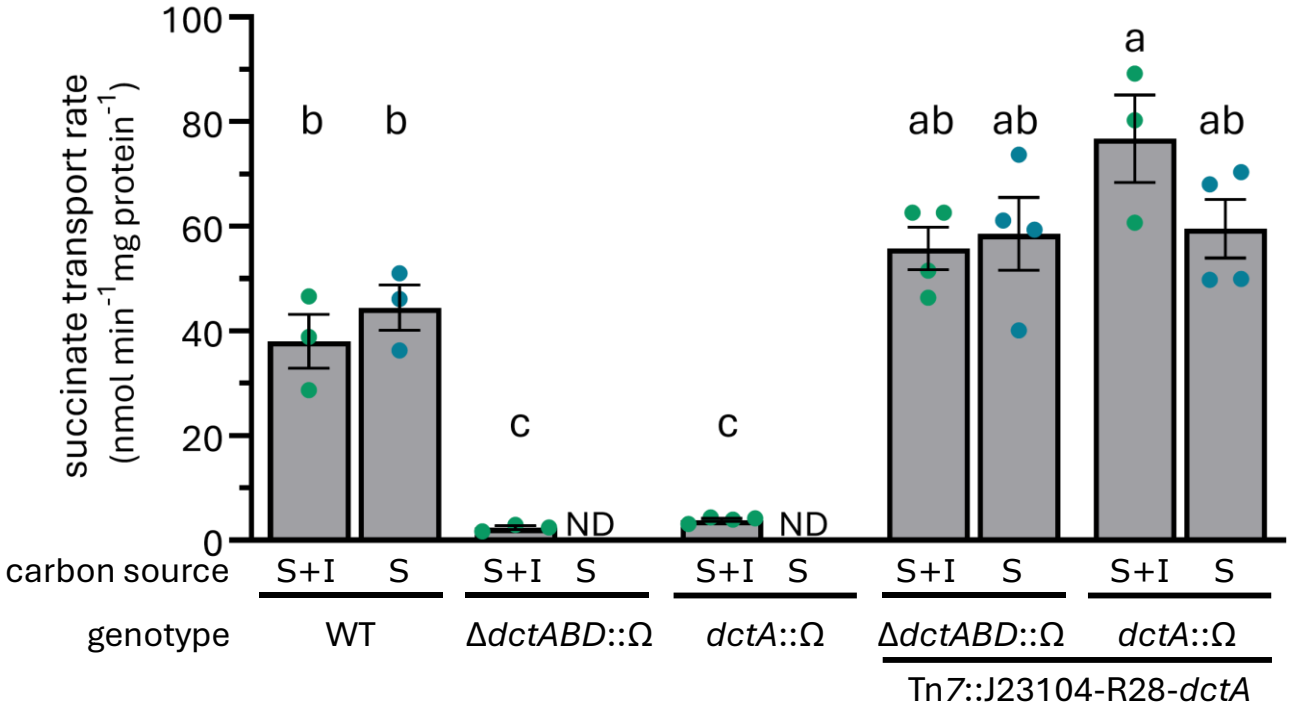


Figure 3.9 Constitutive *dctA* expression restores succinate transport in *dct* mutants to WT levels. Succinate transport rates were measured in WT, Δ*dctABD*::Ω, and *dctA*::Ω strains, as well as the corresponding mutant complemented with a Tn*7* insertion carrying *dctA* expressed constitutively from the J23104 promoter with synthetic ribosome binding site R28. Cells were grown in either succinate and *myo*-inositol (S+I, green) or succinate alone (S, blue). Bars represent mean ± SEM, with individual biological replicates shown. The data stems from two independent experiments. Different letters above bars denote statistical differences (α<0.5), determined by one-way ANOVA followed by Tukey's multiple comparisons. ND (not determined) indicates conditions where transport could not be measured because Δ*dctABD*::Ω and *dctA*::Ω mutants do not grow on succinate as the sole carbon source.

The same constitutive *dctA* complementation strains were then tested for succinate-mediated CCR using the inositol biosensor. Despite restoring transport, J23104-R28-*dctA* did not restore CCR in either the *dctABD* or *dctA* mutant background (Figure 3.10). The inability to restore CCR was also observed when malate rather than succinate was used together with *myo*-inositol (Figure S3.8).

More broadly, none of the constitutive *dctA* constructs restored succinate-mediated repression of the inositol reporter, even when assessed using the modified inoculation protocol used for slowly growing strains (Figure S3.9). These findings separate transporter activity from the regulatory phenotype: although C_4-dicarboxylate uptake can be

reintroduced artificially, this alone is not sufficient to rebuild the signalling or metabolic state required for normal CCR.

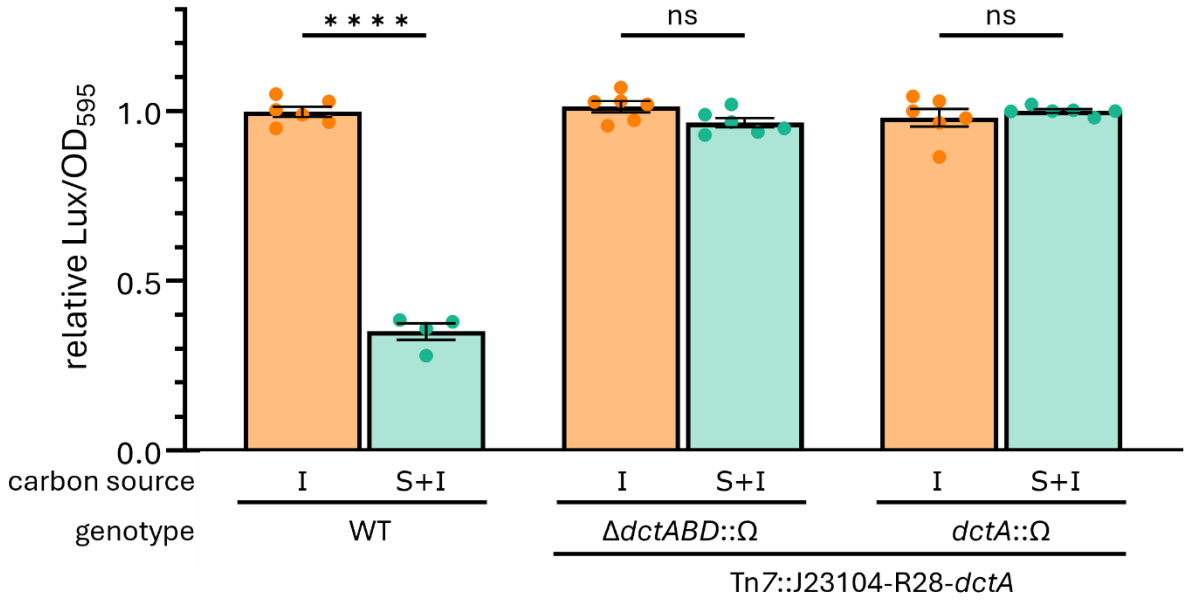


Figure 3.10 Constitutive *dctA* expression do not restore CCR. Luminescence of a inositol biosensor in WT *Rlv*3841 and two Dct mutants complemented with constitutive *dctA* expression, normalised to optical density (Lux/OD_{595}) and expressed relative to WT grown in *myo*-inositol. Luminescence was quantified from liquid cultures grown in MM containing 10 mM *myo*-inositol (I, orange) or 20 mM succinate plus 10 mM myo-inositol (S+I, green). Bars represent mean ± SEM (n ≥ 4). Note that the data stems from two independent experiments. Statistical significance reflects Sidak-corrected comparisons between growth conditions within each genotype following a mixed-effects model, where **** $p < 0.0001$, and ns not significant.

Reinstating dctA *expression is not enough to recover full symbiotic performance*

Rhizobial mutans lacking the DctA permease display a well-characterised Fix^- phenotype, reflecting the requirement for C_4-dicarboxylate uptake for bacteroid survival and nitrogen fixation. To determine whether constitutive *dctA* transcription could restore this function, *dct* mutant strains carrying the best-performing constitutive construct, J23104-R28-*dctA*, were inoculated onto pea plants (Figure 3.11).

Inoculation of pea plants with complemented *dct* mutant strains produced nodules in numbers comparable to WT (Figure 3.11A), but those induced by Golden-Gate complemented *dct* strains were significantly smaller in size (Figure 3.11B) and more heterogeneous in both morphology and colour (Figure 3.11F). Many appeared as small, white, pin-like nodules, whereas others showed (partial) accumulation of red leghaemoglobin, and a subset exhibited elongation resembling the characteristic indeterminate nodules formed on pea, albeit still smaller than the average WT infected nodule. This increased heterogeneity was associated with reduced nitrogen fixation efficiency, reaching ~25-30% of WT levels when normalised per plant and approximately 55% when normalised to nodule weight (Figure 3.11C,D). Plants were significantly smaller than those inoculated with the WT strain (Figure 3.11E).

Engineered constitutive *dctA* expression therefore provided only partial symbiotic function and did not restore WT nitrogen fixation.

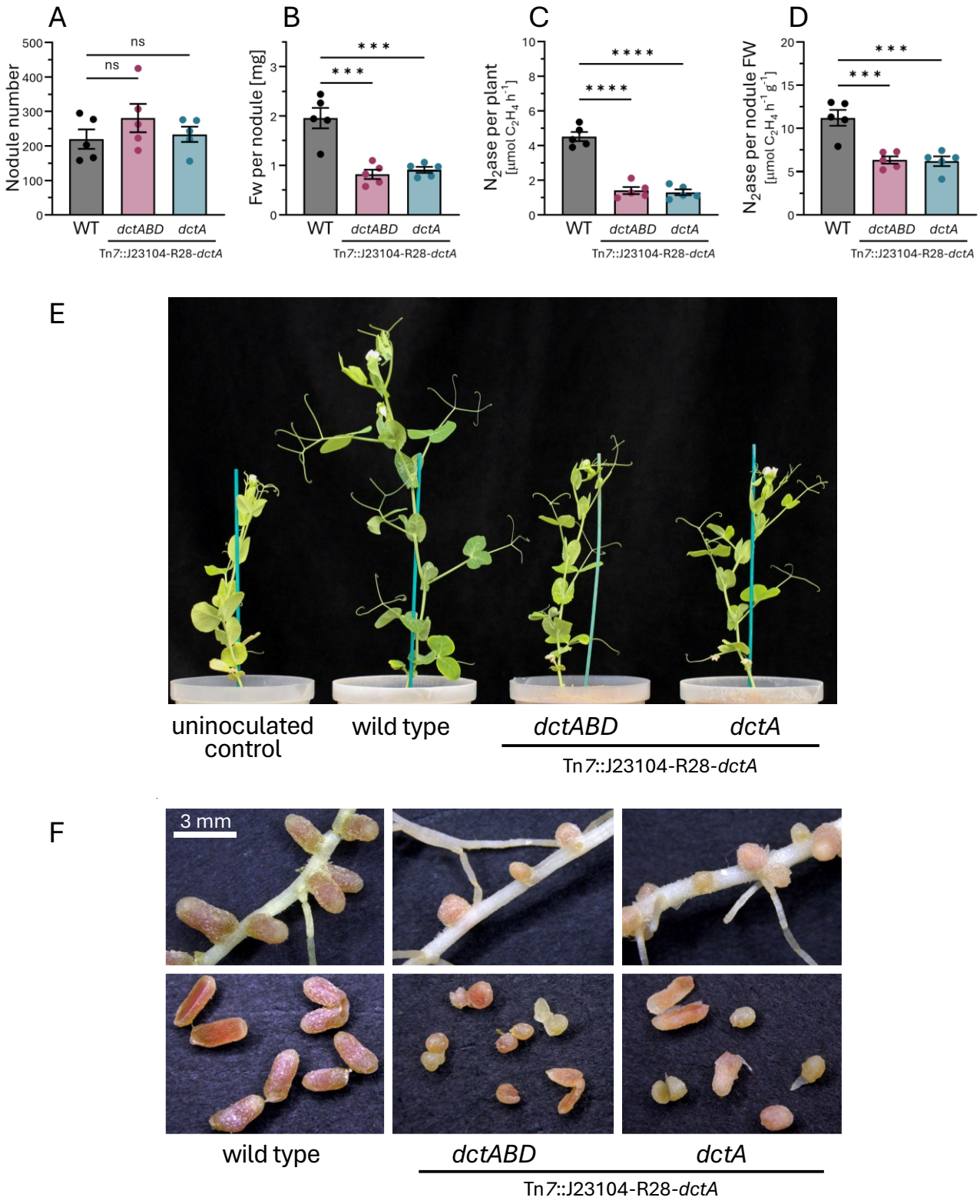


Figure 3.11 Constitutive *dctA* expression does not restore nitrogen fixation. *Pisum sativum* cv. Avola seedlings were inoculated with *Rlv*3841 wild-type (WT), a Δ*dctABD*::Ω, or a *dctA*::Ω mutant complemented with a Tn*7* insertion carrying *dctA* expressed constitutively from the J23104 promoter with synthetic ribosome binding site R28, and grown for 24 dpi. Plants were assayed for nodule number **(A)**, fresh weight (FW) per nodule **(B)**, nitrogenase activity per plant **(C)**, and nitrogenase activity per nodule FW **(D)**. Representative plants **(E)** as well as nodules and nodule cross sections **(F)** are shown for the indicated strains. The scale bar in (F) applies to all images. Each strain was tested on n = 5 plants, with bars indicating mean ± SD. Statistical analysis was performed using one-way ANOVA followed by Tukey's multiple comparisons tests. Asterisks indicate significant differences (**** $p < 0.0001$, *** $p < 0.001$); ns, not significant.

Native promoter dctA complementation as a control

As all attempts to restore growth and CCR in *dctABD* or *dctA* mutant by reintroducing *dctA* under synthetic control had proven more difficult than initially expected, this raised the question of whether *dctA* transcription can only be complemented within its native regulatory context. In a final attempt to resolve the growth defects observed in the abovementioned Golden Gate – based constructs, a native *dctA* complementation strain was generated as a control. For this, the native *dctA*, including its native promoter, the full coding sequence, and the downstream intergenic region containing the native terminator, was cloned into a Tn7-delivery plasmid and conjugated into the *dctA* and *dctABD* strain. Because this construct retained native DctBD-dependent regulation, it was expected to behave more similarly to WT.

In the *dctA* mutant, the native promoter construct restored growth on succinate, demonstrating that the insert was functional. As expected, no rescue was observed in the *dctABD* mutant, confirming that activation of the Tn*7* insert required DctBD.

However, even in the *dctA* background, growth remained slower than WT, with a prolonged lag phase following transfer from rich medium to minimal medium, similar to that observed for constitutive *dctA* complementation constructs (Figure S3.7).

While the complemented *dctA* strain showed substantial growth when plated onto succinate/ammonia, it was noted that growth in liquid cultures remained impaired, with cultures requiring substantially longer than WT to reach stationary phase.

When tested for CCR, the native promoter complementation still failed to restore succinate-mediated repression of the inositol reporter (Figure S3.10). Thus, even restoration of *dctA* under native transcriptional control was insufficient to recover a fully WT phenotype.

Discussion

In this chapter, we employed two complementary approaches to examine whether C_4-dicarboxylate transport by the DctA permease can be uncoupled from its native DctBD regulatory circuit, in order to disentangle contributions of the Dct system to downstream phenotypes. The first involved analysis of the spontaneous regulatory mutant RU150 and its suppressor derivative RU152-22, whereas the second employed engineered *dctA* expression via synthetic constitutive promoters. Despite these distinct strategies, both approaches produced strains with constitutive *dctA* expression leading to comparable growth defects and, importantly, failed to restore CCR or nitrogen fixation to WT-levels. The only exception was the suppressor strain RU152-22, which is discussed in more detail below. Notably, the similarity of phenotypes observed in RU150 and the engineered *dctA* complementation strains suggests a shared underlying regulatory imbalance, and these systems are therefore discussed jointly in the following sections.

RU150 demonstrates that C4-dicarboxylate transport alone is insufficient for normal physiological function

The spontaneous regulatory mutant RU150, in which native *dct* regulation is disrupted by a Tn*5* insertion (Figure S3.2), provides a key example demonstrating that C_4-dicarboxylate transport alone is insufficient to support normal physiological function. Although *dctA* transcript levels in RU150 are reduced to a fraction of those observed in induced WT cells (Reid & Poole, 1998, Figure S3.5), succinate transport rates remain comparable to WT (Figure S3.4). This indicates that C_4-dicarboxylate transport saturates at relatively low levels of *dctA* expression, suggesting that transporter expression is not the primary rate-limiting factor for uptake under these conditions. This is consistent with previous findings showing that fivefold transcriptional overexpression of *dctA* in *S. meliloti* does not result in increased succinate transport rates (Rastogi et al., 1992), further supporting the notion that transport is not proportional to P_{dctA} activity and that near-maximal transport activity is achieved at or below WT expression levels.

Instead, these observations raise the question of whether the higher levels of *dctA* transcription observed under inducing conditions in the WT serve functions beyond substrate transport. One proposed role is the modulation of DctBD signalling, as

suggested by Reid & Poole (1998), who hypothesised that DctA may influence the activity of the DctB sensor kinase. In this context, reduced *dctA* expression in RU150 may not limit transport per se, but instead disrupts the regulatory coordination between transport and signalling within the Dct system (see below).

While C_4-dicarboxylate transport is preserved in RU150, the strain exhibits pronounced defects across multiple physiological functions: Growth is severely impaired when succinate is provided as the sole carbon source in combination with ammonia (Reid, 1995), and RU150 fails to mount normal CCR of the alternative carbon source *myo*-inositol (Figure 3.3). In addition, RU150 displays a marked reduction in symbiotic nitrogen fixation, forming small, white nodules on pea with only minimal residual nitrogenase activity (Figure 3.6). Consistent with this, no acetylene reduction was detected when RU150 was inoculated on *Vicia sativa* (Reid & Poole, 1998), indicating that, depending on the host, the strain produces a near- to complete Fix^- phenotype.

Taken together, these observations demonstrate that the phenotype of RU150 cannot be readily explained by impaired substrate uptake, but instead reflects a broader disruption of physiological processes that likely depend on correct *dct* regulation. At present, it remains unclear whether this misregulation arises primarily from the uncoupling of *dctA* expression from DctBD control, from constitutive expression per se, or from a combination of both. Notably, a similar phenotype has been reported for a *dctB* mutant in which *dctA* expression is constitutive, resulting in nitrogen fixation rates below 20% of the WT (Mavridou et al., 1995). Collectively, these findings corroborate the idea that, although C_4-dicarboxylate uptake is essential for nitrogen fixation, proper *dct* regulation is equally indispensable. Uncontrolled or misregulated *dctA* expression adversely affects symbiotic function, although the underlying mechanism remains to be elucidated.

Engineered DctA complementation restores transport but fails to recreate the native regulatory state

To determine whether restoration of *dctA* expression is sufficient to recover normal physiological function, *dctA* was reintroduced into *dct* mutant backgrounds under the control of synthetic constitutive promoters. This design uncoupled *dctA* expression from native DctBD-dependent regulation and, in principle, allowed transport to be restored

independently of the signalling system. Several constructs supported measurable *dctA* expression (Figure 3.8); however, even the single-copy design employed here proved challenging, as higher-expression constructs were not tolerated in *E. coli* or *R. leguminosarum*. This is consistent with earlier studies reporting instability and toxicity associated with plasmid-based *dctA* (over)expression (Rastogi et al., 1992; Reid, 1995). Of the successfully obtained constructs, even the weakest constitutive promoters generated *dctA* expression levels at or above those observed in the WT (Figure 3.8), indicating that constitutive expression readily exceeds physiological levels. This may contribute to the growth defects observed in several strains and suggests that no fixed level of constitutive *dctA* expression can replicate the dynamic regulation required for, and achieved by, the native system.

Despite these limitations, one construct produced *dctA* expression levels not significantly different from those of induced WT, restored succinate transport to near- or above wild-type levels, and recovered growth on succinate in combination with ammonia to levels approaching those of the WT, although full WT growth was not recapitulated. This demonstrates that functional DctA-mediated uptake had been re-established.

However, none of the engineered complementation strains restored CCR, and even the best-performing construct remained impaired in symbiotic function, with complemented strains displaying reduced nitrogen fixation relative to wild type. These findings indicate that, although transport can be restored experimentally, constitutive *dctA* expression - even at near-native transcript levels and across different genetic backgrounds - does not recreate the regulatory conditions required for normal physiological function and is insufficient to re-establish the full *dct*-dependent phenotype. The inability of constitutive *dctA* expression to restore function therefore points to a requirement for regulatory integration beyond transporter activity alone. The engineered strains instead mirror the phenotype of the regulatory mutant RU150, albeit slightly less severe growth and symbiotic impairment.

In *S. meliloti*, an alternative symbiotic activation (ASA) of *dctA* that is independent of DctBD has been extensively described (Boesten et al., 1998; Watson, 1990; Yarosh et al., 1989), although its mechanism has not been identified. Whether a similar regulatory mechanism exists in *R. leguminosarum* is unknown; however, if present, constitutive

dctA expression would likely interfere with this secondary regulation and may account for the partially impaired symbiotic phenotype observed in engineered strains. In addition, we observed a heterogeneous distribution of nodule morphologies on pea plants infected with the engineered *dctA* strains. A similar phenotype has been reported by Yurgel & Kahn (2005), who described both small, white ineffective nodules and elongated, partially pink nodules in *M. sativa* plants inoculated with *dctA* mutants retaining partial transport capacity.

These observations suggest that not only the presence of DctA transport, but also its temporal and spatial regulation during nodule development, is critical for effective symbiotic function. Constitutive or misregulated expression is therefore unlikely to reproduce the dynamic metabolic transitions required during bacteroid differentiation. While the Dct system is not crucial for colonisation and infection, it becomes essential in bacteroids (Wheatley et al., 2020), yet *dctA* expression appears to vary across developmental zones of the nodules (Boesten et al., 1998).

To our surprise, even reintroduction of *dctA* under control of its native promoter did not fully restore WT behaviour, as assessed by growth on succinate, and consequently failed to recover normal CCR (Figure S3.10). Although partial complementation was observed, restoration of native transcriptional control alone was insufficient to re-establish full Dct function. The basis for this incomplete restoration of function remains to be determined. A likely explanation is that complementation at the Tn*7* insertion site fails to recapitulate the genomic context of the *dct* locus, where spatial and regulatory coupling to *dctBD* may be essential. Alternatively, yet unidentified regulatory interactions not captured in the cloned fragment may contribute to functional coupling within the system. It is also possible that the native *dctABD* locus, or part of its sequence, contains additional features, such as small regulatory RNAs, that were disrupted by the Ω insertion, although no such features are currently known to us in this region.

Balanced *dctA* expression and DctBD signalling are required for functional coupling of transport and regulation

The combined analysis of RU150, RU152-22, and the engineered *dctA* complementation strains points to a central role for balanced regulation within the Dct system. A key

observation emerging from this study is that transport capacity can be maintained across a wide range of *dctA* expression levels, whereas physiological function is highly sensitive to disruption of regulatory coupling. This suggests that accurate function depends not on absolute DctA abundance, but on its coordinated interaction with the DctBD signalling system.

In his thesis, Reid (1995) proposed a model in which DctA and DctB may form a complex within the membrane, thereby linking substrate transport to signal transduction. In this framework, DctA would fulfil a dual role, functioning not only as a transporter but also as a regulator of DctBD signalling, thereby linking substrate uptake to regulatory output. Supporting this view, the absence of DctA has been shown to render the DctBD system hypersensitive to induction, including to substrates normally not recognized by DctBD in the presence of DctA, suggesting that DctA contributes to stabilising or modulating DctB signalling behaviour (Reid, 1998).

Although a direct physical interaction between DctA and DctB has long been proposed, experimental evidence for such interactions remains limited. This is likely due to the membrane-bound nature of both proteins, which complicates biochemical and structural analysis. Attempts to model potential interactions using AlphaFold multimer did not yield high-confidence predictions for a DctA-DctB interaction. However, this does not exclude such interactions, as current prediction tools remain similarly limited in their ability to model dynamic and/or membrane-associated protein complexes (Agarwal & McShan, 2024).

Disruption of Dct regulation impairs carbon - nitrogen coordination

A striking feature shared between RU150 and the engineered *dctA* complementation strains is their impaired growth on succinate with ammonia as the nitrogen source. All strains grew normally on glucose with ammonia or on succinate when amino acids were provided as a nitrogen source, although it should be noted that all tested amino acids also serve as (poor) carbon sources. Consequently, these experiments could not distinguish whether the observed phenotype arises from impaired succinate transport and/or metabolism, ammonia assimilation, or an interaction between the two, as no condition tested allowed either process to be assessed independently while controlling

for the other. Nevertheless, these observations are consistent with the growth defect not being due to a general inability to utilise either succinate or ammonia individually, but rather with a failure to properly coordinate carbon and nitrogen metabolism when Dct regulation is disrupted, although this argumentation remains speculative.

Reid (1998) proposed that this phenotype arises from inappropriate activity of the DctBD signalling system, whereby phosphorylated DctD may engage in cross-regulation with other σ^{54}-dependent pathways involved in ammonia assimilation. In support of this model, disruption of either *dctB* or *dctD* in the RU150 background restores growth on succinate/ammonia. More broadly, the shared domain architecture of σ^{54}-dependent regulators such as DctD, NtrC, and NifA suggests that cross-regulation between these systems is mechanistically plausible and has been reported previously (e.g Labes & Finan, 1993; Reid & Poole, 1998). Conversely, it remains unclear whether such interactions represent a physiological regulatory mechanism or an artefact of perturbed systems.

In an attempt to explore this possibility, transcript levels of the nitrogen regulator *ntrC* and key ammonia assimilation genes *glnA* and *glnII* were assessed under succinate/ammonia conditions (Figure S3.11). Although a dysregulated *dct* system indeed seems to negatively affect expression of *glnA* and *glnII*, no consistent transcriptional pattern was observed that could substantiate impaired ammonia assimilation in RU150 and the *dct* complementation strains compared to the WT or RU152-22. This suggests that the observed growth defect is unlikely to be explained solely at the transcriptional level of carbon and nitrogen regulators. However, this does not negate the possibility that regulatory crosstalk occurs at a different level or may involve other factors, which will require further investigation to resolve this phenotype.

Importantly, the present findings indicate that the RU150 phenotype cannot be explained solely by inappropriately phosphorylated DctD, as similar growth defects were observed in engineered strains lacking the native *dctABD* locus. This demonstrates that impaired growth on succinate/ammonia can arise independently of DctBD signalling and may instead be attributed to an imbalance within the Dct system more generally. Our observations further indicate that *dctA* expression is only tolerated within a narrow range

around native induced levels, and that deviations in either direction have regulatory consequences. According to qPCR analysis (Figure 3.8), engineered *dctA* expression closely matched induced WT levels, yet still resulted in aberrant behaviour. The original model can therefore be extended to reflect that proper carbon-nitrogen coordination requires a balanced relationship between DctA and DctBD, as both reduced *dctA* expression in the presence of active DctBD signalling (as in RU150) and the inverse condition of excess or misregulated *dctA* in the absence of coordinated signalling (as in the engineered strains) give rise to similar growth defects. Likewise, constitutive expression of *dctA*, as opposed to inducible expression, may be responsible for the observed phenotype.

Together, these findings highlight the difficulty of attributing the observed growth impairment to a single underlying cause, and instead indicate a broader disruption of carbon–nitrogen coordination when *dct* regulation is perturbed. Rather than representing a complete inability to utilise C_4-dicarboxylates, the phenotype appears to arise from a failure to adapt to conditions requiring simultaneous carbon uptake and nitrogen assimilation. In this context, disruption of *dct* regulation may impair the integration of carbon uptake with nitrogen metabolism, leading to a condition in which growth is possible but not efficiently sustained. This interpretation also provides a potential framework for understanding the associated defects in CCR and symbiotic performance, both of which depend on effective utilisation of C_4-dicarboxylates.

Importantly, this indicates that the observed phenotype reflects a failure of metabolic adaptation rather than a fundamental inability to utilise succinate or ammonia, reinforcing the view that proper regulatory coordination is required to sustain growth under these conditions. More broadly, these findings further highlight the sensitivity of the Dct system to perturbation, where even targeted modifications give rise to complex and unanticipated phenotypes.

Not all transport restoration recreates the same metabolic state

The finding that restoration of DctA-mediated transport does not recover downstream physiological functions in a variety of strains contrasts with observations from the preceding chapter, where complementation with the heterologous malate transporter

MaeP restored CCR (Figure 2.7) and facilitated symbiotic nitrogen fixation levels indistinguishable from WT (Mitsch et al., 2018). This discrepancy indicates that not all modes of C_4-dicarboxylate uptake are functionally equivalent, even when measurable transport activity is supported. Alternatively, it is conceivable that the growth defects observed in RU150 and engineered *dctA* strains – likely linked to impaired carbon-nitrogen coordination – mask or limit restoration of normal physiological behaviour.

One explanation for this observation is that excess DctA production may perturb membrane integrity or promote protein misfolding and aggregation. As protein levels were not determined, it remains unclear to what extent the measured dctA transcript levels translate into functional DctA protein.

Another explanation for this difference lies in the regulatory context in which transport occurs. In the native system, *dctA* expression is dynamically induced in response to C_4-dicarboxylate availability sensed by DctB, allowing coordinated integration of transport with downstream metabolic responses. In contrast, uncontrolled C_4-dicarboxylate influx permitted by constitutive expression of *dctA* may overwhelm and therefore disrupt temporal regulation required for proper metabolic coordination. As concluded in Chapter 2, CCR operates via an inducer exclusion mechanism that depends on timely repression of alternative carbon pathways. If C_4-dicarboxylate uptake is not properly synchronised with cellular metabolism, particularly under conditions where ammonia assimilation is possibly also perturbed, this regulatory response may fail, preventing effective repression of alternative carbon sources.

Importantly, this discrepancy cannot be attributed to a specific C_4-dicarboxylate used, as CCR was not restored in engineered strains when tested with either succinate or malate in combination with *myo*-inositol (Figure S3.9). Instead, it suggests that fundamental differences exist between MaeP- and DctA-mediated transport in how they interface with the cellular regulatory network. In addition, this observation suggests that DctA may interact with proteins other than DctBD, indicating the presence of additional, yet unidentified interaction partners.

Interestingly, MaeP is a relatively low-affinity transporter compared to DctA, with a K_m for malate of approximately 41 µM and a V_{max} of ~1 nmol min^{-1} mg protein $^{-1}$ (Mitsch, 2000),

whereas DctA exhibits a K_m for succinate between 1-5 µM depending on the rhizobial species (Yurgel & Kahn, 2004). Despite this, MaeP-mediated uptake may generate intracellular metabolite pools or flux dynamics sufficient to trigger CCR, potentially because it bypasses the regulatory coupling and feedback control to which DctA is subject, for example through interaction with DctB. This could explain why restoration of transport via DctA in most cases does not reproduce the same physiological outcome as MaeP-mediated uptake.

Further support for the interpretation that CCR is not mediated directly by the Dct system comes from the suppressor strain RU152-22, which restores growth, CCR, and symbiotic performance despite disruption of the native *dct* architecture**.** Although the genetic basis of this restoration is complex, RU152-22 represents a configuration in which DctA-mediated transport is re-established, although the canonical *dct* regulon is no longer intact, yet full physiological function is recovered. This indicates that DctBD signalling itself is not strictly required for CCR or symbiotic function, provided that an appropriate metabolic state is established. In this respect, the behaviour of RU152-22 aligns with MaeP complementation, reinforcing the conclusion that restoration of function depends on metabolism of C_4-dicarboxylates rather than transport alone.

The Dct system functions as an integrated transport-regulatory module

Taken together, the findings in this chapter support a model in which the Dct system operates as an integrated module linking C_4-dicarboxylate uptake to broader physiological regulation. In this framework, DctA functions not only as a transporter, but also as part of a regulatory system that coordinates carbon uptake with downstream metabolic and signalling processes. Disruption of this coordination – whether through altered transcription levels or loss of regulatory control – leads to widespread physiological consequences. This perspective helps reconcile the diverse phenotypes observed across the different experimental approaches: while transport is clearly required, it is not sufficient to establish the physiological state necessary for growth, CCR, or symbiotic nitrogen fixation. Instead, these processes depend on the proper integration of transport within a regulatory network that balances carbon and nitrogen metabolism.

These findings also have implications for our understanding of bacteroid metabolism. Although C_4-dicarboxylates are well established as the main carbon source during symbiosis, the underlying regulatory rationale for the metabolic preference remains unclear. The host plant supplies sucrose to the nodule, which is subsequently converted into C_4-dicarboxylates for uptake by DctA (Poole & Allaway, 2000); yet rhizobia possess at least two transport systems capable of sucrose uptake, both of which are repressed in bacteroids, along with many other carbon transport and metabolic pathways (Green et al., 2019; Karunakaran et al., 2009; Wheatley et al., 2020). In parallel, nitrogen assimilation is downregulated to enable nitrogen export to the host, resulting in bacteroids becoming auxotrophic for certain nitrogenous compounds (Prell et al., 2009, 2010). While direct evidence is lacking, it is plausible that regulatory coupling between Dct activity, CCR, and nitrogen metabolism contributes to this coordinated reprogramming. In this context, components such as *glnII*, which appear to be dispensable during free-living growth (Wheatley et al., 2017, 2020) but may be regulated in a Dct-dependent manner (Figure S3.11; Reid, 1995), represent potential links between carbon uptake and nitrogen metabolism. Although the underlying mechanisms remain unresolved, these observations point to an integrated regulatory network coordinating carbon and nitrogen metabolism in bacteroids. Elucidating this integration represents an important avenue for future research and may provide targets for improving symbiotic nitrogen fixation.

Future work, in particular, direct measurements of intracellular metabolite pools, analysis of regulatory network activity, and development of systems allowing controlled modulation of *dctA* expression will be important for disentangling the contributions of transport and regulation. Approaches that more closely approximate native regulation, such as weaker promoters, alternative ribosome binding sites, inducible systems, or modification of native regulatory elements affecting P_{dctA} control, may help to resolve the limitations observed with constitutive constructs. More broadly, these findings highlight the Dct system as a key node in metabolic coordination, with implications for understanding and potentially engineering symbiotic nitrogen fixation.

Conclusion

Across both the spontaneous and engineered systems, a consistent pattern emerged. Reduced or inappropriately expressed *dctA* impaired growth on succinate/ammonia, abolished succinate-mediated CCR, and disrupted normal symbiotic nitrogen fixation. Increasing *dctA* expression could restore transport and, in some contexts, growth. However, neither constitutive expression nor reintroduction under native promoter control was sufficient to recover all downstream phenotypes. The data therefore indicate that DctA-mediated transport and DctBD-dependent regulatory output are closely linked but not interchangeable: restoration of transport does not automatically restore the broader physiological and symbiotic functions associated with an intact Dct system. Together, these findings redefine the Dct system as an integrated regulatory module rather than a just a transport pathway.

References

Agarwal, V., & McShan, A. C. (2024). The power and pitfalls of AlphaFold2 for structure prediction beyond rigid globular proteins. *Nature Chemical Biology*, *20*(8), 950–959. https://doi.org/10.1038/s41589-024-01638-w

Arwas, R., McKay, I. A., Rowney, F. R. P., Dilworth, M. J., & Glenn, A. R. (1985). Properties of organic acid utilization mutants of Rhizobium leguminosarum strain 300. *Microbiology*, *131*(8), 2059–2066. https://doi.org/10.1099/00221287-131-8-2059

Batista, S., Catalán, A. I., Hernández-Lucas, I., Martínez-Romero, E., Aguilar, O. M., & Martínez-Drets, G. (2001). Identification of a system that allows a Rhizobium tropici dctA mutant to grow on succinate, but not on other C_4-dicarboxylates. *Canadian Journal of Microbiology*, *47*(6), 509–518. https://doi.org/10.1139/w01-041

Beringer, J. E. (1974). R factor transfer in Rhizobium leguminosarum. *Microbiology*, *84*(1), 188–198. https://doi.org/10.1099/00221287-84-1-188

Birkenhead, K., Noonan, B., Reville, W. J., Boesten, B., Manian, S. S., & O'Gara, F. (1990). Carbon utilization and regulation of nitrogen fixation genes in Rhizobium meliloti. *Molecular Plant-Microbe Interactions*, *3*, 167–173.

Boesten, B., Batut, J., & Boistard, P. (1998). DctBD-dependent and -independent expression of the Sinorhizobium (Rhizobium) meliloti C_4-dicarboxylate transport gene (dctA) during symbiosis. *Molecular Plant-Microbe Interactions*, *11*(9), 878–886. https://doi.org/10.1094/MPMI.1998.11.9.878

Burriolo, C. A. (2024). *C_4-dicarboxylate uptake and metabolism in free-living Mesorhizobium ciceri CC1192*. Honours thesis, Murdoch University.

Choi, K.-H., Gaynor, J. B., White, K. G., Lopez, C., Bosio, C. M., Karkhoff-Schweizer, R. R., & Schweizer, H. P. (2005). A Tn7-based broad-range bacterial cloning and expression system. *Nature Methods*, *2*(6), 443–448. https://doi.org/10.1038/nmeth765

Choi, K.-H., Mima, T., Casart, Y., Rholl, D., Kumar, A., Beacham, I. R., & Schweizer, H. P. (2008). Genetic tools for select-agent-compliant manipulation of Burkholderia pseudomallei. *Applied and Environmental Microbiology*, *74*(4), 1064–1075. https://doi.org/10.1128/AEM.02430-07

Davies, S. J., Golby, P., Omrani, D., Broad, S. A., Harrington, V. L., Guest, J. R., Kelly, D. J., & Andrews, S. C. (1999). Inactivation and regulation of the aerobic C_4-dicarboxylate transport (*dctA*) gene of Escherichia coli. *Journal of Bacteriology*, *181*(18), 5624–5635. https://doi.org/10.1128/JB.181.18.5624-5635.1999

Day, D. A., & Copeland, L. (1991). Carbon metabolism and compartmentation in nitrogen-fixing legume nodules. *Plant Physiology and Biochemistry*, *29*(2) 185–201.

Ditta, G., Stanfield, S., Corbin, D., & Helinski, D. R. (1980). Broad host range DNA cloning system for gram-negative bacteria: Construction of a gene bank of Rhizobium meliloti. *Proceedings of the National Academy of Sciences*, *77*(12), 7347–7351. https://doi.org/10.1073/pnas.77.12.7347

Dombrecht, B., Marchal, K., Vanderleyden, J., & Michiels, J. (2002). Prediction and overview of the RpoN-regulon in closely related species of the rhizobiales. *Genome Biology*, *3*(12), research0076.1. https://doi.org/10.1186/gb-2002-3-12-research0076

Finan, T. M., Wood, J. M., & Jordan, D. C. (1983). Symbiotic properties of C_4-dicarboxylic acid transport mutants of Rhizobium leguminosarum. *Journal of Bacteriology*, *154*(3), 1403–1413. https://doi.org/10.1128/jb.154.3.1403-1413.1983

Geddes, B. A., Mendoza-Suárez, M. A., & Poole, P. S. (2019a). A bacterial expression vector archive (BEVA) for flexible modular assembly of Golden Gate-compatible vectors. *Frontiers in Microbiology*, *9*, 3345. https://doi.org/10.3389/fmicb.2018.03345

Geddes, B. A., Paramasivan, P., Joffrin, A., Thompson, A. L., Christensen, K., Jorrin, B., Brett, P., Conway, S. J., Oldroyd, G. E. D., & Poole, P. S. (2019b). Engineering transkingdom signalling in plants to control gene expression in rhizosphere bacteria. *Nature Communications*, *10*(1), 3430. https://doi.org/10.1038/s41467-019-10882-x

Giblin, L., Boesten, B., Turk, S., Hooykaas, P., & O'gara, F. (1995). Signal transduction in the Rhizobium meliloti dicarboxylic acid transport system. *FEMS Microbiology Letters*, *126*(1), 25–30. https://doi.org/10.1111/j.1574-6968.1995.tb07385.x

Glenn, A. R., & Brewin, N. J. (1981). Succinate-resistant mutants of Rhizobium leguminosarum. *Microbiology*, *126*(1), 237–241. https://doi.org/10.1099/00221287-126-1-237

Glenn, A. R., Poole, P. S., & Hudman, J. F. (1980). Succinate uptake by free-living and bacteroid forms of Rhizobium leguminosarum. *Microbiology*, *119*(1), 267–271. https://doi.org/10.1099/00221287-119-1-267

Green, R. T., East, A. K., Karunakaran, R., Downie, J. A., & Poole, P. S. (2019). Transcriptomic analysis of Rhizobium leguminosarum bacteroids in determinate and indeterminate nodules. *Microbial Genomics*, *5*(2). https://doi.org/10.1099/mgen.0.000254

Hanahan, D. (1983). Studies on transformation of Escherichia coli with plasmids. *Journal of Molecular Biology*, *166*(4), 557–580. https://doi.org/10.1016/S0022-2836(83)80284-8

Hardy, R. W. F. (1977). Rate-limiting steps in biological photoproductivity. In A. Hollaender, R. H. Burris, P. R. Day, R. W. F. Hardy, D. R. Helinski, M. R. Lamborg, L. Owens, & R. C. Valentine (Eds), *Genetic Engineering for Nitrogen Fixation* (pp. 369–399). Springer US. https://doi.org/10.1007/978-1-4684-0880-5_23

Hoffman, B. M., Lukoyanov, D., Yang, Z.-Y., Dean, D. R., & Seefeldt, L. C. (2014). Mechanism of nitrogen fixation by nitrogenase: The next stage. *Chemical Reviews*, *114*(8), 4041–4062. https://doi.org/10.1021/cr400641x

Hosie, A. H. F., Allaway, D., Galloway, C. S., Dunsby, H. A., & Poole, P. S. (2002). Rhizobium leguminosarum has a second general amino acid permease with unusually broad substrate specificity and high similarity to branched-chain amino acid transporters (Bra/LIV) of the ABC family. *Journal of Bacteriology*, *184*(15), 4071–4080. https://doi.org/10.1128/JB.184.15.4071-4080.2002

Johnston, A. W. B., & Beringer, J. E. (1975). Identification of the Rhizobium strains in rea root nodules using genetic markers. *Journal of General Microbiology*, *87*(2), 343–350. https://doi.org/10.1099/00221287-87-2-343

Jording, D., Sharma, P. K., Schmidt, R., Engelke, T., Uhde, C., & Pühler, A. (1993). Regulatory aspects of the C_4-dicarboxylate transport in Rhizobium meliloti: Transcriptional activation and dependence on effectave symbiosis. *Journal of Plant Physiology*, *141*(1), 18–27. https://doi.org/10.1016/S0176-1617(11)80846-1

Jorrin, B., Haskett, T. L., Knights, H. E., Martyn, A., Underwood, T. J., Dolliver, J., Ledermann, R., & Poole, P. S. (2024). Stable, fluorescent markers for tracking synthetic communities and assembly dynamics. *Microbiome*, *12*(1), 81. https://doi.org/10.1186/s40168-024-01792-2

Karunakaran, R., Ramachandran, V. K., Seaman, J. C., East, A. K., Mouhsine, B., Mauchline, T. H., Prell, J., Skeffington, A., & Poole, P. S. (2009). Transcriptomic analysis of Rhizobium leguminosarum biovar viciae in symbiosis with host plants Pisum sativum and Vicia cracca. *Journal of Bacteriology*, *191*(12), 4002–4014. https://doi.org/10.1128/JB.00165-09

Kustu, S., Santero, E., Keener, J., Popham, D., & Weiss, D. (1989). Expression of sigma 54 (ntrA)-dependent genes is probably united by a common mechanism. *Microbiological Reviews*, *53*(3), 367–376. https://doi.org/10.1128/mr.53.3.367-376.1989

Labes, M., & Finan, T. M. (1993). Negative regulation of sigma 54-dependent dctA expression by the transcriptional activator DctD. *Journal of Bacteriology*, *175*(9), 2674–2681. https://doi.org/10.1128/jb.175.9.2674-2681.1993

Ledebur, H., Gu, B., Sojda, J., & Nixon, B. T. (1990). Rhizobium meliloti and Rhizobium leguminosarum dctD gene products bind to tandem sites in an activation sequence located upstream of sigma 54-dependent dctA promoters. *Journal of Bacteriology*, *172*(7), 3888–3897. https://doi.org/10.1128/jb.172.7.3888-3897.1990

Ledebur, H., & Nixon, B. T. (1992). Tandem DctD-binding sites of the Rhizobium meliloti dctA upstream activating sequence are essential for optimal function despite a 50- to 100-fold difference in affinity for DctD. *Molecular Microbiology*, *6*(23), 3479–3492. https://doi.org/10.1111/j.1365-2958.1992.tb01783.x

Mavridou, A., Barny, M.-A., Poole, P., Plaskitt, K., Davies, A. E., & Johnston, A. W. B. (1995). Rhizobium leguminosarum nodulation gene (nod) expression is lowered by an allele-specific mutation in the dicarboxylate transport gene dctB. *Microbiology*, *141*(1), 103–111. https://doi.org/10.1099/00221287-141-1-103

Mitsch, M. J. (2000). *Characterization of the NADP(+)-dependent malic enzyme of Sinorhizobium (Rhizobium) meliloti and investigations into the requirements of malate uptake and malic enzyme activity in bacteroids*. PhD thesis, McMaster University. https://macsphere.mcmaster.ca/handle/11375/7165?mode=full

Mitsch, M. J., diCenzo, G. C., Cowie, A., & Finan, T. M. (2018). Succinate transport is not essential for symbiotic nitrogen fixation by Sinorhizobium meliloti or Rhizobium leguminosarum. *Applied and Environmental Microbiology*, *84*(1), e01561-17. https://doi.org/10.1128/AEM.01561-17

Nan, B., Liu, X., Zhou, Y., Liu, J., Zhang, L., Wen, J., Zhang, X., Su, X., & Wang, Y. (2010). From signal perception to signal transduction: Ligand-induced dimeric switch of DctB sensory domain in solution. *Molecular Microbiology*, *75*(6), 1484–1494. https://doi.org/10.1111/j.1365-2958.2010.07069.x

Nixon, B. T., Ronson, C. W., & Ausubel, F. M. (1986). Two-component regulatory systems responsive to environmental stimuli share strongly conserved domains with the nitrogen assimilation regulatory genes ntrB and ntrC. *Proceedings of the National Academy of Sciences*, *83*(20), 7850–7854. https://doi.org/10.1073/pnas.83.20.7850

Pini, F., East, A. K., Appia-Ayme, C., Tomek, J., Karunakaran, R., Mendoza-Suárez, M., Edwards, A., Terpolilli, J. J., Roworth, J., Downie, J. A., & Poole, P. S. (2017). Bacterial biosensors for in vivo spatiotemporal mapping of root secretion. *Plant Physiology*, *174*(3), 1289–1306. https://doi.org/10.1104/pp.16.01302

Poole, P., & Allaway, D. (2000). Carbon and nitrogen metabolism in Rhizobium. In *Advances in Microbial Physiology* (Vol. 43, pp. 117–163). Elsevier. https://doi.org/10.1016/S0065-2911(00)43004-3

Poole, P. S., Blyth, A., Reid, C. J., & Walters, K. (1994). Myo-inositol catabolism and catabolite regulation in Rhizobium leguminosarum bv. viciae. *Microbiology*, *140*(10), 2787–2795. https://doi.org/10.1099/00221287-140-10-2787

Prell, J., Bourdès, A., Kumar, S., Lodwig, E., Hosie, A., Kinghorn, S., White, J., & Poole, P. (2010). Role of symbiotic auxotrophy in the rhizobium-legume symbioses. *PLoS ONE*, *5*(11), e13933. https://doi.org/10.1371/journal.pone.0013933

Prell, J., White, J. P., Bourdes, A., Bunnewell, S., Bongaerts, R. J., & Poole, P. S. (2009). Legumes regulate Rhizobium bacteroid development and persistence by the supply of branched-chain amino acids. *Proceedings of the National Academy of Sciences*, *106*(30), 12477–12482. https://doi.org/10.1073/pnas.0903653106

Rastogi, V., Labes, M., Finan, T., & Watson, R. (1992). Overexpression of the dctA gene in Rhizobium meliloti: Effect on transport of C_4 dicarboxylates and symbiotic nitrogen fixation. *Canadian Journal of Microbiology*, *38*(6), 555–562. https://doi.org/10.1139/m92-091

Reid, C. J. (1995). *The regulation of the DCT system in Rhizobium leguminosarum biovar viciae*. PhD thesis, University of Reading.

Reid, C. J., & Poole, P. S. (1998). Roles of DctA and DctB in signal detection by the dicarboxylic acid transport system of Rhizobium leguminosarum. *Journal of Bacteriology*, *180*(10), 2660–2669. https://doi.org/10.1128/JB.180.10.2660-2669.1998

Reid, C. J., Walshaw, D. L., & Poole, P. S. (1996). Aspartate transport by the Dct system in Rhizobium leguminosarum negatively affects nitrogen-regulated operons. *Microbiology*, *142*(9), 2603–2612. https://doi.org/10.1099/00221287-142-9-2603

Ronson, C. W., Astwood, P. M., Nixon, T. B., & Ausubel, F. M. (1987). Deduced products of C_4-dicarboxylate transport regulatory genes of Rhizobium leguminosarum are homologous to nitrogen regulatory gene products. *Nucleic Acids Research*, *15*(19), 7921–7934. https://doi.org/10.1093/nar/15.19.7921

Ronson, C. W., Lyttleton, P., & Robertson, J. G. (1981). C_4-dicarboxylate transport mutants of Rhizobium trifolii form ineffective nodules on Trifolium repens. *Proceedings of the National Academy of Sciences*, *78*(7), 4284–4288. https://doi.org/10.1073/pnas.78.7.4284

Sambrook, J., Fritsch, E. F., Maniatis, T., Russell, D. W., & Green, M. R. (1989). *Molecular cloning: A laboratory manual*. Cold Spring Harbor Laboratory Press.

Six, S., Andrews, S. C., Unden, G., & Guest, J. R. (1994). Escherichia coli possesses two homologous anaerobic C_4-dicarboxylate membrane transporters (DcuA and DcuB) distinct from the aerobic dicarboxylate transport system (Dct). *Journal of Bacteriology*, *176*(21), 6470–6478. https://doi.org/10.1128/jb.176.21.6470-6478.1994

Sojda, J., Gu, B., Lee, J., Hoover, T. R., & Nixon, B. T. (1999). A rhizobial homolog of IHF stimulates transcription of dctA in Rhizobium leguminosarum but not in Sinorhizobium meliloti. *Gene*, *238*(2), 489–500. https://doi.org/10.1016/S0378-1119(99)00366-2

Thoma, S., & Schobert, M. (2009). An improved Escherichia coli donor strain for diparental mating. *FEMS Microbiology Letters*, *294*(2), 127–132. https://doi.org/10.1111/j.1574-6968.2009.01556.x

Tjahjono, O. (2025). *Regulation of global metabolism by PTS-NTR in Rhizobium leguminosarum*. PhD thesis, University of Oxford.

Udvardi, M., & Poole, P. S. (2013). Transport and metabolism in legume-rhizobia symbioses. *Annual Review of Plant Biology*, *64*(1), 781–805. https://doi.org/10.1146/annurev-arplant-050312-120235

Van Slooten, J. C., Bhuvanasvari T. V., Bardin S., & Stanley J. (1992). Two C_4-dicarboxylate transport systems in Rhizobium sp. NGR234: Rhizobial dicarboxylate transport is essential for nitrogen fixation in tropical legume symbioses. *Molecular Plant-Microbe Interactions*, *5*(2), 179. https://doi.org/10.1094/MPMI-5-179

Vance, C. P., Miller, S. S., Driscoll, B. T., Robinson, D. L., Trepp, G., Gantt, J. S., & Samas, D. A. (1998). Nodule carbon metabolism: Organic acids for N_2 Fixation. In C. Elmerich, A. Kondorosi, & W. E. Newton (Eds), *Biological Nitrogen Fixation for the 21st Century* (Vol. 31, pp. 443–448). Springer Netherlands. https://doi.org/10.1007/978-94-011-5159-7_274

Wang, Y., Lee, J. H., Brewer, J. M., & Hoover, T. R. (1997). A conserved region in the σ^{54}-dependent activator DctD is involved in both binding to RNA polymerase and coupling ATP hydrolysis to activation. *Molecular Microbiology*, *26*(2), 373–386. https://doi.org/10.1046/j.1365-2958.1997.5851955.x

Watson, R. J. (1990). Analysis of the C_4-dicarboxylate transport genes of Rhizobium meliloti: Nucleotide sequence and deduced products of dctA, dctB, and dctD. *Molecular Plant-Microbe Interactions*, *3*(3), 174. https://doi.org/10.1094/MPMI-3-174

Watson, R. J., Rastogi, V. K., & Chan, Y.-K. (1993). Aspartate transport in Rhizobium meliloti. *Journal of General Microbiology*, *139*(6), 1315–1323. https://doi.org/10.1099/00221287-139-6-1315

Wheatley, R. M., Ford, B. L., Li, L., Aroney, S. T. N., Knights, H. E., Ledermann, R., East, A. K., Ramachandran, V. K., & Poole, P. S. (2020). Lifestyle adaptations of Rhizobium from rhizosphere to symbiosis. *Proceedings of the National Academy of Sciences*, *117*(38), 23823–23834. https://doi.org/10.1073/pnas.2009094117

Wheatley, R. M., Ramachandran, V. K., Geddes, B. A., Perry, B. J., Yost, C. K., & Poole, P. S. (2017). Role of O_2 in the growth of Rhizobium leguminosarum bv. viciae 3841 on glucose and succinate. *Journal of Bacteriology*, *199*(1). https://doi.org/10.1128/JB.00572-16

Yarosh, O. K., Charles, T. C., & Finan, T. M. (1989). Analysis of C_4-dicarboxylate transport genes in Rhizobium meliloti. *Molecular Microbiology*, *3*(6), 813–823. https://doi.org/https://doi.org/10.1111/j.1365-2958.1989.tb00230.x

Yurgel, S., Mortimer, M. W., Rogers, K. N., & Kahn, M. L. (2000). New substrates for the dicarboxylate transport system of Sinorhizobium meliloti. *Journal of Bacteriology*, *182*(15), 4216–4221. https://doi.org/10.1128/JB.182.15.4216-4221.2000

Yurgel, S. N., & Kahn, M. L. (2004). Dicarboxylate transport by rhizobia. *FEMS Microbiology Reviews*, *28*(4), 489–501. https://doi.org/10.1016/j.femsre.2004.04.002

Yurgel, S. N., & Kahn, M. L. (2005). Sinorhizobium meliloti *dctA* mutants with partial ability to transport dicarboxylic acids. *Journal of Bacteriology*, *187*(3), 1161–1172. https://doi.org/10.1128/JB.187.3.1161-1172.2005

Supplementary Information

Table S3.2 Primers used in this work.

Primer	Sequence 5' → 3'	Description
Tn*5*	GAACGTTACCATGTTAGGAGGT	Tn*5* mapping primer (A. Downie)
oxp6485	CTTCAGCTGGGTGCCGAATT	FW and RV sequencing primers amplifying the *dctA-dctB* intergenic region
oxp6486	GACATGGCGGATTTGTGCAT	
oxp6975	CATGCATGAGCTCACTAGTGTTTT CTGCACGAAACGCAAATAG	FW and RV amplification primer for *Rlv*3841 native *dctA* for HiFi assembly of pOPS2284
oxp6976	TTCGCGAGGTACCGGGCCCAGT GGAACGAGAACGGCTC	
oxp6980	GATGAAGTCGATCGGCAATCTG	RT-qPCR primers for *rpoD*
oxp6981	GCTTCGACCATTTCCTTCTTGG	
oxp7500	TACAACGGCTTCTCGATCGT	RT-qPCR primers for *dctA*
oxp7501	CAGCCGGCCTTTTCCATCTT	
oxp7624	CACCGATGCAGGGATGGTAA	RT-qPCR primers for *dctB*
oxp7625	TCGCCGACGATATCCTTGGA	
oxp7626	GGACGGCGCCTATGATTTCA	RT-qPCR primers for *dctD*
oxp7627	ATCAGCGGCAAGTTCTCCTG	
oxp7628	CGATGGCTATTTGCAGACGC	RT-qPCR primers for *glnA*
oxp7629	AGATAGAGGCAATCGTCTGCG	
oxp7630	AATCGTCGAAGAGCACCTCG	RT-qPCR primers for *glnII*
oxp7631	AGGTAGCGTGCCATCCAGAT	
oxp7632	CTGGATTTCGGCAGGTGAGG	RT-qPCR primers for *ntrC*
oxp7633	ATGGCGGTCATGAAGGTGTT	
oxp2898	TTTTGAAGACAAGGAGGATCCA TAAGGGTTCGCAATCGC	FW and RV amplification primer for P_{rpoD} for Golden Gate assembly of pOGG446
oxp6509	TTTTGAAGACAAAGTATGGGTTG CCATTTATATCGTCGCC	
oxp6558	CACTCTGTGGTCTCAAATGATC GCAGCACCACTCGATGC	FW and RV amplification primer for *dctA* ORF for assembly of pOGG447 (GoldenGate-like module)
oxp6559	CACTTCGTGGTCTCAAAGCTTA TTCGGCGGGCTGAAG	

oxp2327	GATGATCTTCTCGCTGCCGA	FW and RV PCR primers amplifying the *glmS*-RL2383 intergenic region
oxp2328	GCTCTGGCCAATGAGGTTCT	
oxp3060	CACAGCATAACTGGACTGATTTC	PTn7R – FW PCR primer binding to right end of Tn*7* mobile element (Choi et al. 2005)
oxp3061	ATTAGCTTACGACGCTACACCC	PTn7L – RV PCR primer binding to left end of Tn*7* mobile elem (Choi et al. 2005)

FW: forward; RV: reverse

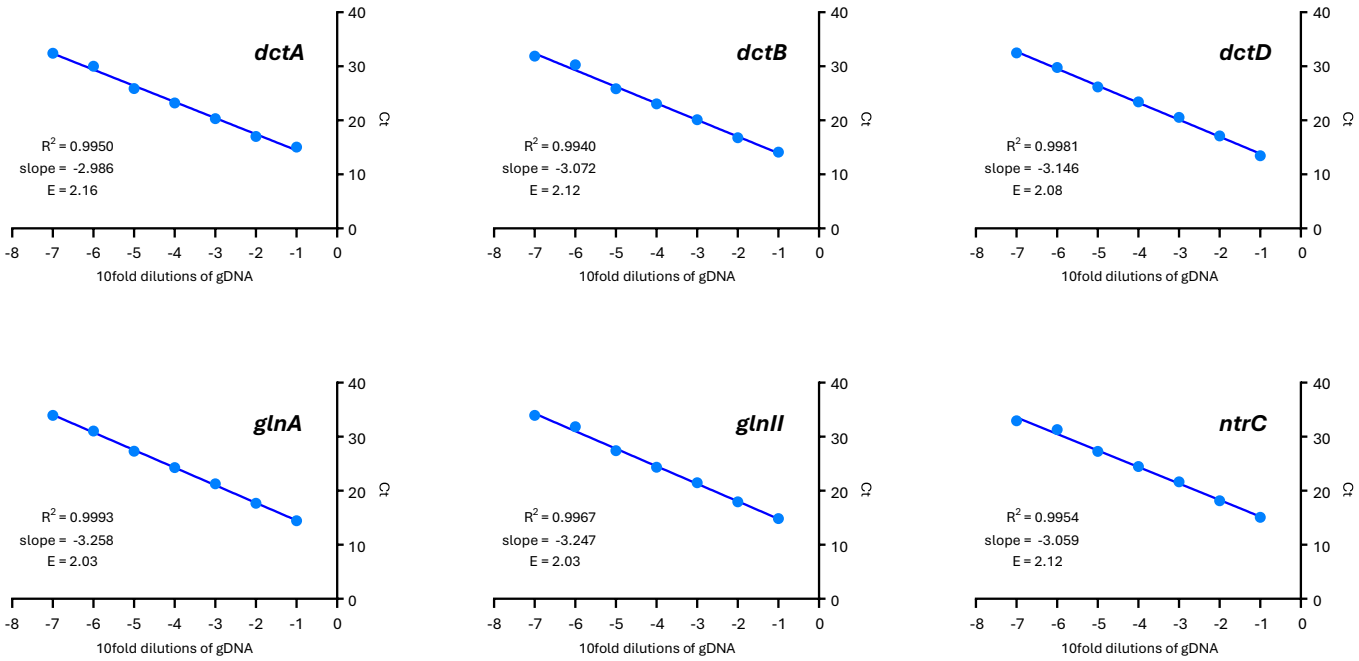


Figure S3.1 Standard curves used to calculate amplification efficiencies for RT-qPCR primers.

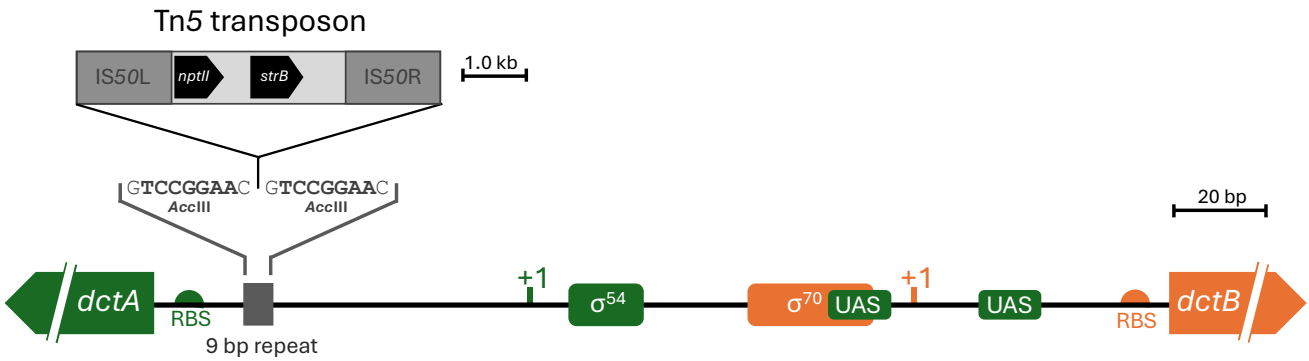


Figure S3.2 Location of the Tn5 insertion in the *dctA* - *dctB* intergenic region of strain RU150. The inserted Tn5 transposon, carrying the antibiotic resistance genes *nptII* and *strB* and flanked by IS50 elements, is inserted 19 bp upstream of the *dctA* startcodon at an *AccIII* site. A 9 bp duplication, characteristic of Tn*5* insertion, is present on either side of the transposon and contains a duplicated *AccIII* site. Genes are depicted as arrows indicating transcriptional orientation, ribosome binding sites (RBS) as half-circles, and predicted transcription start sites (+1) as vertical ticks. Sigma-factor binding sites are shown as rounded boxes, with the *dctA* promoter corresponding to a σ^{54}-dependent −24/−12 element and the *dctB* promoter to a σ^{70}-dependent −35/−10 element. The *dctA* promoter additionally contains two upstream activator sequences (UASs) that serve as binding sites for its transcriptional activator DctD. Regulatory elements associated with *dctA* and *dctB* are indicated in green and orange, respectively. Adapted from Reid and Poole (1998) and extended.

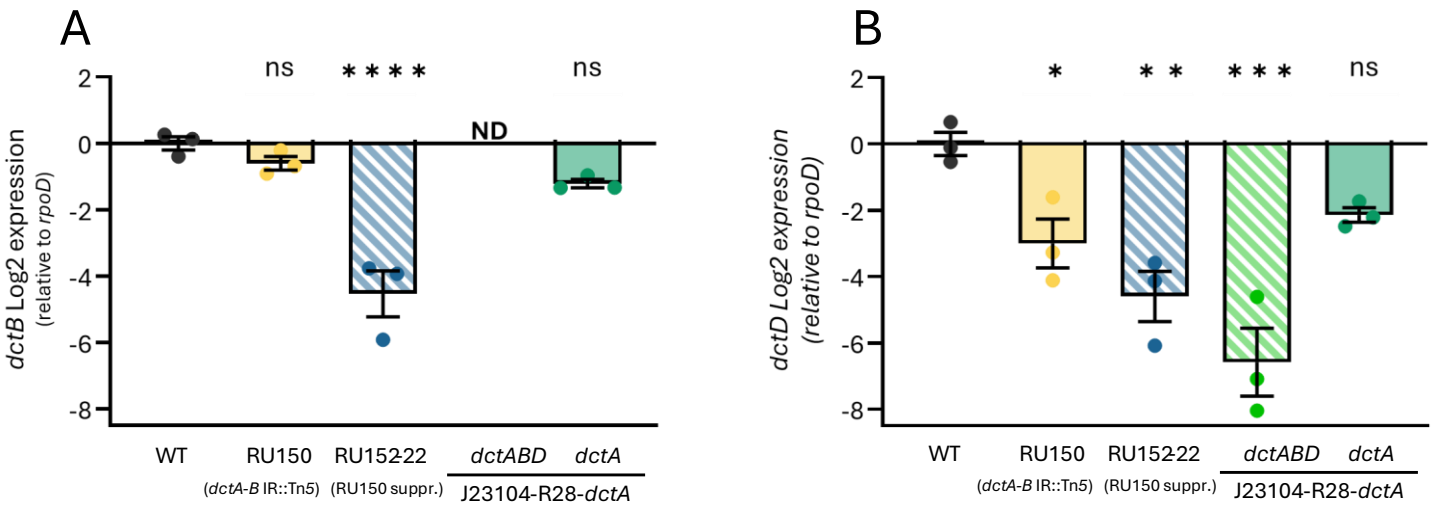


Figure S3.3 Altered *dctB* and *dctD* expression in *dct* regulation and complementation mutants. *dctB* **(A)** and *dctD* **(B)** expression was quantified by qPCR in WT *Rlv*3841, RU150, RU152-22, as well as a Δ*dctABD*::Ω or *dctA*::Ω strain complemented with a Tn*7* insertion carrying *dctA* expressed constitutively from the J23104 promoter with the synthetic ribosome binding site R28. Cells were grown in UMS supplemented with 20 mM succinate and 10 mM NH_4Cl. Expression levels are shown as log_2-transformed relative expression (Pfaffl method), normalised to *rpoD* and expressed relative to WT. Bars represent mean ± SEM (n = 3). Statistical significance was determined by one-way ANOVA with Dunnett's correction compared to WT (ns, not significant, **** $p < 0.0001$,*** $p < 0.001$, ** $p < 0.01$, * $p < 0.05$). ND = not detected (no amplification after 35 cycles); striped bars indicate expression considered not biologically meaningful.

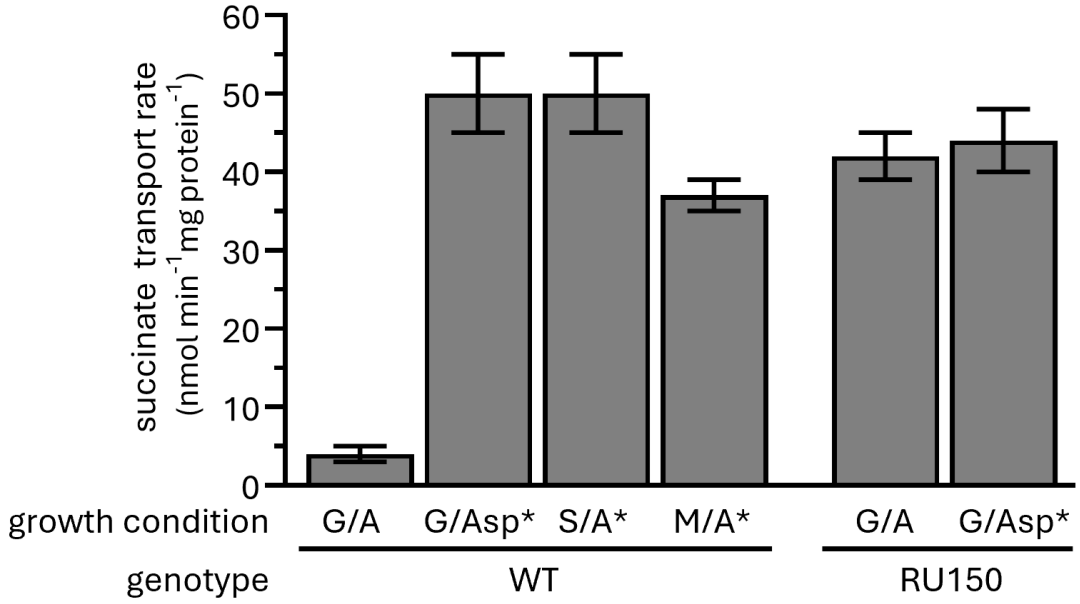


Figure S3.4 RU150 constitutively transports succinate. Succinate uptake rates were measured in *Rlv*3841 WT and the dct regulatory mutant RU150 grown under various dct-inducing (indicated by an asterisk) and non-inducing conditions. Growth substrates: G, 10 mM glucose; S, 20 mM succinate; M, 20 mM malate; A, 10 mM NH_4Cl; Asp, 10 mM aspartate. Bars represent mean ± SEM, with data taken from Poole et al. (1994); Reid and Poole (1998).

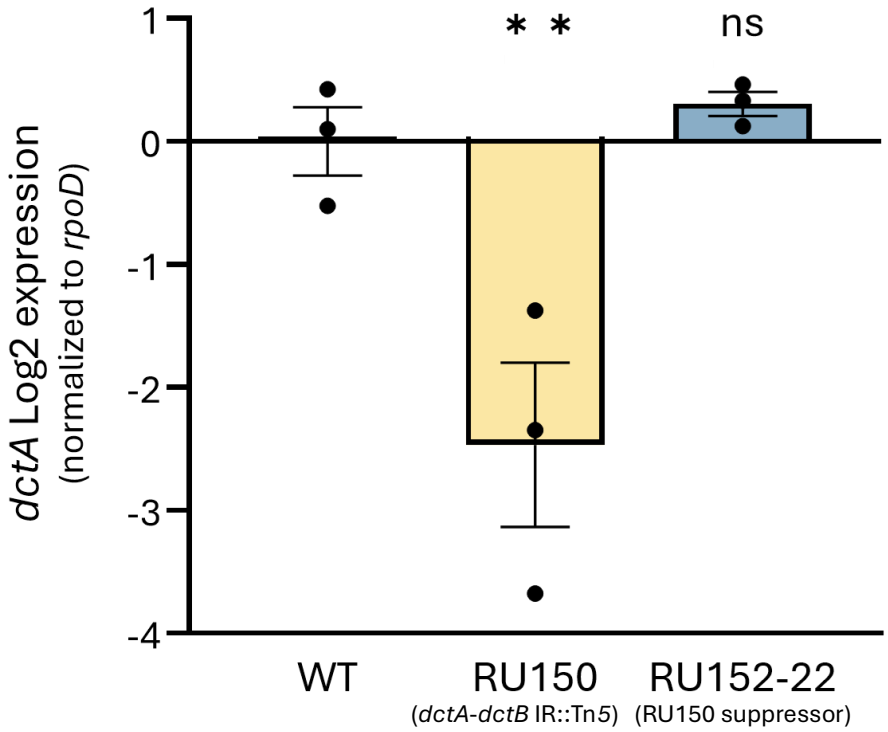


Figure S3.5 Reduced *dctA* expression in RU150 is restored in its suppressor RU152-22. *dctA* expression was quantified by qPCR in WT *Rlv*3841, RU150, and RU152-22. RU150 carries a Tn*5* insertion in the *dctA*-*dctB* intergenic region (IR), resulting in low level constitutive *dctA* expression independent of DctBD signalling. RU152-22 is a spontaneous suppressor of RU150 (see Figure 3.4 for detailed genotype). Cells were grown in UMS supplemented with 20 mM succinate and 10 mM NH_4Cl. Expression levels are shown as $\log_2$-transformed relative expression (Pfaffl method), normalised to *rpoD* and expressed relative to WT. Bars represent mean ± SEM (n = 3). Statistical significance was determined by one-way ANOVA with Dunnett's correction compared to WT (ns, not significant, ** $p < 0.01$).

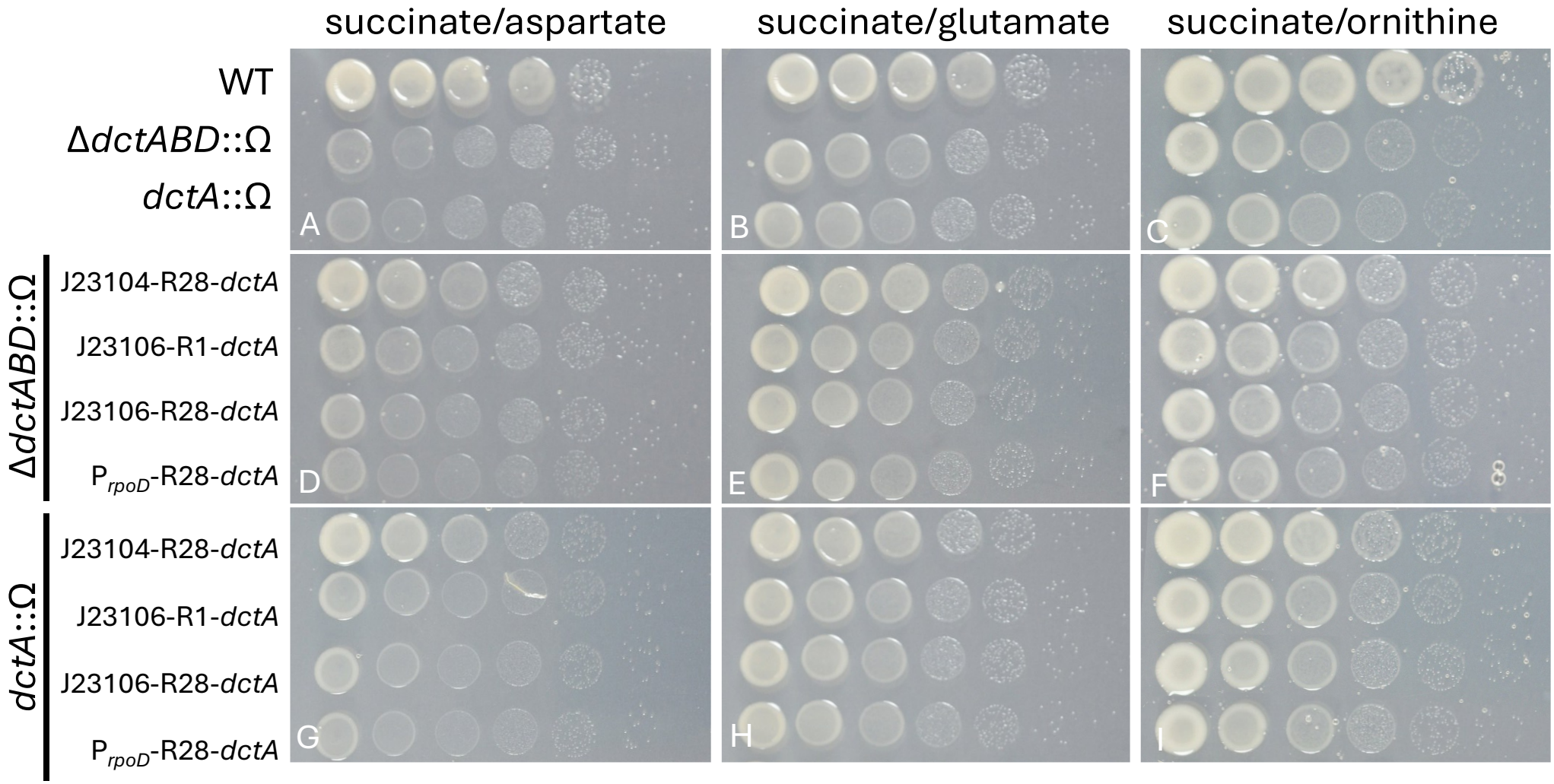


Figure S3.6 Growth of constitutive *dctA* complementation strains on succinate with alternative nitrogen sources. 10 µL of serial tenfold dilutions (starting from OD595 = 0.1) of *R. leguminosarum* bv. *viciae* (*Rlv*) 3841 wild type (WT), Δ*dctABD*::Ω [RU714], *dctA*::Ω [RU727], and constitutive *dctA* complementation strains [OPS3941-44, OPS3948-51] were spotted onto UMS minimal medium supplemented with 20 mM succinate as the carbon source and either 10 mM aspartate **(A,D,G)**, 10 mM glutamate **(B,E,H)**, or 10 mM ornithine **(C,F,I)** as the nitrogen source.

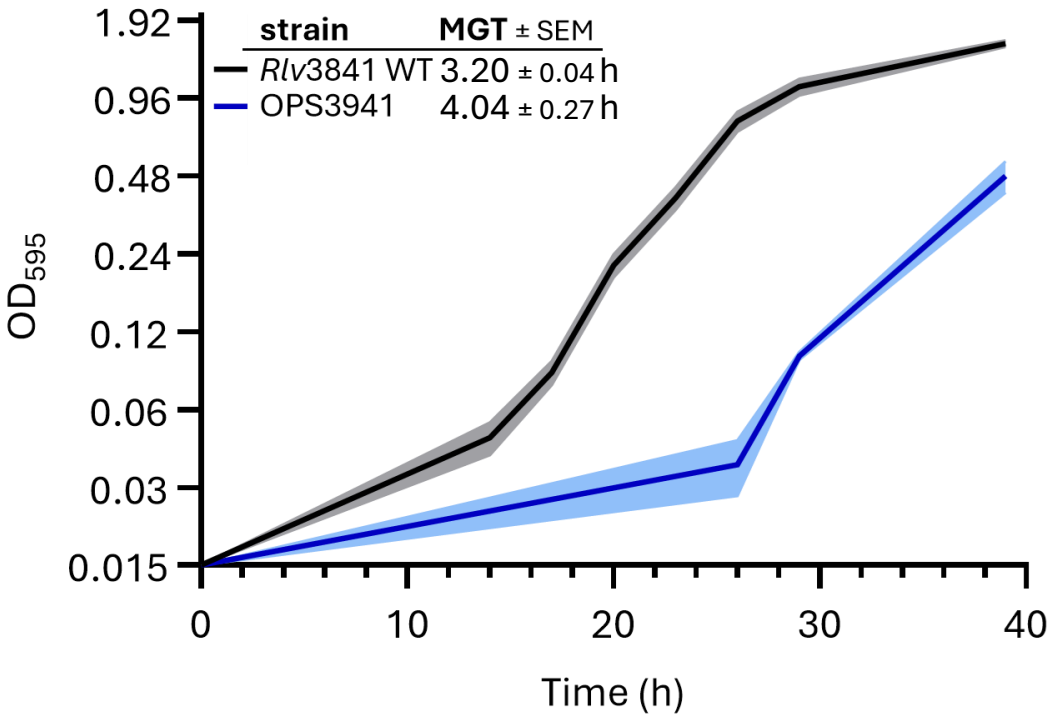


Figure S3.7 Constitutive *dctA* complementation does not restore WT-like growth on succinate/ammonia. Blank-corrected average OD_{595} (mean of three replicates; SEM shown as bands) of *Rlv*3841 WT (black) and a constitutive *dctA* complementation strain (OPS3941; Δ*dctABD*::Ω Tn*7*::J23104-R28-*dctA*, blue) grown in UMS supplemented with 20 mM succinate and 10 mM NH_4Cl. Optical density was measured every 3 h using a plate reader, and the mean generation time (MGT ± SEM) was calculated from the exponential growth phase of each replicate.

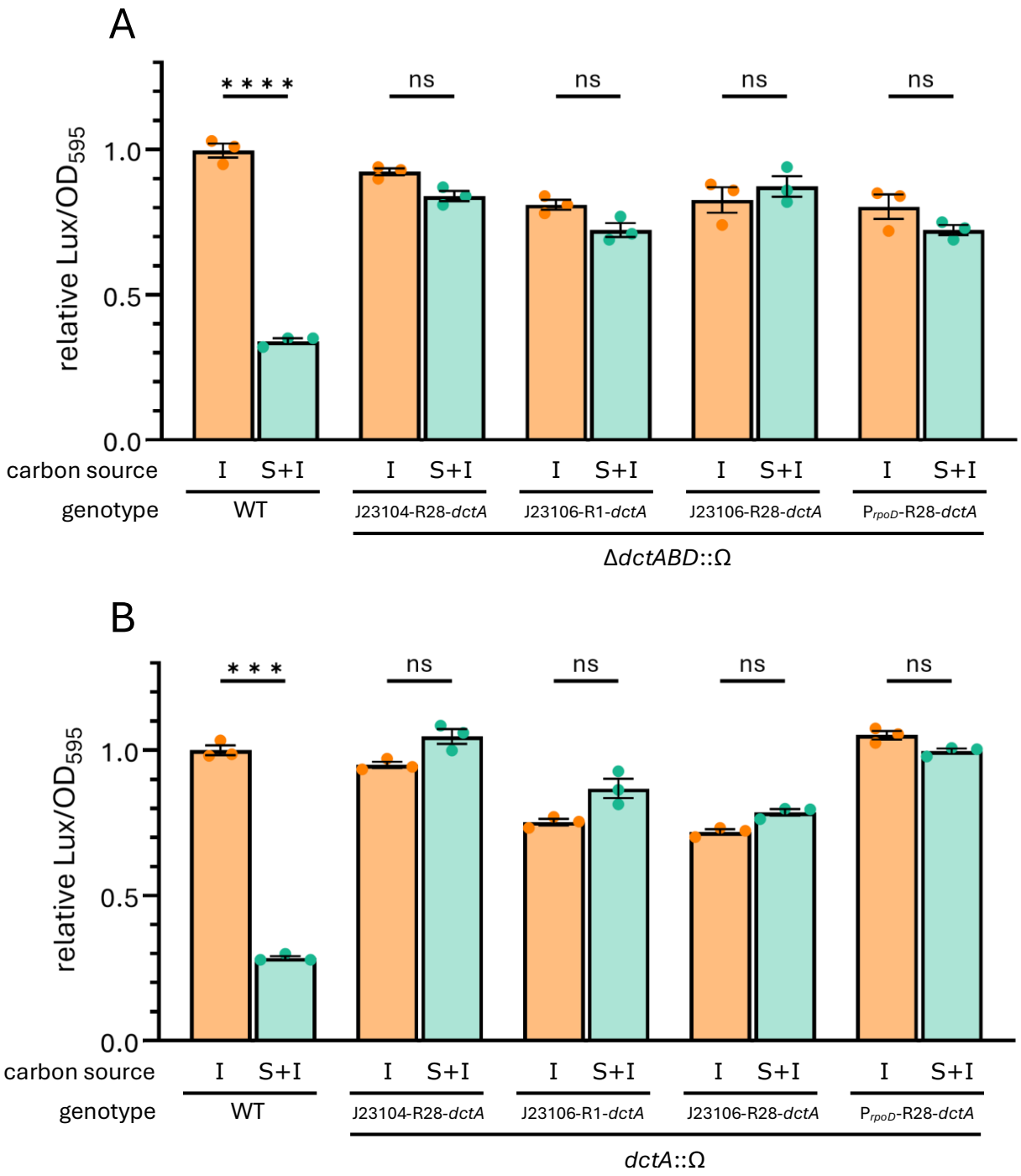


Figure S3.8 Constitutive *dctA* complementation does not restore CCR. Luminescence of an inositol biosensor in WT *Rlv*3841 and *dct* mutant complementation strains, normalised to optical density (Lux/OD_{595}) and expressed relative to WT grown in *myo*-inositol. DctA complementation was achieved by integrating Golden Gate-constructs of varying constitutive *dctA* expression strength (ordered in increasing *dctA* expression strength, see Figure 3.8) into the chromosome of a Δ*dctABD*::Ω **(A)** or *dctA*::Ω **(B)** mutant backgrounds. Luminescence was quantified from liquid cultures grown in TY and inoculated into MM containing either 10 mM *myo*-inositol (I, orange), or 20 mM succinate plus 10 mM *myo*-inositol (S+I, green) at OD_{595} ~ 0.5. Bars represent mean ± SEM (n = 3). Statistical significance reflects Sidak-corrected comparisons between growth conditions within each genotype following a two-way ANOVA, where **** $p < 0.0001$, *** $p < 0.001$, ns not significant.

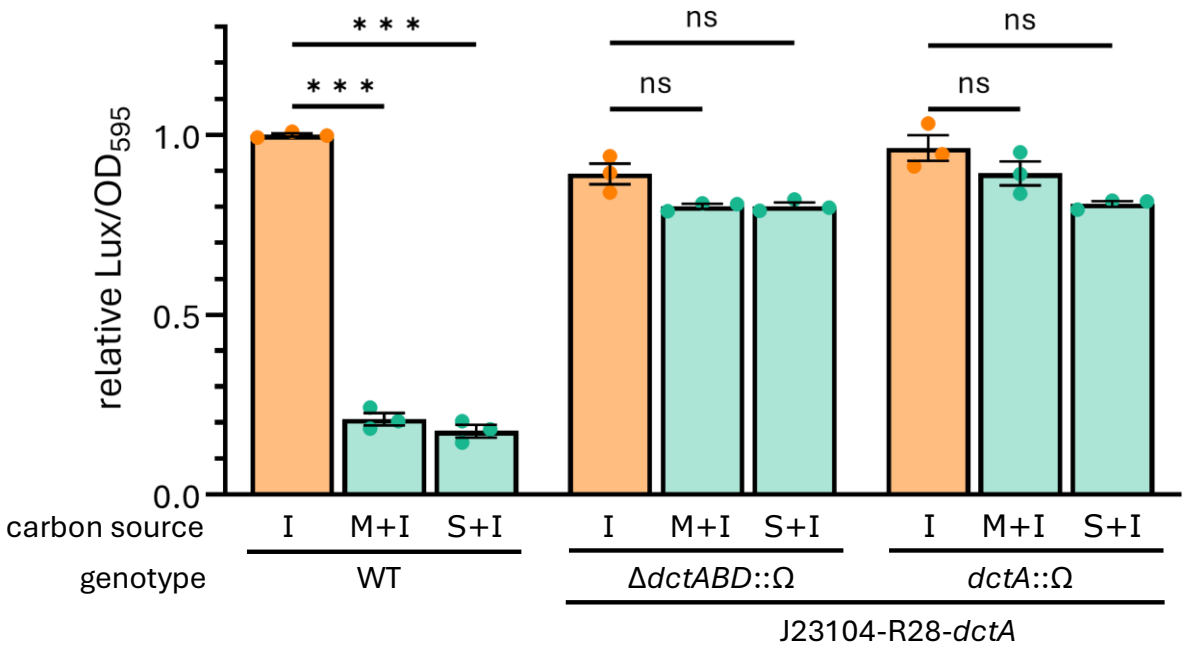


Figure S3.9 Constitutive *dctA* expression does not restore CCR independent of the C_4-dicarboxylate used. Luminescence of an inositol biosensor in WT *Rlv*3841 and two *dct* mutants complemented with constitutive *dctA* expression, normalised to optical density (Lux/OD_{595}) and expressed relative to WT grown in *myo*-inositol. Luminescence was quantified from liquid cultures grown in UMS containing 10 mM *myo*-inositol (I, orange), 20 mM malate plus 10 mM myo-inositol, or 20 mM succinate plus 10 mM *myo*-inositol (M+I, S+I, both in green). Bars represent mean ± SEM (n = 3). Statistical significance reflects Dunnet-corrected comparisons between growth conditions within each genotype following a two-way ANOVA, where *** $p < 0.001$, ns, not significant.

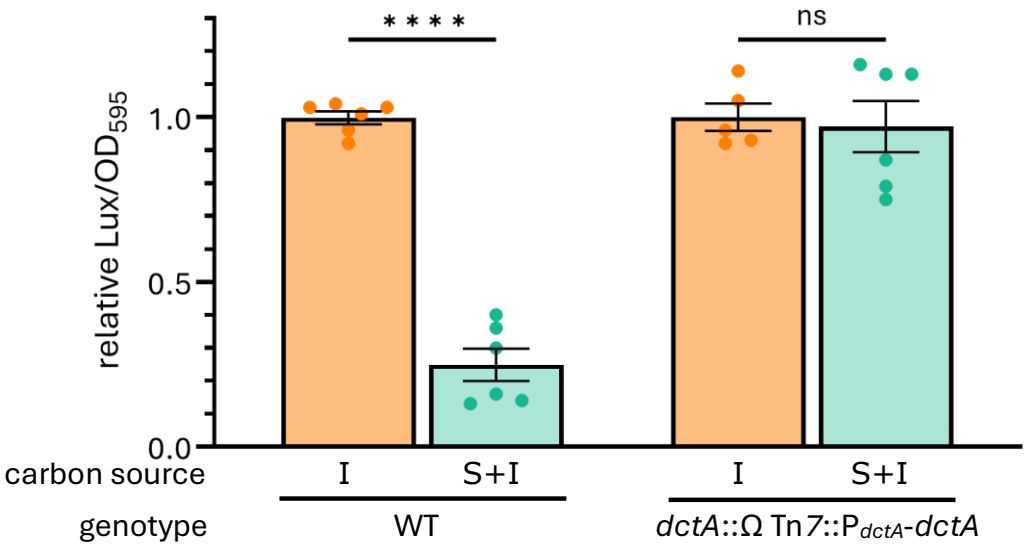


Figure S3.10 Complementation with the native *dctA* does not restore CCR. Luminescence of an inositol biosensor in WT *Rlv*3841 and a *dctA* mutant complemented with a Tn*7*-integrated copy of *dctA* under its native promoter, normalised to optical density (Lux/OD_{595}) and expressed relative to WT grown in *myo*-inositol. Luminescence was quantified from liquid cultures grown in UMS containing 10 mM *myo*-inositol (I, orange), or 20 mM succinate plus 10 mM *myo*-inositol (S+I, green). Bars represent mean ± SEM (n ≥ 5). Note that the data stems from two independent experiments. Statistical significance reflects Sidak-corrected comparisons between growth conditions within each genotype following a mixed-effects model, where **** $p < 0.0001$, ns, not significant.

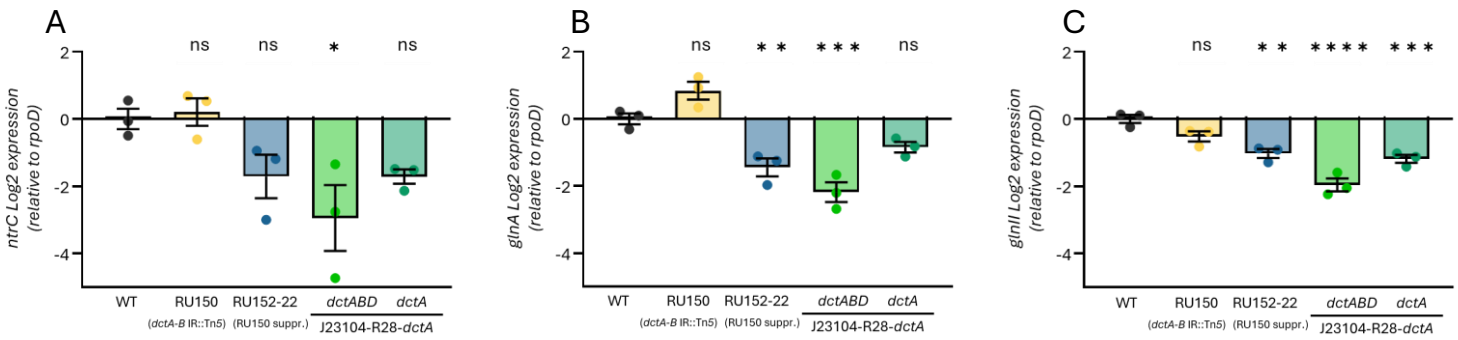


Figure S3.11 Expression of key nitrogen metabolism genes in *dct* regulatory and complementation mutants. *ntrC* **(A)**, *glnA* **(B)**, and *glnII* **(C)** expression was quantified by qPCR in WT *Rlv*3841, RU150, RU152-22, as well as a Δ*dctABD*::Ω or *dctA*::Ω strain complemented with a Tn*7* insertion carrying *dctA* expressed constitutively from the J23104 promoter with the synthetic ribosome binding site R28. Cells were grown in UMS supplemented with 20 mM succinate and 10 mM NH_4Cl. Expression levels are shown as $\log_2$-transformed relative expression (Pfaffl method), normalised to *rpoD* and expressed relative to WT. Bars represent mean ± SEM (n = 3). Statistical significance was determined by one-way ANOVA with Dunnett's correction compared to WT (ns, not significant, **** $p < 0.0001$,*** $p < 0.001$, ** $p < 0.01$, * $p < 0.05$). ND = not detected (no amplification after 35 cycles).

4

Functional diversification of canonical and oxygen-responsive DksA homologues in *Rhizobium leguminosarum*

Chapter 4

This thesis chapter is presented in the form of a completed manuscript intended for publication. Minor formatting changes have been made to the manuscript to fit the format of this thesis.

The work presented in this chapter is not directly related to the previous chapters.

Functional diversification of canonical and oxygen-responsive DksA homologues in *Rhizobium leguminosarum*

Ann-Kathrin Maurer[1], Raphael Ledermann[1,], Philip Poole[1]

[1] Department of Biology, University of Oxford, Oxford, UK

Abstract

The stringent response is a widespread bacterial regulatory mechanism that coordinates bacterial adaptation to nutritional limitation and environmental stresses and is mediated by the alarmone (p)ppGpp and the transcription factor DksA. Recent studies suggest that this regulatory system may also contribute to the molecular adjustments required for establishment and/or maintenance of the nitrogen-fixing symbiosis between rhizobia and legumes. Here, we investigated the regulation and function of the three DksA homologues in *Rhizobium leguminosarum* in free-living growth and symbiosis with pea (*Pisum sativum* L.) and bean (*Phaseolus vulgaris* L.). We define two phylogenetic and functionally distinctive groups corresponding to canonical DksA proteins and DksA-like paralogs. In *R. leguminosarum* bv. *viciae* 3841 (*Rlv*3841), the two DksA-like proteins, designated DksL1 and DksL2, differ structurally from canonical DksA. Both *dksL* genes possess upstream anaerobox motifs (TTGAT-X_4-ATCAA), placing them under control of the oxygen-responsive FnrN regulatory pathway. Accordingly, both *dksL* copies genes are strongly induced in free-living bacteria under microaerobic conditions and in bacteroids. Despite this induction, deletion of the *dksL* genes caused no detectable transcriptomic or symbiotic defects, suggesting context-dependent or subtle roles rather than canonical stringent response regulation. In contrast, deletion of the canonical *dksA* resulted in pronounced transcriptional reprogramming during symbiosis, including early activation of nitrogen-scavenging pathways followed by stress responses, metabolic imbalance, and a failure to fully commit to the differentiated bacteroid state. Importantly, the requirement for DksA was host-dependent: while defects were largely masked in terminally differentiated pea bacteroids, DksA became essential for recovery from the bacteroid state in bean bacteroids which can resume free-living growth. Together, these findings demonstrate functional diversification among DksA homologues, with canonical DksA maintaining bacteroid metabolic homeostasis and DksL proteins acting as oxygen-responsive regulators whose roles remain to be fully elucidated.

KEYWORDS Rhizobium–legume symbiosis; DksA; stringent response; bacteroid homeostasis; oxygen-responsive regulation; functional diversification

Introduction

The legume-rhizobium symbiosis is one of the most sophisticated mutualistic plant-microbe interactions and involves a highly coordinated developmental program in which soil-dwelling rhizobia transition from free-living growth to an intracellular nitrogen-fixing state within root nodules. This transition requires rhizobia to colonize the rhizosphere, infect root tissue of compatible host plants, and trigger nodule organogenesis through a series of signalling and developmental steps governed by a variety of symbiotic genes (different steps reviewed in Masson-Boivin et al., 2009; Oldroyd et al., 2011; Poole et al., 2018). During nodule development, motile cells differentiate into bacteroids and undergo extensive physiological remodelling to support nitrogen fixation.

This transition from free-living growth to the symbiotic state requires rhizobia to continuously adjust gene expression in response to changing environmental inputs (reviewed in Downie, 2014; Ledermann et al., 2021). Within nodules, rhizobia encounter major constraints, including extremely low oxygen tensions, altered nutrient availability, and the high metabolic demand required to sustain nitrogen fixation. In some hosts, additional stress is imposed by host-derived antimicrobial peptides that force bacteroids into terminal differentiation (Montiel et al., 2017). Rhizobia adapt to these conditions through extensive transcriptional reprogramming, including activation of oxygen-responsive regulatory cascades that, for instance, lead to modification of the electron transport chain through the induction of high-affinity terminal oxidases (Rutten & Poole, 2019). In mature bacteroids, global gene expression is extensively reorganized: many functions associated with free-living growth are downregulated, whereas symbiosis-specific programs – including nitrogen fixation and associated metabolic pathways – are induced (Green et al., 2019).

Together, these observations underscore that successful symbiosis requires robust global regulatory systems capable of integrating environmental and metabolic cues during differentiation. Consistent with the physiological demands of the nodule environment, multiple studies report induction of bacterial stress-response pathways in planta, indicating that establishment and maintenance of symbiosis impose substantial physiological stress on the microsymbiont (Chen et al., 2025; Davies & Walker, 2007;

Djordjevic et al., 2003; Green et al., 2019; Karunakaran et al., 2009). Activation of these stress responses is therefore considered critical for survival within the host and for optimal symbiotic performance (Hawkins & Oresnik, 2022; Ledermann et al., 2021; Schwartzman & Ruby, 2016). Accordingly, mutants defective in stress adaptation frequently display reduced symbiotic performance (Davies & Walker, 2007, 2008; Domingo-Serrano et al., 2025; Oke et al., 2001).

One candidate system for coordinating such broad adaptations is the stringent response, a conserved bacterial stress programme that orchestrates the balance between growth and survival during adverse nutritional and environmental conditions. In free-living bacteria, stringent response signalling is mediated by the alarmone (p)ppGpp (guanosine penta- or tetra-phosphate), produced primarily by RelA in response to ribosome-associated stress signals, which globally reshapes transcriptional priorities from growth toward survival (reviewed in Dalebroux & Swanson, 2012; Ronneau & Hallez, 2019). The transcription factor DksA acts in concert with (p)ppGpp to modulate RNA polymerase activity and fine-tune promoter-specific outputs (Irving et al., 2021; Paul et al., 2004). Under nutrient limitation, for example, the stringent response represses ribosomal RNA (rRNA) transcription and therefore diverts resources from division and growth toward amino acid biosynthesis and stress adaptation (Irving et al., 2021; see also further targets described therein).

DksA was first described in 1990 in *E. coli* as a suppressor of the *dnaK* mutant phenotype (Kang & Craig, 1990). Since then, DksA has been shown to bind within the secondary channel of RNA polymerase, where it acts synergistically with (p)ppGpp to destabilize promoter complexes and thereby modulate transcription initiation at specific promoters (Paul et al., 2004, 2005). Canonical DksA proteins typically contain two major domains: (i) a coiled-coil domain with a conserved DXXDXA motif at its tip, important for RNA polymerase interaction and function, and (ii) a globular domain that in many cases is stabilized by a Cys_4 zinc-binding motif. Variations in these domains across taxa raise the question of whether paralogs are functionally redundant or have evolved specialized roles in distinct regulatory contexts.

Recent work shows that both the (p)ppGpp synthetase RelA and the transcription factor DksA are symbiotically relevant. In *R. leguminosarum*, a *relA* mutant displayed impaired

nitrogen fixation (Tjahjono, 2025), and the (p)ppGpp alarmone has been shown to be required for effective symbiosis in *Rhizobium etli* (Calderón-Flores et al., 2005; Moris et al., 2005). In *Sinorhizobium meliloti*, RelA is essential for nodule formation (Wells & Long, 2002) and possibly bacteroid differentiation (Barnett et al., 2004). Similarly, deletion of *dksA* in *S. meliloti* results in reduced nodulation and lower nitrogen fixation activity on *Medicago sativa* (Wippel & Long, 2016). Transcriptomic analyses previously reported upregulation of *dksA* homologues in bacteroids of bean (*Phaseolus vulgaris* L.) and pea (*Pisum sativum* L.) (Green et al., 2019; Karunakaran et al., 2009).

Although the core mechanisms of the stringent response are broadly conserved across bacteria, structural and functional variants occur (Mittenhuber, 2001). While DksA is often described as an enhancer or cofactor of the stringent response, it can also influence cellular processes beyond classical starvation signalling (c.f. Tehranchi et al., 2010; Trautinger et al., 2005; Zhang et al., 2014). Accordingly, deletion of *dksA* creates pleiotropic phenotypes in diverse bacterial species, and its regulatory roles have been investigated in a number of organisms, including *E. coli* (Parshin et al., 2015), *Pseudomonas aeruginosa* (Perron et al., 2005), and *Rhodobacter sphaeroides* (Lennon et al., 2014), as well as in symbiotic rhizobia such as *Sinorhizobium meliloti* (Wippel & Long, 2016). Interestingly, many bacteria encode more than one DksA homologue, and in most cases it is unknown which protein homologue participates in which regulatory response. In *Rhizobium leguminosarum*, three *dksA* homologues are present, raising the question of whether these paralogs perform redundant or specialized functions during free-living growth and symbiosis.

The aim of this work is therefore to characterize the three *dksA* homologues in *Rhizobium leguminosarum*, focusing on the model strain *R. leguminosarum* bv. *viciae* 3841 (*Rlv*3841), and to determine their regulatory roles and functional contributions to rhizobial symbiosis.

Material and Methods

Bacterial strains and growth conditions

The bacterial strains and plasmids used in this study are listed in Table 4.1 and Table 4.2.

Table 4.1 Strains used in this study.

Strains	Relevant phenotype and genotype	Reference or Source
Escherichia coli		
DH5α	*supE44 ΔlacU169* (ϕ80 *lacZ*ΔM15) *hsdR17 recA1 gyrA96 thi-1 relA2*	Hanahan, 1983
ST18	Sm^r Sp^r *pro thi hsdR* chromosome::RP4-2 Tc::Mu-Kan::Tn*7*/ λ*pir* Δ*hemA*	Thoma & Schobert, 2009
Rhizobium leguminosarum* bv. *viciae		
3841	Sm^r derivative of *R. leguminosarum* bv. *viciae* strain 300;	Johnston & Beringer, 1975; Glenn et al., 1980
OPS1097	Sm^r Sp^r *relA*::ΩSpc	Tjahjono, 2025
OPS3016	Sm^r Gm^r 3841 Tn*7*::$P_{dksA1.1}$-*gusA*	this work
OPS3017	Sm^r Gm^r 3841 Tn*7*::$P_{dksA1.2}$-*gusA*	this work
OPS3018	Sm^r Gm^r 3841 Tn*7*::P_{dksA2}-*gusA*	this work
OPS3019	Sm^r Gm^r 3841 Tn*7*::P_{relA}-*gusA*	this work
OPS3024	Sm^r Sp^r Gm^r *nifH*::ΩSpc Tn*7*::P_{dksL1}-*gusA*	this work
OPS3025	Sm^r Sp^r Gm^r *nifH*::ΩSpc Tn*7*::P_{dksL2}-*gusA*	this work
OPS3026	Sm^r Sp^r Gm^r *nifH*::ΩSpc Tn*7*::P_{dksA}-*gusA*	this work
OPS3030	Sm^r Nm^r Sp^r Gm^r $hFixL_9$::ΩSpc $hFixL_{chr}$::*pK19* Tn*7*::P_{dksL1}-*gusA*	this work
OPS3031	Sm^r Nm^r Sp^r Gm^r $hFixL_9$::ΩSpc $hFixL_{chr}$::*pK19* Tn*7*::P_{dksL2}-*gusA*	this work
OPS3033	Sm^r Tc^r Gm^r *fnrN*::ΩTet Tn*7*::P_{dksL1}-*gusA*	this work
OPS3034	Sm^r Tc^r Gm^r *fnrN*::ΩTet Tn*7*::P_{dksL2}-*gusA*	this work
OPS3036	Sm^r Gm^r Δ$fxkR_9$ Tn*7*::P_{dksL1}-*gusA*	this work
OPS3037	Sm^r Gm^r Δ$fxkR_9$ Tn*7*::P_{dksL2}-*gusA*	this work
OPS3300	Sm^r Δ*dksL1*	this work
OPS3301	Sm^r Δ*dksL2*	this work
OPS3365	Sm^r Δ*dksA*	this work
OPS3367	Sm^r Δ*dksL1* Δ*dksL2*	this work
OPS4310	Sm^r Δ*dksA*::*aacC1* Δ*dksL1* Δ*dksL2*	this work
OPS2516	Sm^r, Gm^r *Rlv*3841 miniTn7-tagged with P_{snifH}-*celB*	this work
OPS4243	Sm^r, Gm^r *Rlv*3841 miniTn7-tagged with P_{snifH}-*gusA*	this work
OPS4244	Sm^r, Gm^r OPS3365 miniTn7-tagged with P_{snifH}-*celB*	this work
OPS4245	Sm^r, Gm^r OPS3367 miniTn7-tagged with P_{snifH}-*celB*	this work

Rhizobium leguminosarum* bv. *phaseoli

4292	Rf^r derivative of *R. leguminosarum* bv. *phaseoli* strain 8002	Johnston et al., 1982
OPS4299	Rf^r Δ*dksA*	this work
OPS4301	Rf^r Δ*dksL1*	this work
OPS4303	Rf^r Δ*dksL2*	this work

Gm: gentamicin; Nm: neomycin; Sm: streptomycin; Sp: spectinomycin; Rf: rifampicin; Tc: tetracycline; ^{r}denotes resistance.

Table 4.2 Plasmids used in this study.

Plasmid	Relevant phenotype and genotype / Description	Reference or Source
pK18mobsacB	Km^r *sacB*, *oriV* pMB1, *oriT* RP4, mobilizable suicide vector for mutagenesis,	Schäfer et al., 1994
pOPS1548	Ap^r, Gm^r (pUC18R6KT-miniTn*7*T) P_{snifH}-*gusA*	Clark, 2021
pOPS1549	Ap^r, Gm^r (pUC18R6KT-miniTn*7*T) P_{snifH}-*celB*	Clark, 2021
pOPS1850	Ap^r Gm^r (pUC18T-mini-Tn*7*T-Gm) promoterless *gusA* in mTn*7* delivery plasmid for promoter fusions	this work
pOPS1851	Ap^r Gm^r (pOPS1850) P_{dksL1}-*gusA*	this work
pOPS1852	Ap^r Gm^r (pOPS1850) P_{dksL2}-*gusA*	this work
pOPS1853	Ap^r Gm^r (pOPS1850) P_{dksA}-*gusA*	this work
pOPS1854	Ap^r Gm^r (pOPS1850) P_{relA}-*gusA*	this work
pOPS1980	Km^r (pK18mobSacB) 3841 *dksL1* up- and downstream regions	this work
pOPS1981	Km^r (pK18mobSacB) 3841 *dksL2* up- and downstream regions	this work
pOPS1982	Km^r (pK18mobSacB) 3841 *dksA* up- and downstream regions	this work
pOPS2380	Km^r (pK18mobSacB) 4292 *dksA* up- and downstream regions	this work
pOPS2381	Km^r (pK18mobSacB) 4292 *dksL1* up- and downstream regions	this work
pOPS2382	Km^r (pK18mobSacB) 4292 *dksL2* up- and downstream regions	this work
pOPS2405	Km^r Gm^r (pOPS1982) 3841 *dksA* flanking regions with *aacC1*	this work
pRGD-GmR	Ap^r Gm^r *aacC1* donor plasmid	Ledermann et al., 2016
pRK2013	Km^r self-transmissible helper plasmid	Ditta et al., 1980
pTNS3	Ap^r *oriT oriV*(R6K) *tnsABCD* Tn*7* helper plasmid	Choi et al., 2008
pUC18T-mini-Tn*7*T-Gm	Ap^r Gm^r *oriT oriV*(ColE1) Tn*7* delivery vector	Choi et al., 2005

Ap: Ampicillin; Gm: gentamicin; Km: kanamycin; ^{r} denotes resistance.

E. coli strains were grown at 37°C in liquid or solid lysogeny broth (LB) (Sambrook et al., 1989) with appropriate antibiotics at the following concentrations (μg mL^{-1}): ampicillin 100, kanamycin 50, gentamicin 10. Strain ST18 was supplemented with 50 μg mL^{-1} 5-aminolevulinic acid.

R. leguminosarum strains were grown at 28°C in either tryptone yeast (TY) complex medium (Beringer, 1974) or universal minimal salts (UMS) minimal medium (Pini et al., 2017). If not indicated otherwise, UMS was supplemented with 10 mM NH_4Cl as nitrogen source and 20 mM succinate as carbon source. Antibiotics were added when necessary, at the following concentrations (µg mL^{-1}): gentamicin 20, neomycin 40, streptomycin 500, spectinomycin 10, tetracycline 5 (in solid media) or 1 (in liquid media), and rifampicin 50.

Strain construction

Markerless in-frame deletion mutants of *dksA* homologues in *Rlv*3841 were generated using the pK18mobSacB system (Schäfer et al., 1994). To illustrate the procedure, deletion of *dksL1* in *Rlv*3841 is described as an example.

Two approximately 750-800 bp fragments corresponding to the up- and downstream regions of *dksL1*, including the first four and last five codons, were PCR-amplified from *Rlv*3841 gDNA using primer pairs oxp5767/5768 and oxp5769/5770 (Table S4.1), respectively, and Q5 High Fidelity DNA Polymerase (NEB). Both fragments were assembled via a HiFi reaction (NEBuilder® HiFi DNA Assembly Master Mix; NEB) into a *Hind*III- and *Bam*HI-digested pK18mobsacB backbone, resulting in plasmid pOPS1980 (Table 4.2).

Biparental mating was performed to introduce pOPS1980 into WT *Rlv*3841, and transconjugants were selected for neomycin resistance. Single-crossover exconjugants were cultivated in liquid TY without neomycin to allow a second homologous recombination event to occur. Double-crossover candidates were selected on TY supplemented with 5% (w/v) sucrose (Quandt & Hynes, 1993).

Resulting candidates were screened for loss of neomycin resistance, and the correct deletion in the final strain (OPS3300) was verified by colony PCR using primers oxp5924/5925, which amplify the entire deletion region, and oxp5866/5867 as a negative control, which amplify an internal fragment of the deleted region. All colony PCRs used OneTaq DNA Polymerase (NEB). Deletion of the respective gene was confirmed by Sanger sequencing (Source Bioscience).

Markerless deletion mutants of the remaining genes were generated analogously, using the corresponding primers listed in Table S4.1, the generated plasmids in Table 4.2, and the resulting strains in Table 4.1. For *Rlv*3841, a double mutant (Δ*dksL1* Δ*dksL2*; OPS3367) was generated by introducing pOPS1981 into the existing Δ*dksL1* mutant (OPS3300). Multiple attempts to generate a markerless triple mutant were unsuccessful. Instead, pOPS1982 was digested with *Spe*I (a *Spe*I site had been incorporated between the two flanking regions in the original primer design), and a gentamicin resistance cassette (*aacC1*) excised from pRGD-GmR by *Spe*I digestion was ligated into the linearized plasmid using T4 DNA ligase (NEB), resulting in pOPS2405. The triple mutant (Δ*dksA*::*aacC1* Δ*dksL1* Δ*dksL2*; OPS4310) was subsequently generated by introducing pOPS2405 into the double mutant background.

Corresponding markerless single deletion of *dksA* homologues were generated in the bean-nodulating symbiont *Rhizobium leguminosarum* bv. *phaseoli* 4292 (*Rlp*4292) using the same strategy. Associated primers, plasmids and resulting strains are listed in Table S4.1, Table 4.2, and Table 4.1, respectively. The *dksA* homologues in this strain were identified via BLAST analysis (NCBI).

General plant growth

Pisum sativum cv. Avola seeds or *Phaseolus vulgaris* cv. Tendergreen seeds were surface sterilised for 2 min in 100% ethanol and washed in 2 changes of sterile water, followed by 5 min in ~2% sodium hypochlorite and washed in 10 changes of water. Seeds were germinated at 28 °C on 0.8% water agar plates until emerging radicles were about 1 cm (2-3 days).

Pea seedlings were transplanted into 2 L sterile pots containing either pre-soaked medium-grade vermiculite and 800 mL nitrogen-free rooting solution (Poole et al., 1994) or into1 L sterile pots containing a 1:1 V/V mix of pre-soaked fine vermiculite and silver sand and 150 mL of 2.67x concentrated nitrogen-free rooting solution (as in Poole et al., (1994) but 2.67 times more concentrated).

Bean seedlings were transplanted into 1 L sterile pots containing a 1:1 V/V mix of pre-soaked fine vermiculite and silver sand and 200 mL of Broughton and Dilworth's (1971) nitrogen-free nutrient solution.

If not indicated otherwise, 1 mL of bacterial suspension with an OD_{595} = 0.01 of the respective rhizobial strain was added to each pot as inoculum. For each experiment, plants without inoculum were grown as negative controls. The pots were placed in a growth room (22°C, 16 h light/8 h dark) and watered with sterile deionized (DI) water as necessary from 7 dpi onwards. Bean plants received an additional 100 mL of sterile rooting solution per week from 7 dpi onwards. Pea plants were grown for 25 dpi and bean plants for 28 dpi, if not otherwise stated.

Acetylene reduction assay for nitrogenase activity

Plants were uprooted and placed in 250 mL Schott bottles with injectable seals. 2% of air was removed and replaced with acetylene. Plants were incubated for 1 h, after which triplicate 1 mL gas samples were withdrawn and the conversion of acetylene to ethylene measured was measured using a gas chromatograph (Clarus 480, PerkinElmer). Nitrogenase activity is expressed as nmol ethylene produced per hour per plant or, alternatively, as nmol ethylene produced per hour per gram of nodule fresh weight. Values represent the mean of the three technical replicates measured per Schott bottle.

Recovery and regrowth of nodule-derived bacteria

To assess the viability of nodule-derived bacteria from pea, five nodules per plant were crushed in 1 mL isolation buffer (8 mM K_2HPO_4, 2 mM KH_2PO_4, 300 mM sucrose, 2 mM $MgCl_2$). The crude extract was centrifuged, and 10 µL aliquots of a tenfold serial dilution series of the supernatant was spotted in up to five technical replicates on TY agar supplemented with streptomycin. After approximately three days of incubation, dilutions yielding 10-100 CFU were counted, and original CFU per nodule weight were calculated based on the respective dilution factor.

The same procedure was performed for bean nodules; however only one nodule per plant was used. As bean plants do not induce terminal differentiation in their rhizobial partner, bacteroids recovered from bean nodules retain the ability to dedifferentiate into free-living bacteria. To assess the time required to resume growth, bean nodules were harvested and bacteroids were isolated using the differential spin protocol described above. Isolated bacteroids were inoculated into 50 mL TY supplemented with rifampicin

at an initial OD_{595} of 0.1, and growth was monitored by determining OD_{595} over a 48 h period.

Induction conditions and reporter activity measurements

Bacteria used as reporter strains contain the promoter region of either *dksA*, *dksL1*, *dksL2*, or *relA* fused to the β-glucuronidase gene (*gusA*), which was integrated into their chromosome with a mini-Tn7T transposon. For this, pUC18T-mini-Tn*7*T-Gm was first linearized with *Kpn*I and *Hin*dIII and the *gusA* gene, amplified with oxp5245-46, cloned into the vector using HiFi assembly, to produce pOPS1850, a promoterless *gusA* in mTn*7* delivery plasmid with a multicloning site (MCS) to easily clone in promoter fragments. Promoter regions of the abovementioned genes were amplified from *Rlv*3841 gDNA with primers listed in Table S4.1 and cloned into *Spe*I-*Pst*I-digested pOPS1850 via HiFi reaction, resulting in plasmids pOPS1851-54.

To investigate respective promoter activity under various growth and stress conditions, rhizobial strains were cultivated under different conditions prior to measurment of β-glucuronidase (GusA) activity. Tested conditions included minimal and rich media, exponential and stationary growth phases, nitrogen and carbon starvation, growth under different oxygen concentrations (21%, 1%, 0.5%), and symbiosis with pea. In addition, expression was examined in mutants lacking key components involved in oxygen sensing and regulation or nitrogen fixation, under both free-living and symbiotic conditions.

Unless otherwise stated, free-living cultures were grown overnight and harvested by centrifugation. For starvation assays, rhizobial strains were precultured in complete UMS medium, washed in 10 mM $MgCl_2$, and inoculated into fresh aliquots containing either complete UMS (control), UMS lacking NH_4Cl (nitrogen starvation), or UMS lacking succinate (carbon starvation).

Microaerobic conditions were created by incubating free-living UMS cultures overnight in a glove-box (Belle Technology), wherein oxygen levels were manually adjusted. Oxygen concentrations were monitored using a portable oxygen analyser (Model 200, Quantek Instruments).

For GusA assays performed on bacteroids, pea plants were set up as described above. Three weeks post-inoculation, plants were uprooted and nodules picked. Bacteroids were isolated from nodules utilizing a differential spin protocol (Rutten et al., 2021). For comparison of free-living bacteria and bacteroids (Figure 4.3), bacteroids were purified using a Percoll density gradient (Allaway et al., 2000).

β-Glucuronidase activity was measured according to the protocol described by Ledermann (2017). Briefly, 85 µL of cells (washed twice with 0.9% NaCl, concentrated to OD_{595} < 5.0) were added to 915 µL of β-glucuronidase assay buffer (50 mM $NaPO_4$ pH 7.0, 10 mM β-mercaptoethanol, 2 mM EDTA, 0.1% sarkosyl, 0.1% Triton X-100). Cells were permeabilised by adding 30 µL of chloroform followed by thorough vortexing. The enzymatic reaction was started by adding 200 µL of PNPG solution (13.5 mM p-nitrophenyl-β-glucuronide) and incubated at 37°C. Reactions were terminated by adding 500 µL of 2 M Na_2CO_3 once a visible yellow coloration developed relative to the control (85 µL NaCl instead of cells). Samples were cleared by centrifugation and absorbance of supernatants measured at 405 nm. β-Glucuronidase activity was calculated in analogy to β-galactosidase activity (Miller, 1972) and reported as adapted Miller units (MU):

$$adapted\ MU = \frac{OD_{405} \times 1000}{V \times OD_{600} \times t}$$

where V denotes volume of cell sample in mL and t denotes running time of the reaction in decimal minutes.

For each condition, three biological replicates of each promoter-*gusA* fusion were assayed. One biological replicate was defined as an independent culture or as bacteroids isolated from pooled nodules of plants from one pot. Each biological replicate was analysed as the mean of two technical replicates.

Assessing free-living growth

To assess the effect of *dksA* homologue deletions on free-living growth, 10 µL of cell suspensions of *Rlv*3841 WT and mutant strains were spotted in serial tenfold dilutions starting from OD_{595} = 0.1 onto TY or UMS plates supplemented with different carbon sources. To evaluate growth under low-oxygen conditions, a separate set of plates was

incubated in the glove-box with at 0.5% O_2. Growth was assessed after three or five days of incubation, respectively.

Competition assay with *celB*- and *gusA*-marked strains

WT and *dksA* mutants were tagged with Tn7 insertions of either P_{snifH}-*celB* (pOPS1549) or P_{snifH}-*gusA* (pOPS1548). *Rhizobium* cultures used as inoculum were grown overnight, washed, and adjusted to a final density of 10^5 CFU mL^{-1}. Diluted cultures were mixed at either 1:1 or 10:1 ratios and a total of 10^5 CFUs was added to the nitrogen-free rooting solution used on the day pea seedlings were transplanted into 1 L pots. The actual CFU proportions in each inoculum were determined by plating further dilutions of the inoculum, with counts calculated from three technical replicates.

Plants were harvested at 23 dpi. For sequential double-staining of nodules (Sánchez-Cañizares & Palacios, 2013; Sessitsch et al., 1996), roots were washed before being submerged in phosphate buffer (7 g L^{-1} NaH_2PO_4, 7.2 g L^{-1} Na_2HPO_4, 1 mM ethylenediaminetetraacetic acid [EDTA] [pH 8], 1% Sarkosyl, 1 mL L^{-1} Triton X100) containing 0.2 mg mL^{-1} Magenta-glcA (5-bromo-6-chloro-3-indolyl-β-D-glucuronide) overnight at 28°C. Roots were then transferred to fresh phosphate buffer and heat-treated for 2 h at 70°C to destroy endogenous β-galactosidase activity, before X-gal (5-bromo-4-chloro-3-indolyl-β-D-galactoside) was added to a final concentration of 0.25 mg mL^{-1} and roots incubated overnight at 37°C. Numbers of pink- and blue-stained nodules per rootsystem were counted.

RNA isolation from pea bacteroids

Two sets of pea plants were set-up for harvest at two different timepoints (12 or 28 days post-inoculation, dpi). For the 12 dpi time point, 2 L pots with three pea plants each were prepared as described above and inoculated five days after transplanting. For the 28 dpi time point, 2 L pots containing two pea plants each were prepared as described above and inoculated at the time of transplanting.

At 12 or 28 dpi, plants were uprooted and nodules were harvested directly into liquid nitrogen, with all nodules from plants grown in the same pot pooled into one sample. Bacteroids were isolated from nodules using the differential spin protocol described

above, with the following modifications: frozen nodules were ground under addition of liquid nitrogen, the isolation buffer was pre-chilled to 4°C, and all centrifugation steps were performed at 4°C.

The resulting bacteroid pellet was resuspended in pre-chilled RLT Plus buffer (RNeasy Plus Mini Kit, Qiagen) and lysed using a FastPrep-24 5G instrument (MP Biomedicals). Total RNA was subsequently extracted from the lysate according to the kit manufacturer's instructions. Residual gDNA was removed using the TURBO DNA-*free*™ Kit (Invitrogen). RNA quantity and purity were assessed using a Qbit 2.0 fluorometer (Invitrogen).

RNA sequencing and analysis

Further quality checks as well as RNA sequencing were performed by Novogene (Cambridge, UK) using the NovaSeq X Plus platform to generate 150 bp paired-end reads. Raw read quality was assessed using FastQC (v0.12.1, Andrews, 2010). mRNA reads were mapped to the *Rlv*3841 genome (ASM926v1, Young et al., 2006) using EDGE-pro v1.3.1 (Magoc et al., 2013), which employs Bowtie2 v2.1.0 (Langmead & Salzberg, 2012). Differential gene expression analysis was conducted using DESeq2 (Love et al., 2014) in R Studio (v4.5.1, R Core Team, 2025). Normalised counts were calculated from mapped reads and adjusted *p*-values were obtained using the Benjamini–Hochberg method. Genes with a fold change ≥ 2 and an adjusted *p*-value < 0.01 were considered significantly differentially expressed.

Gene annotations were based on the published genome and BioCyc annotations from the *Rlv*3841 Genome Explorer (Herson et al., 2024). Venn diagrams were generated using InteractiVenn (Heberle et al., 2015).

The complete set of analysed data, including all condition comparisons, is provided in Supplementary Table A (.xlsx) and raw sequencing reads will be deposited to NCBI.

Phylogeny

The phylogenetic tree was inferred from an amino acid sequence alignment generated using MUSCLE (v5.1; Edgar, 2022) with default parameters. Maximum likelihood analysis was performed using RAxML (v8.2.11; Stamatakis, 2014) under the BLOSUM62 substitution model with gamma-distributed rate heterogeneity among sites. Branch

support was assessed using rapid bootstrap analysis with 1,000 replicates, and bootstrap support values were mapped onto the best-scoring maximum likelihood tree. The resulting tree was visualized as unrooted. All analyses were conducted in Geneious Prime v2026.0.2 via plugins.

Statistical analyses

All statistical analyses and visualizations were performed using GraphPad Prism (v10.6.1). Differences between groups were evaluated by analysis of variance (ANOVA) with appropriate multiple-comparison corrections. When assumptions of equal variance were not met, Welch's ANOVA was applied. Where necessary, data were log-transformed prior to analysis to satisfy normality assumptions.

Results

Phylogenetic analysis of rhizobial *dksA* homologues

The genome of *R. leguminosarum* bv. *viciae* encodes three predicted DksA homologues (Figure 4.1, Table S4.5) compared to a single copy in *E. coli*. The three *Rlv*3841 homologues were identified through BLAST searches against known homologues in other species. One *dksA* homologue overlaps with the putative gene RL2268 on the opposite strand and was not assigned a separate locus identifier in the original *Rlv*3841 genome annotation (Young et al., 2006); we therefore designated this ORF RL2268A. All three encode a small protein between 107 and 139 amino acids in size, sharing between 19.3–40.2% pairwise identity.

To investigate the evolutionary relationships among these homologues, amino acid sequences of known DksA proteins from representative rhizobia and related α-proteobacteria were aligned, and a maximum likelihood phylogenetic tree was inferred (Figure 4.1). The dataset included the three *Rlv*3841 homologues, corresponding homologues from *R. leguminosarum* bv. *phaseoli* 4292 (*Rlp*4292), as well as reported homologues from *Mesorhizobium* spp. and *Bradyrhizobium* spp. In addition, homologues from other α-proteobacteria and γ-proteobacteria were considered in the analysis as these proteins have been previously studied.

While *E. coli* and *Agrobacterium fabrum* encode only one DksA protein, two homologues have been reported for *P. aeruginosa* and *R. sphaeroides*. Other rhizobial species likewise encode one or multiple copies, with single homologues identified in *B. diazoefficiens* and *M. loti*, and two copies in *S. meliloti*. The closely related strain *Rlp*4292 also encodes three homologues. The presence of multiple homologues in *Rlv*3841 and selected α-proteobacteria and γ-proteobacteria lineages suggests independent lineage-specific duplication events and raises the possibility of functional diversification. Notably, copy number variation does not correlate with symbiotic lifestyle, as both symbiotic and non-symbiotic members of the Rhizobiaceae encode either single or multiple homologues.

The resulting phylogeny resolved two major clades (Figure 4.1): One clade comprises DksA proteins that cluster with the well-characterized *E. coli* DksA and includes *Rlv*3841 RL2643, hereafter referred to as DksA. These proteins share the conserved coiled-coil tip motif (DXXDXA), which has been shown to be required for interaction with RNA polymerase in canonical *E. coli* DksA (Parshin et al., 2015).

The two additional DksA versions in *Rlv*3841 (RL1870, RL2268A) are here referred to as DksA-like (DksL) proteins, as they form a separate clade and differ from canonical DksA proteins not only in fold structure (Figure S4.2) but also in motif conservation (Figure S4.1). Notably, only DksL2 (RL2268A) retains both the conserved DXXDXA motif and an intact Cys_4 zinc-finger motif, while DksL1 (RL1870) has a aspartate-to-glutamate substitution within the coiled-coil domain motif (Figure S4.1; Figure S4.2). Based on conserved motif architecture, DksL2 most closely resembles canonical DksA proteins, whereas DksL1 appears more divergent.

In general, amino acid conservation is higher within the canonical DksA group, while DksL proteins show greater sequence variation, although many substitutions are between amino acids with similar physiochemical properties (Figure S4.1). In contrast, all DksL proteins retain all four cysteine residues of the zinc-finger motif, whereas several canonical DksA proteins lack two or three of these residues (Figure S4.1).

The presence of three DksA homologues in *Rlv*3841 and the amino acid variation between them therefore raise the question whether all three proteins fulfil canonical DksA functions or have undergone functional specialisation. Based solely on conserved motif architecture, DksL2 is the most likely candidate for a canonical DksA-like regulator in *Rlv*3841; nevertheless, all three homologues were included in subsequent functional analyses.

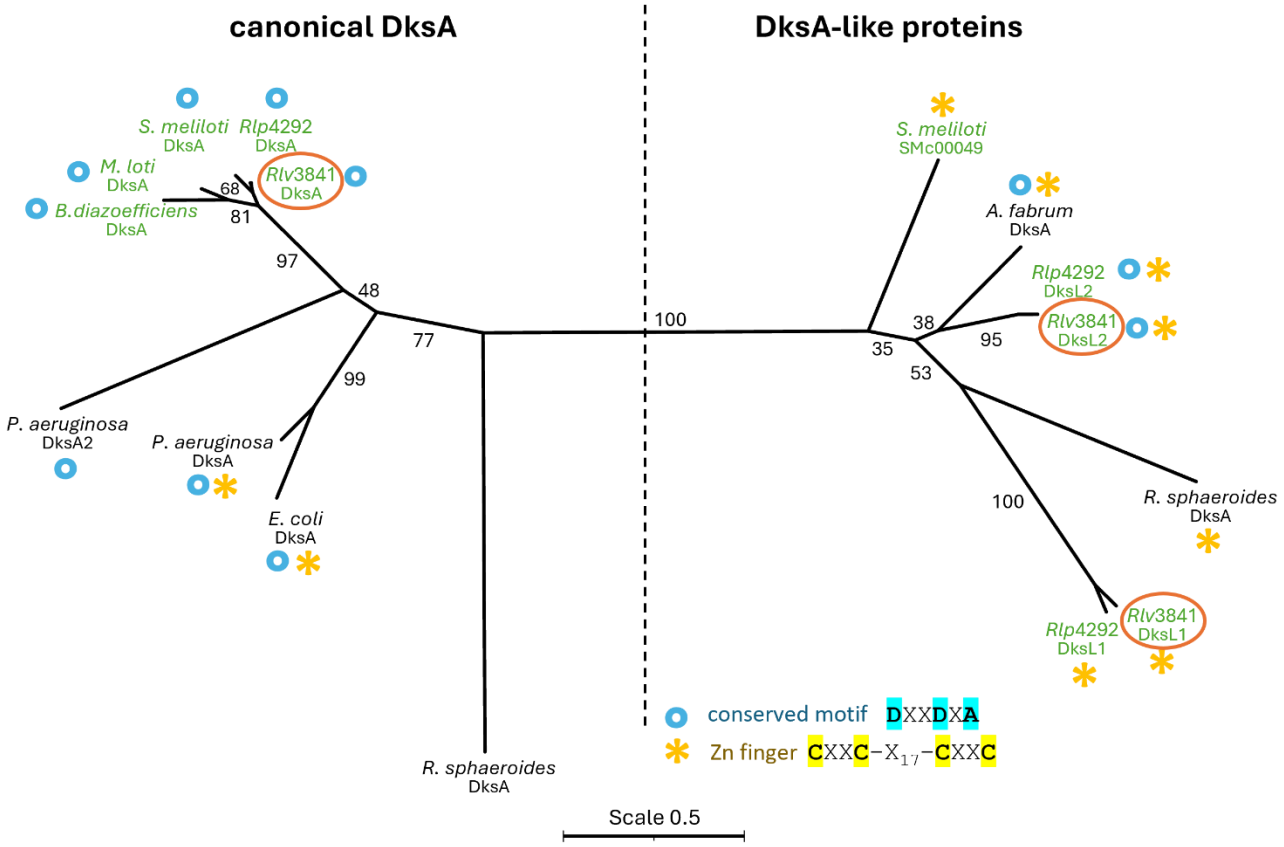


Figure 4.1 Phylogeny of different DksA homologues in different bacteria. The tree separates into two major clades: canonical DksA proteins (left) and DksA-like (DksL) proteins (right). Blue circles indicate the presence of the conserved coiled-coil tip motif (DXXDXA), characteristic of canonical DksA proteins. Yellow asterisks indicate the presence of a complete Cys_4 zinc-finger motif (CXXC–X_{17}–CXXC). DksA proteins from symbiotic species are highlighted in green, with the three homologues from *Rhizobium leguminosarum* bv. *viciae* (*Rlv*) 3841 circled in orange. The tree was inferred by maximum likelihood from MUSCLE-aligned amino acid sequences using RAxML (BLOSUM62). Bootstrap support values (1,000 replicates) are shown at the branches. The tree is unrooted.

Transcriptional regulation of *dksA* homologues

To determine whether environmental stresses affect transcription of the *dksA* homologues in *Rlv*3841, respective promoter-*gusA* fusions were assayed under various free-living conditions, including different growth media, growth phases, nutrient limitations, and oxygen levels, as well as during symbiosis with pea. In some assays, a P_{relA}-*gusA* fusion was included for comparison.

Limited transcriptional regulation of dksA homologues and relA under classical stress conditions

Given the established role of DksA and RelA in the stringent response and its association with amino acid starvation (Krol & Becker, 2011; Perron et al., 2005), we examined conditions involving nutrient limitation or amino acid deprivation. TY medium contains amino acids originating from e.g. yeast extracts or peptone salts, whereas cells grown in minimal medium (UMS) must synthesize amino acids from ammonium. Similarly, stationary phase represents a physiologically stressful condition characterized by nutrient depletion and accumulation of metabolic byproducts (cf. Nyström, 2004).

Under these conditions, *dksA* homologues and *relA* exhibited only minor transcriptional changes (Figure S4.3). No biologically relevant induction was observed in any of the four promoter-*gusA* fusions when cultures were grown in complete versus minimal medium (Figure S4.3A), or subjected to nitrogen or carbon starvation (Figure S4.3C). Fold changes between paired conditions were below two-fold for all reporters.

In contrast, *dksA* and *relA* promoter activities were modestly but significantly elevated in stationary phase compared to exponential growth (Figure S4.3B). Given the stability of the GusA reporter protein, this increase may partly reflect protein accumulation rather than true transcriptional induction and may therefore overestimate promoter activity in stationary phase.

Across all non-inducing conditions, expression of *dksA* and *relA* was consistently higher than that of *dksL1* and *dksL2*. Promoter activities of the latter remained below 10 adapted Miller Units (MU), implying very low basal expression indistinguishable from background noise.

Together, these results suggest that the *dksA* homologues and *relA* are not strongly transcriptionally induced under classical free-living stress conditions. Instead, *dksA* and *relA* appear to be under control of a (weak) constitutive promoter, while the *dksL* genes remain minimally expressed in the absence of specific inducing signals.

Microaerobic conditions induce promoters of dksL genes

To determine whether the induction of *dksL* genes observed in bacteroids (Green et al., 2019) is linked to the microaerobic environment within nodules, reporter strains were grown under controlled microaerobic conditions in an oxygen cabinet.

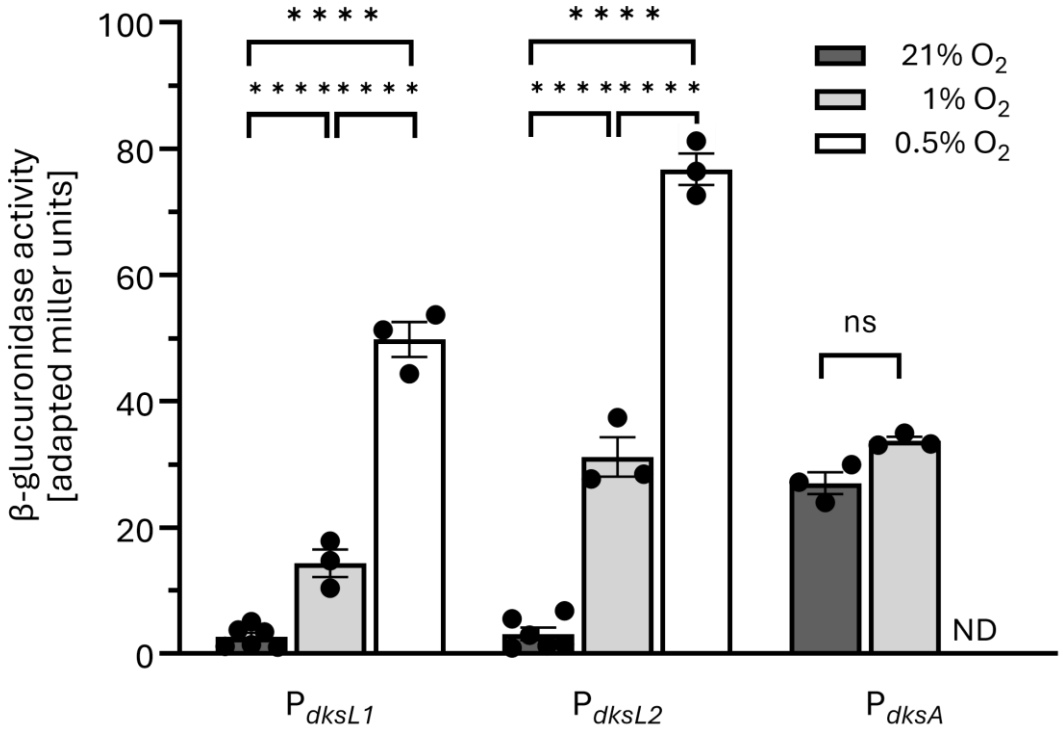


Figure 4.2 Microaerobiosis induces *dksL1* and *dksL2* but not *dksA* in free-living *Rlv*3841. Promoter fusions of the respective genes to *gusA* were conjugated into *Rlv*3841 WT and β-glucuronidase activities assayed after free-living cultures were grown for at least 12 h in either atmospheric oxygen conditions (filled bars) or in an oxygen cabinet set to 1% oxygen (grey bars) or 0.5% oxygen (open bars). Bars represent mean ± SEM from three biological replicates. Statistical significance reflects Tukey-corrected comparisons between growth conditions for each reporter following a two-way ANOVA, where ns not significant, **** $p < 0.0001$. ND = not determined.

Exposure to 1% O_2 resulted in approximately three- and six-fold increases in promoter activity for *dksL1* and *dksL2*, respectively, compared to cultures grown at atmospheric oxygen (21%). Further reduction to 0.5% O_2 led to induction levels exceeding 40- and 60-

fold, respectively (Figure 4.2), indicating a strong oxygen-dependent response in which promoter activity increases proportionally with decreasing oxygen concentrations.

In contrast, induction was not significantly changed for the *dksA* promoter (Figure 4.2) or *relA* (not shown) under any tested microaerobic condition.

dksL genes, but not dksA nor relA, are induced in bacteroids

To confirm the previously reported upregulation of *dksA* homologues in bacteroids (Green et al., 2019; Karunakaran et al., 2009), promoter activity was examined during symbiosis by inoculating reporter strains onto pea plants. Bacteroids were isolated from three-week-old nodules and β-glucuronidase activities were compared to those of aerobic, free-living cultures (Figure 4.3).

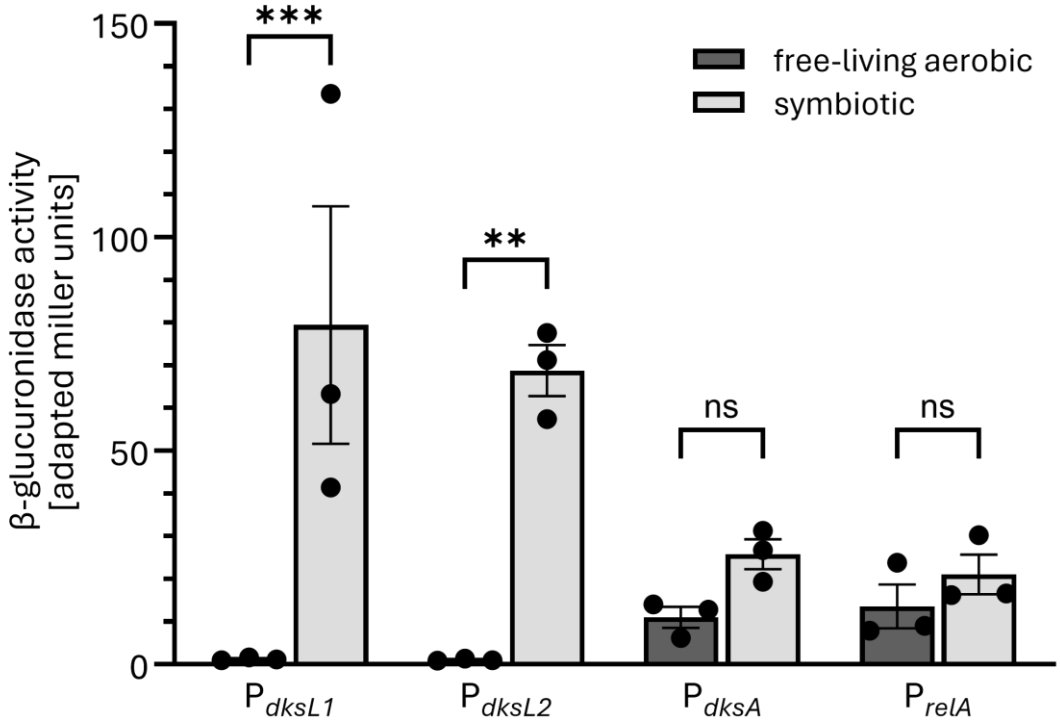


Figure 4.3 In bacteroids, dksL1 and dksL2 are induced while dksA and relA show no relevant increase. Promoter fusions of the respective genes to *gusA* were conjugated into *Rlv*3841 WT and β-glucuronidase activities assayed after in cell grown under free-living aerobic conditions for 12 h in UMS (dark bars) and in respective bacteroids (light bars). Bacteroids were isolated from 21 dpi pea nodules using a Percoll gradient. Bars represent mean ± SEM from three biological replicates. Statistical significance reflects Sidak-corrected comparisons between growth conditions for each reporter following a two-way ANOVA, where ns not significant, *** $p < 0.001$, ** $p < 0.01$.

Both *dksL* promoters exhibited a strong induction in bacteroids, whereas *dksA* and *relA* showed no significant increase in expression relative to free-living conditions. β-glucuronidase activities and fold changes observed for *dksL1* and *dksL2* in bacteroids were among the highest measured across all assays but still comparable to those detected under the lowest microaerobic condition (0.5% O_2; Figure 4.2).

Together, these results confirm that the *dksL* genes are induced under symbiotic conditions, likely driven by the low oxygen levels within nodules.

dksL genes are under control of FnrN

Upregulation of symbiotic genes during the transition from free-living cells to bacteroids is governed by oxygen-responsive regulatory pathways. In *Rlv*3841, the hFixL–FxkR cascade and FnrN – of which hFixL and FnrN function as direct oxygen sensors – together with the master regulator NifA, coordinate oxygen-dependent gene expression required for bacteroid differentiation and nitrogen fixation as oxygen levels decline within the developing nodule (reviewed in detail in Dixon & Kahn, 2004; Rutten et al., 2021).

Given that *dksL* genes are strongly induced in bacteroids (Figure 4.3) and under low oxygen (Figure 4.2), we hypothesized that their expression is controlled by one or more of these oxygen-responsive regulators. To assess their contribution, induction of *dksL1* and *dksL2* was examined in the *Rlv*3841 WT and in mutants lacking hFixL, FxkR, and FnrN.

In bacteroids of the mutant lacking both *hFixL* copies, as well as in those of the *fxkR* mutant, expression of *dksL1* and *dksL2* was only slightly reduced compared to the WT (Figure 4.4A). In contrast, induction of both promoters was nearly abolished in the *fnrN* mutant bacteroids, indicating that FnrN is the primary regulator of *dksL* gene expression during symbiosis.

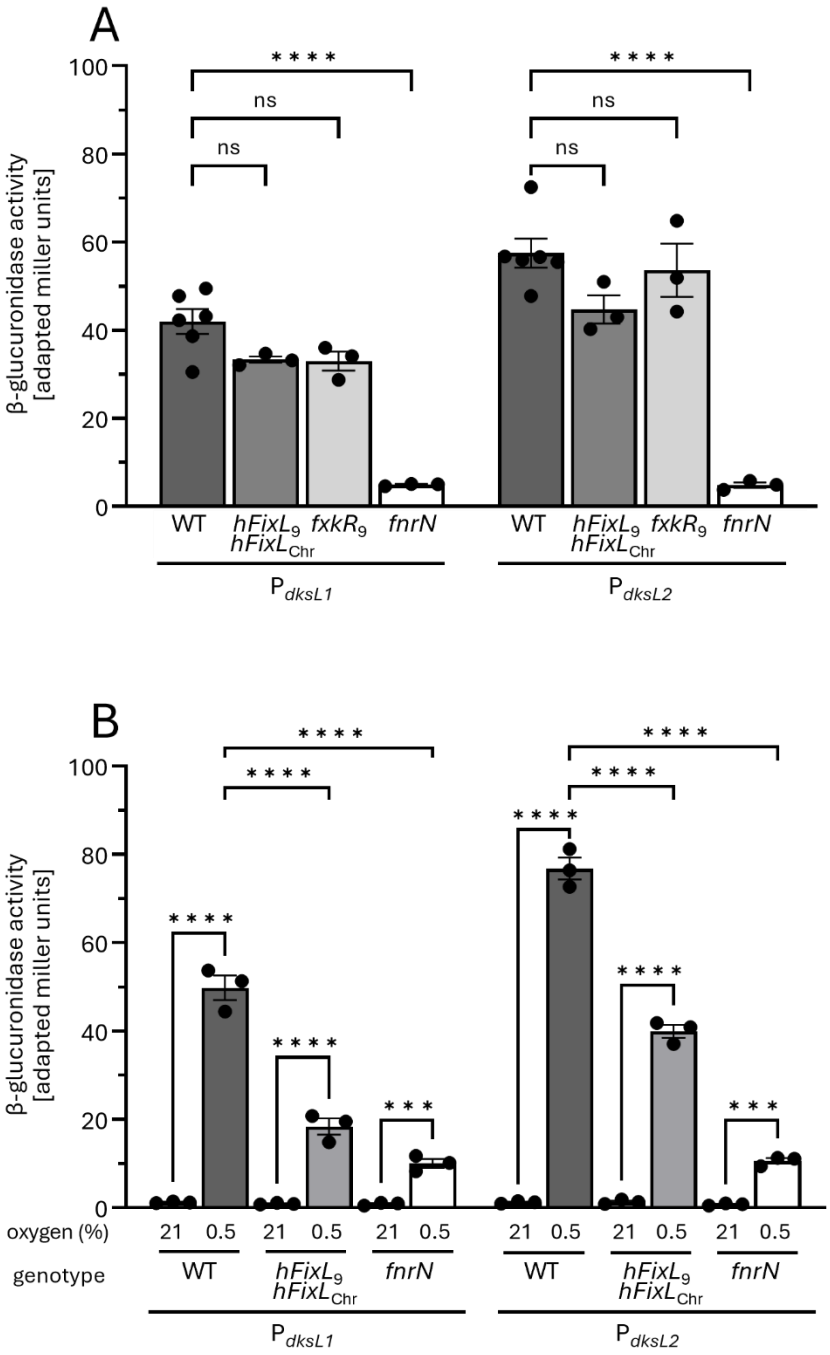


Figure 4.4 Expression of *dksL* genes depends on the oxygen regulators hFixL and FnrN. *Rlv*3841 WT (dark bars) and mutant strains (grey to white bars; $hFixL_9\ hFixL_{chr}$ [LMB496]; $fxkR_9$ [OPS1808]; *fnrN* [LMB648]) containing promoter-*gusA* fusions of either *dksL1* or *dksL2* were assayed for their β-glucuronidase activities. Subscripts indicate gene location (9, plasmid 9; Chr, chromosome).

(A) Promoter activity in bacteroids isolated from three-week-old pea nodules using a differential spin protocol. Activity of both promoters was nearly abolished in the *fnrN* mutant background, whereas little or no reduction in β-glucuronidase activity was observed in the double *hFixL* and *fxkR* mutant.

(B) Promoter activity in free-living cultures grown for at least 12 h under atmospheric (21% O_2) or microaerobic (0.5% O_2) conditions. In the double *hFixL* mutant, induction of both *dksA*–like promoters was reduced by about half while mutation of *fnrN* further reduced β-glucuronidase activity to a fraction of WT induction.

Bars represent mean ± SEM from three biological replicates. Statistical significance reflects Sidak-corrected comparisons between growth conditions for each reporter following a two-way ANOVA, where ns not significant, **** $p < 0.0001$, *** $p < 0.001$.

To determine whether this loss of *dksL* induction in *fnrN* mutants is an indirect consequence of impaired nitrogen fixation, promoter activity was additionally examined in a *nifH* mutant background, which lacks a functional nitrogenase and exhibits a Fix$^-$ phenotype. No relevant differences in induction of *dksL* expression were observed between fixing and non-fixing nodules (Figure S4.4). This demonstrates that *dksL* expression is independent of nitrogen fixation activity and is instead directly regulated by the oxygen-responsive pathway, foremost by FnrN.

Previous work suggested that hFixL primarily responds to free-living microaerobic conditions, whereas FnrN autoactivation occurs only under near-anaerobic conditions within nodules (Rutten et al., 2021). To assess the contribution of these regulators under microoxic conditions, promoter activity was measured in free-living cultures of WT, the double *hFixL* mutant, and the *fnrN* mutant grown at atmospheric oxygen and at 0.5% O_2 (Figure 4.4B).

At atmospheric oxygen levels, *dksL1* and *dksL2* remained uninduced across all strains, consistent with previous observations. At 0.5% O_2, induction of *dksL1* and *dksL2* was reduced by approximately half in the double *hFixL* mutant. Notably, disruption of *fnrN* critically reduced β-glucuronidase activity to approximately 20% and 14% of WT level induction for *dksL1* and *dksL2*, respectively. These results refine the model proposed by Rutten et al. (2021), which did not examine oxygen levels below 1%, by indicating that FnrN already becomes functionally active under free-living conditions at sufficiently low oxygen levels (e.g. 0.5% O_2).

To determine whether the oxygen-responsive regulators directly control expression of the *dksL* genes, we examined their promoter regions for conserved anaerobox motifs. The canonical FixK/FnrN operator sequence (TTGAT-X_4-ATCAA) was identified upstream of both *dksL1* and *dksL2*, whereas no such motif was detected in the *dksA* promoter region (Figure 4.5). As both FixK and FnrN are known to bind these conserved sequences to induce expression of downstream genes (Kaminski et al., 1991; Rutten et al., 2021; Schlüter et al., 1992), the presence of anaeroboxes upstream of the *dksL* genes provides strong support for direct regulation by the oxygen-sensing pathway and is consistent with their FixK/FnrN-dependent induction observed in bacteroids and under microaerobic conditions.

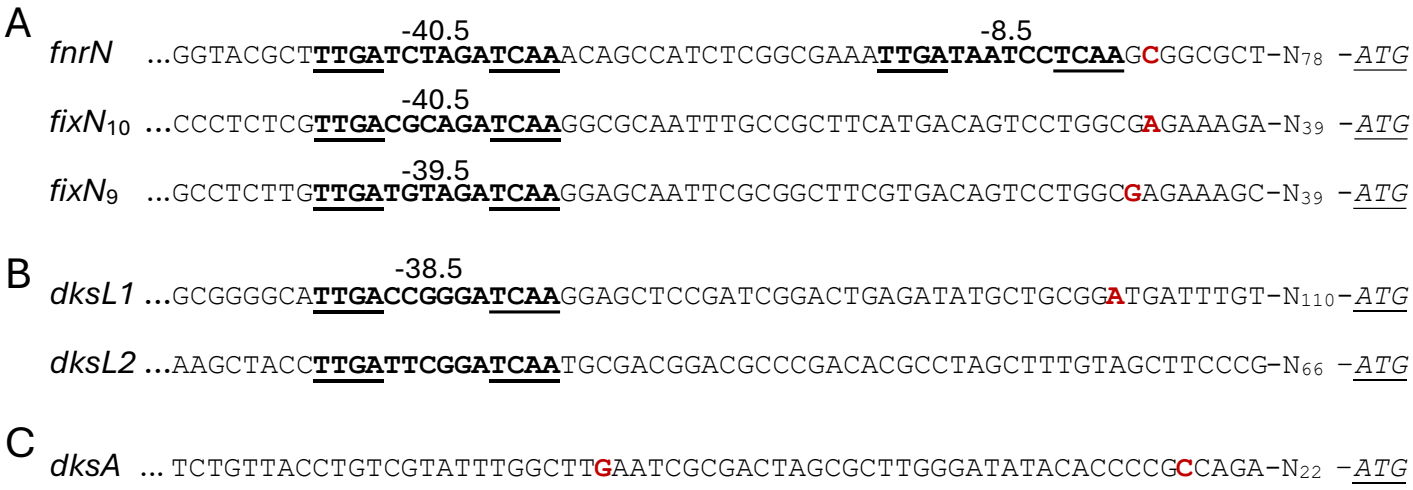


Figure 4.5 Sequence alignment of selected *Rlv*3841 FnrN-controlled promoters. The consensus anaerobox motif (TTGA-N_6-TCAA) is shown in bold. Predicted transcription start sites (TSS) are highlighted in red. Numbers above each anaerobox indicate the distance of the motif centre relative to the predicted TSS. **(A)** Confirmed FnrN-regulated promoters (*fnrN*, *fixN*$_{10}$, and *fixN*$_9$) show a conserved anaerobox sequence positioned at a similar distance upstream of the TSS. **(B)** The *dksA*-like homologues *dksL1* and *dksL2* contain putative anaerobox motifs with comparable spacing relative to the TSS. No TSS was predicted upstream of *dksL2*. **(C)** In contrast, the *dksA* promoter lacks a recognizable anaerobox motif.

Loss of *dksA* homologues does not impair growth or symbiosis

As transcriptional regulation of *dksL* genes is strongly associated with the microaerobic conditions within nodules, we hypothesized that these homologues might contribute to symbiosis with legume hosts. To test this, we generated deletion mutants of each individual homologue (OPS3300, OPS3301, OPS3365) as well as higher-order mutants, specifically a *dksL1 dksL2* double mutant (OPS3367) and a *dksA dksL1 dksL2* triple mutant (OPS4310).

Repeated attempts to construct a markerless triple mutant were unsuccessful. Among approximately 200 double-crossover candidates screened, none carried an in-frame deletion of *dksA*; instead, all isolates had reverted to the WT allele during the second recombination. This observation suggests selective pressure against simultaneous loss of all three genes, potentially due to functional redundancy among the *dksA* homologues.

Nevertheless, deletion of *dksA* in the *dksL1 dksL2* double mutant background was ultimately achieved by replacing *dksA* with an antibiotic resistance cassette through double recombination, demonstrating that the triple mutant is viable. This suggests that recovery of a markerless triple mutant was likely limited due to substantial selective constraints rather than non-viability.

The high sequence conservation and similar induction profiles of DksL1 and DksL2 suggested functional overlap. As initial characterization of the respective single mutants revealed no detectable symbiotic phenotype, we prioritized the double mutant for detailed analysis to evaluate their combined contribution.

Deletion of *dksA* homologues had only minor effects on free-living growth, including under microoxic conditions (Figure S4.5). The *dksA* triple mutant most closely resembled a *relA* mutant in overall growth pattern; however, neither strain displayed a pronounced growth defect compared to the WT. Notably, colonies of the *relA* mutant and the triple mutant appeared more mucoid, whereas the WT, the *dksA* mutant, and the *dksL1* and *dksL2* double mutant displayed a drier morphology.

Under microoxic conditions (Figure S4.5D-F), growth was reduced for all strains compared to normoxia (Figure S4.5A-C). Even after 5 days of incubation, growth

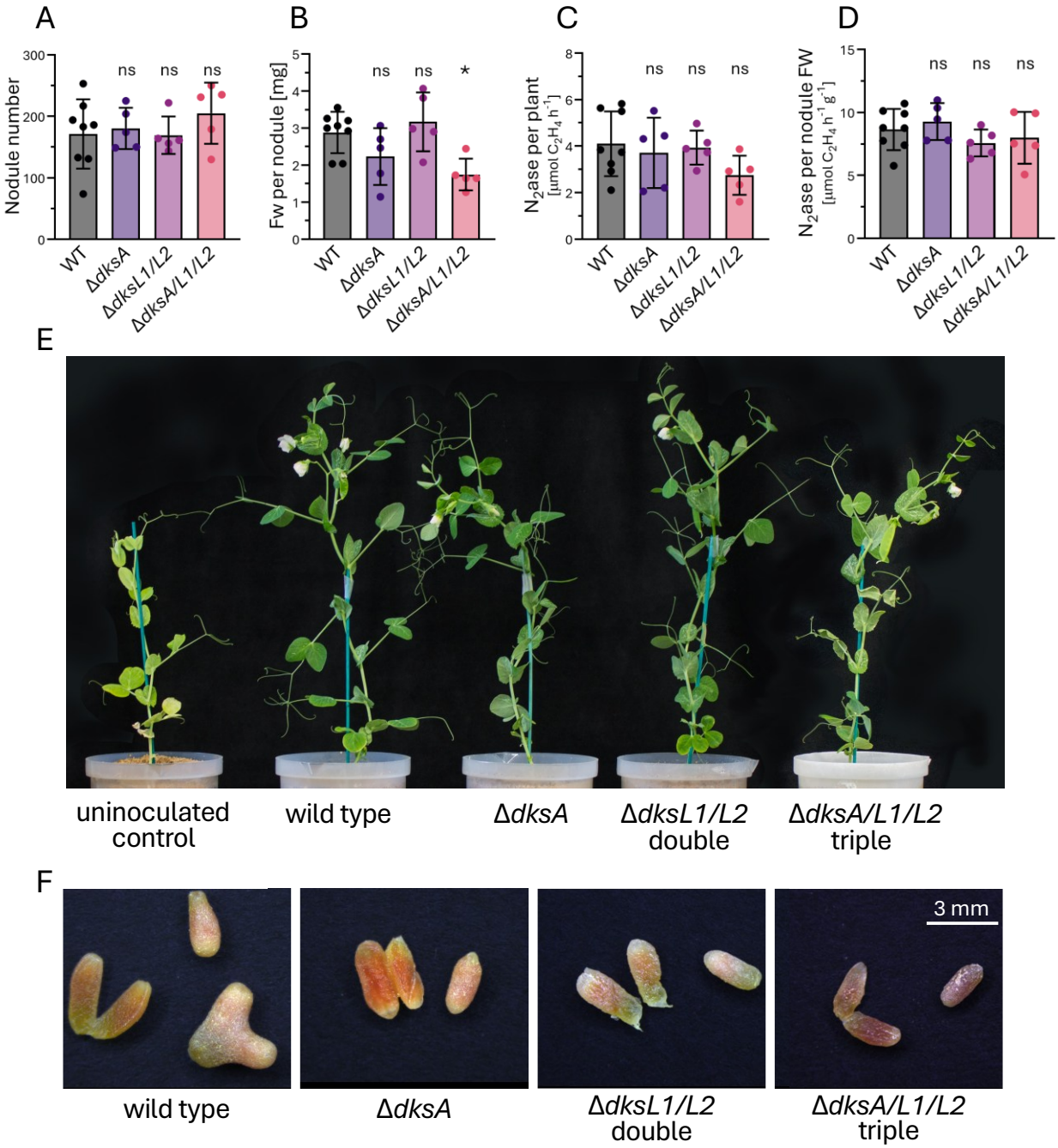


Figure 4.6 Deletion of *dksA* homologues does not affect nodulation or fixation in mature peas. *Pisum sativum* cv. Avola seedlings were inoculated with *Rlv*3841 wild type (WT), a Δ*dksA* single mutant, a Δ*dksL1* Δ*dksL2* double mutant, or a Δ*dksA*::*aacC1* Δ*dksL1* Δ*dksL2* triple mutant and grown for 28 dpi. Plants were assayed for nodule number **(A)**, fresh weight (FW) per nodule **(B)**, nitrogenase activity per plant **(C)**, and nitrogenase activity per nodule FW **(D)**. Representative plants **(E)** as well as nodules and nodule cross sections **(F)** are shown for the indicated strains. Each strain was tested on $n \geq 5$ plants, with bars representing mean ± SD. Statistical analysis was performed using one-way ANOVA followed by Dunnett's multiple comparisons test versus WT ($\alpha \leq 0.05$). Asterisks indicate significant differences; ns, not significant.

remained limited, particularly on minimal media, with glucose supporting the least growth. Strain-dependent differences were subtle and inconsistent across media. The *dksL1 dksL2* double mutant appeared slightly less viable under microoxic conditions, although this trend was not reflected in the triple mutant's growth. Interestingly, the *relA* mutant showed a tendency toward slightly improved growth under microoxia relative to the other strains.

All mutant strains formed nodules at levels comparable to WT, with no significant differences in nodule number (Figure 4.6A). Although the triple mutants produced significantly smaller nodules (Figure 4.6B), this reduction in size did not translate into decreased nitrogen fixation activity (Figure 4.6C,D). Nitrogenase activity, quantified by acetylene reduction assay (ARA), showed no significant differences at 28 dpi in either per plant or when normalized to nodule fresh weight (Figure 4.6C,D), indicating that nodule functionality was not significantly impaired. Plants inoculated with mutant strains were indistinguishable from WT controls (Figure 4.6E) and nodules were comparable in morphology and coloration (Figure 4.6F). All inoculated plants had dark green leaves indicative of sufficient nitrogen supply, as opposed to chlorotic and smaller uninoculated controls.

Interestingly, quantification of viable, non-differentiated bacteria within pea nodules revealed approximately a 10-fold reduction in CFU in the *dksA* and an approximately 1000-fold reduction in the triple mutant compared to the WT (Figure 4.7), demonstrating a substantial reduction in mutant viability inside pea nodules.

Previous studies in *S. meliloti* reported a delay in nodule development when canonical *dksA* was deleted, with effects most evident at early stages and largely compensated in mature nodules. To detect potential developmental defects, symbiotic performance was therefore additionally assessed at 12 dpi (Figure S4.6). No significant differences were observed in any measured parameters. Young nodules formed by the mutant strains were indistinguishable from WT with respect to nodule number, size, morphology, or nitrogen fixation activity. The triple mutant displayed greater variability among individual plants, yet without a statistically significant effect.

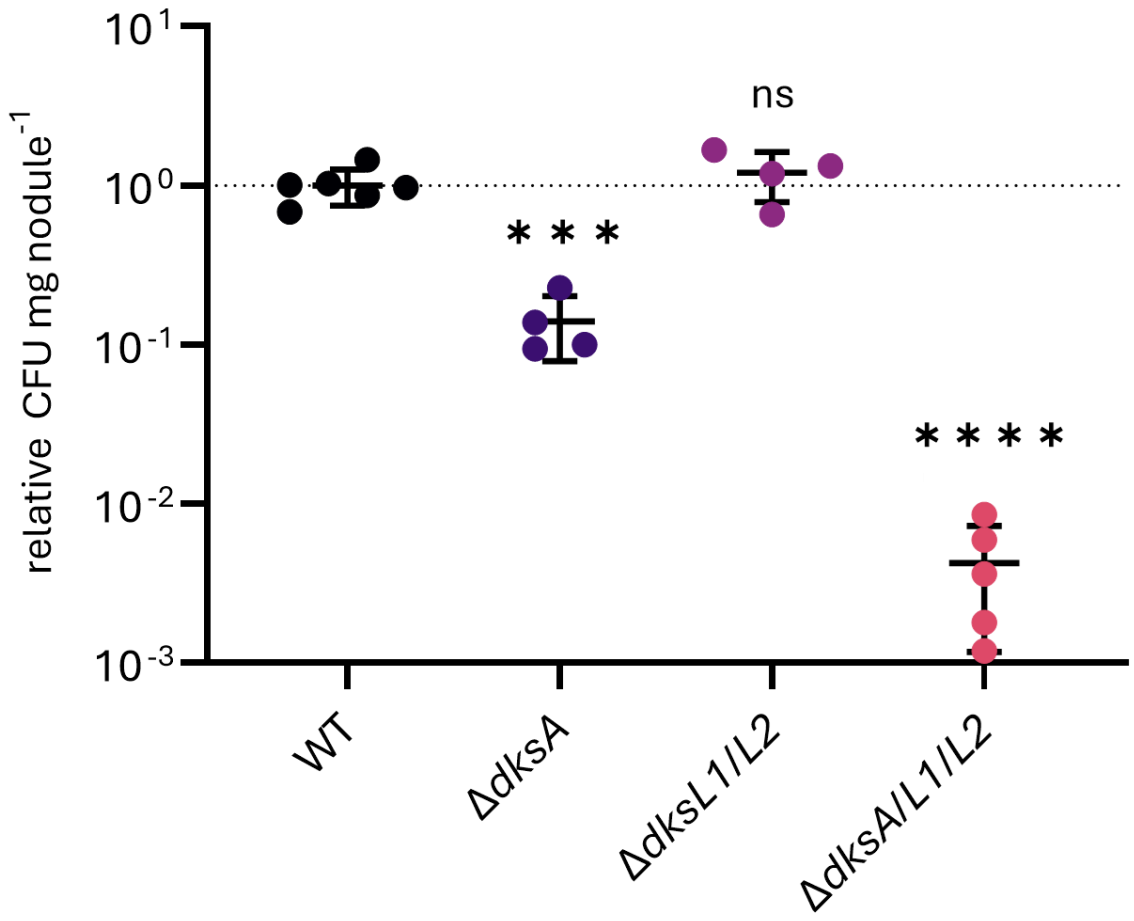


Figure 4.7 The *dksA* single and *dksA dksL1 dksL2* triple mutants show reduced rhizobial viability in pea nodules. Numbers of viable, non-differentiated bacteria recovered from *Pisum sativum* cv. Avola nodules. Bacteroids from *Rhizobium leguminosarum* bv. *viciae* 3841 wild type (WT), a Δ*dksA* single mutant, a Δ*dksL1* Δ*dksL2* double mutant, or a Δ*dksA*::*aacC1* Δ*dksL1* Δ*dksL2* triple mutant were isolated from 28 dpi-old nodules, serially diluted, and plated to determine colony forming units (CFU) per mg of nodule tissue. Data represent 5 biological replicates, each assayed in 5 technical replicates. Results are derived from two independent experiments and were normalized to the WT to account for experimental variability. Statistical analysis was performed on log-transformed data using Brown-Forsythe and Welch ANOVA, followed by Dunnett's T3 multiple-comparisons test against the WT. **** $p < 0.0001$, *** $p < 0.001$; ns, not significant.

DksA homologues affect competitive abilities differently

Given the absence of major symbiotic defects in single-inoculation assays, we asked whether more subtle phenotypes may only become apparent under competitive conditions and therefore assessed nodule occupancy of *dksA* homologue mutants in direct competition against *Rlv*3841 WT (Figure 4.8). Differentially marked strains were co-inoculated at defined ratios, and the relative abundance of nodules induced by the WT or a *dksA* homologue mutant strain was compared against the inoculum ratios.

The relative proportions in nodules induced by differently marked WT strains closely reflected the input ratio, indicating that the markers do not interfere with competitive ability on pea, consistent with previous reports (Clark, 2021). In contrast, deletion of *dksA* significantly increased competitive nodule occupancy. Across both inoculation ratios, more nodules were occupied by the CelB-marked Δ*dksA* strain than expected based on the inoculum, indicating an increased competitiveness relative to the WT.

In opposite, deletion of both *dksL*s resulted in reduced competitiveness. The CelB-marked Δ*dksL1* Δ*dksL2* double mutant occupied significantly fewer nodules than predicted from the inoculum ratio, particularly in the 10:1 input ratio, demonstrating a competitive disadvantage to the WT. All reported differences were significant at $p < 0.05$ according to Welch's unpaired *t*-test. Together, these results indicate that DksA negatively affects competitive fitness and a deletion of *dksA* may aid the competitive abilities, whereas *dksL1* and *dksL2* positively contribute to competitive nodule occupancy in pea plants.

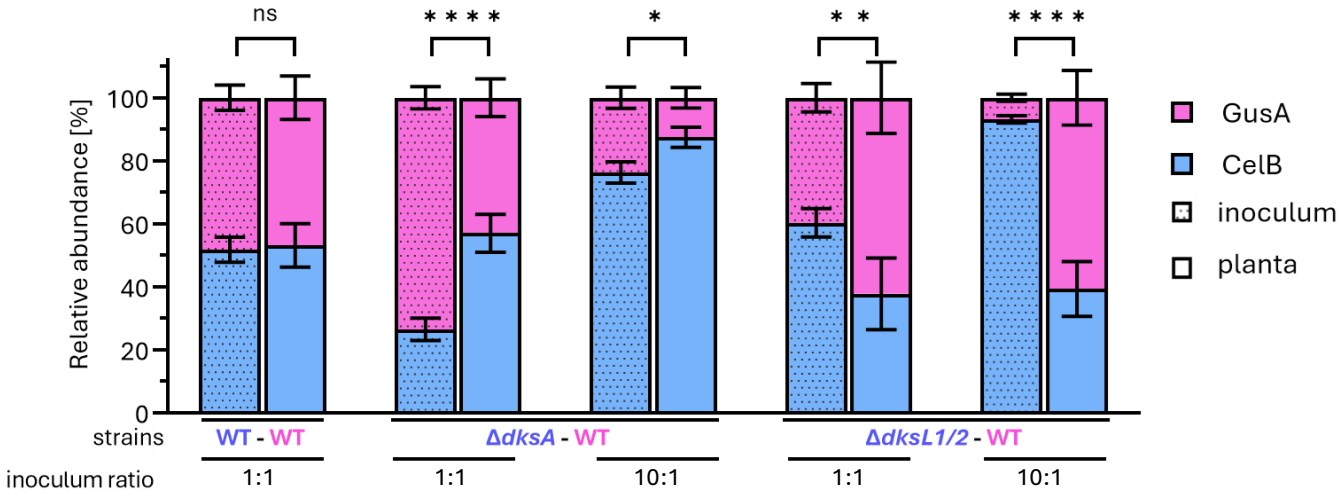


Figure 4.8 Δ*dksA* exhibits increased and Δ*dksL1/2* reduced competitiveness relative to WT during nodule occupancy. *celB*-marked strains (WT-*celB*, Δ*dksA*-celB, or Δ*dksL1/2*-*celB*; green) were co-inoculated with *gusA*-marked WT (orange) at the indicated input ratios (aiming at 1:1 or 10:1). Stacked bars show the relative abundance of GusA- and CelB-expressing CFU in the inoculum (dotted bars) and in nodules subjected to sequential double staining (solid bars), expressed as percentage of the total population. Error bars indicate SD (inoculum n = 3; plants n = 8). Statistical significance compares the GusA-fraction in inoculum and plant populations for each competition using Welch's unpaired t-test (two-tailed); ns, not significant; * $p < 0.05$; ** $p < 0.01$; **** $p < 0.0001$.

Transcriptome analysis on bacteroids collected from developing (12 dpi) and mature (28 dpi) nodules

Promoter analysis revealed strong upregulation of *dksL*s under low-oxygen conditions and in bacteroids. Despite this, *P. sativum* plants inoculated with *dksA* homologue mutants appeared phenotypically normal and showed no substantial reduction in symbiotic performance, even in the triple mutant background. To determine whether more subtle transcriptional alterations might occur without overt effects on symbiotic efficiency, we performed a transcriptomic analysis.

Given that Wippel & Long (2016) reported effects predominantly during early stages of *S. meliloti* - *M. sativa* symbiosis rather than in mature nodules, we included two developmental time points, young (12 dpi) and fully developed (28 dpi) nodules, in our analysis. Total RNA was isolated from *P. sativum* nodules formed by either the *Rlv*3841 WT, Δ*dksA* mutant, or Δ*dksL1* Δ*dksL2* double mutant, and RNA sequencing was performed on biological triplicates.

On average, 42,374,035 ± 3,724,754 paired-end reads (mean ± SD) were obtained per sample. Of these, 41.08 ± 11.87% (mean ± SD) aligned to the *R. leguminosarum* genome (Table S4.2), which is higher than previously reported percentages (Pardo Díaz, 2022). This corresponds to approximately 17.5 ± 5.7 million mapped bacterial reads per sample.

The alignment rate was significantly lower (unpaired *t*-test, $p < 0.0001$) in RNA extracted from 12 dpi nodules (31.73 ± 7.29%, mean ± SD) compared to 28 dpi nodules, (50.43 ± 7.02%, mean ± SD). This difference likely reflects the developmental progression of the nodules, including increased bacterial biomass and transcriptional activity in mature nodules. Nevertheless, even the lower alignment rates resulted in sequencing depths well above the commonly accepted threshold of 5-10 million reads required for robust differential gene expression analysis in bacteria (Haas et al., 2012).

Transcript abundance was quantified as transcripts per million (TPM) and differential expression analysis between genotypes and time points was performed using DESeq2 on normalized, regularized log (rlog)-transformed count data. Differential expression

analysis was conducted for 7,425 coding sequences. The full dataset is available in Supplementary Table A (.xlsx).

Principal component analysis (PCA, Figure S4.7) revealed tight clustering of biological triplicates, indicating high reproducibility. The first principal component (PC1), explaining 62.46% of the variance, primarily separated samples by developmental stage (12 vs 28 dpi), demonstrating that nodule age is the main driver of transcriptional variation. The second principal component (PC2; 11.79% of the variance) further resolved samples according to inoculum genotype.

WT and Δ*dksL1* Δ*dksL2* bacteroids clustered closely at both time points, indicating that deletion of the two *dksL* genes does not elicit large-scale changes in gene expression. In contrast, Δ*dksA* bacteroids formed a distinct cluster, particularly at 28 dpi, suggesting a stronger transcriptional impact of *dksA* deletion on the bacterial transcriptome.

Differential gene expression during nodule maturation

Consistent with the PCA, the most pronounced transcriptional differences were observed between developmental stages. Across genotypes, comparison of 12 dpi and 28 dpi samples showed extensive transcriptional reprogramming, with 862-1095 differentially expressed genes (DEGs) identified per genotype (Figure S4.8). Notably, 534 DEGs were shared among all three genotypes, indicating a conserved developmental transcriptional program during nodule maturation.

Among shared DEGs, 243 genes were upregulated at 28 dpi and were predominantly associated with carbon and energy metabolism, as well as stress response and chaperone functions. Conversely, 291 genes were downregulated and were enriched for functions typically no longer required in mature bacteroids. These included genes associated with motility (flagella and chemotaxis), alternative carbon uptake and catabolic pathways, as well as features shared with growth-arrested cells, i.e. downregulated ribosomal and translational machinery. Together, these transcriptional changes reflect the metabolic reprogramming characteristic of differentiated bacteroids.

Deletion of dksL1 and dksL2 does not affect global gene expression

Strikingly, no DEGs were identified between the Δ*dksL1* Δ*dksL2* mutant and the WT at either time point when applying a threshold of α=0.01 and |log2FC| ≥ 1 (≥2-fold change), apart from the two deleted loci themselves. Even under less stringent criteria (*p adj* < 0.05), only a small number of genes exhibited marginal expression changes.

At 12 dpi, the only additional gene with *p adj* < 0.05 encoded a putative transmembrane cation ATPase transporter (RL1871), which showed a modest 1.8-fold decrease in expression. Importantly, RL1871 is located immediately downstream of *dksL1*, suggesting that the observed effect likely reflect local transcriptional effect resulting from the markerless deletion rather than a regulatory consequence of *dksL1* loss.

Similarly, at 28 dpi, only four genes met the relaxed significance threshold. RL2871 and RL2269, both positioned immediately next to the deleted loci, displayed mild downregulation (1.7-fold and 1.3-fold decreases, respectively), again consistent with local promoter or transcriptional effects. Two additional genes encoding conserved hypothetical proteins displayed moderate changes (RL2269: ~1.3-fold decrease; pRL100242: ~2.7-fold increase), while *clpA* (RL2213) exhibited only a minor decrease (~1.25-fold).

Collectively, these findings indicate that simultaneous deletion of the two *dksL* genes does nor measurably alter the global bacteroid transcriptome, consistent with the absence of a detectable symbiotic performance phenotype (Figure 4.6; Figure S4.5).

Deletion of dksA alters transcriptional regulation

Deletion of dksA strongly induces nitrogen scavenging and amino acid catabolism in early nodules

In contrast, deletion of Δ*dksA* had pronounced impact on global gene expression. Using a threshold of α = 0.01 and |log2FC| ≥ 1 (i.e. ≥2-fold change), 45 genes were differentially expressed at 12 dpi, of which 40 were upregulated and five were downregulated (Figure S4.9A,C; Table S4.3). Of these, 17 genes displayed substantial expression changes (log2FC ≥ 2; ≥4-fold change), 16 of which were strongly upregulated. The only gene

exhibiting strong apparent downregulation was *dksA* itself, reflecting the absence of mapped reads at the deleted locus.

A clear enrichment of nitrogen acquisition and amino acid transport systems emerged. The ammonium uptake and assimilation system (*amtB*, 5.5-fold; *glnK*, 6.1-fold; *glnII*, 3.8-fold) was coordinately induced, indicating activation of the canonical ammonium sensing and assimilation pathway. Consistently, two PAAT (polar amino acid transporter) ABC transporter systems were induced: the chromosomal cluster RL0981-84 (~3.8–4.1-fold) and a plasmid-encoded PAAT system on pRL10 (pRL100070–72; ~2.3–2.4-fold). In both cases directly adjacent genes were similarly upregulated. According to BioCyc annotations (Herson et al., 2024), these genes are organized in operons, with the first gene classically showing the strongest induction.

In addition to amino acid transport, several other ABC transporter systems were upregulated, including RL3368-71 and components of the NitT anionic substrate transporter. Genes linked to alternative carbon utilization, such as s *eryH* and *melA*, were also induced.

The most pronounced transcriptional change was observed for a large gene cluster on pRL10 (pRL100242-252). This region comprises the GABA-specific POPT ABC transporter (*gtsABCD*), strongly induced (12-24-fold), and an adjacent operon (pRL100242-247) upregulated 15- to 38-fold. The latter encodes predicted amino acid catabolic enzymes, including flavin-dependent oxidoreductases, a hydrolase, an aldehyde dehydrogenase, and a NIPSNAP domain protein, suggesting coordinated activation of GABA or broader amino acid catabolism. Induction of *gabD4* (3.2-fold), encoding NAD-dependent succinate-semialdehyde dehydrogenase, further supports increased GABA assimilation. As GABA assimilation shares downstream reactions with the GABA shunt, increased GABA catabolism may thereby link amino acid catabolism to central carbon metabolism via succinate production for TCA cycle entry.

More than half of the DEGs are plasmid-encoded, with approximately 40% located on the symbiotic plasmid pRL10, suggesting that DksA contributes to repression of plasmid-borne catabolic functions during early bacteroid development. In addition, several transcriptional regulators were differentially expressed, including induction of a LysR-

family regulator and *dksL1* (~2-fold), alongside repression of GntR- and TetR-family regulators, indicating broader regulatory rewiring in the absence of DksA.

Collectively, these data indicate that loss of DksA triggers strong activation of nitrogen scavenging, amino acid uptake, and GABA catabolic pathways, suggesting that DksA restrains nitrogen assimilation (e.g. NH_3 assimilation) during symbiosis. This dysregulation is consistent with a metabolic state resembling nitrogen and/or carbon limitation.

Deletion of dksA causes widespread stress-associated transcriptional reprogramming in mature nodules

At 28 dpi, the transcriptional impact of *dksA* deletion was more pronounced, with 175 DEGs identified (Figure S4.9B-C; Table S4.4). The majority (137 genes) were downregulated in the mutant relative to the WT, while 38 were upregulated, indicating a broad role for DksA in mature nodule development gene regulation. Although more genes were affected than at 12 dpi, the magnitude of expression changes was generally less pronounced, with only 16 downregulated and 9 upregulated genes showing ≥4-fold differences. Notably, the overall directionality shifted from predominantly upregulated genes at 12 dpi to mainly downregulated genes at 28 dpi, suggesting that DksA primarily repressed pathways in early nodules but contributed more substantially to transcriptional activation in mature bacteroids. Merely 17 genes are shared between both time points.

Evidence of sustained nitrogen limitation persisted at 28 dpi. The key ammonium assimilation genes remained strongly upregulated (*amtB,* 3.2-fold; *glnK*, 7.0-fold; *glnII,* 4.0-fold), alongside the beforementioned chromosomal PAAT transporter (RL0979–RL0984; ~4–4.6-fold) and the expression of the plasmid-encoded PAAT component pRL100072 is still elevated. Together, these data indicate that the Δ*dksA* mutant continues to exhibit a nitrogen-limited transcriptional profile in mature bacteroids.

As observed at 12 dpi, several transcriptional regulators remained differentially expressed relative to the WT, indicating continued regulatory imbalance. In addition, mature nodules exhibited a broader induction of stress-associated functions. Alongside

the flavin reductase (RL0979), which was already upregulated earlier, the chaperone systems *dnaK/dnaJ* and *groEL/groES* were now also induced, consistent with proteotoxicity and potentially redox stress.

Strikingly, numerous symbiotic plasmid functions were repressed. Core nodulation genes (*nodN*, *nodE*, *nodF*, *nodA*, *nodC*) were ~2–3-fold downregulated, and rhizosphere-induced genes (*rhiA*, *rhiB*, *rhiC*) were even more strongly repressed (~6–7-fold). In addition, expression of several surface- and envelope-associated genes, including glycosyltransferases (e.g. RL1155), exported proteins (e.g., RL0469, RL0530, RL1154), and *ndvA* (RL4640) was reduced. Similarly, a broad range of transport systems were downregulated, including CUT1 and CUT2 carbohydrate ABC transporter components (pRL90285-86, pRL100462, pRL120393), PepT peptide transporter components (pRL100278, pRL110446, pRL110454), a TRAP transporter (pRL120400–402), and several MFS/RND efflux systems (*salA*, RL2938, *rmrAB*, RL4274), consistent with overall metabolic attenuation.

In contrast, plasmid conjugation machinery (*traG, traC, trbL, trbE, trbB*) was strongly induced (up to ~7-fold), indicating derepression of plasmid transfer functions in the absence of DksA.

In summary, while the Δ*dksA* mutant remained nitrogen-starved, mature bacteroids additionally exhibited widespread repression of symbiotic and metabolic functions alongside activation of stress and plasmid mobility pathways. This pattern suggests progressive regulatory imbalance and impaired maintenance of the differentiated bacteroid state in the absence of DksA.

Phenotypic characterization of *dksA* homologues in bean-symbiont *Rlp*4292

The wild-type like symbiotic performance of *dksA* and *dksL* mutants in pea suggested that host context may influence the functional requirement for DksA. To determine whether these roles are conserved across related but biologically distinct symbioses, we extended our analysis to the bean symbiont *Rlp*4292. The three paralogs identified in *Rlp*4292 share high sequence similarity with the *Rlv*3841 homologues, with 92-96% nucleotide sequence similarity and 86-98.6% amino acid sequence similarity (Table

S4.5). Importantly, the conserved motif architecture, including the presence or absence of the coiled-coil and Zn-finger domains, is maintained between the two strains (Figure S4.2), suggesting congruent functionality.

Interest in examining the bean symbiont was further motivated by recent insertion sequencing (INSeq) predictions. INSeq a powerful approach to assess gene contributions to bacterial fitness across developmental stages (Wheatley et al., 2017, 2020). Recent INSeq screens performed in pea- and bean-nodulating rhizobia by our group enabled direct comparison of gene requirements in these closely related yet biologically distinct symbioses (Knights, Ledermann et al., in preparation; Wheatley et al., 2020).

In both hosts, disruption of the canonical *dksA* gene resulted in markedly reduced recovery of bacteroids from nodules, indicating a conserved requirement during symbiosis (Table S4.5; Table S4.6). In contrast, *dksL1* displayed largely neutral or minor fitness effects in both strains. The second paralog, *dksL2*, was not evaluated in *Rlv*3841 due to annotation limitations described earlier. However, in *Rlp*4292, INSeq-derived fitness estimates (log_2FC) predicted, similar to *dksA*, a pronounced defect for *dksL2* in bacteroids and during regrowth. This pattern suggests that *dksL2* may contribute to bacterial survival or adaptation during transitions out of the differentiated state in bean nodules.

Differences between the INSeq datasets likely reflect the distinct biology of the two symbioses. Pea plants impose terminal differentiation of bacteroids, such that only undifferentiated bacteria are released from senescing nodules (Mergaert et al., 2006). By contrast, bean bacteroids retain the capacity to dedifferentiate and resume free-living growth, enabling assessment of the regrowth stage and implicating potential roles of *dksA* and *dksL2* during this transition.

To determine whether the symbiotic contribution of *dksA* homologues is host-dependent, we generated analogous markerless single deletions of all three homologues in the bean symbiont *Rlp*4292 and characterized their symbiotic phenotypes.

In contrast to the results obtained with the pea symbiont *Rlv*3841, inoculation of bean plants revealed distinct phenotypes among the mutants (Figure 4.9). Despite INSeq

indicating a fitness defect for *dksL1* and *dksL2* mutants, no differences were observed in plant phenotypes, as bean plants inoculated with these mutants were indistinguishable from those inoculated with the WT across all measured parameters (Figure 4.9A-D).

In contrast, plants inoculated with the Δ*dksA* mutant displayed a paler green to yellowish phenotype (Figure 4.9E), resembling chlorotic uninoculated controls and indicative of reduced nitrogen supply. Although nodule number and total nodule fresh weight were not significantly altered (Figure 4.9A,B), nodules formed by the *dksA* mutant were white to light pink in cross-sections compared to the characteristic red derived from leghaemoglobin observed in functional WT and *dksL* mutant nodules (Figure 4.9F). In addition, ARA revealed significantly reduced nitrogenase activity in plants inoculated with the Δ*dksA* mutant (Figure 4.9C).

To assess regrowth ability following symbiotic differentiation, bacteroids were isolated from 28 dpi bean nodules, reinoculated into TY medium, and growth monitored over 48 h. (Figure 4.10A). All strains displayed a pronounced lag phase after reinoculation, consistent with the transition from the bacteroid state back to free-living bacteria.

The *dksA* mutant displayed a markedly extended lag phase compared to the lag phase of all other strains. While WT, *dksL1*, and *dksL2* resumed exponential growth approximately 16-18 h after reinoculation into rich media, *dksA* did not enter exponential phase until approximately 20-24 h (Figure 4.10A).

In addition to the delayed onset of exponential growth, the *dksA* mutant showed a substantially reduced growth rate once exponential growth was established. The mean generation time (MGT) of *dksA* was 12.71 ± 1.42 h (mean ± SEM), more than twice that of the WT and the d*ksL1* and *dksL2* mutants, which exhibited MGTs of approximately 5.3 h (Figure 4.10A).

This impairment in growth is consistent with drop-count assays performed on rhizobia isolated from bean nodules to assess post-symbiotic viability. When normalized to nodule weight, CFU recovery from the Δ*dksA* strain was reduced by approximately seven orders of magnitude (Figure 4.10B), indicating a severe loss of viability compared to the WT.

Collectively, these data demonstrate that deletion of *dksA*, but not *dksL1* or *dksL2*, results in reduced rhizobial viability, and both an extended adaptation period from the bacteroid state and a reduced growth rate once adapted.

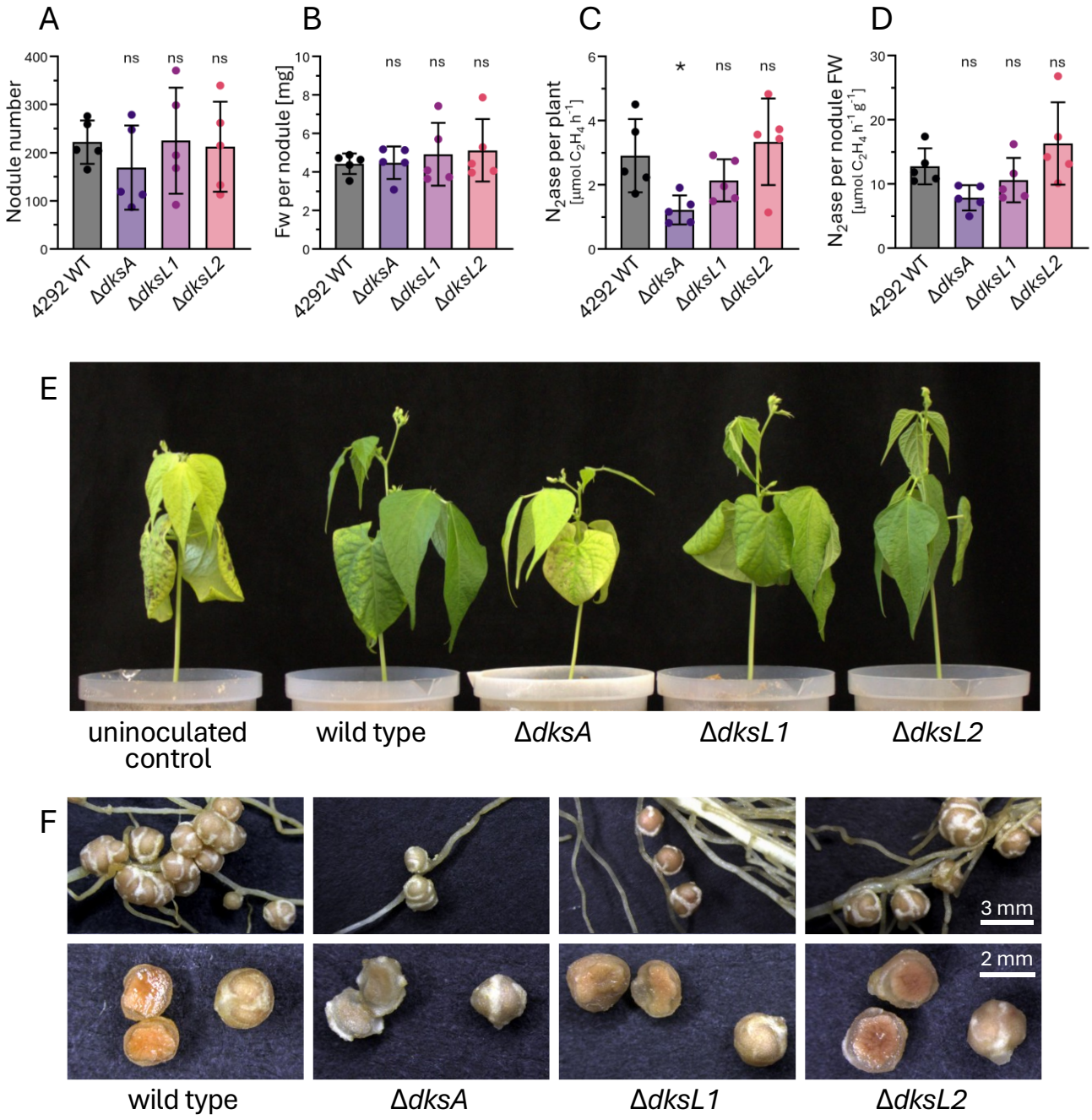


Figure 4.9 Deletion of *dksA*, but not *dksL* homologues, affects nitrogen fixation in beans. *Phaseolus vulgaris* cv. Tendergreen seedlings were inoculated with *Rlp*4292 wild type (WT) or Δ*dksA*, Δ*dksL1*, or Δ*dksL2* single mutant and grown for 28 dpi. Plants were assayed for nodule number **(A)**, fresh weight (FW) per nodule **(B)**, nitrogenase activity per plant **(C)**, and nitrogenase activity per nodule FW **(D)**. Representative plants **(E)** as well as nodules and nodule cross sections **(F)** are shown for the indicated strains. Scale bars in (F) apply per row. Each strain was tested on n = 5 plants, with bars representing mean ± SD. Statistical analysis was performed using one-way ANOVA followed by Dunnett's multiple comparisons test versus WT ($\alpha \leq 0.05$). Asterisks indicate significant differences; ns, not significant.

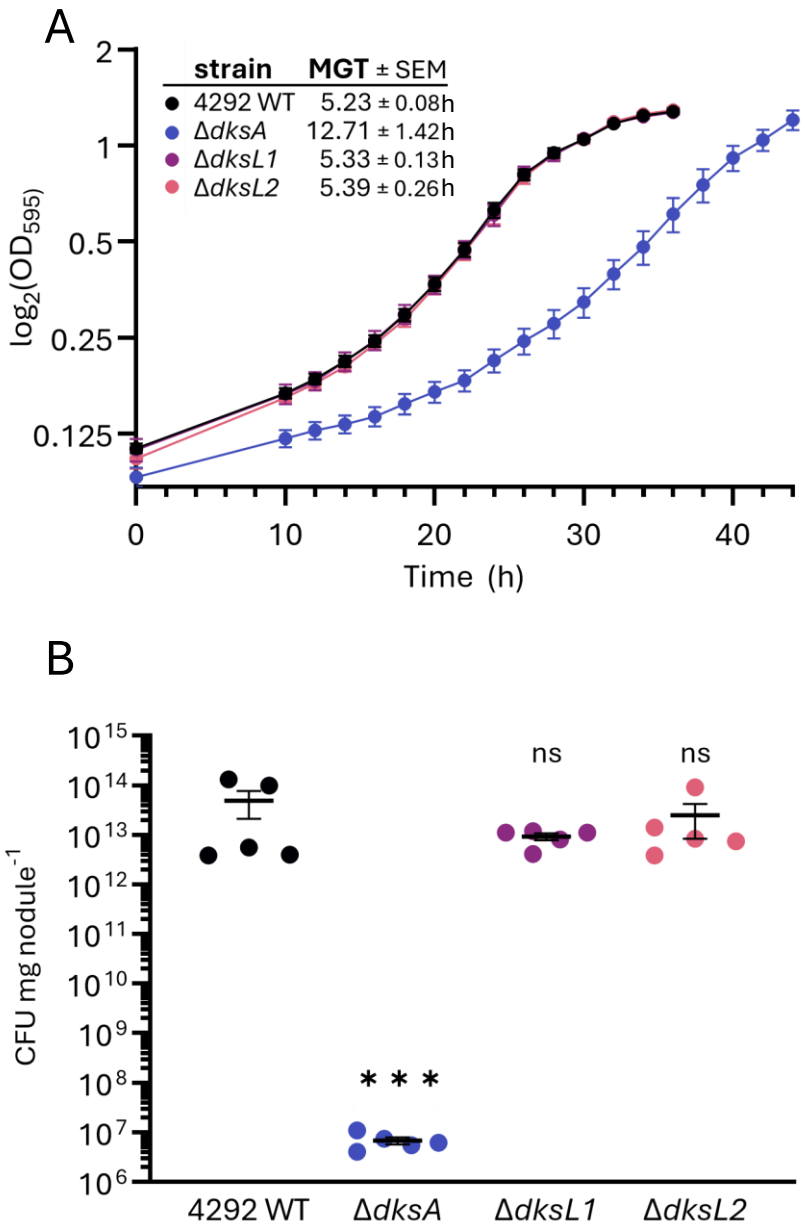


Figure 4.10 Deletion of *dksA*, but not *dksL1* or *dksL2*, reduced rhizobial viability and delays regrowth from bean nodules. (A) Regrowth curves of *Rhizobium leguminosarum* bv. *phaseoli* 4292 wild type (WT) and single deletion mutants Δ*dksA,* Δ*dksL1*, and Δ*dksL2*. Bacteroids were isolated from 28 dpi *Phaseolus vulgaris* cv. Tendergreen nodules and inoculated into TY medium. Growth is shown as $\log_2(OD_{595})$ over time. Data represent the mean ± SEM of 5 biological replicates. Mean generation time (MGT ± SEM) was calculated from the exponential growth phase of each replicate. **(B)** Viable bacteria recovered from bean nodules. Isolated bacteroids were serially diluted and plated to determine colony forming units (CFU) per mg of nodule tissue. Data represent 5 biological replicates, each assayed in 5 technical replicates. Statistical analysis was performed on log-transformed data using Brown-Forsythe and Welch ANOVA, followed by Dunnett's T3 multiple comparisons against the WT. *** $p < 0.001$; ns, not significant.

Discussion

DksA is a highly conserved RNA polymerase-binding transcription factor best known for its role in the stringent response, where it cooperates with (p)ppGpp to globally reprogram bacterial transcription during nutrient limitation and other adverse conditions. While many bacteria encode a single DksA protein, several α-proteobacteria, including rhizobia, harbour multiple homologues whose functional relationships have remained largely unexplored. The presence of three DksA homologues in *R. leguminosarum* raises the question whether gene duplication has facilitated functional specialization in this species, particularly in the context of its complex life cycle requiring dynamic transitions between metabolically distinct free-living and symbiotic states.

Here, we combined phylogenetic, regulatory, genetic, and transcriptomic analyses to dissect the roles of the three homologues across diverse physiological conditions. Focusing primarily on the pea symbiont *Rlv*3841, we set out to define regulatory control, physiological function, and potential functional divergence of the paralogs. In addition, by extending our analysis to the bean symbiont *Rlp*4292, we assessed whether the contribution of individual DksA homologues is contingent on host-imposed symbiotic development.

Diversification of DksA homologues

Phylogenetic analysis resolved two principal clades corresponding to canonical DksA proteins and DksA-like homologues (Figure 4.1). It is important to note that this phylogeny does not fully reconstruct the evolutionary history of this protein family, as the dataset was intentionally biased toward species with available experimental data and those encoding multiple homologues. Nevertheless, the observed distribution of copies across related taxa suggests independent duplication and/or loss events, as closely related species do not necessarily encode the same number of DksA homologues.

Most DksA variants retain the coiled-coil tip motif (DXXDXA), which has been demonstrated to be critical for DksA function as a transcriptional regulator in *E. coli, R. sphaeroides*, and *P. aeruginosa* (Furman et al., 2013; Lee et al., 2012; Lennon et al., 2014). In line with this, neither Wippel and Long (2016) nor we observed a clear

phenotype for DksL proteins with variations in the coiled-coil tip motif in *S. meliloti*, *Rlv*3841, or *Rlp*4292 under the conditions tested. Interestingly, however, the amino acid variations represent relatively conservative substitutions. For example, *S. meliloti* Smc0049 contains an alanine-to-valine substitution (DXXDXV), while several *R. leguminosarum* DksL proteins contain an aspartate-to-glutamate substitution (DXXEXA).

Nevertheless, motif conservation alone does not guarantee functional equivalence. In *S. meliloti*, restoration of the DksA-like protein Smc00049 to match the coiled-coil sequence of the strain's canonical DksA did not rescue the phenotype of a *dksA* mutant in either *E. coli* or *S. meliloti* (Wippel & Long, 2016), indicating that the presence of this motif alone is insufficient to confer canonical activity. Instead, deletion of the N-terminus of DksA led to a loss of function, suggesting that this region contributes to at least structural stability and/ or RNA polymerase interaction. Notably, DksL proteins possess a shortened N-terminus compared to canonical DksA homologues (Figure S4.2). Yet, even a chimeric fusion of the DksA N-terminus to Smc00049 failed to restore activity (Wippel & Long, 2016), demonstrating that despite apparent structural similarity, DksL proteins are functionally distinct from the canonical DksA.

In contrast, the functional significance of the Cys_4 zinc finger motif in DksA remains less clear. In the proteins analysed here, the complete Cys_4 Zn-finger motif is mostly conserved within the DksL clade, while several canonical DksA proteins lack one or more cysteine residues (Figure S4.1; Figure S4.2). Zinc finger motifs are typically associated with structural stabilization of protein domains and, in some contexts, nucleic acid interactions (Krishna et al., 2003).

Historically, the Cys_4 motif was considered essential for proper DksA folding and activity, supported by experimental evidence from *E. coli* and *P. aeruginosa* (Furman et al., 2013; Lee et al., 2012; Paul et al., 2004; Perron et al., 2005). However, later work revealed that for instance the *P. aeruginosa* paralog DksA2 lacks the complete Zn-finger motif and yet retains a similar fold, globular domain structure, and RNA polymerase binding properties to those of Zn-dependent DksA (Furman et al., 2013).

Instead, zinc-finger conservation may be linked to environmental specialization or species-specific requirements, rather than canonical function. In *P. aeruginosa*, zinc-independent paralog DksA2 may serve as a back-up copy for the canonical Zn-dependent DksA in zinc-poor environments (Blaby-Haas et al., 2011). Conversely, in *R. sphaeroides* and *S. meliloti*, only one of the encoded homologues complements an *E. coli* Δ*dksA* mutant despite differences in zinc-finger conservation (Lennon et al., 2014; Wippel & Long, 2016), further indicating that the presence of the Zn motif alone does not reliably define canonical activity.

These comparisons suggest that DksA paralogs have diversified along distinct evolutionary trajectories in different bacterial species. In *R. leguminosarum*, the phylogeny is consistent with specialization into one dominant canonical regulator (DksA) and two DksA-like paralogs. The broader distribution of multiple DksA copies across both symbiotic and non-symbiotic α-proteobacteria indicates that gene duplication is not strictly linked to symbiosis but may rather reflect adaptation to fluctuating environmental pressures. Consistent with this, unlike canonical *dksA*, both *dksL* genes are expressed only under a subset of tested conditions, suggesting that they may represent environmentally specialized regulators, particularly in response to oxygen availability.

Oxygen-dependent regulation of *dksL* genes

Transcriptional analyses demonstrated that *dksL1* and *dksL2* are strongly induced under microaerobic conditions and in bacteroids, whereas *dksA* and *relA* remain largely constitutively expressed. Across all promoter-reporter assays conducted, *dksA* and *relA* displayed predominantly constitutive expression, with no substantial stress-dependent induction. Promoter activity of *dksA* remained within a relatively narrow range (20-50 MU) across all tested environments, including starvation conditions. This pattern suggests that *dksA* is expressed from a weak constitutive promoter and likely represents the housekeeping DksA variant in *Rlv*3841. This is in line with findings in *S. meliloti*, where Wippel and Long (2016) observed no increase of *dksA* transcript levels at either 10 or 21 dpi compared to levels in rich medium.

The lack of transcriptional control indicates a posttranscriptional regulation mechanism of DksA as its activity is induced in response to starvation (Blaby-Haas et al., 2011; Krol

& Becker, 2011; Parshin et al., 2015; Perron et al., 2005). This is often the case with stringent response regulators. For instance, *relA* is constitutively expressed at low levels (this work, Krol & Becker, 2011) but becomes activated upon sensing uncharged tRNA at the ribosome, thereby triggering (p)ppGpp synthesis (Wendrich et al., 2002). Similarly, in *P. aeruginosa*, DksA expression follows a biphasic pattern and is regulated largely via mRNA stability rather than promoter induction (Perron et al., 2005).

By contrast, *dksL1* and *dksL2* showed no relevant expression under uninduced conditions but were substantially upregulated under microaerobic conditions and in bacteroids (Figure 4.2; Figure 4.3). This regulatory pattern is consistent with observations in *R. sphaeroides*, where a *dksA*-like homologue is specifically induced under anaerobic conditions while canonical *dksA* is expressed constitutively (Arai et al., 2008; Dufour et al., 2010; Lennon et al., 2014). Together, these data suggest that DksL proteins may have evolved specialized oxygen-associated functions rather than acting as canonical stringent regulators.

Assays conducted in oxygen-regulation mutant backgrounds revealed that FnrN is the principal activator of *dksL* expression. Induction of both *dksL1* and *dksL2* was nearly abolished in an *fnrN* mutant during symbiosis (Figure 4.4A) and strongly reduced under microaerobic free-living conditions (Figure 4.4B). Induction of *dksL1* and *dksL2* is therefore a consequence of decreasing oxygen levels, mediated through the hFixL-FxkR-FixK and FnrN oxygen-sensing cascade (Figure 1.4). Expression of *dksL* genes is activated by binding of FnrN to canonical anaerobox operator sites (TTGAT-X_4-ATCAA) located upstream of their transcription start sites (Figure 4.5). Anaeroboxes are recognized by both FixK and FnrN, which bind these motifs to induce expression of oxygen-responsive genes (Kaminski et al., 1991; Schlüter et al., 1992). FnrN is assumed to have a greater affinity for anaerobox motifs than FixK (Rutten et al., 2021), potentially allowing FnrN to outcompete FixK for binding as oxygen levels decrease.

Notably, FnrN-dependent activation was already evident at 0.5% O_2 under free-living conditions, indicating that FnrN becomes functionally active at higher oxygen concentrations than previously proposed. Rutten et al. (2021) detected limited *fnrN* expression at 1% oxygen and suggested a stepwise activation model in which hFixL primes the system before FnrN autoregulation takes over at lower oxygen levels. Our data

are consistent with a gradual induction model but suggest that oxygen thresholds for activation may be lower and more finely tuned than previously appreciated.

Residual induction in the *fnrN* mutant likely reflects partial compensation by FixK proteins, which recognize the same anaerobox sequences (Rutten & Poole, 2019). As *Rlv*3841 encodes three FixK homologues, future analysis of *fixK* or *fixK fnrN* mutants may clarify the relative contributions of these regulators to fine-tuning *dksL* expression under different oxygen conditions.

Importantly, induction of *dksL* genes was independent of nitrogen fixation, as expression remained intact in a *nifH* mutant background (Figure 4.3). Together, these findings demonstrate that *dksL* genes are integrated into the established hFixL–FxkR–FixK and FnrN oxygen-sensing pathway that governs the transition from free-living cells to bacteroids, rather than the classical stringent response pathway. This suggests that *dksL* function may be important in nodule bacteria prior to full bacteroid differentiation, at earlier stages of infection (i.e. before 12 dpi) when oxygen is declining but nitrogen fixation is not yet fully established.

Despite their strong induction during symbiosis, deletion of both *dksL* genes caused neither major transcriptional reprogramming nor strong defects in nodulation or nitrogen fixation in pea or bean, indicating that their function is not essential for core symbiotic metabolism. Nevertheless, more subtle phenotypic differences suggest a contributory role under certain conditions. In particular, the pronounced reduction in viability observed in the triple mutant suggests a role in maintaining bacterial persistence during later stages of infection. Together, these findings suggest that *dksL* genes may function during the transition into the symbiotic state and contribute to the longer-term bacterial viability within nodules.

Canonical DksA maintains bacteroid homeostasis

In free-living bacteria, deletion of *dksA* results in pleiotropic phenotypes across diverse bacterial species (Lennon et al., 2014; Parshin et al., 2015; Perron et al., 2005). In the context of symbiosis, however, the role of the stringent response regulator remains comparatively unexplored.

In *Rlv*3841, deletion of *dksA* homologues had only minor effects on free-living growth (Figure S4.5). The *dksA* triple mutant most closely resembled a *relA* mutant in overall growth pattern but neither strain exhibited a pronounced defect compared to the WT. Strikingly, despite their strong oxygen-dependent induction, deletion of *dksL1* and *dksL2* did not result in detectable phenotypes under low-oxygen free-living conditions (Figure S4.5) or during symbiosis with pea (Figure 4.6, Figure S4.6). Unexpectedly, transcriptomic analysis revealed no significant differentially expressed genes beyond the deleted loci themselves in either developing or mature nodules. This absence of global transcriptional impact argues strongly against functional redundancy with canonical DksA and suggests that DksL proteins do not substitute for DksA in regulating the symbiotic transcriptome. However, transcriptomic analysis of the triple mutant would be needed to definitively exclude functional redundancy between all homologues.

The only strong phenotype associated with loss of *dksL* genes was reduced competitiveness during nodule occupancy. This may point to a role during early infection or initial adaptation to the nodule environment. Since colonisation, infection thread formation, and early nodule development are themselves oxygen-sensitive processes, it remains possible that DksL proteins contribute to fine-tuning gene expression during these early transitions, even if their role is not apparent once symbiosis is fully established. In addition, it remains possible that, analogous to the zinc-dependent specialization described in *P. aeruginosa*, DksL proteins respond to environmental cues not yet tested, such as metal availability or redox stress.

In contrast to the minimal effects observed upon deletion of the DksL genes, loss of canonical *dksA* resulted in pronounced transcriptional alterations during symbiosis. Early nodules (12 dpi) exhibited strong but targeted induction of genes associated with nitrogen scavenging and amino acid uptake, including *amtB*, *glnK*, *glnII*, and multiple ABC transporters, including PAAT systems. A plasmid-encoded GABA uptake and catabolic cluster were the most upregulated loci. Activation of the GABA shunt is commonly associated with nitrogen or carbon limitation and may serve to replenish TCA cycle intermediates and maintain C/N balance. The coordinated induction of these pathways suggests that Δ*dksA* bacteroids adopt a transcriptional state resembling nitrogen starvation or at least metabolic imbalance during early differentiation. This phenotype

may reflect a failure to properly integrate metabolic signals in the absence of DksA, leading to inappropriate activation of nutrient acquisition systems. Alternatively, DksA may normally repress free-living metabolic programs during symbiosis, and its deletion partially reverts cells toward a free-living transcriptional state. Consistent with this line of argumentation could be the differential expression of various transcriptional regulators, which are either directly controlled by DksA or are secondary regulators trying to compensate for its loss. In either case, Δ*dksA* bacteroids appear unable to fully commit to the differentiated bacteroid program.

By 28 dpi, this transcriptional imbalance became more pronounced and shifted toward broader stress-associated reprogramming, characterised by persistent nitrogen starvation signatures alongside repression of transport and symbiotic plasmid functions and induction of chaperone systems. The downregulation of *nod* and *rhi* genes at this stage, despite their primary role in early symbiosis, likely reflects this global plasmid dysregulation rather than stage-specific regulation. Together with the concurrent repression of plasmid-encoded surface and transport functions and induction of conjugation genes, these patterns suggest a loss of coordinated control over plasmid-encoded functions. This dysregulation may be linked to increased proteotoxic or redox stress in the mutant, a hypothesis that could be tested in future work by assessing redox tolerance or sensitivity to antimicrobial nodule-specific cysteine-rich (NCR) peptides.

Despite extensive transcriptional dysregulation, nodule number and overall nitrogenase activity remained comparable to WT in pea (Figure 4.6). However, recovery of viable bacteria from nodules was substantially reduced in the Δ*dksA* mutant (Figure 4.7), indicating that DksA is dispensable for nitrogen fixation per se but required for maintaining long-term bacteroid viability. The absence of a strong fixation defect likely reflects the terminal differentiation of pea bacteroids, where bacteria do not require means for survival past their nitrogen-fixating state. In *S. meliloti*, Δ*dksA* mutants exhibit delayed nodule development (Wippel & Long, 2016). Our data suggest that such delays may result from progressive metabolic instability, which could ultimately predispose nodules to earlier senescence. Analysis of later time points would help clarify whether DksA contributes to sustained nodule longevity. Interestingly, Δ*dksA* mutants displayed increased competitiveness for nodule occupancy, a phenotype that is difficult to

interpret but may likewise point to altered regulatory states during early infection. This supports the notion, also proposed by Wippel and Long (2016), that DksA contributes to early symbiotic processes that are impaired rather than completely blocked.

An important direction for future work will therefore be to distinguish direct DksA-dependent transcriptional effects from secondary consequences of the metabolic imbalance observed here. As DksA regulates transcription through its interaction with RNA polymerase rather than by conventional sequence-specific DNA binding, approaches examining DksA or RNA polymerase occupancy, such as ChIP-seq (chromatin immunoprecipitation sequencing; Myers et al., 2015) using epitope-tagged DksA, could help identify genomic regions associated with DksA-containing transcription complexes. Candidate promoters identified from the transcriptomic analysis, particularly those associated with nitrogen scavenging and amino acid uptake, could then be tested using promoter fusions and in vitro transcription assays to determine whether their regulation is directly dependent on DksA.

Collectively, the developmental trajectory observed in *dksA* bacteroids resembles a failure to maintain metabolic homeostasis during symbiosis. Initially nutrient scavenging pathways are activated, followed by progressive stress and regulatory imbalance, suggesting progressive loss of metabolic balance. These findings clearly establish DksA as the dominant global regulator among the three paralogs and underscore its role in sustaining transcriptional stability during symbiosis.

Host-dependent requirements for DksA during symbiosis

The importance of DksA became more pronounced in the bean symbiont *Rlp*4292. In pea, where bacteroids undergo terminal differentiation, deletion of *dksA* did not result in a strong nitrogen fixation defect despite extensive transcriptional dysregulation and reduced recovery of viable bacteria from nodules. Because terminally differentiated pea bacteroids do not need to resume free-living growth, defects in long-term cellular stability may remain phenotypically masked.

In contrast to pea, bean bacteroids retain the ability to dedifferentiate and resume growth. In this context, deletion of *dksA* resulted in reduced nitrogenase activity, pale

nodules, and impaired bacterial viability. Moreover, the Δ*dksA* mutant displayed both an extended lag phase and a markedly reduced growth rate upon reinoculation into rich medium, indicating a defect in coordinating the transition from the differentiated state back to free-living growth. These findings suggest that while DksA function supports nitrogen fixation, it is essential for efficient recovery from the bacteroid state and for maintaining metabolic competence in a reversible symbiosis.

The reduced recovery of viable Δ*dksA* bacteria from bean nodules raises an important mechanistic question. It could reflect either a lower initial bacterial population within nodules or impaired survival and dedifferentiation during transition back to the free-living state, or reduced viability or recovery of the mutant during specifically the plating process. Because nodule size was not significantly reduced, one of the latter explanations appear more likely. Nevertheless, direct assessment of bacteroid viability, for example through quantification of bacterial abundance directly from nodule tissue, for example by qPCR or flow cytometry, will be required to distinguish between these possibilities.

Interestingly, deletion of *dksL2* did not reproduce the fitness effects predicted by INSeq analyses under single-strain inoculation conditions, suggesting that INSeq results may capture fitness differences that only become apparent under competitive or complex soil and rhizosphere conditions not represented in such assays, and supporting the notion that DksL proteins contribute to context-dependent fitness rather than core symbiotic functions.

Together, these results reveal a host-dependent requirement for DksA. In terminally differentiated pea bacteroids, long-term viability is largely irrelevant to symbiotic success, whereas in bean – where bacteria must survive and re-enter the free-living stage – DksA becomes critical. The contrasting phenotypes between pea and bean symbionts underscore how the functional importance of global transcriptional regulators depends on host-imposed developmental programs.

Conclusion

This study reveals a clear functional division among the three DksA homologues in *R. leguminosarum*. Canonical DksA acts as the primary global stringent-response

regulator and is required to maintain metabolic homeostasis during bacteroid differentiation. In its absence, bacteroids display a transcriptional trajectory marked by early activation of nitrogen-scavenging pathways, followed by progressive stress responses and plasmid-associated dysregulation, ultimately compromising long-term viability. Loss of DksA likely disrupts ppGpp-dependent regulation, leading to metabolic imbalance and failure to fully commit to the differentiated bacteroid program

In contrast, the two DksA-like paralogs DksL1 and DksL2 are oxygen-induced, FnrN-controlled regulators that do not substitute for canonical DksA. Despite strong microaerobic induction, their deletion caused no major transcriptomic or symbiotic defects. The absence of detectable phenotypes raises the possibility that DksL proteins play only minor or condition-specific roles that were not revealed under the experimental settings employed here.

Importantly, the requirement for DksA is host-dependent. While defects are masked in terminally differentiated pea bacteroids, DksA becomes critical in reversible bean symbiosis, where recovery from the differentiated state is required. Together, these results illustrate how duplication of a global regulator can enable functional specialization while preserving core stringent-response functions during complex lifestyle transitions.

References

Abramson, J., Adler, J., Dunger, J., Evans, R., Green, T., Pritzel, A., Ronneberger, O., Willmore, L., Ballard, A. J., Bambrick, J., Bodenstein, S. W., Evans, D. A., Hung, C.-C., O'Neill, M., Reiman, D., Tunyasuvunakool, K., Wu, Z., Žemgulytė, A., Arvaniti, E., … Jumper, J. M. (2024). Accurate structure prediction of biomolecular interactions with AlphaFold 3. *Nature*, *630*(8016), 493–500. https://doi.org/10.1038/s41586-024-07487-w

Allaway, D., Lodwig, E. M., Crompton, L. A., Wood, M., Parsons, R., Wheeler, T. R., & Poole, P. S. (2000). Identification of alanine dehydrogenase and its role in mixed secretion of ammonium and alanine by pea bacteroids. *Molecular Microbiology*, *36*(2), 508–515. https://doi.org/10.1046/j.1365-2958.2000.01884.x

Andrews, S. (2010). *FastQC: A Quality Control Tool for High Throughput Sequence Data* http://www.bioinformatics.babraham.ac.uk/projects/fastqc/

Arai, H., Roh, J. H., & Kaplan, S. (2008). Transcriptome dynamics during the transition from anaerobic photosynthesis to aerobic respiration in Rhodobacter sphaeroides 2.4.1. *Journal of Bacteriology*, *190*(1), 286–299. https://doi.org/10.1128/JB.01375-07

Barnett, M. J., Toman, C. J., Fisher, R. F., & Long, S. R. (2004). A dual-genome symbiosis chip for coordinate study of signal exchange and development in a prokaryote–host interaction. *Proceedings of the National Academy of Sciences*, *101*(47), 16636–16641. https://doi.org/10.1073/pnas.0407269101

Beringer, J. E. (1974). R factor transfer in Rhizobium leguminosarum. *Microbiology*, *84*(1), 188–198. https://doi.org/10.1099/00221287-84-1-188

Blaby-Haas, C. E., Furman, R., Rodionov, D. A., Artsimovitch, I., & De Crécy-Lagard, V. (2011). Role of a Zn-independent DksA in Zn homeostasis and stringent response: Role of a DksA homolog in Zn homeostasis. *Molecular Microbiology*, *79*(3), 700–715. https://doi.org/10.1111/j.1365-2958.2010.07475.x

Broughton, W. J., & Dilworth, M. J. (1971). Control of leghaemoglobin synthesis in snake beans. *Biochemical Journal*, *125*(4), 1075–1080. https://doi.org/10.1042/bj1251075

Calderón-Flores, A., Du Pont, G., Huerta-Saquero, A., Merchant-Larios, H., Servín-González, L., & Durán, S. (2005). The stringent response is required for amino acid and nitrate utilization, Nod factor regulation, nodulation, and nitrogen fixation in Rhizobium etli. *Journal of Bacteriology*, *187*(15), 5075–5083. https://doi.org/10.1128/JB.187.15.5075-5083.2005

Chen, M., Raisin, A., Judkins, N., Allard, P., Défossez, E., Stumpe, M., Yruela, I., Becana, M., & Reinhardt, D. (2025). Inhibition of rhizobial cheaters by the host Medicago truncatula involves repression of symbiotic functions and induction of defense. *New Phytologist*, *248*(3), 1458–1474. https://doi.org/10.1111/nph.70494

Choi, K.-H., Gaynor, J. B., White, K. G., Lopez, C., Bosio, C. M., Karkhoff-Schweizer, R. R., & Schweizer, H. P. (2005). A Tn7-based broad-range bacterial cloning and expression system. *Nature Methods*, *2*(6), 443–448. https://doi.org/10.1038/nmeth765Choi, K.-H., Mima, T., Casart, Y., Rholl, D., Kumar, A., Beacham, I. R., & Schweizer, H. P. (2008). Genetic tools for select-agent-compliant manipulation of Burkholderia pseudomalle*i*. *Applied and Environmental Microbiology*, *74*(4), 1064–1075. https://doi.org/10.1128/AEM.02430-07

Clark, L. J. (2021). *Host regulation of the legume-rhizobia symbiosis*. PhD thesis, University of Oxford.

Dalebroux, Z. D., & Swanson, M. S. (2012). ppGpp: Magic beyond RNA polymerase. *Nature Reviews Microbiology*, *10*(3), 203–212. https://doi.org/10.1038/nrmicro2720

Davies, B. W., & Walker, G. C. (2007). Identification of novel Sinorhizobium meliloti mutants compromised for oxidative stress protection and symbiosis. *Journal of Bacteriology*, *189*(5), 2110–2113. https://doi.org/10.1128/JB.01802-06

Davies, B. W., & Walker, G. C. (2008). A highly conserved protein of unknown function is required by Sinorhizobium meliloti for symbiosis and environmental stress protection. *Journal of Bacteriology*, *190*(3), 1118–1123. https://doi.org/10.1128/JB.01521-07

Ditta, G., Stanfield, S., Corbin, D., & Helinski, D. R. (1980). Broad host range DNA cloning system for gram-negative bacteria: Construction of a gene bank of Rhizobium meliloti. *Proceedings of the National Academy of Sciences*, *77*(12), 7347–7351. https://doi.org/10.1073/pnas.77.12.7347

Dixon, R., & Kahn, D. (2004). Genetic regulation of biological nitrogen fixation. *Nature Reviews Microbiology*, *2*(8), 621–631. https://doi.org/10.1038/nrmicro954

Djordjevic, M. A., Chen, H. C., Natera, S., Van Noorden, G., Menzel, C., Taylor, S., Renard, C., Geiger, O., & Weiller, G. F. (2003). A global analysis of protein expression profiles in Sinorhizobium meliloti: Discovery of new genes for nodule occupancy and stress adaptation. *Molecular Plant-Microbe Interactions®*, *16*(6), 508–524. https://doi.org/10.1094/MPMI.2003.16.6.508

Domingo-Serrano, L., Sanchis-López, C., Alejandre, C., Soldek, J., Palacios, J. M., & Albareda, M. (2025). A microaerobically induced small heat shock protein contributes to Rhizobium leguminosarum / Pisum sativum symbiosis and interacts with a wide range of bacteroid proteins. *Applied and Environmental Microbiology*, *91*(1), e01385-24. https://doi.org/10.1128/aem.01385-24

Downie, J. A. (2014). Legume nodulation. *Current Biology*, *24*(5), R184–R190. https://doi.org/10.1016/j.cub.2014.01.028

Dufour, Y. S., Kiley, P. J., & Donohue, T. J. (2010). Reconstruction of the core and extended regulons of global transcription factors. *PLoS Genetics*, *6*(7), e1001027. https://doi.org/10.1371/journal.pgen.1001027

Edgar, R. C. (2022). Muscle5: High-accuracy alignment ensembles enable unbiased assessments of sequence homology and phylogeny. *Nature Communications*, *13*(1), 6968. https://doi.org/10.1038/s41467-022-34630-w

Furman, R., Biswas, T., Danhart, E. M., Foster, M. P., Tsodikov, O. V., & Artsimovitch, I. (2013). DksA2, a zinc-independent structural analog of the transcription factor DksA. *FEBS Letters*, *587*(6), 614–619. https://doi.org/10.1016/j.febslet.2013.01.073

Glenn, A. R., Poole, P. S., & Hudman, J. F. (1980). Succinate uptake by free-living and bacteroid forms of Rhizobium leguminosarum. *Microbiology*, *119*(1), 267–271. https://doi.org/10.1099/00221287-119-1-267

Green, R. T., East, A. K., Karunakaran, R., Downie, J. A., & Poole, P. S. (2019). Transcriptomic analysis of Rhizobium leguminosarum bacteroids in determinate and indeterminate nodules. *Microbial Genomics*, *5*(2). https://doi.org/10.1099/mgen.0.000254

Haas, B. J., Chin, M., Nusbaum, C., Birren, B. W., & Livny, J. (2012). How deep is deep enough for RNA-Seq profiling of bacterial transcriptomes? *BMC Genomics*, *13*(1), 734. https://doi.org/10.1186/1471-2164-13-734

Hanahan, D. (1983). Studies on transformation of Escherichia coli with plasmids. *Journal of Molecular Biology*, *166*(4), 557–580. https://doi.org/10.1016/S0022-2836(83)80284-8

Hawkins, J. P., & Oresnik, I. J. (2022). The rhizobium-legume symbiosis: Co-opting successful stress management. *Frontiers in Plant Science*, *12*, 796045. https://doi.org/10.3389/fpls.2021.796045

Heberle, H., Meirelles, G. V., Da Silva, F. R., Telles, G. P., & Minghim, R. (2015). InteractiVenn: A web-based tool for the analysis of sets through Venn diagrams. *BMC Bioinformatics*, *16*(1), 169. https://doi.org/10.1186/s12859-015-0611-3

Herson, J., Krummenacker, M., Spaulding, A., O'Maille, P., & Karp, P. D. (2024). The Genome Explorer genome browser. *mSystems*, *9*(7), e00267-24. https://doi.org/10.1128/msystems.00267-24

Irving, S. E., Choudhury, N. R., & Corrigan, R. M. (2021). The stringent response and physiological roles of (pp)pGpp in bacteria. *Nature Reviews Microbiology*, *19*(4), 256–271. https://doi.org/10.1038/s41579-020-00470-y

Johnston, A. W. B., & Beringer, J. E. (1975). Identification of the Rhizobium strains in pea root nodules using genetic markers. *Journal of General Microbiology*, *87*(2), 343–350. https://doi.org/10.1099/00221287-87-2-343

Johnston, A. W. B., Hombrecher, G., Brewin, N. J., & Cooper, M. C. (1982). Two transmissible plasmids in Rhizobium leguminosarum strain 300. *Microbiology*, *128*(1), 85–93. https://doi.org/10.1099/00221287-128-1-85

Kaminski, P. A., Mandon, K., Arigoni, F., Desnoues, N., & Elmerich, C. (1991). Regulation of nitrogen fixation in Azorhizobium caulinodans: Identification of a fixK -like gene, a positive regulator of nifA. *Molecular Microbiology*, *5*(8), 1983–1991. https://doi.org/10.1111/j.1365-2958.1991.tb00820.x

Kang, P. J., & Craig, E. A. (1990). Identification and characterization of a new Escherichia coli gene that is a dosage-dependent suppressor of a dnaK deletion mutation. *Journal of Bacteriology*, *172*(4), 2055–2064. https://doi.org/10.1128/jb.172.4.2055-2064.1990

Karunakaran, R., Ramachandran, V. K., Seaman, J. C., East, A. K., Mouhsine, B., Mauchline, T. H., Prell, J., Skeffington, A., & Poole, P. S. (2009). Transcriptomic analysis of Rhizobium leguminosarum biovar viciae in symbiosis with host plants Pisum sativum and Vicia cracca. *Journal of Bacteriology*, *191*(12), 4002–4014. https://doi.org/10.1128/JB.00165-09

Knights, H. E., Ledermann, R., Jorrin, B., Abreu, I., Campbell, M. J., Cocker, C. R., Dolliver, J., East, A. K., Hague, K., Maurer, A.-K., Palomero-Gómez, M., Prescott, H., Terpolilli, J., Tjahjono, O., Tronca, M. N., Underwood, T. J., & Poole, P. S. (in preparation). *Mechanisms behind nodule infection and bacteroid dedifferentiation in Rhizobium leguminosarum* [Unpublished manuscript].

Knights, H. E., Ramachandran, V. K., Jorrin, B., Ledermann, R., Parsons, J. D., Aroney, S. T. N., & Poole, P. S. (2024). Rhizobium determinants of rhizosphere persistence and root colonization. *The ISME Journal*, *18*(1), wrae072. https://doi.org/10.1093/ismejo/wrae072

Krishna, S. S., Majumdar, I., & Grishin, N. V. (2003). Structural classification of zinc fingers: SURVEY AND SUMMARY. *Nucleic Acids Research*, *31*(2), 532–550. https://doi.org/10.1093/nar/gkg161

Krol, E., & Becker, A. (2011). ppGpp in Sinorhizobium meliloti: Biosynthesis in response to sudden nutritional downshifts and modulation of the transcriptome. *Molecular Microbiology*, *81*(5), 1233–1254. https://doi.org/10.1111/j.1365-2958.2011.07752.x

Langmead, B., & Salzberg, S. L. (2012). Fast gapped-read alignment with Bowtie 2. *Nature Methods*, *9*(4), 357–359. https://doi.org/10.1038/nmeth.1923

Ledermann, R. (2017). *Role of general stress response in trehalose biosynthesis for functional rhizobia-legume symbiosis*. PhD thesis, ETH Zurich. https://doi.org/10.3929/ETHZ-B-000202317

Ledermann, R., Schulte, C. C. M., & Poole, P. S. (2021). How rhizobia adapt to the nodule environment. *Journal of Bacteriology*, *203*(12). https://doi.org/10.1128/JB.00539-20

Ledermann, R., Strebel, S., Kampik, C., & Fischer, H.-M. (2016). Versatile vectors for efficient mutagenesis of Bradyrhizobium diazoefficiens and other alphaproteobacteria. *Applied and Environmental Microbiology*, *82*(9), 2791–2799. https://doi.org/10.1128/AEM.04085-15

Lee, J.-H., Lennon, C. W., Ross, W., & Gourse, R. L. (2012). Role of the coiled-coil tip of Escherichia coli DksA in promoter control. *Journal of Molecular Biology*, *416*(4), 503–517. https://doi.org/10.1016/j.jmb.2011.12.028

Lennon, C. W., Lemmer, K. C., Irons, J. L., Sellman, M. I., Donohue, T. J., Gourse, R. L., & Ross, W. (2014). A Rhodobacter sphaeroides protein mechanistically similar to Escherichia coli DksA regulates photosynthetic growth. *mBio*, *5*(3), e01105-14. https://doi.org/10.1128/mBio.01105-14

Love, M. I., Huber, W., & Anders, S. (2014). Moderated estimation of fold change and dispersion for RNA-seq data with DESeq2. *Genome Biology*, *15*(12), 550. https://doi.org/10.1186/s13059-014-0550-8

Magoc, T., Wood, D., & Salzberg', S. L. (2013). EDGE-pro: Estimated degree of gene expression in prokaryotic genomes. *Evolutionary Bioinformatics*, *9*, EBO.S11250. https://doi.org/10.4137/EBO.S11250

Masson-Boivin, C., Giraud, E., Perret, X., & Batut, J. (2009). Establishing nitrogen-fixing symbiosis with legumes: How many rhizobium recipes? *Trends in Microbiology*, *17*(10), 458–466. https://doi.org/10.1016/j.tim.2009.07.004

Mergaert, P., Uchiumi, T., Alunni, B., Evanno, G., Cheron, A., Catrice, O., Mausset, A.-E., Barloy-Hubler, F., Galibert, F., Kondorosi, A., & Kondorosi, E. (2006). Eukaryotic control on bacterial cell cycle and differentiation in the Rhizobium –legume symbiosis. *Proceedings of the National Academy of Sciences*, *103*(13), 5230–5235. https://doi.org/10.1073/pnas.0600912103

Miller, J. H. (1972). *Experiments in Molecular Genetics*. Cold Spring Harbor Laboratory Press.

Mittenhuber, G. (2001). Comparative genomics and evolution of genes encoding bacterial (p)ppGpp synthetases/hydrolases (the Rel, RelA and SpoT proteins). *Journal of Molecular Microbiology and Biotechnology*, *3*(4), 585–600.

Montiel, J., Downie, J. A., Farkas, A., Bihari, P., Herczeg, R., Bálint, B., Mergaert, P., Kereszt, A., & Kondorosi, É. (2017). Morphotype of bacteroids in different legumes correlates with the number and type of symbiotic NCR peptides. *Proceedings of the National Academy of Sciences*, *114*(19), 5041–5046. https://doi.org/10.1073/pnas.1704217114

Moris, M., Braeken, K., Schoeters, E., Verreth, C., Beullens, S., Vanderleyden, J., & Michiels, J. (2005). Effective Symbiosis between Rhizobium etli and Phaseolus vulgaris requires the

alarmone ppGpp. *Journal of Bacteriology*, *187*(15), 5460–5469. https://doi.org/10.1128/JB.187.15.5460-5469.2005

Myers, K. S., Park, D. M., Beauchene, N. A., & Kiley, P. J. (2015). Defining bacterial regulons using ChIP-seq. *Methods*, *86*, 80-88.

Nyström, T. (2004). Stationary-phase physiology. *Annual Review of Microbiology*, *58*(1), 161–181. https://doi.org/10.1146/annurev.micro.58.030603.123818

Oke, V., Rushing, B. G., Fisher, E. J., Moghadam-Tabrizi, M., & Long, S. R. (2001). Identification of the heat-shock sigma factor RpoH and a second RpoH-like protein in Sinorhizobium meliloti. *Microbiology*, *147*(9), 2399–2408. https://doi.org/10.1099/00221287-147-9-2399

Oldroyd, G. E. D., Murray, J. D., Poole, P. S., & Downie, J. A. (2011). The rules of engagement in the legume-rhizobial symbiosis. *Annual Review of Genetics*, *45*(1), 119–144. https://doi.org/10.1146/annurev-genet-110410-132549

Pardo Díaz, J. (2022). *Construction of gene coexpression networks and transcriptomic analysis for Rhizobium leguminosarum*. PhD thesis, University of Oxford.

Parshin, A., Shiver, A. L., Lee, J., Ozerova, M., Schneidman-Duhovny, D., Gross, C. A., & Borukhov, S. (2015). DksA regulates RNA polymerase in Escherichia coli through a network of interactions in the secondary channel that includes Sequence Insertion 1. *Proceedings of the National Academy of Sciences*, *112*(50). https://doi.org/10.1073/pnas.1521365112

Parsons, J. (2019). *Characterising root attachment in Rhizobium-legume symbioses*. PhD thesis, University of Oxford.

Paul, B. J., Barker, M. M., Ross, W., Schneider, D. A., Webb, C., Foster, J. W., & Gourse, R. L. (2004). DksA: A critical component of the transcription initiation machinery that potentiates the regulation of rRNA Promoters by ppGpp and the initiating NTP. *Cell*, *118*(3), 311–322. https://doi.org/10.1016/j.cell.2004.07.009

Paul, B. J., Berkmen, M. B., & Gourse, R. L. (2005). DksA potentiates direct activation of amino acid promoters by ppGpp. *Proceedings of the National Academy of Sciences*, *102*(22), 7823–7828. https://doi.org/10.1073/pnas.0501170102

Perederina, A., Svetlov, V., Vassylyeva, M. N., Tahirov, T. H., Yokoyama, S., Artsimovitch, I., & Vassylyev, D. G. (2004). Regulation through the secondary channel—Structural framework for ppGpp-DksA synergism during transcription. *Cell*, *118*(3), 297–309. https://doi.org/10.1016/j.cell.2004.06.030

Perron, K., Comte, R., & Van Delden, C. (2005). DksA represses ribosomal gene transcription in *Pseudomonas aeruginosa* by interacting with RNA polymerase on ribosomal

promoters. *Molecular Microbiology*, *56*(4), 1087–1102. https://doi.org/10.1111/j.1365-2958.2005.04597.x

Pini, F., East, A. K., Appia-Ayme, C., Tomek, J., Karunakaran, R., Mendoza-Suárez, M., Edwards, A., Terpolilli, J. J., Roworth, J., Downie, J. A., & Poole, P. S. (2017). Bacterial biosensors for in vivo spatiotemporal mapping of root secretion. *Plant Physiology*, *174*(3), 1289–1306. https://doi.org/10.1104/pp.16.01302

Poole, P., Ramachandran, V., & Terpolilli, J. (2018). Rhizobia: From saprophytes to endosymbionts. *Nature Reviews Microbiology*, *16*(5), 291–303. https://doi.org/10.1038/nrmicro.2017.171

Poole, P. S., Blyth, A., Reid, C. J., & Walters, K. (1994). Myo-inositol catabolism and catabolite regulation in Rhizobium leguminosarum bv. viciae. *Microbiology*, *140*(10), 2787–2795. https://doi.org/10.1099/00221287-140-10-2787

Quandt, J., & Hynes, M. F. (1993). Versatile suicide vectors which allow direct selection for gene replacement in gram-negative bacteria. *Gene*, *127*(1), 15–21. https://doi.org/10.1016/0378-1119(93)90611-6

R Core Team. (2025). *R: A language and environment for statistical computing*. R Foundation for Statistical Computing. https://www.R-project.org/

Ronneau, S., & Hallez, R. (2019). Make and break the alarmone: Regulation of (p)ppGpp synthetase/hydrolase enzymes in bacteria. *FEMS Microbiology Reviews*, *43*(4), 389–400. https://doi.org/10.1093/femsre/fuz009

Rutten, P. J., & Poole, P. S. (2019). Oxygen regulatory mechanisms of nitrogen fixation in rhizobia. In *Advances in Microbial Physiology* (Vol. 75, pp. 325–389). Elsevier. https://doi.org/10.1016/bs.ampbs.2019.08.001

Rutten, P. J., Steel, H., Hood, G. A., Ramachandran, V. K., McMurtry, L., Geddes, B., Papachristodoulou, A., & Poole, P. S. (2021). Multiple sensors provide spatiotemporal oxygen regulation of gene expression in a Rhizobium-legume symbiosis. *PLOS Genetics*, *17*(2), e1009099. https://doi.org/10.1371/journal.pgen.1009099

Sambrook, J., Fritsch, E. F., Maniatis, T., Russell, D. W., & Green, M. R. (1989). *Molecular cloning: A laboratory manual*. Cold Spring Harbor Laboratory Press.

Sánchez-Cañizares, C., & Palacios, J. (2013). Construction of a marker system for the evaluation of competitiveness for legume nodulation in Rhizobium strains. *Journal of Microbiological Methods*, *92*(3), 246–249. https://doi.org/10.1016/j.mimet.2012.12.022

Schäfer, A., Tauch, A., Jäger, W., Kalinowski, J., Thierbach, G., & Pühler, A. (1994). Small mobilizable multi-purpose cloning vectors derived from the Escherichia coli plasmids pK18 and pK19: Selection of defined deletions in the chromosome of Corynebacterium glutamicum. *Gene*, *145*(1), 69–73. https://doi.org/10.1016/0378-1119(94)90324-7

Schlüter, A., Patschkowski, T., Unden, G., & Priefer, U. B. (1992). The Rhizobium leguminosarum FnrN protein is functionally similar to Escherichia coli Fnr and promotes heterologous oxygen-dependent activation of transcription. *Molecular Microbiology*, *6*(22), 3395–3404. https://doi.org/10.1111/j.1365-2958.1992.tb02207.x

Schwartzman, J. A., & Ruby, E. G. (2016). Stress as a normal cue in the symbiotic environment. *Trends in Microbiology*, *24*(5), 414–424. https://doi.org/10.1016/j.tim.2016.02.012

Sessitsch, A., Wilson, K. J., Akkermans, A. D., & De Vos, W. M. (1996). Simultaneous detection of different Rhizobium strains marked with either the Escherichia coli gusA gene or the Pyrococcus furiosus celB gene. *Applied and Environmental Microbiology*, *62*(11), 4191–4194. https://doi.org/10.1128/aem.62.11.4191-4194.1996

Stamatakis, A. (2014). RAxML version 8: A tool for phylogenetic analysis and post-analysis of large phylogenies. *Bioinformatics*, *30*(9), 1312–1313. https://doi.org/10.1093/bioinformatics/btu033

Tehranchi, A. K., Blankschien, M. D., Zhang, Y., Halliday, J. A., Srivatsan, A., Peng, J., Herman, C., & Wang, J. D. (2010). The transcription factor DksA prevents conflicts between DNA replication and transcription machinery. *Cell*, *141*(4), 595–605. https://doi.org/10.1016/j.cell.2010.03.036

Thoma, S., & Schobert, M. (2009). An improved Escherichia coli donor strain for diparental mating. *FEMS Microbiology Letters*, *294*(2), 127–132. https://doi.org/10.1111/j.1574-6968.2009.01556.x

Tjahjono, O. (2025). *Regulation of global metabolism by PTS-NTR in Rhizobium leguminosarum*. PhD thesis, University of Oxford.

Trautinger, B. W., Jaktaji, R. P., Rusakova, E., & Lloyd, R. G. (2005). RNA Polymerase modulators and DNA repair activities resolve conflicts between DNA replication and transcription. *Molecular Cell*, *19*(2), 247–258. https://doi.org/10.1016/j.molcel.2005.06.004

Wells, D. H., & Long, S. R. (2002). The Sinorhizobium meliloti stringent response affects multiple aspects of symbiosis. *Molecular Microbiology*, *43*(5), 1115–1127. https://doi.org/10.1046/j.1365-2958.2002.02826.x

Wendrich, T. M., Blaha, G., Wilson, D. N., Marahiel, M. A., & Nierhaus, K. H. (2002). Dissection of the mechanism for the stringent factor RelA. *Molecular Cell*, *10*(4), 779–788. https://doi.org/10.1016/S1097-2765(02)00656-1

Wheatley, R. M., Ford, B. L., Li, L., Aroney, S. T. N., Knights, H. E., Ledermann, R., East, A. K., Ramachandran, V. K., & Poole, P. S. (2020). Lifestyle adaptations of Rhizobium from rhizosphere to symbiosis. *Proceedings of the National Academy of Sciences*, *117*(38), 23823–23834. https://doi.org/10.1073/pnas.2009094117

Wheatley, R. M., Ramachandran, V. K., Geddes, B. A., Perry, B. J., Yost, C. K., & Poole, P. S. (2017). Role of O_2 in the growth of Rhizobium leguminosarum bv. viciae 3841 on glucose and succinate. *Journal of Bacteriology*, *199*(1). https://doi.org/10.1128/JB.00572-16

Wippel, K., & Long, S. R. (2016). Contributions of Sinorhizobium meliloti transcriptional regulator DksA to bacterial growth and efficient symbiosis with Medicago sativa. *Journal of Bacteriology*, *198*(9), 1374–1383. https://doi.org/10.1128/JB.00013-16

Young, J. P. W., Crossman, L. C., Johnston, A. W., Thomson, N. R., Ghazoui, Z. F., Hull, K. H., Wexler, M., Curson, A. R., Todd, J. D., Poole, P. S., Mauchline, T. H., East, A. K., Quail, M. A., Churcher, C., Arrowsmith, C., Cherevach, I., Chillingworth, T., Clarke, K., Cronin, A., … Parkhill, J. (2006). The genome of Rhizobium leguminosarum has recognizable core and accessory components. *Genome Biology*, *7*(4), R34. https://doi.org/10.1186/gb-2006-7-4-r34

Zhang, Y., Mooney, R. A., Grass, J. A., Sivaramakrishnan, P., Herman, C., Landick, R., & Wang, J. D. (2014). DksA guards elongating RNA Polymerase against ribosome-stalling-induced arrest. *Molecular Cell*, *53*(5), 766–778. https://doi.org/10.1016/j.molcel.2014.02.005

Supplementary Information

Table S4.1 Primers used in this work.

Primer	Sequence 5' → 3'	Description
oxp5245	GCTGCAGGAATTCCTCGAGA TAGACTGAGGTAATCATGGTC	FW and RV amplification primer for *gusA* for HiFi assembly of pOPS1850
oxp5246	GCAAGGCCTTCGCGAGGTAC TCATTGTTTGCCTCCCTG	
oxp5247	TTCGATCATGCATGAGCTCAG TTAGGTCCGAGCTCGGC	FW and RV amplification primer for *Rlv*3841 P_{dksL1} for HiFi assembly of pOPS1851
oxp5248	TATCTCGAGGAATTCCTGCAC CTAACCAATGCTGGCCC	
oxp5249	TATCTCGAGGAATTCCTGCATG CTTTGGTGGGAATTTC	FW and RV amplification primer for *Rlv*3841 P_{dksL2} for HiFi assembly of pOPS1852
oxp5250	TTCGATCATGCATGAGCTCACT CATGTCACATTGACGG	
oxp5251	TTCGATCATGCATGAGCTCAAT CCAGCGGGCCTTTTCAG	FW and RV amplification primer for *Rlv*3841 P_{dksA} for HiFi assembly of pOPS1853
oxp5252	TATCTCGAGGAATTCCTGCATC TCATCTGGCGGGGTGTATATC	
oxp5253	TTCGATCATGCATGAGCTCAA CCAGATGTCGGAAGAAG	FW and RV amplification primer for *Rlv*3841 P_{relA} for HiFi assembly of pOPS1854
oxp5254	TATCTCGAGGAATTCCTGCAA TAAAAATAAAAGCGCGCC	
oxp5767	ATTCGAGCTCGGTACCCGGGA TAGGCCCTTTGGGGACC	FW and RV for amplicon upstream of *Rlv*3841 *dksL1*, for cloning into pK18mobSacB and markerless mutant generation
oxp5768	ATTTACTAGTGCTTTTGTTCATT TTAGTGCCTTC	
oxp5769	GAACAAAAGCACTAGTAAATC GTTCCGCTGAGAC	FW and RV for amplicon downstream of *Rlv*3841 *dksL1*, for cloning into pK18mobSacB and markerless mutant generation
oxp5770	TAAAACGACGGCCAGTGCCA TCCACGAGCCTGACTATTC	
oxp5771	ATTCGAGCTCGGTACCCGGG GCGGAAGCATCGAAATCG	FW and RV for amplicon upstream of *Rlv*3841 *dksA*, for cloning into pK18mobSacB and markerless mutant generation
oxp5772	CGCGATAGACACTAGTCTTC TCACTCAACGCGATTC	
oxp5773	GAAGACTAGTGTCTATCGCG ACGAATGAG	FW and RV for amplicon downstream of *Rlv*3841 *dksA*, for cloning into pK18mobSacB and markerless mutant generation
oxp5774	TAAAACGACGGCCAGTGCC ACTGGTGGACTTCCGAACG	
oxp5807	ATTCGAGCTCGGTACCCGG GCTCGAATGTATCGCGGAC	FW and RV for amplicon upstream of *Rlv*3841 *dksL2*, for cloning into pK18mobSacB and markerless mutant generation
oxp5808	ACTGACAGAAACTAGTCTG CTTCTGCATGATCGC	

oxp5809	GCAGACTAGTTTCTGTCAG TCTTGCGCTC	FW and RV for amplicon downstream of *Rlv*3841 *dksL2*, for cloning into pK18mobSacB and markerless mutant generation
oxp5810	TAAAACGACGGCCAGTGC CATCGATTTGCAATGGGCTG	
oxp5866	ACCTTGCCCGTCGTCTCG	FW and RV mapping primers for *Rlv*3841 *dksL1* mutagenesis – negative control
oxp5867	GCAGAACGGCGTATAGGGG	
oxp5868	TCCGCACATCCCCAACGC	FW and RV mapping primers for *Rlv*3841 *dksL2* mutagenesis – positive control
oxp5869	GCTGGCACGCTCTATCCGG	
oxp5870	CGAGCTAGAAACCCGCCTGC	FW and RV mapping primer for *Rlv*3841 *dksL2* mutagenesis – negative control
oxp5871	GTCAAGCCTCCTCTCGCCG	
oxp5924	GTACCCGTAGCGGTCACG	FW and RV mapping primer for *Rlv*3841 *dksL1* mutagenesis – positive control
oxp5925	CGACCAGGAACCAGAGCG	
oxp5874	TCATGAACGTAAACCAGCGCG	FW and RV mapping primers for *Rlv*3841 *dksA* mutagenesis – negative control
oxp5875	GCTCCTGCGCTTCGATCG	
oxp5927	AGGCGCTAATCCGGTTGG	FW and RV mapping primers for *Rlv*3841 *dksA* mutagenesis – positive control
oxp5873	CTCAGCTCTTCCGCCGCC	
oxp7502	ATTCGAGCTCGGTACCCGGGC GGCGGAAGCATCGTAATC	FW and RV for amplicon upstream of *Rlp*4292 *dksA*, for cloning into pK18mobSacB and markerless mutant generation
oxp7503	CGTCGCGATAACTAGTGATCTT CTCACTCAACGCG	
oxp7504	GATCACTAGTTATCGCGACGAA TGAGAGTTTTCATG	FW and RV for amplicon downstream of *Rlp*4292 *dksA*, for cloning into pK18mobSacB and markerless mutant generation
oxp7505	TAAAACGACGGCCAGTGCCAAA GACAGCTCCCCAGCCTTG	
oxp7506	ATTCGAGCTCGGTACCCGGGCT TTGGAGACCGGCATCG	FW and RV for amplicon upstream of *Rlp*4292 *dksL1*, for cloning into pK18mobSacB and markerless mutant generation
oxp7507	ATTTACTAGTTGAGCTTCTAATCA TTTTAGTGCC	
oxp7508	TAGAAGCTCAACTAGTAAATCGT TCCGCTGAGGC	FW and RV for amplicon downstream of *Rlp*4292 *dksL1*, for cloning into pK18mobSacB and markerless mutant generation
oxp7509	TAAAACGACGGCCAGTGCCATC CACGAGTCTGACTATTCC	
oxp7510	ATTCGAGCTCGGTACCCGGGTG CCTCTATTGCACGAGAC	FW and RV for amplicon upstream of *Rlp*4292 *dksL2*, for cloning into pK18mobSacB and markerless mutant generation
oxp7511	ACGAACTAGTGGACTGCTTCTG CATGATC	
oxp7512	GAAGCAGTCCACTAGTTCGTTT GAAGCCTGAGTTG	FW and RV for amplicon downstream of *Rlp*4292 *dksL2*, for cloning into pK18mobSacB and markerless mutant generation
oxp7513	TAAAACGACGGCCAGTGCCAA TCAACCAGGGCCTCTTC	

oxp7516	CTCGCAATATAGGGAGGGCG	FW and RV mapping primers for *Rlp*4292 *dksA* mutagenesis – positive control
oxp7517	TCTTGGTGGACTTCCGAACG	
oxp7514	AACGTAAACCAGCGTGCCTA	FW and RV mapping primers for *Rlp*4292 *dksA* mutagenesis – negative control
oxp7515	TCGCCAGTTTCCTCGCAATA	
oxp7520	ACGCTGCCAATCCTACGAAA	FW and RV mapping primers for *Rlp*4292 *dksL1* mutagenesis – positive control
oxp7521	CAGGAACCAGACCGAGAACC	
oxp7518	GTCGCGCTAGAGAAGGACAG	FW and RV mapping primers for *Rlp*4292 *dksL1* mutagenesis – negative control
oxp7519	ATCGATGCAGAACGGCGTAT	
oxp7524	GCGAACGCCATGGTTGAATT	FW and RV mapping primers for *Rlp*4292 *dksL2* mutagenesis – positive control
oxp7525	CGCTCTTCCTCGACGAGATC	
oxp7522	CCTGCAAGCGATCGAGAATG	FW and RV mapping primers for *Rlp*4292 *dksL2* mutagenesis – negative control
oxp7523	TGACAGAAAGGTGTGTGGGG	

*Rlv*3841: *Rhizobium leguminosarum* bv. *viciae* 3841; *Rlp*4292: *Rhizobium leguminosarum* bv. *phaseoli* 4292; FW: forward; RV: reverse

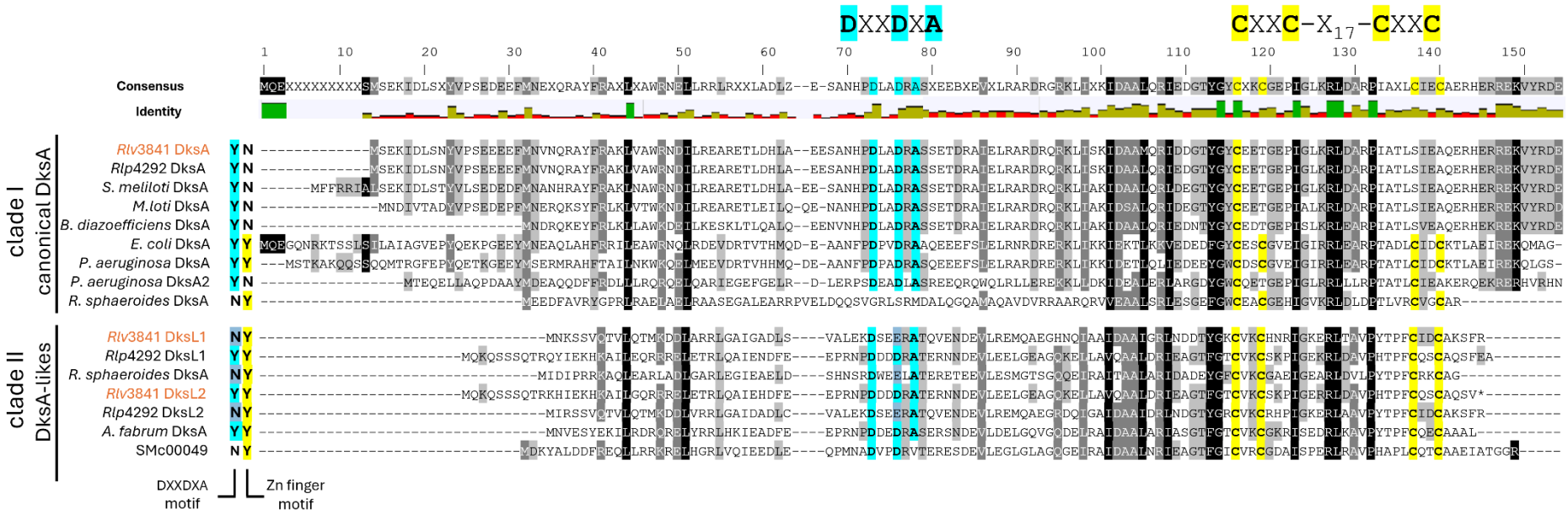


Figure S4.1 Multiple sequence alignment of DksA and DksA-like (DksL) proteins. Amino acid alignment of representative DksA homologues from α- and γ-proteobacteria, grouped according to the two phylogenetic clades defined in Figure 4.1. Clade I comprises canonical DksA proteins, whereas Clade II contains DksL homologues. BLOSUM62-based amino acid similarity is indicated by shading: black, 100%; dark grey, 80–<100%; light grey, 60–<80%; and white, <60% similarity. The conserved coiled-coil tip motif (DXXDXA) is highlighted in blue, which is retained in most homologues. The Cys_4 zinc-finger motif (CXXC–X_{17}–CXXC) is highlighted in yellow. Conservation within this region varies across homologues: all DksA-like proteins retain a complete Cys_4 motif, whereas several members of Clade I lack one or more of the conserved cysteine residues. Presence/absence of both motifs is indicated next to each sequence name (Y = present; N= absent). The three *Rlv*3841 homologues are highlighted in orange for reference.

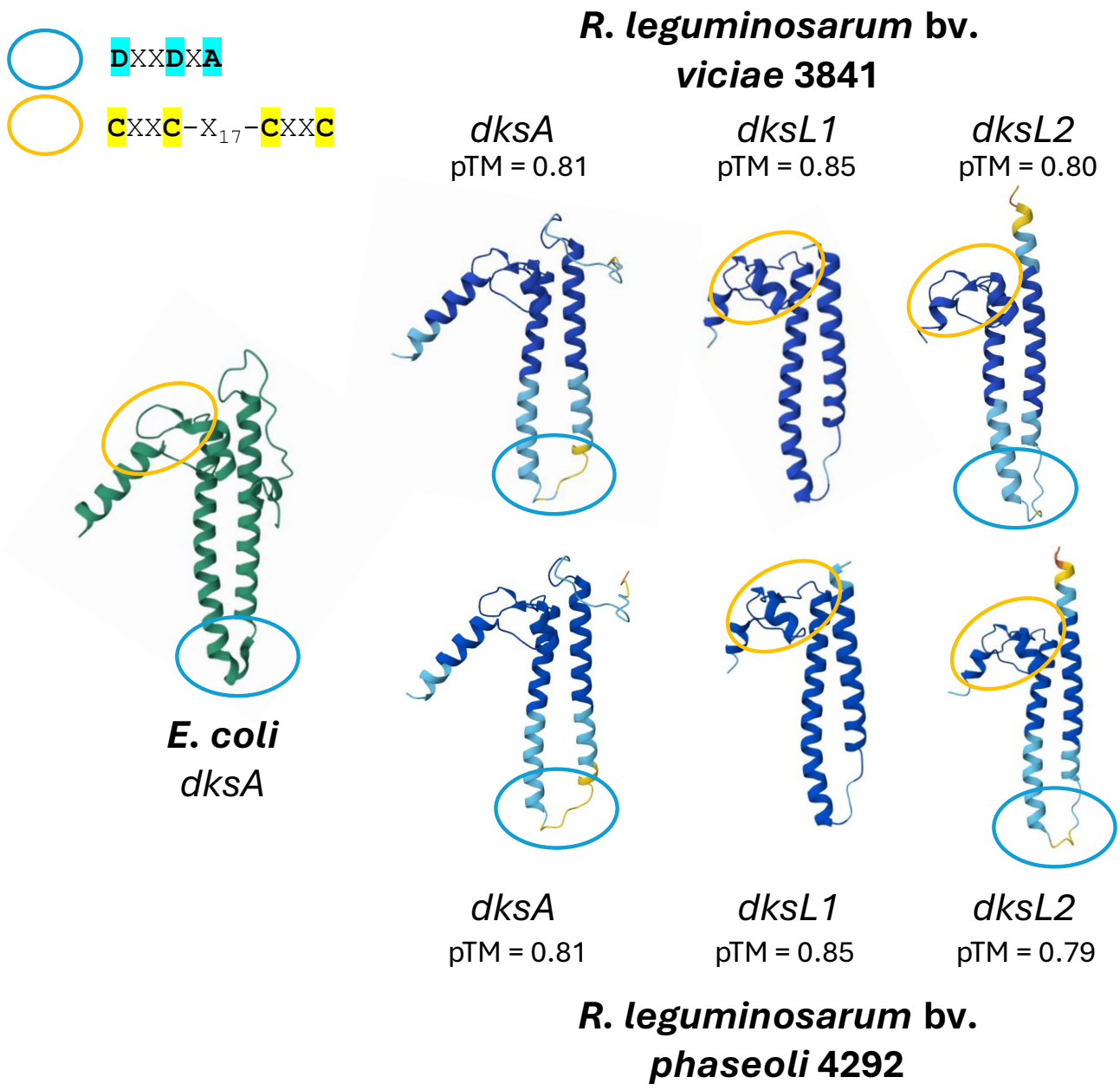


Figure S4.2 Protein structures of the *E. coli* DksA and the three DksA homologues from *Rlv*3841 and *Rlp*4292. The *E. coli* DksA structure was determined by X-ray crystallography (Perederina et al., 2004; PDB ID: 1TJL), while all other structures were predicted using AlphaFold3 (Abramson et al., 2024). The pTM (predicted template modelling) score, reflecting confidence in the overall fold and domain organization, is reported; pTM > 0.5 are generally indicative of a correct global topology. Residues are coloured by pLDDT (predicted Local Distance Difference Test) confidence score: dark blue (>90, very high confidence), light blue (70–90, high confidence), yellow (50–70, low confidence), and orange/red (<50, very low confidence). Presence of the conserved DXXDXA motif and complete Zn finger motif are indicated with blue and yellow ellipses, respectively.

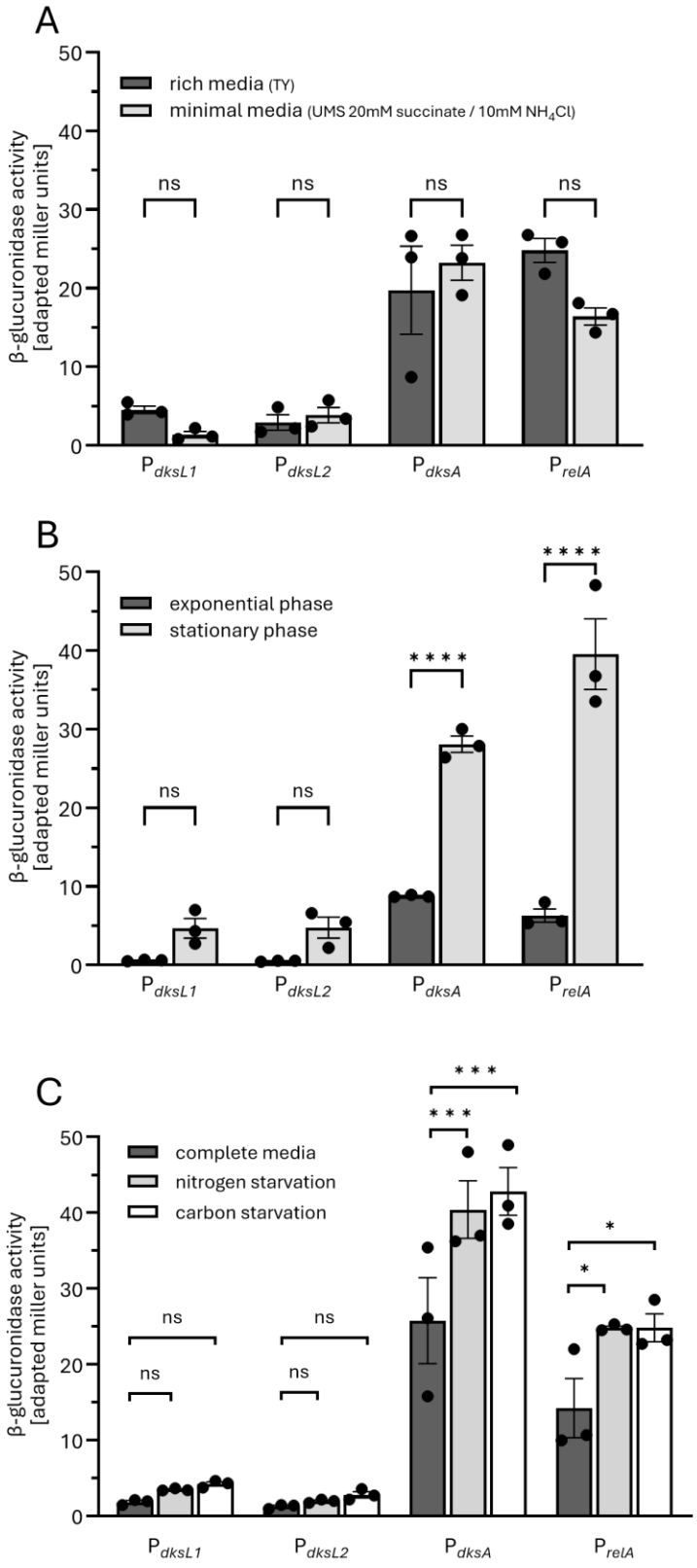


Figure S4.3 Expression of *dksA* homologues and *relA* under different non-inducing conditions. Promoter fusions of the respective genes to *gusA* were conjugated into *Rlv*3841 WT and assayed after free-living cultures were grown in their respective test condition for at least 12h. **(A)** β-Glucuronidase activities in cells grown in rich media (TY, dark bars) and minimal medium (UMS, light bars). **(B)** β-Glucuronidase activities in cells grown in complete UMS for 12h (exponential phase, dark bars) or 36h (stationary phase, light bars). **(C)** β-Glucuronidase activities in cells grown in complete media (UMS 20 mM succinate / 10 mM NH_4Cl; filled bars), in UMS without ammonia (grey bars) or in UMS without succinate (open bars). Bars represent mean ± SEM from three biological replicates. Statistical significance reflects Sidak-corrected comparisons between growth conditions for each reporter following a two-way ANOVA, where ns not significant, **** $p < 0.0001$, *** $p < 0.001$, * $p < 0.05$.

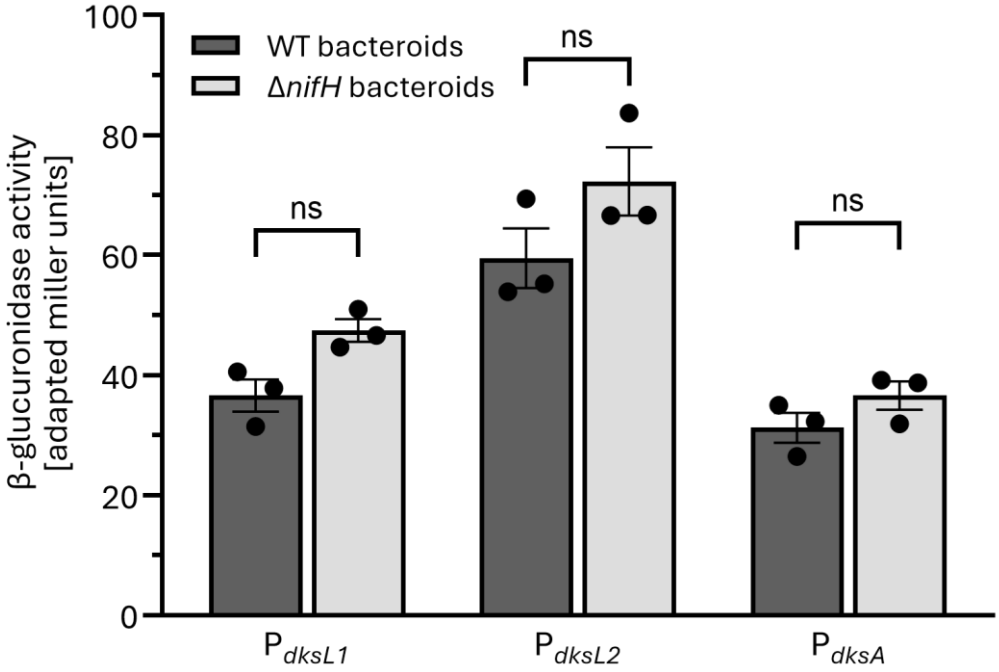


Figure S4.4 In bacteroids, induction of *dksL1* and *dksL2* is independent of fixation ability. *Rlv*3841 WT (dark bars) or *nifH* mutant (RU3940, light bars) strains with integrated promoter-gusA fusions were inoculated on pea plants and isolated from nodules at 21 dpi using a differential spin protocol and assayed for their β-glucuronidase activities. Bars represent mean ± SEM from three biological replicates with statistical significance reflecting Sidak-corrected comparisons between genotypes for each reporter following a two-way ANOVA, with ns = not significant.

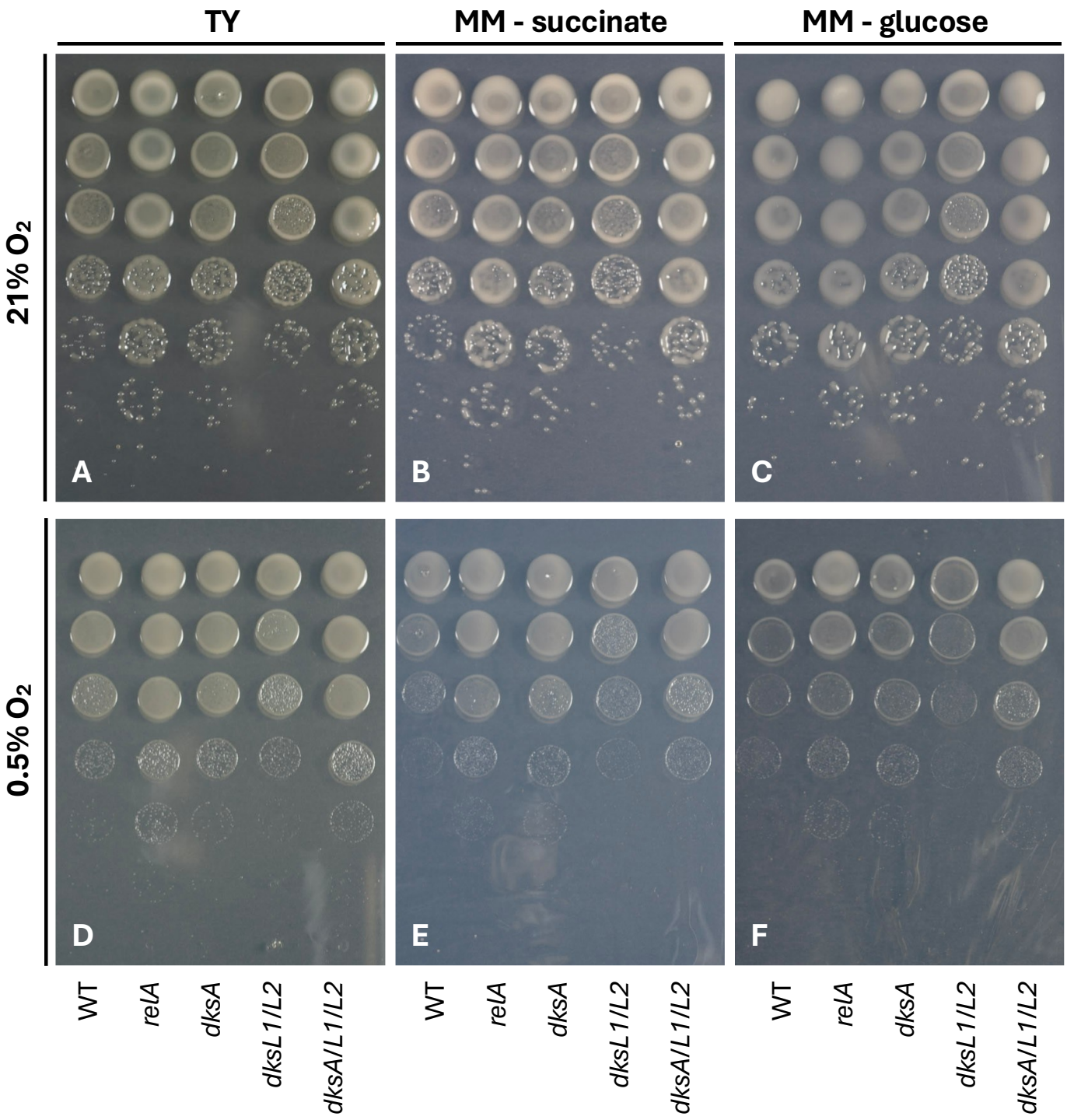


Figure S4.5 Effects of *dksA* homologue deletions on free-living growth of *R. leguminosarum* bv. *viciae* (*Rlv*) 3841 under normoxic and microoxic conditions. 10 µL of serial tenfold dilutions (starting from OD595 = 0.1) of *Rlv* wild type (WT), *relA*::ΩSpc [OPS1097], Δ*dksA* [OPS3365], Δ*dksL1* Δ*dksL2* [OPS3367], and Δ*dksA*::*aacC1* Δ*dksL1* Δ*dksL2* [OPS4310] were spotted onto TY rich medium **(A,D)** or UMS minimal medium (MM) supplemented with 10 mM NH_4Cl as the nitrogen source and either 20 mM succinate **(B,E)** or 10 mM glucose **(C,F)** as the carbon source. Plates were incubated at 21% O_2 for 3 days **(A-C)** or at 0.5% O_2 for for 5 days **(D-F)**.

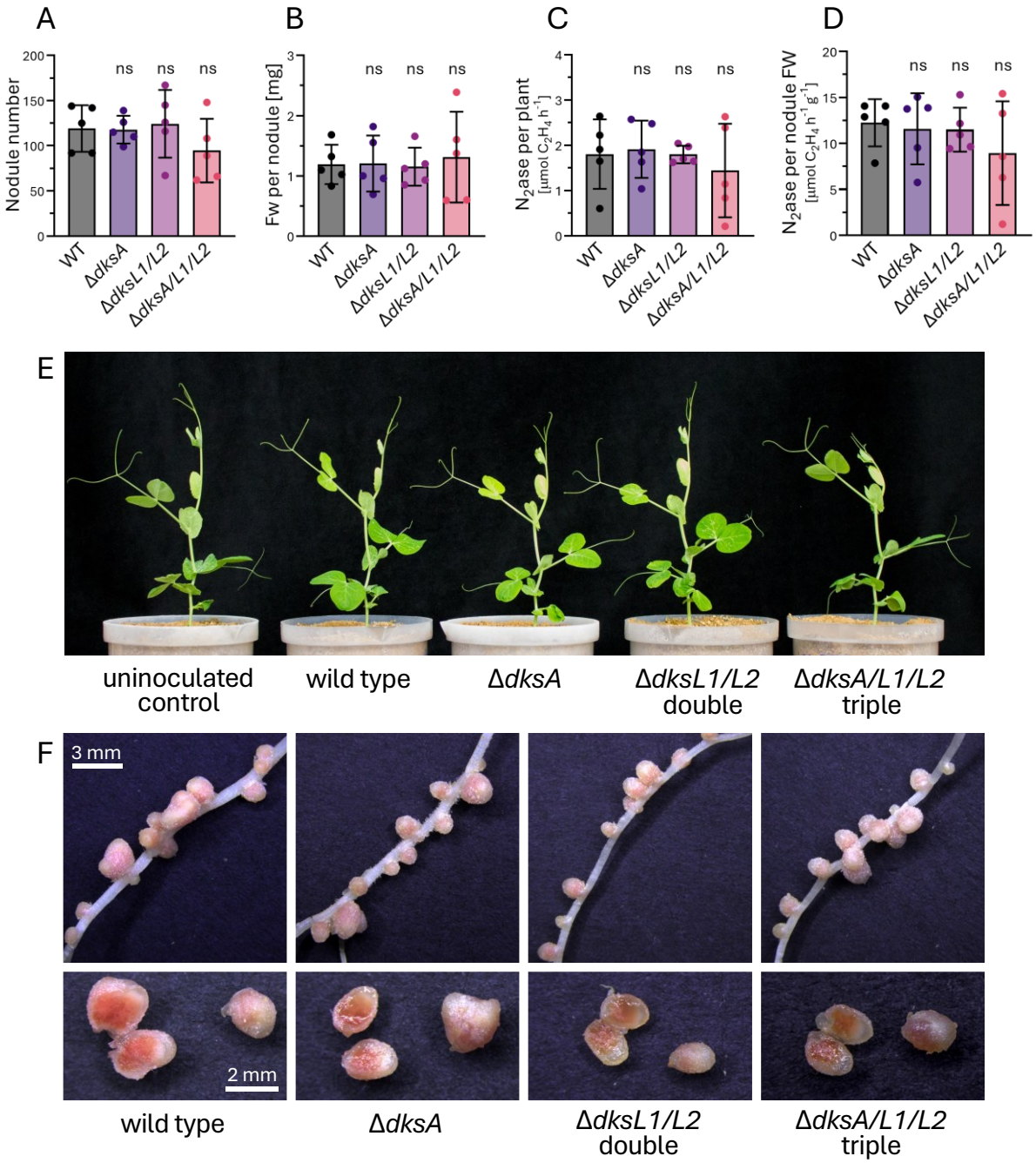


Figure S4.6 Deletion of *dksA* homologues does not affect nodulation or fixation in young peas. *Pisum sativum* cv. Avola seedlings were inoculated with *Rlv*3841 wild type (WT), a Δ*dksA* single mutant, a Δ*dksL1* Δ*dksL2* double mutant, or a Δ*dksA*::*aacC1* Δ*dksL1* Δ*dksL2* triple mutant and grown for 12 dpi. Plants were assayed for nodule number **(A)**, fresh weight (FW) per nodule **(B)**, nitrogenase activity per plant **(C)**, and nitrogenase activity per nodule FW **(D)**. Representative plants **(E)** as well as nodules and nodule cross sections **(F)** are shown for the indicated strains. Scale bars in (F) apply per row. Each strain was tested on n = 5 plants, with bars representing mean ± SD. Statistical analysis was performed using one-way ANOVA followed by Dunnett's multiple comparisons test versus WT ($\alpha \leq 0.05$), with ns, not significant.

Table S4.2 Overview of RNA sequencing output.

timepoint	inoculum strain	biol. rep.	total paired reads	alignment rate*
12 dpi	**WT**	1	45,198,683	36.96%
		2	41,069,441	27.33%
		3	39,028,522	19.60%
	Δ*dksA*	1	41,947,804	42.17%
		2	44,649,056	27.40%
		3	42,487,420	41.33%
	Δ*dksL1* Δ*dksL2*	1	47,286,475	28.53%
		2	37,768,783	31.64%
		3	41,183,176	30.58%
28 dpi	**WT**	1	52,216,865	56.91%
		2	39,007,986	48.79%
		3	41,095,873	42.36%
	Δ*dksA*	1	41,590,833	55.22%
		2	43,634,004	55.14%
		3	46,781,216	53.66%
	Δ*dksL1* Δ*dksL2*	1	40,029,301	36.86%
		2	38,027,380	48.21%
		3	39,729,811	56.74%

* = % of total reads aligned to *Rlv*3841 genome

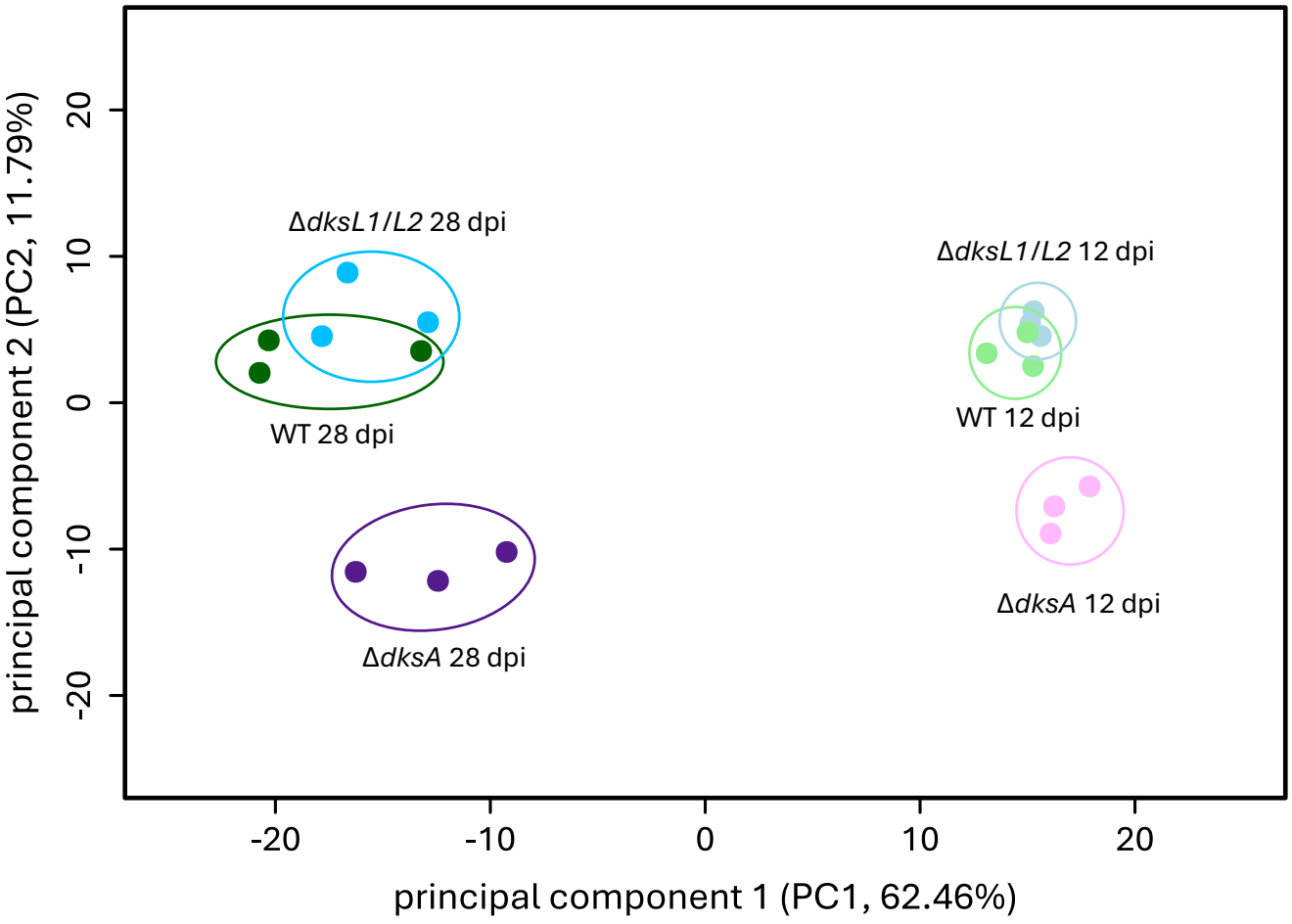


Figure S4.7 Principal component analysis (PCA) of bacteroid transcriptome samples across genotypes and timepoints. PCA was performed on regularized log (rlog)-transformed counts computed with DESeq2 to assess global transcriptional differences among samples. The first two principal components are shown, with PC1 explaining 62.46% of the total variance and PC2 explaining 11.79%. Each point represents an individual biological replicate. Samples cluster according to genotype (WT, Δ*dksA*, Δ*dksL1/L2*) and time post-inoculation (12 dpi and 28 dpi).

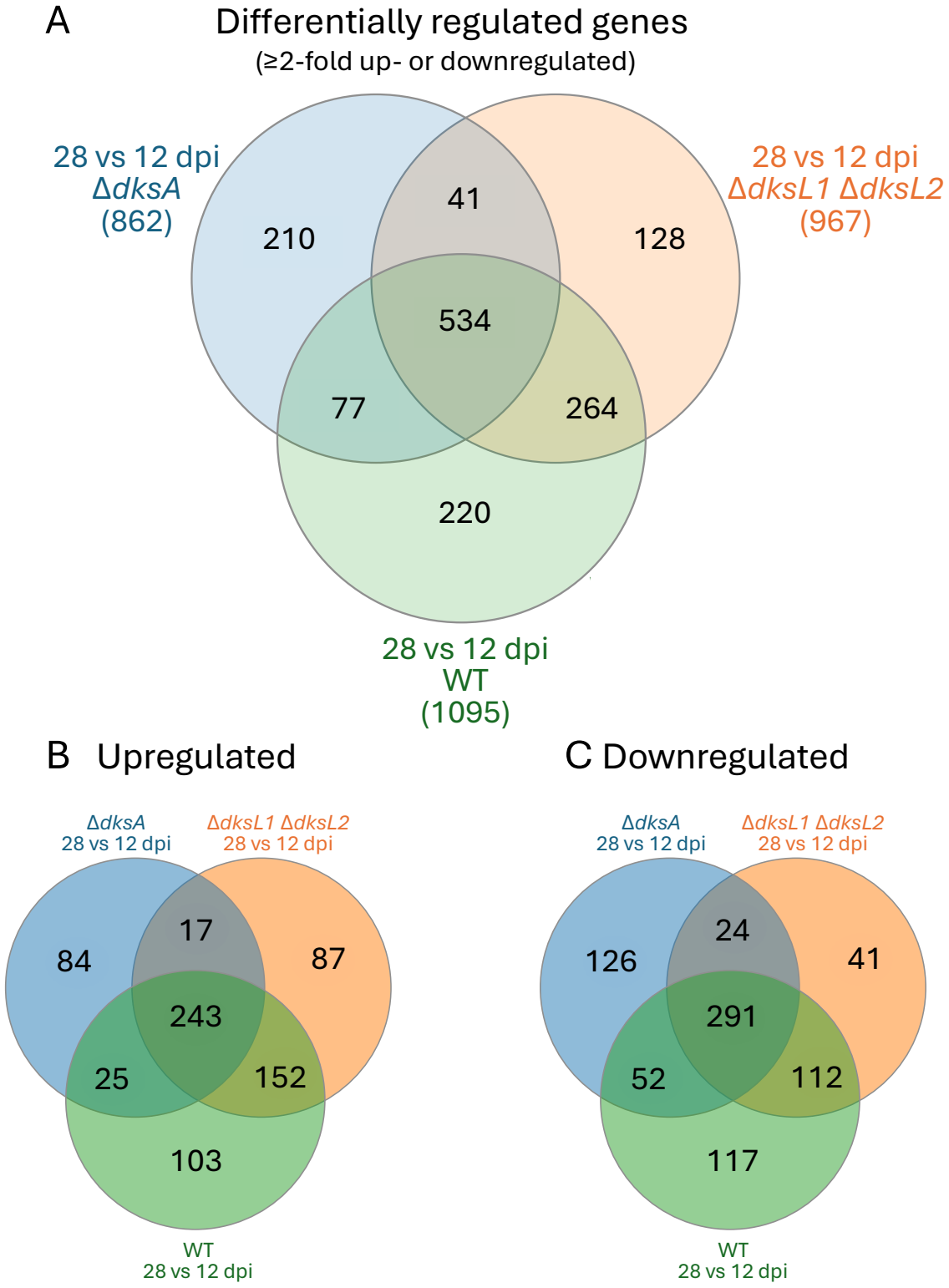
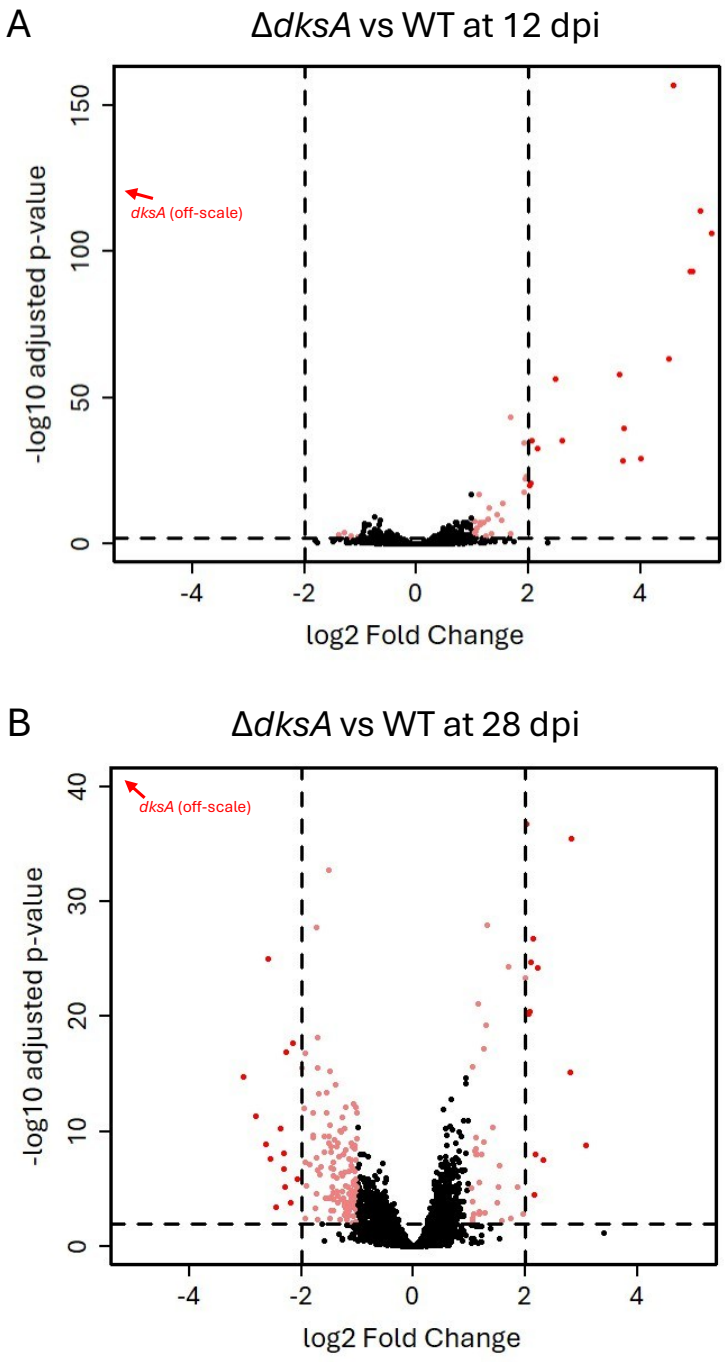


Figure S4.8 Differentially expressed genes (DEGs) between developmental stages (28 vs 12 dpi) in Δ*dksA*, Δ*dksL1* Δ*dksL2*, and WT bacteroids. (A) Venn diagrams showing total DEGs identified in each genotype. **(B)** Overlap of genes upregulated at 28 dpi relative to 12 dpi. **(C)** Overlap of genes downregulated at 28 dpi relative to 12 dpi. Numbers within each section indicate the number of genes unique to or shared among the indicated genotypes. Differential expression was defined as *p adj* < 0.01 and |log2FC| ≥ 1 (≥2-fold change).



C

		12 dpi	28dpi
not significant	FDR ≥ 0.01	**7380**	**7250**
significant	FDR < 0.01, |log2FC| ≥ 1	**45** (40↑ / 5↓)	**175** (38↑ / 137↓)
large effect size	FDR < 0.01, |log2FC| ≥ 2	**17** (16↑ / 1↓)	**25** (9↑ / 16↓)

Figure S4.9 Volcano plots of differential gene expression between the Δ*dksA* mutant and *Rlv*3841 WT at (A) 12 dpi and (B) 28 dpi. Each point represents one gene, with the x-axis showing the log2 fold change (FC) (Δ*dksA* vs WT), and the y-axis showing the −log10 adjusted *p*-value (Benjamini–Hochberg FDR). Genes with FDR < 0.01 and |log2FC| > 1 (≥2-fold change) are shown in light red, while genes with |log2FC| > 2 (≥4-fold change) are highlighted in dark red. Black points represent genes that do not meet these thresholds. Dashed lines indicate the fold change cutoff (vertical; |log2FC| = 2) and FDR significance threshold (horizontal; 0.01). Positive log2 fold change values denote genes upregulated in Δ*dksA* relative to WT, while negative values indicate higher expression in the WT. Axes were truncated for visualisation; the deleted *dksA* gene lies outside the plotting range and is indicated by an arrow. **(C)** Summary of differentially expressed genes. For full list of differentially expressed genes see Table S4.3 and S4.4.

Table S4.3 Significantly differentially expressed genes in the Δ*dksA* mutant relative to *Rlv*3841 wild type in 12 dpi nodules. Subset of genes with at least a 2-fold change in expression (fold change (FC ≥ 2 for upregulated genes, highlighted in orange; FC ≤ 0.5 for downregulated genes, highlighted in blue) and an adjusted *p*-values < 0.01. Genes with particularly strong expression changes (FC ≥ 4 or FC ≤ 0.25) are indicated in bold. Neighbouring genes are highlighted in green; continuous green blocks indicate potential operon structures according to the BioCyc Genome Explorer (Herson et al., 2024). Genes that are still differentially expressed at 28 dpi (Table S4.4) are indicated in bold.

Genes	Names	Description of putative proteins encoded/product	FC	*p adj*
RL0585		RibD family protein	0.48	4.29E-03
RL0979		flavin reductase family protein	3.88	2.03E-23
RL0980		aminopeptidase P family protein	**4.03**	1.02E-20
RL0981		permease component of ABC transporter PAAT	3.78	1.42E-18
RL0982		permease component of ABC transporter PAAT	3.87	5.92E-24
RL0983		SBP of ABC transporter PAAT	3.81	3.67E-23
RL0984		ATP-binding component of ABC transporter PAAT	**4.07**	1.23E-21
RL1870	*dksL1*	DksA-like protein 1 RNA polymerase-binding transcription factor	2.04	2.50E-05
RL1993		SBP of ABC transporter NitT anionic substrate	2.15	1.23E-17
RL2643	*dksA*	RNA polymerase-binding transcription factor DksA	**0.01**	4.45E-94
RL3366		flavoprotein	2.07	1.50E-03
RL3368		permease component of ABC transporter	2.85	6.60E-09
RL3369		permease component of ABC transporter	2.89	1.33E-14
RL3370		SBP of ABC transporter	**4.42**	3.07E-33
RL3371		ATP-binding component of ABC transporter	**4.16**	3.37E-36
RL3549	*glnII*	bifunctional glutamine synthetase II	3.78	2.78E-35
RL3594		dihydrodipicolinate synthase	2.45	5.82E-13
RL4564	*amtB*	transmembrane ammonium transporter	**5.54**	3.34E-57
RL4565	*glnK*	nitrogen regulatory protein PII	**6.07**	5.34E-36
pRL70094	*repCp7c*	replication protein RepC	2.69	9.76E-11
pRL80054		conserved hypothetical protein	0.41	1.68E-04
pRL80142	*trbBp8*	conjugal transfer protein TrbB	3.20	3.08E-04
pRL90257		GntR family transcriptional regulator	0.38	7.98E-04
pRL100068		aminohydrolase	2.12	3.35E-06
pRL100069		conserved hypothetical protein	2.19	1.85E-07
pRL100070		ATP-binding component of ABC transporter PAAT	2.27	6.61E-08
pRL100072		SBP of ABC transporter PAAT	2.40	2.08E-09
pRL100149		conserved hypothetical protein	2.05	2.64E-08
pRL100223		conserved hypothetical protein	2.35	1.28E-03
pRL100242		amino acid synthesis family protein	**15.94**	8.22E-30
pRL100243		hydrolase	**30.16**	6.28E-94
pRL100244		flavin monooxygenase/reductase	**38.35**	5.06E-107
pRL100245		flavin-dependent oxidoreductase	**33.36**	1.53E-114
pRL100246		aldehyde dehydrogenase	**29.34**	8.90E-94
pRL100247		NIPSNAP family protein	**22.49**	7.87E-64
pRL100248	*gtsA*	SBP of ABC transporter POPT GABA transporter	**23.87**	1.32E-157
pRL100249	*gtsB*	permease component of ABC transporter POPT GABA transporter	**12.94**	3.07E-40
pRL100250	*gtsC*	permease component of ABC transporter POPT GABA transporter	**12.71**	5.22E-29
pRL100251	*gtsD*	ATP-binding component of ABC transporter POPT GABA transporter	**12.33**	1.19E-58
pRL100252	*gabD4*	NAD-dependent succinate-semialdehyde dehydrogenase	3.20	5.68E-44
pRL100345		permease component of ABC transporter NitT	2.04	9.06E-05

pRL110105		LysR family transcriptional regulator	2.50	3.79E-04
pRL120070		TetR family transcriptional regulator	0.45	2.41E-03
pRL120203	*eryH*	periplasmic lipoprotein, potentially involved in erythritol uptake/metabolism	2.06	3.69E-05
pRL120256	*melA*	bifunctional alpha-galactosidase (melibiase)	2.18	6.31E-08

ABC: ATP-binding cassette (subclasses of ABC systems: PAAT: polar amino acid transporter; POPT: Polar Oligo-Peptide Transporter); SBP: solute-binding protein

Table S4.4 Significantly differentially expressed genes in the Δ*dksA* mutant relative to *Rlv*3841 wild type in 28 dpi nodules. Subset of genes with at least a 2-fold change in expression (fold change (FC ≥ 2 for upregulated genes, highlighted in orange; FC ≤ 0.5 for downregulated genes, highlighted in blue) and an adjusted *p*-values < 0.01. Particularly strong expression changes (FC ≥ 4 or FC ≤ 0.25) are indicated in bold. Neighbouring genes are highlighted in green; continuous green blocks indicate potential operon structures according to the BioCyc Genome Explorer (Herson et al., 2024). Genes that were already differentially expressed at 12 dpi (Table S4.3) are indicated in bold.

Genes	Names	Description of putative proteins encoded/product	FC	*p adj*
RL0088		conserved hypothetical protein	0.47	9.09E-05
RL0151	*dnaJ*	chaperone protein DnaJ	2.07	2.14E-16
RL0152	*dnaK*	heat shock chaperone protein DnaK	2.23	7.80E-22
RL0190		transmembrane protein	0.41	1.10E-10
RL0238		conserved hypothetical protein	2.38	5.81E-18
RL0274		conserved hypothetical protein	**0.21**	1.08E-17
RL0469		exported surface protein	**0.12**	1.51E-15
RL0506		conserved hypothetical protein	0.26	4.33E-08
RL0530		hypothetical exported protein	0.36	1.42E-07
RL0598		conserved hypothetical protein	0.30	1.94E-08
RL0633		conserved hypothetical protein	0.45	6.62E-04
RL0870	*ldt3*	ErfK/YbiS/YhnG family protein	0.49	5.13E-05
RL0883	*groLch1*	60 kda chaperonin (protein cpn60)	2.45	5.06E-20
RL0884	*groSch1*	10 kda chaperonin (protein cpn10)	2.48	1.06E-28
RL0979		flavin reductase family protein	**4.26**	1.64E-25
RL0980		aminopeptidase P family protein	**4.12**	5.04E-21
RL0981		permease component of ABC transporter PAAT	**4.21**	3.47E-21
RL0982		permease component of ABC transporter PAAT	3.97	3.76E-24
RL0983		SBP of ABC transporter PAAT	**4.37**	1.51E-27
RL0984		ATP-binding component of ABC transporter PAAT	**4.62**	5.07E-25
RL1154		hypothetical exported protein	0.39	2.02E-09
RL1155		glycosyltransferase	0.28	6.65E-08
RL1164		conserved hypothetical protein	0.46	3.21E-05
RL1172		transmembrane protein	0.41	1.60E-05
RL1215		transmembrane protein	**0.20**	6.94E-06
RL1216		conserved hypothetical protein	**0.22**	1.31E-04
RL1329	*salA*	MFS family efflux transporter (membrane fusion protein)	0.37	1.75E-07
RL1485		conserved hypothetical protein	0.43	3.80E-09
RL1521	*sodC*	superoxide dismutase	0.39	9.34E-10
RL1631	*napC*	cytochrome c type nitrate reductase NapC exported to periplasm	0.31	4.44E-14
RL1644		hypothetical exported protein	0.40	1.44E-08
RL1832	*exoA*	exodeoxyribonuclease	0.45	1.61E-03

RL1833		conserved hypothetical protein	0.36	2.42E-11
RL1840		transmembrane protein	0.36	7.83E-04
RL2025		transmembrane protein	0.31	3.04E-16
RL2145		conserved hypothetical protein	0.45	2.64E-05
RL2200		conserved hypothetical protein	0.30	2.63E-05
RL2416		conserved hypothetical protein	0.45	1.15E-04
RL2430		conserved hypothetical protein	0.49	2.03E-12
RL2430A		conserved hypothetical protein	0.46	1.53E-05
RL2444		conserved hypothetical protein with DUF1445	2.18	8.86E-09
RL2467		conserved hypothetical protein	0.42	9.78E-09
RL2469		pseudogene	0.41	8.08E-11
RL2491		hypothetical exported protein	0.48	1.90E-04
RL2553		conserved hypothetical protein	0.48	1.93E-06
RL2643	*dksA*	RNA polymerase-binding transcription factor DksA	**0.01**	5.92E-130
RL2912		hypothetical exported protein	0.36	3.18E-03
RL2938		transmembrane transporter protein MFS superfamily	**0.17**	9.29E-26
RL3065		hypothetical exported protein	0.45	2.24E-08
RL3085		hypothetical exported protein	0.30	1.52E-28
RL3096		truncated pseudogene, putative arginine deiminases (pfam02274)	0.38	1.06E-06
RL3180		conserved hypothetical protein	0.43	1.93E-03
RL3186		transmembrane protein	0.42	6.87E-07
RL3371		ATP-binding component of ABC transporter	2.15	2.70E-09
RL3378	*cinI*	autoinducer synthesis protein	0.46	1.27E-05
RL3384		hypothetical exported protein	0.48	1.87E-07
RL3457		conserved hypothetical protein	0.34	2.46E-12
RL3549	*glnII*	bifunctional glutamine synthetase II	**4.02**	1.87E-37
RL3684		transmembrane protein	0.31	6.16E-19
RL3889		transmembrane protein	0.44	5.89E-06
RL3950		phage-related protein	2.17	8.49E-09
RL4133		hypothetical exported protein	0.47	1.75E-09
RL4194		bifunctional succinate-semialdehyde dehydrogenase	0.43	5.73E-11
RL4195		transmembrane protein	0.31	2.13E-07
RL4196		hypothetical exported protein	0.36	5.77E-06
RL4231	*araF*	SBP of ABC transporter CUT2	2.16	3.02E-10
RL4274		RND family efflux transporter (membrane fusion protein)	0.37	7.41E-07
RL4306		hypothetical exported protein	0.42	5.94E-05
RL4370		conserved hypothetical protein	0.48	1.70E-09
RL4426	*xerC*	site-specific tyrosine recombinase XerC	0.48	4.92E-04
RL4564	*amtB*	transmembrane ammonium transporter	3.24	4.63E-25
RL4565	*glnK*	nitrogen regulatory protein PII	**6.99**	3.59E-36
RL4578	*ggt2*	bifunctional gamma-glutamyl transpeptidase precursor	0.39	1.59E-04
RL4579		pilin protein	0.44	4.37E-03
RL4640	*ndvA*	ATP-binding permease component of ABC transporter; Glucan export	0.48	3.04E-09
RlC84		RlC84	2.14	4.63E-09
pRL70054		conserved hypothetical protein	0.36	4.30E-05
pRL80104		methylase	2.65	4.16E-11
pRL80118		nuclease	2.10	1.28E-03
pRL80119		conserved hypothetical protein	2.82	1.47E-04
pRL80120	*traGp8*	conjugal transfer protein TraG	2.41	1.17E-03
pRL80121	*traCp8*	conjugal transfer protein TraC	**4.50**	8.86E-09
pRL80137	*trbLp8*	conjugal transfer protein TrbL	3.32	3.07E-03
pRL80139	*trbEp8*	conjugal transfer protein TrbE	2.85	6.43E-06

pRL80142	*trbBp8*	conjugal transfer protein TrbB	**6.95**	6.17E-16
pRL90054		conserved hypothetical protein	0.31	5.41E-07
pRL90055		conserved hypothetical protein	**0.20**	1.78E-07
pRL90059	*rmrA*	MFS family efflux transporter (membrane fusion protein)	0.43	7.81E-13
pRL90060	*rmrB*	MFS family efflux transporter (inner membrane protein)	0.46	2.65E-08
pRL90069		hypothetical exported protein	0.48	2.68E-05
pRL90070		acetyltransferase	0.46	4.52E-05
pRL90129		conserved hypothetical protein	**0.19**	5.74E-11
pRL90196		conserved hypothetical protein	0.35	2.41E-10
pRL90257		GntR family transcriptional regulator	0.49	7.41E-03
pRL90285		permease component of ABC transporter CUT1	0.45	5.13E-04
pRL90286		SBP of ABC transporter CUT1	0.43	4.54E-06
pRL100072		SBP of ABC transporter PAAT	2.38	7.35E-10
pRL100163		hypothetical protein with homology to asparagine synthase	0.43	3.17E-07
pRL100169	*rhiA*	rhizosphere-induced protein RhiA	**0.14**	4.66E-12
pRL100170	*rhiB*	rhizosphere-induced protein RhiB	**0.16**	1.19E-09
pRL100171	*rhiC*	rhizosphere-induced protein RhiC	**0.18**	3.38E-04
pRL100179	*nodN*	nodulation protein NodN	0.45	2.82E-04
pRL100182	*nodE*	nodulation protein NodE homology with beta-ketoacyl synthases	0.35	1.90E-33
pRL100183	*nodF*	nodulation protein NodF acyl carrier protein	0.36	4.96E-16
pRL100185	*nodA*	nodulation protein NodA	0.48	4.46E-06
pRL100187	*nodC*	bifunctional N-acetylglucosaminyltransferase NodC	0.48	2.77E-07
pRL100242		conserved hypothetical protein	3.60	5.89E-06
pRL100243		hydrolase	2.90	8.00E-08
pRL100278		permease component of ABC transporter PepT	0.49	6.80E-03
pRL100300		short-chain dehydrogenase/reductase	0.48	6.44E-05
pRL100398		SBP of ABC transporter	0.47	8.36E-03
pRL100405		transmembrane protein	0.40	4.11E-03
pRL100460		lipid biosynthesis 3-oxoacyl-[acyl-carrier-protein] reductase	0.49	7.81E-13
pRL100462		permease component of ABC transporter CUT2	0.48	3.70E-13
pRL110011	*treY*	bifunctional trehalose synthase / putative trehalose synthase	0.26	1.36E-17
pRL110016		conserved hypothetical protein	0.49	4.71E-06
pRL110033		ATP-binding permease component of ABC transporter Export	0.42	5.80E-12
pRL110034		ATP-binding permease component of ABC transporter Export	0.49	3.69E-10
pRL110105		LysR family transcriptional regulator	2.25	9.19E-04
pRL110108		conserved hypothetical protein	0.35	6.62E-05
pRL110257A		conserved hypothetical protein	0.43	2.69E-04
pRL110257B		conserved hypothetical protein	0.46	3.41E-04
pRL110268		conserved hypothetical protein	0.46	1.02E-09
pRL110289	*pcaF*	beta-ketoadipyl CoA thiolase	2.07	1.16E-04
pRL110304	*treX*	glycosylhydrolase	0.38	8.00E-15
pRL110305		bifunctional topoisomerase I / putative topoisomerase I	0.34	3.54E-14
pRL110306	*(ligD)*	pseudogene, DNA polymerase LigD, polymerase domain	0.50	6.80E-06
pRL110317		conserved hypothetical protein	0.31	4.54E-03
pRL110326		conserved hypothetical protein	0.44	1.32E-03
pRL110327		conserved hypothetical protein	0.38	4.50E-10
pRL110328		conserved hypothetical protein	0.43	1.47E-04
pRL110446		ATP-binding component of ABC transporter PepT	0.47	2.15E-03
pRL110454		SBP of ABC transporter PepT	0.45	2.68E-07
pRL110506		transmembrane protein	2.08	3.42E-03
pRL110604		trifolitoxin-related protein	0.46	8.77E-08

pRL110605		conserved hypothetical protein	**0.23**	1.74E-18
pRL110615	*nadC*	bifunctional nicotinate-nucleotide pyrophosphorylase [carboxylating]	2.07	5.65E-03
pRL110616	*nadB*	L-aspartate oxidase	2.25	1.41E-03
pRL120298		conserved hypothetical protein	0.49	1.28E-05
pRL120299		conserved hypothetical protein	0.49	2.61E-05
pRL120301	*yagS*	bifunctional xanthine dehydrogenase YagS, FAD-binding subunit	0.49	1.39E-06
pRL120302	*yagT*	bifunctional xanthine dehydrogenase YagT, iron-sulfur binding subunit	0.49	2.82E-08
pRL120320	*vbsC*	acetylase	2.25	2.67E-06
pRL120374		bifunctional transmembrane ribonuclease domain protein	0.45	3.97E-04
pRL120393		SBP of ABC transporter CUT2	0.43	4.12E-04
pRL120394		conserved hypothetical protein	0.43	1.52E-04
pRL120398		hypothetical exported protein	0.29	1.83E-10
pRL120399		GntR family transcriptional regulator	0.36	1.92E-09
pRL120400		SBP of TRAP transporter	**0.25**	2.57E-16
pRL120401		small permease (DctQ-like) component of TRAP transporter	0.34	5.55E-05
pRL120402		large permease (DctM-like) component of TRAP transporter	0.33	6.05E-09
pRL120403		dehydrogenase	**0.24**	1.27E-06
pRL120494		short-chain dehydrogenase/reductase	0.49	1.05E-03
pRL120504	*fcS*	feruloyl-CoA synthetase	**0.17**	2.03E-08
pRL120505	*ech*	bifunctional enoyl CoA hydratase/lyase	**0.20**	6.61E-09
pRL120506		aryl-alcohol dehydrogenase	0.36	6.29E-09
pRL120507	*calB*	coniferyl aldehyde dehydrogenase	0.35	9.50E-10
pRL120509		molybdopterin-binding oxidoreductase	2.33	8.86E-09
pRL120537		FAD/NAD/ferredoxin protein	0.32	1.16E-07
pRL120538		Rieske 2Fe2S dioxygenase	0.29	2.38E-12
pRL120600		GntR family transcriptional regulator	2.03	7.22E-06
pRL120652		conserved hypothetical protein	0.41	7.95E-05
pRL120653		conserved hypothetical protein	0.26	4.54E-06
pRL120708		bifunctional alpha-amylase	0.37	2.13E-05
pRL120709	*treS*	trehalose synthase	0.33	2.45E-10
pRL120710	*glgB2*	bifunctional 1,4-alpha-glucan/glycogen branching protein	0.26	8.57E-13
pRL120717		conserved hypothetical protein	0.37	4.18E-08
pRL120722		bifunctional alpha-amylase	0.39	3.91E-05
pRL120723	*malQ*	4-alpha-glucanotransferase	0.29	2.92E-10
pRL120730		conserved hypothetical protein	0.43	2.35E-04
pRL120733		SBP of ABC transporter PAAT	0.37	6.69E-04
pRL120736		conserved hypothetical protein	0.43	1.14E-03
pRL120737		conserved hypothetical protein	0.38	1.45E-05
pRL120738		transmembrane protein	0.37	8.30E-05
pRL120739		phospholipase	0.41	4.70E-07

ABC: ATP-binding cassette (subclasses of ABC systems: CUT1: Carbohydrate Uptake Transporter 1; CUT2: Carbohydrate Uptake Transporter 2; PAAT: polar amino acid transporter; PepT: peptide transporter; POPT: Polar Oligo-Peptide Transporter);
SBP: solute-binding protein; TRAP: Tripartite ATP-independent Periplasmic transporter; DUF: Domain of Unknown Function;
MFS: Major Facilitator Superfamily; RND: Resistance-Nodulation-Division (efflux family);

Table S4.5 Comparison of the three DksA homologues in *Rhizobium leguminosarum* bv. *viciae* 3841 (*Rlv*3841) and *Rhizobium leguminosarum* bv. *phaseoli* (*Rlp*4292).

category	***Rlv*3841**		***Rlp*4292**		**Comparison of *Rlv*3841 & *Rlp*4292 homologues**			
					shared identity		conserved motifs	
	gene (locus)	AA (bp)	gene (locus)	AA (bp)	nucleotide % (shared/all nts)	protein % (shared/all AA)	Zn finger	DXXDXA
"canonical"	***dksA*** (RL2643)	139 (420)	***dksA*** (RHL1447)	139 (420)	96.2% (404/420)	98.6% (137/139)	No	Yes
"likes"	***dksL1*** (RL1870)	107 (324)	***dksL1*** (RHLb6067)	107 (324)	92.0% (298/324)	86% (92/107)	Yes	No
"likes"	***dksL2*** (RL2268A)	116 (351)	***dksL2*** (RHL1099)	118 (357)	93.4% (328/358)	94.8% (110/118)	Yes	Yes

Table S4.6 Comparison of *dksA* homologue gene fitness in pea (*Rhizobium leguminosarum* bv. *viciae* 3841; *Rlv*3841) and bean (*Rhizobium leguminosarum* bv. *phaseoli* 4292; *Rlp*4292) symbionts determined by insertion sequencing (INSeq).

category	gene	**Pea INSeq (*Rlv*3841)**[1]					**Bean INSeq (*Rlp*4292)**[2]					
		HMM			gene fitness value (log2FC)		HMM			gene fitness value (log2FC)		
		free-living	bacteroids	nodule bacteria	free-living vs bacteroids	free-living vs nodule bacteria	free-living	bacteroids	regrowth	free-living vs bacteroids	free-living vs regrowth	bacteroid vs regrowth
"canonical"	***dksA***	NE	DE	NE	**-6.01**	**-6.02**	NE	ES	ES	**-5.1**	**-5.1**	0
"like"	***dksL1***	NE	NE	NE	**1.55**	-0.15	NE	NE	NE	0.59	0.55	-0.04
"like"	***dksL2***	nd	nd	nd	nd	nd	NE	NE	NE	**2.42**	**-4.15**	**-6.93**

[1] Wheatley et al., (2020) with fitness values (log2 fold change) calculated by Hayley Knights; [2] Knights, Ledermann, et al., (in preparation). Note that, in *Rlv*3841, 'nodule bacteria' refers to undifferentiated bacteria in the nodule and, in *Rlp*4292, 'regrowth' includes nodule bacteria plus dedifferentiated bacteroids.
Gene fitness was calculated with two methods: HMM (Hidden Markov Model) classification: NE: neutral (insertion has neutral impact on fitness); DE: defective (insertion impairs fitness); ES: essential (no or very few insertions are tolerated); for more details see Wheatley et al., (2020); and
Gene fitness value (log2 ratio of relative mutant abundance between conditions), where log2FC ~ 0: neutral fitness; log2FC < -2: severely disadvantaged fitness; log2FC > 0.42: advantageous fitness; for more details see Knights et al., (2024).
nd: not determined (gene fitness of *dksL2* was not assessed due to improper annotation of the gene in an earlier version of the *Rlv*3841 genome)

Table S4.7 *Rhizobium leguminosarum* bv. *viciae* 3841INSeq (insertion sequencing) fitness assignments of *dksA* and *dksL1* mutants.

category	gene	free-living laboratory[1]			root attachment, 1h post-inoculation[2]					symbiosis with pea[3]			
					pea			soybean	barley				
		TY 21% O_2	UMS 21% O_2	UMS 1% O_2	pH 6.5	pH 7.0	pH 7.5	pH 7.0	pH 7.0	rhizosphere	root attached	nodule bacteria	bacteroids
"canonical"	***dksA***	NE	NE	NE	NE	DE	DE	DE	DE	NE	NE	DE	NE
"like"	***dksL1***	NE	NE	NE	NE	NE	NE	NE	NE	AD	NE	NE	NE

[1] Wheatley et al., (2017); [2] Parsons, (2019); [3] Wheatley et al., (2020).
HMM classification: NE: neutral (insertion has neutral impact on fitness); DE: defective (insertion impairs fitness); AD: advantaged (insertion enhances fitness); for more details see Wheatley et al., (2020).
Note, gene fitness of *dksL2* was not assessed due to improper annotation of the gene in an earlier version of the *Rlv*3841 genome.

Supplementary Table A RNA-seq analysis of dksA homologues in bacteroids

Full analysis of the RNA-seq data, including all condition comparisons (WT, *dksA*, *dksL1 dksL2* bacteroids from 12 and 28 dpi), is provided in an Excel file **"Supplementary Table A_RNAseq on dksA homologs bacteroids_complete results.xlsx"** submitted alongside this thesis.

5

GENERAL DISCUSSION AND FUTURE PERSPECTIVES

GENERAL DISCUSSION AND FUTURE PERSPECTIVES

In summary, in this thesis I investigated how metabolic and regulatory processes are coordinated in *Rhizobium leguminosarum* across its life cycle, with a particular focus on carbon utilisation, transport systems, and global regulatory mechanisms. The work presented here addresses three interconnected questions: how carbon source hierarchy is established, how transport systems contribute to physiological adaptation, and how global regulators integrate environmental signals to shape bacterial behaviour during different stages of symbiosis.

By addressing these questions, I examined key factors that govern bacteroid metabolism. Consequently, the results presented here advance our understanding of regulatory circuits that underpin rhizobial adaptation, including those that drive carbon catabolite repression and promoter preference in *R. leguminosarum*. These processes are central to how rhizobia respond to fluctuating nutrient environments, coordinate metabolic activity, and ultimately establish and maintain an efficient symbiosis with legume hosts.

In **Chapter 2,** I characterised the basis of the carbon source preference in *R. leguminosarum* under conditions where multiple substrates are available, particularly, the preferential uptake of C_4-dicarboxylates. While various individual catabolic pathways in rhizobia have been investigated (Fry et al., 2001; Vanderlinde et al., 2014; Yost et al., 2006), these approaches often consider substrates in isolation and do not reflect the complex environments encountered in soil or during host infection, where multiple carbon sources are present simultaneously (Knights et al., 2024; Ramachandran et al., 2011). Under such conditions, rhizobia must prioritise substrate utilisation to maintain metabolic efficiency and competitiveness, as inappropriate or simultaneous expression of catabolic pathways impairs the transition to the nodule environment (Pardo Díaz, 2022).

The dicarboxylate transport system (Dct), which mediates the uptake of C_4-dicarboxylates, has repeatedly been identified as essential in genome-wide mutant screens (Knights, Ledermann et al., in preparation; Wheatley et al., 2020), and transcriptomic studies (Green et al., 2019; Ramachandran et al., 2011). This is consistent

with metabolic network analyses across multiple stages of the symbiotic cycle, which identify C_4-dicarboxylate uptake as a key requirement (diCenzo et al., 2016, 2020; Schulte et al., 2022). While modelling approaches can capture aspects of these metabolic dependencies, their predictive power is limited by the accuracy of imposed flux constraints, particularly when regulatory mechanisms and feedback control are not fully understood (diCenzo et al., 2020). This highlights that understanding regulatory and metabolic interactions is essential for identifying the determinants of bacterial behaviour.

Although the Dct emerged as the primary target in the conducted mutant screen, our results show that carbon catabolite repression (CCR) is driven by intracellular metabolite availability rather than by direct Dct-mediated signalling. Restoration of CCR using a heterologous malate transporter supports this conclusion. Thus, a central finding of this thesis is that carbon source hierarchy in *R. leguminosarum* is governed by intracellular metabolite levels rather than a dedicated extracellular sensing mechanism, although the nature of the underlying signal remains unknown.

Utilising the inositol pathway as an example, I showed that this uptake-driven mechanism acts via an inducer exclusion model, in which presence of C_4-dicarboxylates suppresses alternative substrate utilisation by limiting their uptake and preventing inducer accumulation. Unlike classical CCR systems in *Escherichia coli*, which rely on defined global regulators (Görke & Stülke, 2008), rhizobial carbon regulation appears to be more distributed and metabolite-driven. Such a metabolite-driven regulatory system is well suited to the heterogeneous soil environment, where rapid and flexible responses to changing substrate availability are essential. It remains to be determined whether CCR operates uniformly across all carbon sources through this shared mechanism and whether additional hierarchies exist among alternative pathways. Preliminary observations suggest a graded response, indicating a nuanced (hierarchical) regulatory network. Such variation may arise from differences in transport capacity, specificity, and affinity, as well as the interplay between global and pathway-specific regulators, as demonstrated here with IolR, or as described for repression of succinate in *E. coli* (Schubert & Unden, 2024). These hypotheses can be tested by extending similar analyses to additional, well-characterised substrates of *Rlv*3841, such as mannitol, which is

chemically and metabolically distinct from C_4-dicarboxylates and supported by defined metabolic pathways and extensive growth data (Perry et al., 2016).

Furthermore, the role of post-transcriptional regulation in CCR warrants further investigation. Recent studies have implicated sRNAs, and thereby the RNA chaperone Hfq, in the (post-) transcriptional control of various ABC transporters in rhizobia (García-Tomsig et al., 2022, 2023), raising the possibility that CCR may involve sRNA-mediated control. Future work could address this by functionally analysing *hfq* mutants or systematically identifying such RNA-based regulatory elements, for instance by utilising MAPS (MS2-affinity purification; Lalaouna et al., 2017) or CLASH (cross-linking ligation and sequencing of hybrids; Helwak & Tollervey, 2014) on succinate-grown rhizobial cultures.

The preferential utilisation of C_4-dicarboxylates in free-living rhizobia likely reflects both metabolic efficiency and regulatory adaptation (McGill et al., 2021; Schulte et al., 2021), and may underlie their central role in bacteroid metabolism (Poole & Allaway, 2000; Udvardi & Poole, 2013). This warranted a more detailed investigation of the Dct system and its potential (cross-) regulatory function beyond substrate uptake. Thus, linkages between the Dct system, carbon hierarchy, and symbiotic performance were explored in **Chapter 3**, employing genetic and synthetic approaches to uncouple C_4-dicarboxylate sensing from transport.

A key finding is that disruption of the native regulatory context of the Dct system causes pronounced growth and symbiotic defects, even when transport capacity is restored. This indicates that the phenotype cannot be explained by impaired substrate uptake alone but instead reflects a failure to properly coordinate metabolic responses. As first proposed by Reid & Poole (1998), this may reflect interference between carbon and nitrogen signalling pathways. Consistently, complementation with native *dctA* failed to restore wild-type growth, suggesting that the regulatory architecture of the *dct* locus extends beyond *dctA* itself and warrants further investigation.

Much of the foundational work on the rhizobial Dct system predates modern systems-level approaches. Consistent with this, the most recent dedicated review dates to Yurgel

& Kahn (2004), and the integration of transport, metabolism, and regulation has likely been underestimated.

While the evidence remains indirect, our findings refine the functional understanding of the Dct system as an integrated module, positioning it at the core of carbon and nitrogen coordination and highlighting its distinct role in rhizobial species compared to other bacteria, where C_4-dicarboxylates play only secondary roles. This may explain why all mutants defective in CCR identified in this thesis also exhibited impaired symbiotic performance, suggesting a functional link between carbon source prioritisation and nitrogen fixation efficiency, even if a direct causal relationship has yet to be established.

The apparent discrepancy between Chapters 2 and 3 can therefore be resolved by considering CCR as a metabolite-driven regulatory outcome and Dct as the system that enforces its physiological implementation. Additional support for a metabolite-driven model of CCR is provided by the suppressor mutant RU152-22, in which *dctA* expression is restored in the absence of DctBD signalling, yet regulation remains non-native. This demonstrates that metabolic state – potentially involving metabolite pool sizes and fluxes through key metabolic checkpoints –, rather than Dct-mediated signalling, is sufficient to drive CCR, while at the same time highlighting the importance of regulatory context for proper physiological function.

More broadly, these findings suggest that transport processes in *R. leguminosarum* may be closely integrated with regulatory processes that coordinate cellular responses to environmental inputs. Transporters are increasingly recognised as components of regulatory networks beyond substrate uptake, for example through protein-protein interactions or coupling to global regulatory pathways (Mulley et al., 2011; Prell et al., 2012; Tjahjono, 2025; Torres-Quesada et al., 2014). The possibility that Dct components interact with additional, as yet unidentified partners therefore represents an important avenue for future research. In *E. coli*, DctA has been shown to interact with its sensor kinase DcuS (Stopp et al., 2021; Witan et al., 2012) and to be inhibited by $EIIA^{Glc}$ (Schubert & Unden, 2024), illustrating this principle. However, Dct components in *E. coli* share only limited sequence similarity with their rhizobial homologues and, importantly, its Dct system is itself subject to repression under CCR conditions via cAMP-dependent

regulation (Davies et al., 1999). Therefore, the possibility of extrapolation of regulatory mechanisms from one organism to another is certainly limited.

The suppressor mutant RU152-22 also highlights the value of suppressor analysis, as (spontaneous) mutations selectable under physiological conditions circumvent issues with cellular viability and regulatory constraints (Bautista et al., 2021). However, the genetic basis of suppression can be difficult to resolve and may complicate interpretation, as observed here. Together, these considerations emphasise the importance of combining targeted and evolutionary approaches to dissect complex regulatory systems.

While in Chapters 2 and 3 I demonstrate that carbon prioritisation in *R. leguminosarum* arises from the coordination of substrate uptake with cellular physiology, they do not explain how these metabolic signals are integrated into broader regulatory networks. **Chapter 4** addresses this gap by focusing on global regulators, in particular the stringent response and its effector DksA.

DksA is a conserved transcriptional regulator, first described in *E. coli* (Kang & Craig, 1990), that modulates bacterial adaptation to nutrient limitation and stress, both processes important during rhizobial lifestyle transitions. Although *dksA* homologues are widely distributed across diverse bacterial lineages (Boutte & Crosson, 2013), and their role in stress adaptation is well established in model organisms (Hauryliuk et al., 2015; Irving et al., 2021), their role in rhizobial symbiosis remains poorly resolved. Given that relatively few regulators of the bacteroid state have been characterised, and those studied in detail predominantly regulate symbiosis-specific gene expression (Dixon & Kahn, 2004; Rutten & Poole, 2019), leaves broader regulatory mechanisms governing bacteroid differentiation less well understood. Consistent with this, disruption of the stringent response, for example through *relA* mutation, impairs symbiotic performance including reduced nitrogen fixation capabilities (Tjahjono, 2025; Wippel & Long, 2016). Against this background, in Chapter 4 I investigated the function of the three DksA homologues encoded in the *R. leguminosarum* genome, with particular emphasis on their contribution to symbiotic adaptation.

Phylogenetic analysis revealed that these homologues cluster into two distinct groups, suggesting potential functional divergence; however, more comprehensive analyses will be required to confirm this classification.

The results presented in this thesis demonstrate convincingly that the canonical DksA protein is the primary contributor to stringent response-associated transcriptional remodelling under symbiotic conditions. In contrast, the DksA-like proteins (DksLs), although transcriptionally induced under microaerobic conditions via FnrN, do not exhibit a clear functional role under the conditions tested. This suggests that their contribution may be context-dependent or subtle, although further analysis of higher-order mutants in both pea- and bean-nodulating rhizobia will be required to clarify their role.

During symbiosis, DksA contributes to metabolic homeostasis by repressing free-living metabolic programmes and promoting the bacteroid state. In particular, the strong upregulation of ammonia assimilation pathways in the *dksA* mutant raises the question of whether these cells experience nitrogen starvation or, alternatively, fail to properly downregulate nitrogen assimilation during symbiosis. More generally, the mechanisms underlying the transition from autonomous nitrogen assimilation to host-dependent auxotrophy in bacteroids remain poorly understood (Prell & Poole, 2006; Udvardi & Poole, 2013). The results presented here suggest that DksA contributes to this metabolic reprogramming, although the precise regulatory mechanisms remain to be elucidated.

Despite these advances, several questions remain. First, the direct targets of DksA in *R. leguminosarum* have not been comprehensively identified, and it remains unclear how DksA integrates signals from carbon and nitrogen metabolism at the molecular level. Future work should therefore aim to dissect the regulatory networks downstream of DksA in greater detail. This could include genome-wide identification of promoters whose activity is altered by DksA interacting with RNA polymerase as well as integration of transcriptomic and metabolomic datasets, particularly in bean bacteroids to complement extensive studies in pea. Likewise, transmission electron microscopy (TEM) or confocal microscopy could provide insight into infection thread development, bacteroid morphology and packing density within nodules. The host-dependent effects observed here further suggest that regulatory requirements differ between reversible and

terminally differentiated bacteroids, indicating that NCR peptide function may override or mask certain regulatory requirements.

Second, the interplay between DksA and other components of the stringent response, particularly RelA and (p)ppGpp, warrants further investigation, especially given that this system acts in concert with other global regulatory systems such as PTS^{Ntr} system to shape global transcriptional responses (Tjahjono, 2025).

In addition, the strong upregulation of genes encoding the GABA-specific ABC transporter (*gtsABCD*) and adjacent operon justifies further functional analysis, particularly as the same operon was found to be also upregulated in earlier stages of symbiosis (Cocker et al., in preparation) and enzymes catabolizing GABA are highly induced in pea bacteroids (Prell et al., 2009). Given that GABA is a major component of plant root exudates and accumulates in nodules (Pini et al., 2017; Sulieman, 2011; Wang et al., 2022), these observations strongly suggest a potential role for the GABA shunt in symbiotic adaptation and possibly bacteroid metabolism.

In summary, in this thesis I demonstrate that bacterial adaptation in *Rhizobium leguminosarum* is governed by the integration of metabolic and regulatory processes across multiple layers of control. In Chapter 2 I established that carbon source hierarchy is driven primarily by intracellular metabolite availability rather than by dedicated sensing mechanisms. In Chapter 3 I show that this hierarchy must be implemented through coordinated regulation of substrate uptake, with the Dct system acting as a key interface linking environmental carbon availability to cellular physiology. Building on this, in Chapter 4 I demonstrate that global regulatory systems, and DksA in particular, integrate these metabolic signals to fine-tune gene expression and coordinate adaptation during symbiosis.

Together, these findings support a model in which rhizobial behaviour is shaped by a hierarchical regulatory framework: intracellular metabolites define metabolic state, transport systems align substrate uptake with cellular demand, and global regulators integrate these inputs to orchestrate transcriptional responses. This multi-layered regulation ultimately determines the ability of rhizobia to transition between free-living

and symbiotic lifestyles and to establish efficient nitrogen-fixing interactions with their plant hosts.

References

Bautista, D. E., Carr, J. F., & Mitchell, A. M. (2021). Suppressor mutants: History and today's applications. *EcoSal Plus*, *9*(2), eESP-0037-2020. https://doi.org/10.1128/ecosalplus.ESP-0037-2020

Boutte, C. C., & Crosson, S. (2013). Bacterial lifestyle shapes stringent response activation. *Trends in Microbiology*, *21*(4), 174–180. https://doi.org/10.1016/j.tim.2013.01.002

Cocker, C. R., Pardo Díaz, J., Jorrin, B., Abreu, I., Ledermann, R., East, A. K., & Poole, P. S. (in preparation). *Gene expression in Rhizobium leguminosarum from rhizosphere to mature nitrogen-fixing bacteroids* [Unpublished manuscript].

Davies, S. J., Golby, P., Omrani, D., Broad, S. A., Harrington, V. L., Guest, J. R., Kelly, D. J., & Andrews, S. C. (1999). Inactivation and regulation of the aerobic C_4-dicarboxylate transport (*dctA*) gene of Escherichia coli. *Journal of Bacteriology*, *181*(18), 5624–5635. https://doi.org/10.1128/JB.181.18.5624-5635.1999

diCenzo, G. C., Checcucci, A., Bazzicalupo, M., Mengoni, A., Viti, C., Dziewit, L., Finan, T. M., Galardini, M., & Fondi, M. (2016). Metabolic modelling reveals the specialization of secondary replicons for niche adaptation in Sinorhizobium meliloti. *Nature Communications*, *7*(1), 12219. https://doi.org/10.1038/ncomms12219

diCenzo, G. C., Tesi, M., Pfau, T., Mengoni, A., & Fondi, M. (2020). Genome-scale metabolic reconstruction of the symbiosis between a leguminous plant and a nitrogen-fixing bacterium. *Nature Communications*, *11*(1), 2574. https://doi.org/10.1038/s41467-020-16484-2

Dixon, R., & Kahn, D. (2004). Genetic regulation of biological nitrogen fixation. *Nature Reviews Microbiology*, *2*(8), 621–631. https://doi.org/10.1038/nrmicro954

Fry, J., Wood, M., & Poole, P. S. (2001). Investigation of myo-inositol catabolism in Rhizobium leguminosarum bv. viciae and its effect on nodulation competitiveness. *Molecular Plant-Microbe Interactions*, *14*(8), 1016–1025. https://doi.org/10.1094/MPMI.2001.14.8.1016

García-Tomsig, N. I., García-Rodriguez, F. M., Guedes-García, S. K., Millán, V., Becker, A., Robledo, M., & Jiménez-Zurdo, J. I. (2023). A double-negative feedback loop between NtrBC and a small RNA rewires nitrogen metabolism in legume symbionts. *mBio*, *14*(6), e02003-23. https://doi.org/10.1128/mbio.02003-23

García-Tomsig, N. I., Robledo, M., diCenzo, G. C., Mengoni, A., Millán, V., Peregrina, A., Uceta, A., & Jiménez-Zurdo, J. I. (2022). Pervasive RNA regulation of metabolism enhances the root colonization ability of nitrogen-fixing symbiotic α-rhizobia. *mBio*, *13*(1), e03576-21. https://doi.org/10.1128/mbio.03576-21

Görke, B., & Stülke, J. (2008). Carbon catabolite repression in bacteria: Many ways to make the most out of nutrients. *Nature Reviews Microbiology*, *6*(8), 613–624. https://doi.org/10.1038/nrmicro1932

Green, R. T., East, A. K., Karunakaran, R., Downie, J. A., & Poole, P. S. (2019). Transcriptomic analysis of Rhizobium leguminosarum bacteroids in determinate and indeterminate nodules. *Microbial Genomics*, *5*(2). https://doi.org/10.1099/mgen.0.000254

Hauryliuk, V., Atkinson, G. C., Murakami, K. S., Tenson, T., & Gerdes, K. (2015). Recent functional insights into the role of (p)ppGpp in bacterial physiology. *Nature Reviews Microbiology*, *13*(5), 298–309. https://doi.org/10.1038/nrmicro3448

Helwak, A., & Tollervey, D. (2014). Mapping the miRNA interactome by cross-linking ligation and sequencing of hybrids (CLASH). *Nature Protocols*, *9*(3), 711–728. https://doi.org/10.1038/nprot.2014.043

Irving, S. E., Choudhury, N. R., & Corrigan, R. M. (2021). The stringent response and physiological roles of (pp)pGpp in bacteria. *Nature Reviews Microbiology*, *19*(4), 256–271. https://doi.org/10.1038/s41579-020-00470-y

Kang, P. J., & Craig, E. A. (1990). Identification and characterization of a new Escherichia coli gene that is a dosage-dependent suppressor of a dnaK deletion mutation. *Journal of Bacteriology*, *172*(4), 2055–2064. https://doi.org/10.1128/jb.172.4.2055-2064.1990

Knights, H. E., Ledermann, R., Jorrin, B., Abreu, I., Campbell, M. J., Cocker, C. R., Dolliver, J., East, A. K., Hague, K., Maurer, A.-K., Palomero-Gómez, M., Prescott, H., Terpolilli, J., Tjahjono, O., Tronca, M. N., Underwood, T. J., & Poole, P. S. (in preparation). *Mechanisms behind nodule infection and bacteroid dedifferentiation in* Rhizobium leguminosarum [Unpublished manuscript].

Knights, H. E., Ramachandran, V. K., Jorrin, B., Ledermann, R., Parsons, J. D., Aroney, S. T. N., & Poole, P. S. (2024). Rhizobium determinants of rhizosphere persistence and root colonization. *The ISME Journal*, *18*(1), wrae072. https://doi.org/10.1093/ismejo/wrae072

Lalaouna, D., Prévost, K., Eyraud, A., & Massé, E. (2017). Identification of unknown RNA partners using MAPS. *Methods*, *117*, 28–34. https://doi.org/10.1016/j.ymeth.2016.11.011

McGill, S. L., Yung, Y., Hunt, K. A., Henson, M. A., Hanley, L., & Carlson, R. P. (2021). Pseudomonas aeruginosa reverse diauxie is a multidimensional, optimized, resource utilization strategy. *Scientific Reports*, *11*(1), 1457. https://doi.org/10.1038/s41598-020-80522-8

Mulley, G., White, J. P., Karunakaran, R., Prell, J., Bourdes, A., Bunnewell, S., Hill, L., & Poole, P. S. (2011). Mutation of GOGAT prevents pea bacteroid formation and N_2 fixation by globally downregulating transport of organic nitrogen sources. *Molecular Microbiology*, *80*(1), 149–167. https://doi.org/10.1111/j.1365-2958.2011.07565.x

Pardo Díaz, J. (2022). *Construction of gene coexpression networks and transcriptomic analysis for Rhizobium leguminosarum*. PhD thesis, University of Oxford.

Perry, B. J., Akter, M. S., & Yost, C. K. (2016). The use of transposon insertion sequencing to interrogate the core functional genome of the legume symbiont Rhizobium leguminosarum. *Frontiers in Microbiology*, *7*. https://doi.org/10.3389/fmicb.2016.01873

Pini, F., East, A. K., Appia-Ayme, C., Tomek, J., Karunakaran, R., Mendoza-Suárez, M., Edwards, A., Terpolilli, J. J., Roworth, J., Downie, J. A., & Poole, P. S. (2017). Bacterial biosensors for in vivo spatiotemporal mapping of root secretion. *Plant Physiology*, *174*(3), 1289–1306. https://doi.org/10.1104/pp.16.01302

Poole, P., & Allaway, D. (2000). Carbon and nitrogen metabolism in Rhizobium. In *Advances in Microbial Physiology* (Vol. 43, pp. 117–163). Elsevier. https://doi.org/10.1016/S0065-2911(00)43004-3

Prell, J., Mulley, G., Haufe, F., White, J. P., Williams, A., Karunakaran, R., Downie, J. A., & Poole, P. S. (2012). The PTS^{Ntr} system globally regulates ATP-dependent transporters in Rhizobium leguminosarum. *Molecular Microbiology*, *84*(1), 117–129. https://doi.org/10.1111/j.1365-2958.2012.08014.x

Prell, J., & Poole, P. (2006). Metabolic changes of rhizobia in legume nodules. *Trends in Microbiology*, *14*(4), 161–168. https://doi.org/10.1016/j.tim.2006.02.005

Ramachandran, V. K., East, A. K., Karunakaran, R., Downie, J. A., & Poole, P. S. (2011). Adaptation of Rhizobium leguminosarumto pea, alfalfa and sugar beet rhizospheres investigated by comparative transcriptomics. *Genome Biology*, *12*(10), R106. https://doi.org/10.1186/gb-2011-12-10-r106

Reid, C. J., & Poole, P. S. (1998). Roles of DctA and DctB in signal detection by the dicarboxylic acid transport system of Rhizobium leguminosarum. *Journal of Bacteriology*, *180*(10), 2660–2669. https://doi.org/10.1128/JB.180.10.2660-2669.1998

Rutten, P. J., & Poole, P. S. (2019). Oxygen regulatory mechanisms of nitrogen fixation in rhizobia. In *Advances in Microbial Physiology* (Vol. 75, pp. 325–389). Elsevier. https://doi.org/10.1016/bs.ampbs.2019.08.001

Schubert, C., & Unden, G. (2024). Regulation of aerobic succinate transporter dctA of E. coli by cAMP-CRP, DcuS-DcuR, and $EIIA^{Glc}$: Succinate as a carbon substrate and signaling molecule. *Microbial Physiology*, *34*(1), 108–120. https://doi.org/10.1159/000538095

Schulte, C. C. M., Borah, K., Wheatley, R. M., Terpolilli, J. J., Saalbach, G., Crang, N., De Groot, D. H., Ratcliffe, R. G., Kruger, N. J., Papachristodoulou, A., & Poole, P. S. (2021). Metabolic control of nitrogen fixation in rhizobium-legume symbioses. *Science Advances*, *7*(31), eabh2433. https://doi.org/10.1126/sciadv.abh2433

Schulte, C. C. M., Ramachandran, V. K., Papachristodoulou, A., & Poole, P. S. (2022). Genome-scale metabolic modelling of lifestyle changes in Rhizobium leguminosarum. *mSystems*, *7*(1), 22.

Stopp, M., Schubert, C., & Unden, G. (2021). Conversion of the sensor kinase DcuS to the fumarate sensitive state by interaction of the bifunctional transporter DctA at the

TM2/PASC-linker region. *Microorganisms*, *9*(7), 1397. https://doi.org/10.3390/microorganisms9071397

Sulieman, S. (2011). Does GABA increase the efficiency of symbiotic N_2 fixation in legumes? *Plant Signaling & Behavior*, *6*(1), 32–36. https://doi.org/10.4161/psb.6.1.14318

Tjahjono, O. (2025). *Regulation of global metabolism by PTS-NTR in Rhizobium leguminosarum*. PhD thesis, University of Oxford.

Torres-Quesada, O., Reinkensmeier, J., Schlüter, J.-P., Robledo, M., Peregrina, A., Giegerich, R., Toro, N., Becker, A., & Jiménez-Zurdo, J. I. (2014). Genome-wide profiling of Hfq-binding RNAs uncovers extensive post-transcriptional rewiring of major stress response and symbiotic regulons in *Sinorhizobium meliloti*. *RNA Biology*, *11*(5), 563–579. https://doi.org/10.4161/rna.28239

Udvardi, M., & Poole, P. S. (2013). Transport and metabolism in legume-rhizobia symbioses. *Annual Review of Plant Biology*, *64*(1), 781–805. https://doi.org/10.1146/annurev-arplant-050312-120235

Vanderlinde, E. M., Hynes, M. F., & Yost, C. K. (2014). Homoserine catabolism by Rhizobium leguminosarum bv. viciae 3841 requires a plasmid-borne gene cluster that also affects competitiveness for nodulation. *Environmental Microbiology*, *16*(1), 205–217. https://doi.org/10.1111/1462-2920.12196

Wang, P., Lopes, L. D., Lopez-Guerrero, M. G., Van Dijk, K., Alvarez, S., Riethoven, J.-J., & Schachtman, D. P. (2022). Natural variation in root exudation of GABA and DIMBOA impacts the maize root endosphere and rhizosphere microbiomes. *Journal of Experimental Botany*, *73*(14), 5052–5066. https://doi.org/10.1093/jxb/erac202

Wheatley, R. M., Ford, B. L., Li, L., Aroney, S. T. N., Knights, H. E., Ledermann, R., East, A. K., Ramachandran, V. K., & Poole, P. S. (2020). Lifestyle adaptations of Rhizobium from rhizosphere to symbiosis. *Proceedings of the National Academy of Sciences*, *117*(38), 23823–23834. https://doi.org/10.1073/pnas.2009094117

Wippel, K., & Long, S. R. (2016). Contributions of Sinorhizobium meliloti transcriptional regulator DksA to bacterial growth and efficient symbiosis with Medicago sativa. *Journal of Bacteriology*, *198*(9), 1374–1383. https://doi.org/10.1128/JB.00013-16

Witan, J., Bauer, J., Wittig, I., Steinmetz, P. A., Erker, W., & Unden, G. (2012). Interaction of the Escherichia coli transporter DctA with the sensor kinase DcuS: Presence of functional DctA/DcuS sensor units. *Molecular Microbiology*, *85*(5), 846–861. https://doi.org/10.1111/j.1365-2958.2012.08143.x

Yost, C. K., Rath, A. M., Noel, T. C., & Hynes, M. F. (2006). Characterization of genes involved in erythritol catabolism in Rhizobium leguminosarum bv. viciae. *Microbiology*, *152*(7), 2061–2074. https://doi.org/10.1099/mic.0.28938-0

Yurgel, S. N., & Kahn, M. L. (2004). Dicarboxylate transport by rhizobia. *FEMS Microbiology Reviews*, *28*(4), 489–501. https://doi.org/10.1016/j.femsre.2004.04.00